The Role of Acyl-ACP Thioesterases and Glycerophosphodiester Phosphodiesterases for Gametophyte Development in *Arabidopsis thaliana*

Dissertation

zur
Erlangung des Doktorgrades (Dr. rer. nat.)
der
Mathematisch-Naturwissenschaftlichen Fakultät
der
Rheinischen Friedrich-Wilhelms-Universität Bonn

vorgelegt von

Meike Siebers
aus
Wesel

Bonn, März 2015

Angefertigt mit Genehmigung der Mathematisch-Naturwissenschaftlichen

Fakultät der Rheinischen Friedrich-Wilhelms-Universität Bonn

1. Gutachter: Prof. Dr. Peter Dörmann

2. Gutachter: Prof. Dr. Lukas Schreiber

Tag der Promotion: 21.08.2015

Erscheinungsjahr: 2016

Contents

Table of Figures

Abbreviations

% (v/v)	Percent volume per volume (ml per 100 ml)
% (w/v)	Percent weight per volume (g per 100 ml)
ACP	Acyl carrier protein
ADP	adenosinediphosphate
Amp	Ampicillin
APS	ammonium persulfate
ATP	Adenosine-5'-triphosphate
BCA	Bicinchoninic acid
BHT	3,5-di-*t*-butyl-4-hydroxytoluene
CDP	Cytidin diphosphate
CMP	Cytidine monophosphate
CTP	Cytidine triphosphate
CID	Collision-induced dissociation
CMdum	Complete minimal dropout uracil medium
CoA	Coenzyme A
Col-0	Columbia 0
DAG	Diacylglycerol
ddH_2O	Double deionized water
DGDG	Digalactosyldiacylglycerol
DNA	Deoxyribonucleic acid
dNTP	Deoxyribonucleotide triphosphate
DTT	Dithiothreitol
E. coli	*Escherichia coli*
EDTA	Ethylenediaminetetraacetic acid
ER	Endoplasmic reticulum
ESI	Electrospray ionization
EtBr	Ethidium bromide
FAME	Fatty acid methyl ester
FID	Flame ionization detector
g	Standard gravity (g = 9.81 m s^{-2})
G3P	Glycerol-3-Phosphate
GC	Gas chromatography
Glc	Glucose
His-tag	Histidine tag
IPTG	Isopropyl-ß-D-thiogalactoside
kb	Kilobase pairs
kDa	Kilo Dalton
LB	Lysogeny Broth
LC-MS	Liquid chromatography coupled to mass spectrometry
LPA	Lysophosphatidic acid
Lyso-PC	Lysophosphatidylcholine
m/z	Mass to charge ratio
MGDG	Monogalactosyldiacylglycerol
mol %	Molar percentage
MS	Mass spectrometry
MS/MS	Tandem mass spectrometry
NADPH	Nicotinamide adenine dinucleotide phosphate
OD	Optical density
ORF	Open reading frame
oTP	Without transit peptide
P	Phosphate
PA	Phosphatidic acid
PC	Phosphatidylcholine

PCR	Polymerase chain reaction
PE	Phosphatidylethanolamine
PG	Phosphatidylglycerol
PGP	Phosphatidylglycerol-3-phosphate
Pi	Inorganic phoshpate
PMA1	Plasma membrane ATPase promoter
ppm	Parts per million
Q-TOF MS	Quadrupole Time-of-Flight Mass Spectrometer
rpm	Revolutions per minute
SD	Standard deviation
SDS	Sodium dodecyl sulfate
SDS PAGE	Sodium dodecyl sulphate polyacrylamide gel electrophesis
sn	Stereospecific numbering
SPE	Solid phase extraction
SQDG	Sulfoquinovosyldiacylglycerol
TAE	Tris-acetate-EDTA
TEMED	Tetramethylethylenediamine
TES	n-(hydroxymethyl)-methyl-2-amino ethane sulfonic acid
Tris	Tris(hydroxymethyl)aminomethane
UDP	Uridine diphosphate
UV	Ultra violet
v/v	Volume per volume
w/v	Weight per volume
WT	Wild type

Fatty acids are abbreviated X:Y, where X represents the number of carbon atoms, and Y represents the number of double bonds.

1 Introduction

Plants – often underestimated but fundamental for life on earth. Without photosynthetic plants and algae, the world, as we know, would not exist. Plants are sessile organisms; they absorb water and inorganic substances through their roots. The energy required for sugar synthesis in the leaves originates from the sun and is captured and made available by oxygenic photosynthesis in plants and algae. Thale cress (*Arabidopsis thaliana*, Arabidopsis) is the most widely studied plant today. This small dicotyledonous species belongs to the family of Brassicaceae and is a very suitable genetic, biochemical, and physiological model organism, due to its small genome size, short life cycle, and little space requirements for growth. Arabidopsis produces numerous seeds after selfing. The genome has been completely sequenced (The Arabidopsis Genome Initiative, 2000), and can be easily and rapidly manipulated through genetic engineering.

1.1 Gametophyte Development of Arabidopsis

The mature flower of Arabidopsis is composed of four sepals, four petals, six stamens, each consisting of a filament and an anther and a gynoecium (Fig.: 1.1).

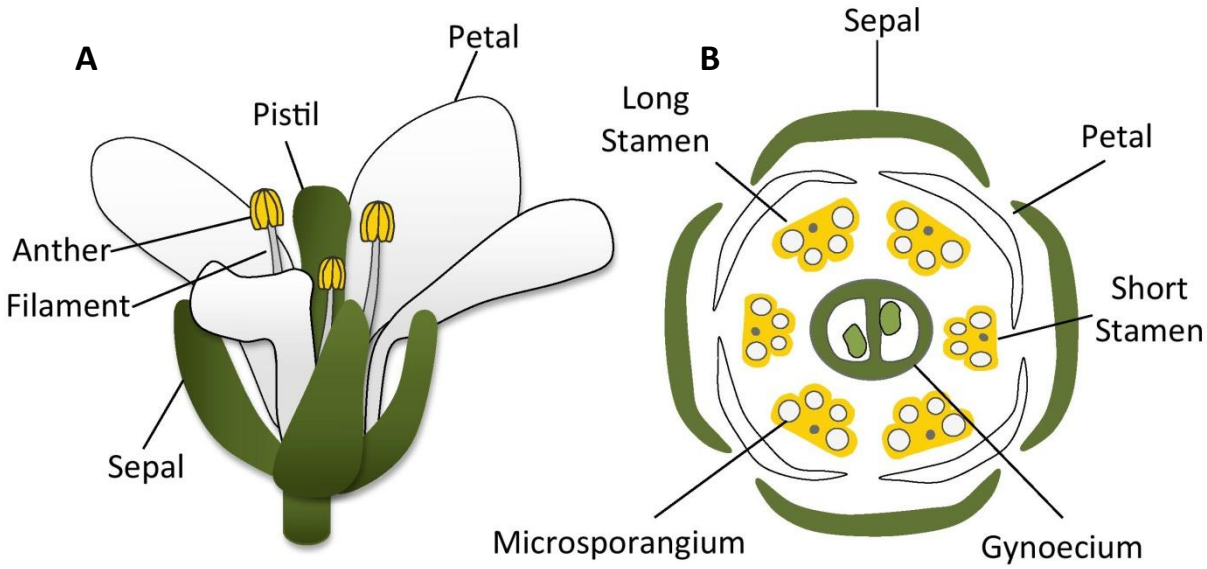

Figure 1.1: The Arabidopsis flower. (A) Scheme of the mature flower of Arabidopsis. **(B)** Transverse section through an Arabidopsis floral bud, showing the number, position, and orientation of the floral organs. The flower is composed of four sepals, four petals, six stamens, and one gynoecium. Stamen and gynoecium represent the reproductive organs.

In Central Europe, Arabidopsis flowers from April to May and is either pollinated by insects or self-pollination (wind). The flower is characterized by being hermaphrodite, having male, as well as female organs, both of which are multicellular, leading to the plant's self-fertility.

In Arabidopsis, the pollen formation takes place in the androecium, formed by six stamens. The stamen consists of the anther positioned on a filament connected to the flower. The male gametophyte, also called pollen grain or microgametophyte, develops inside the anthers. The mature pollen grain contains three cells, two sperm cells encased in a vegetative cell (Gifford and Foster, 1989). The pollen development comprises two sequential phases, the microsporogenesis and the microgametogenesis, which take place inside the anther. Meiotic division of the diploid microsporocyte, which produces four haploid microspores comprising a tetrad, initiates the microsporogenesis. During the subsequent microgametogenesis, the microspores are released from the tetrads and undergo cell expansion, cell wall synthesis, and are released from the anther (Fig.: 1.2).

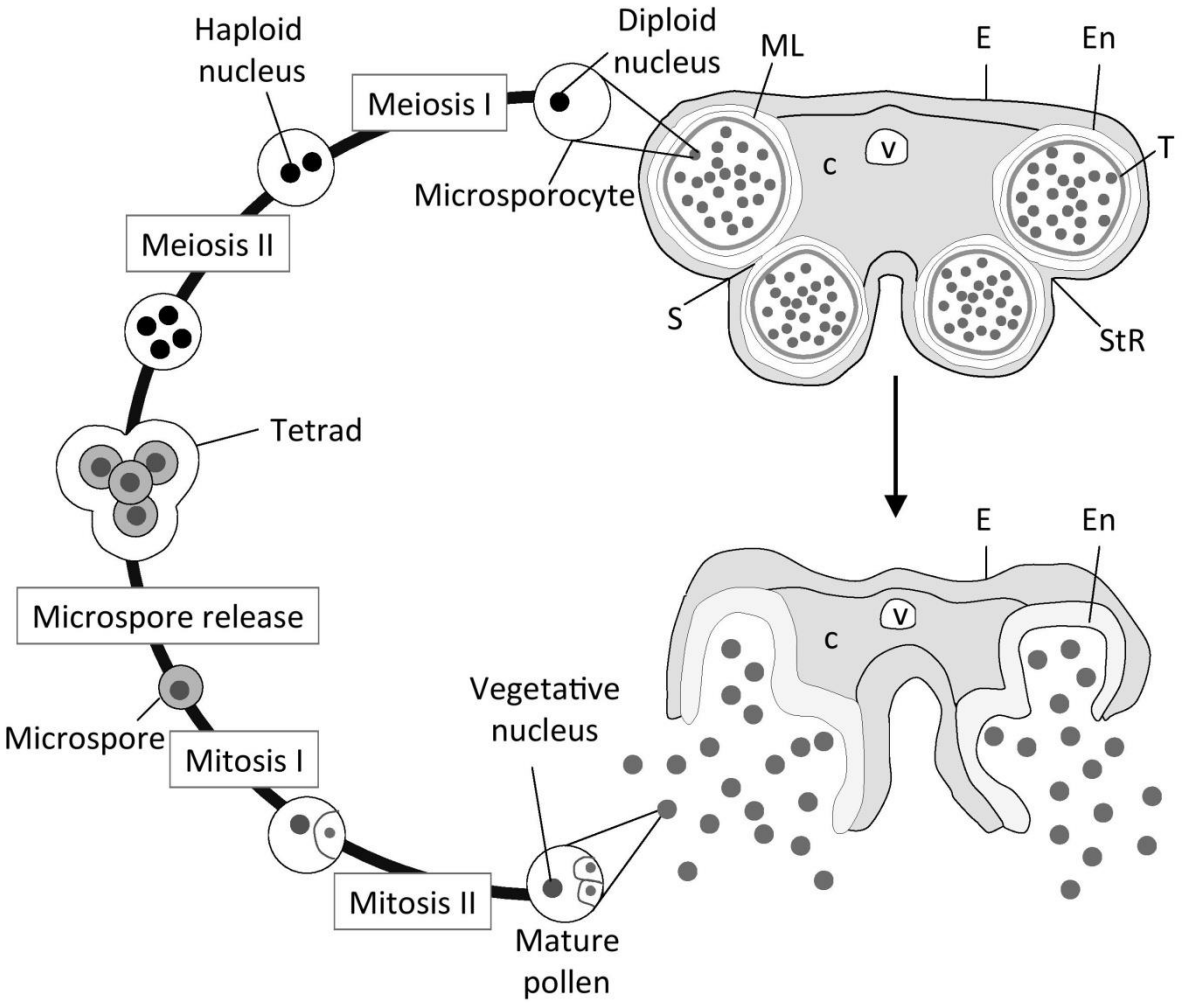

Figure 1.2: Anther and pollen development in Arabidopsis. Transverse sections through Arabidopsis anthers at different developmental stages. c, connective; E, epidermis; En, endothecium; ML, middle layer; S, septum; StR, stomium region; T, tapetum; V, vascular bundle.

Arabidopsis female gametophyte (Fig.: 1.3) development follows the most common Polygonum-type pattern. Over 70 % of flowering plants exhibit this pattern, such as Gramineae (e.g. maize, rice, wheat), Phaseoleae (e.g., beans, soybean), Brassicaceae and Solanaceae (e.g.,

pepper, tobacco, tomato, potato) (Maheshwari and Johri, 1950; Willemse and Van Went, 1984). The gynoecium or ovary of Arabidopsis consists of two fused carpels. These carpels develop as a cylinder divided into two chambers by a false septum harboring the female gametes, the ovules. Around 40-60 ovules are located in four rows within these two chambers (Bowman, 1994). The ovules are specialized somatic structures, which give rise to the egg cells.

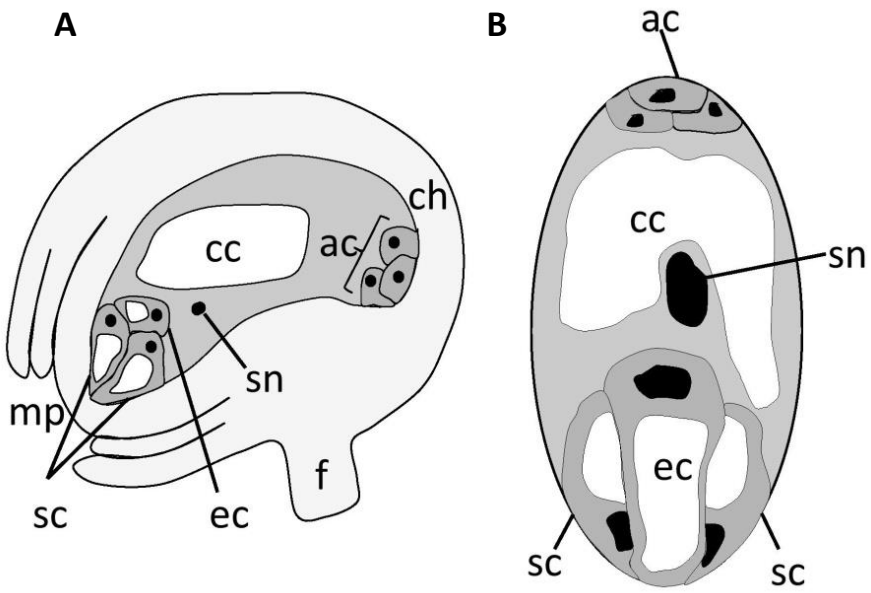

Figure 1.3: The Arabidopsis female gametophyte. (A) Ovule of Arabidopsis comprising the **(B)** mature female gametophyte. The gray, white and black areas represent cytoplasm, vacuoles, and nuclei, respectively. ac, antipodal cells; cc, central cell; ch, chalazal region of the ovule; ec, egg cell; f, funiculus; mp, micropyle; sc, synergid cell; sn, secondary nucleus modified after (Yadegari and Drews, 2004).

Regardless of the developmental pattern, the female gametophyte development occurs within the developing ovule. The development consist of two main phases i.e. megasporogenesis followed by the megagametogenesis. The megasporogenesis is characterized by the formation of four haploid megaspores by meiosis of the diploid megaspore mother cell (Misra, 1962; Webb and Gunning, 1990; Schneitz et al., 1995; Bajon et al., 1999). Megasporogenesis is characterized by three phases, the megaspore mother cell formation, the meiosis to produce haploid megaspores, and the megaspore selection. Only one of the megaspores develops into the functional mature female gametophyte during the subsequent megagametogenesis, while three degenerate. The megagametogenesis is differentiated from three events, a series of mitoses without cytokinesis, followed by cellularization of the nuclei and the subsequent cell differentiation. The female gametophyte, also called embryo sac or megagametophyte, consists of three antipodal cells, one diploid central cell, two synergid cells, and one egg cell, harboring seven to eight nuclei (Bowman, 1994; Schneitz et al., 1995; Christensen et al., 1998). The egg and the synergid are located in the micropylar chamber of the embryo sac. The structure comprising

the synergid, the egg cell and the embryo sac, form the egg apparatus which is separated from the three antipodal cells by the central cell.

In Arabidopsis, the mature pollen grain can be delivered to the pistil's stigma by direct contact due to its self-fertility. The pollen sticks to the stigma by adhesion. The adhesion between pollen and stigma cells is highly selective, requiring cell recognition to prevent inappropriate pollen tube growth from other species, which would deplete female tissue resources (Zinkl et al., 1999). Once placed on the stigma, a pollen tube germinates from the pollen grain and the sperm cells are delivered to the female gametophyte by pollen tube guidance, to surmount the long distance between the stigmatic papillae cells to the embryo sac. The pollen tube penetrates the stigma, and enters into the transmitting tissue, where the different pollen tubes are bundled (Fig.: 1.4). One single pollen tube elongates along the funiculus and enters the micropyle. There it reaches the embryo sac, and two sperm cells are released, leading to a double fertilization of the female gametophyte (Kandasamy et al., 1994; Pruitt and Hülskamp, 1994; Wilhelmi and Preuss, 1997; Lush, 1999; Wilhelmi and Preuss, 1999), which initiates the embryogenesis and seed development.

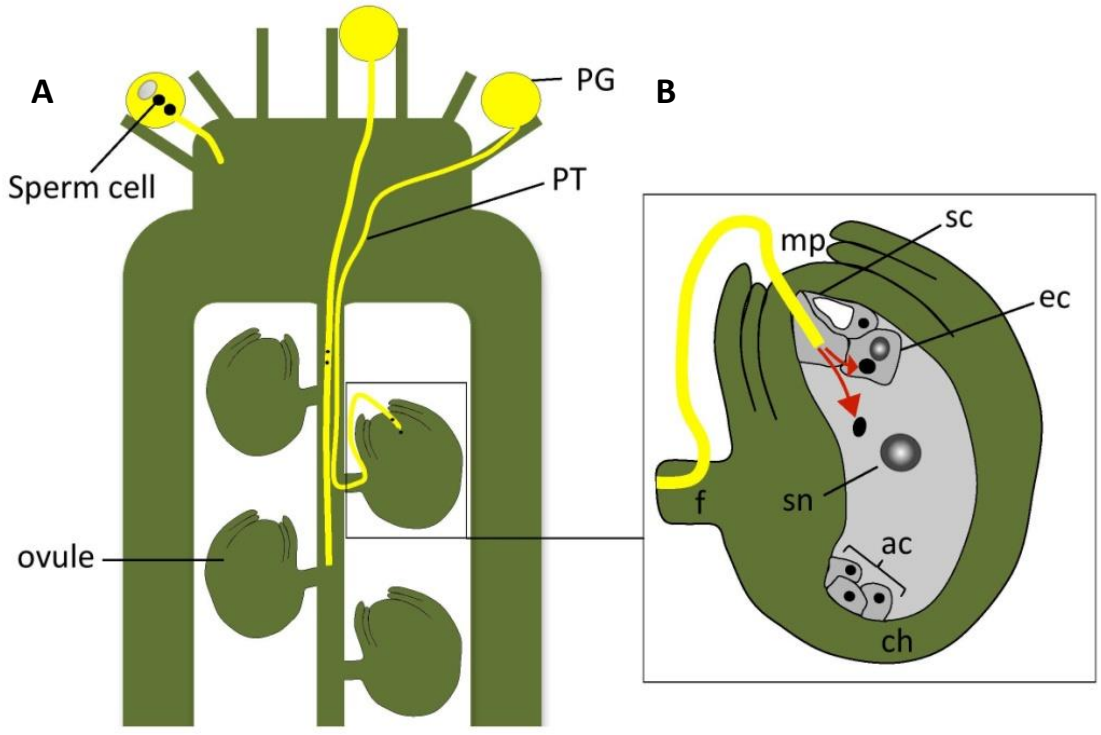

Figure 1.4: Pollen tube guidance in Arabidopsis. (A) Schematic drawing of mature female gametophytes within the gynoecium, showing the path of the pollen tube (PT) through the style and transmitting tissue towards the ovules. **(B)** PT entering the female gametophyte through the receptive synergid, releasing two sperm cells into the egg cell and the central cell.

1.2 Embryogenesis of Arabidopsis

In Arabidopsis the embryo develops from a fertilized egg cell to a mature embryo within three successive phases, (i) embryo morphogenesis, where cell division takes place, (ii) cell expansion, and (iii) subsequent desiccation (Fig.: 1.5). The first phase involves the establishment of the embryo's morphological plan. It is characterized by the differentiation of embryo cell and tissue types, initiated by the fusion of sperm and egg cells forming the diploid zygote, which develops into the embryo during embryogenesis. The second sperm cell unites with the two polar nuclei forming the triploid endosperm (Fig.: 1.5), which sustains high osmotic potential around the embryo and supplies nutrients and hormones to facilitate and support seed germination. The primary organ patterning of the mature plant has been established when the embryo reaches the torpedo stage (Jürgens et al., 1994). In the second phase, the cotyledons and the hypocotyl expand, and storage compound accumulation takes place to prepare for desiccation, germination and early seedling growth. Cell division, as well as cell expansion are highly active during this phase that comes to an end at the mid-late cotyledon stage (Mansfield and Bowman, 1993). In the final phase, the embryo loses water to prepare for quiescence.

The particular phases are grouped in different developmental stages, according to the number of embryo cells and the shape of the developing embryo (Fig.: 1.5). The pro-embryonic phases begin with the 2-celled zygote, ending in the 16-cell stage. The subsequent late phases start by reaching the globular stage, passing heart, torpedo, walking stick stage, stopping by reaching the upturned-U stage. During the development, significant portions of proteins, lipids, starch, and sugar reserves in the embryo are deposited (Bowman, 1994). Further upon the development the protoderm, later becoming the epidermis, the fundamental meristematic tissue, and the innermost procambium, forming the vascular tissue, is established. The cotyledons and the axis, comprising the shoot apical meristem, hypocotyls, root and root apical meristem are defined during this process (Bowman, 1994). Embryo and endosperm are encased in the seed coat (testa), formed by the ovule integuments (Baud et al., 2005) (Fig.: 1.5). This complex progress is coordinated by a high number of distinct genetic programs regulated by numerous genes. To study the regulation of embryogenesis in plants, hundreds of mutants with defects in embryo development were isolated and characterized. These defects can be categorized into five groups, (1) the embryonic lethal mutants in which embryogenesis is arrested, (2) mutants defective in the accumulation of storage products, (3) abnormal seedling mutants with altered pigmentation, (4) mutants altered in seed morphology but do not show any alterations in the maturation program, and (5) mutants showing defects in the regulation of the late embryogenesis (Bowman, 1994; Meinke et al., 1994).

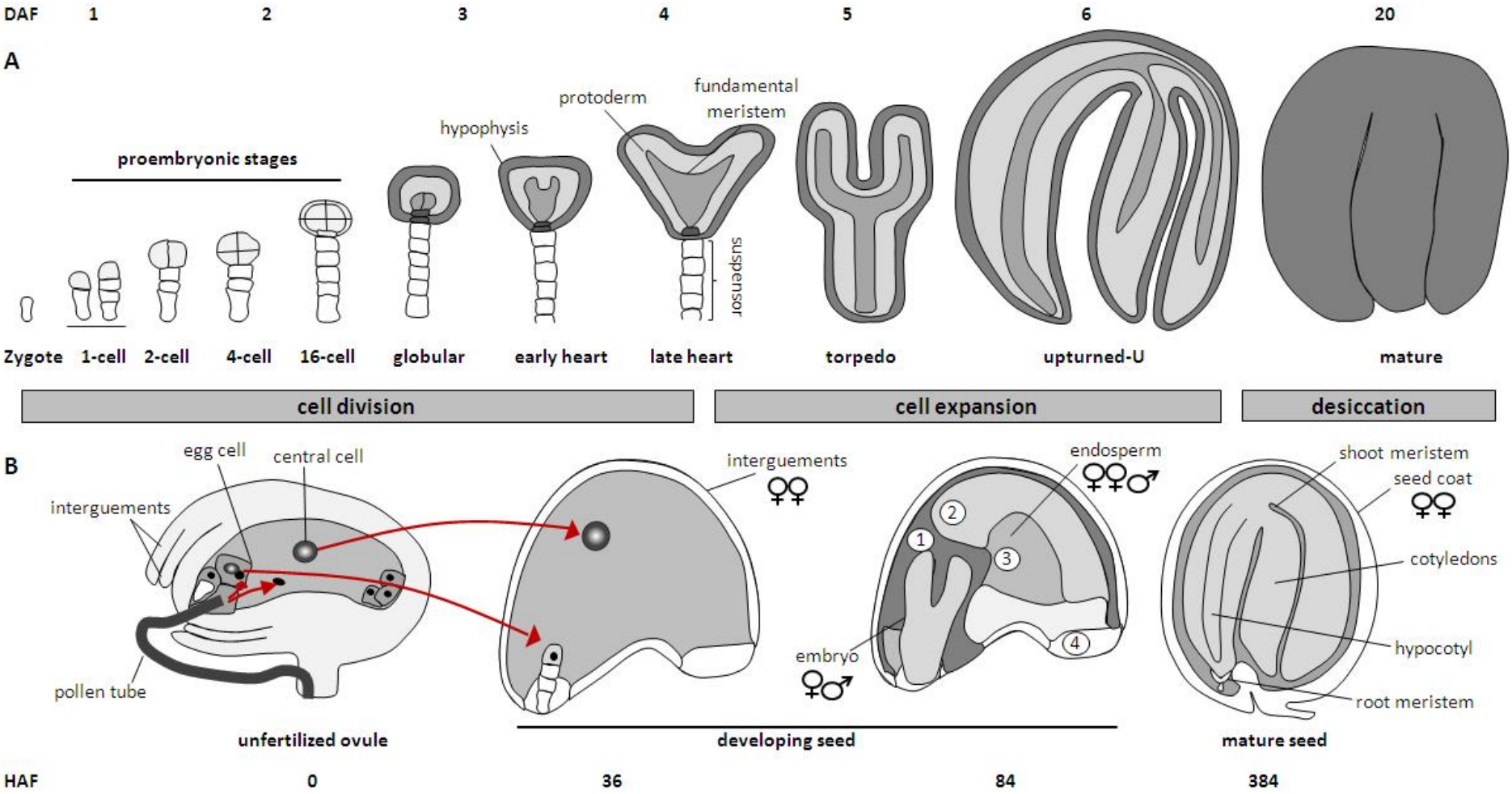

Figure 1.5: Arabidopsis ovule development after fertilization and subsequent embryogenesis. (A) Longitudinal sections of different stages of embryo development. Early (proembryonic) stages are defined according to the cell number, and late stages according to the embryo shapes. DAF, days after flowering. Different shades of grey indicate the tissue differentiation. **(B)** Ovule development after fertilization. The first drawing shows the ovule connected to the ovary wall by the funiculus. The pollen tube enters through the synergid and releases two sperm cells to the egg- and the central cells. The third drawing shows the pattern of endosperm cellularization in the embryo sac: 1, second cellular endosperm, 2 and 3 maturation layers of endosperm; 4, free nuclear endosperm. The mature seed comprises the embryo, awaiting desiccation and enclosed by the seed coat. HAF, hours after fertilization.

1.3 Lipids and Lipid Biosynthesis in Plants

All living cells are surrounded by a plasma membrane, a barrier against the environment. This barrier has to fulfill different functions; it must be partially permeable to allow the entry and export of substances from the environment, but at the same time, somewhat impermeable to prevent an uncontrolled import of compounds, and of leakage of cellular constituents. The plasma membrane is constituted by a lipid bilayer, without no life on earth would exist. Lipids can be found in all cells, with many more functions than the establishment of a lipid bilayer as addressed above. Specific lipids are important structural components of cell membranes (glycerolipids, sphingolipids, sterols), they serve as storage compounds (triacylglycerols) and participate in many biochemical processes such as signaling (jasmonic acid, lyso-PC), protein modification (dolichol) and others. They are defined according to their solubility properties, being insoluble in water, but soluble in non-aqueous solvents such as chloroform or alcohols. Lipids are characterized by a high structural diversity. The most abundant plant lipids are fatty acid containing glycerolipids. Other important lipids include carotenoids, tocopherols, phytols (including chlorophyll), sterols, sphingolipids and waxes (Fig.: 1.6).

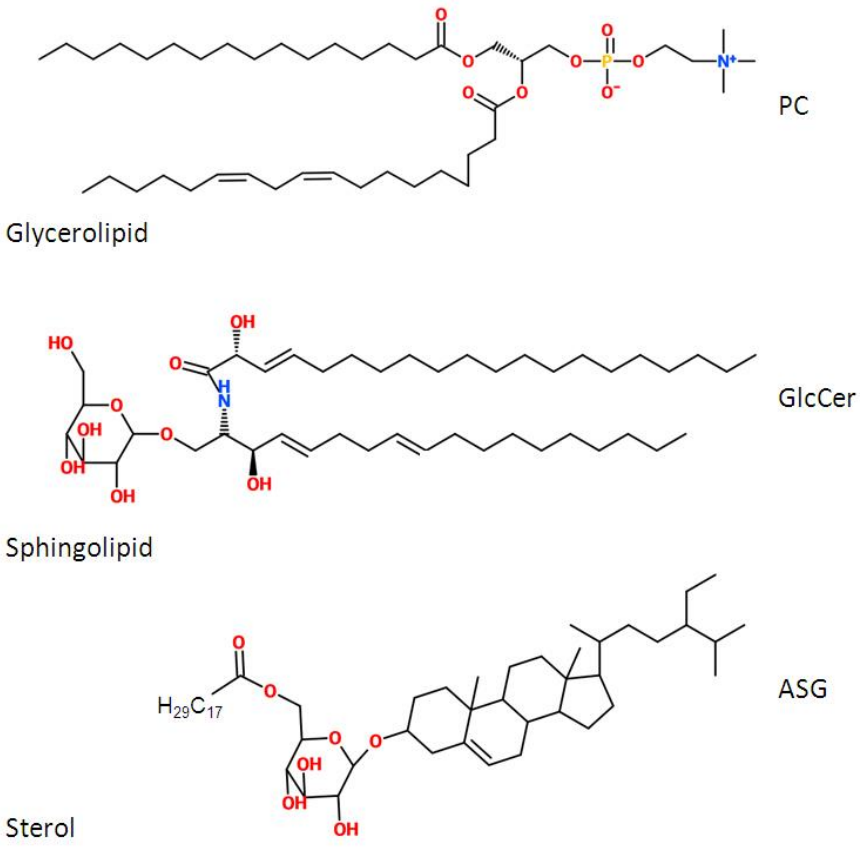

Figure 1.6: Molecular structures of selected membrane lipids. Phosphatidylcholine (PC) as an example for glycerolipids, glucosylceramide (GlcCer) representing the sphingolipids and acylated sterol glucoside (ASG) as representative for the class of sterols.

1.3.1 Fatty Acid Biosynthesis

In Arabidopsis, the major fatty acids are C16-saturated, C16-unsaturated and C18-unsaturated fatty acids (Table 1.1). The fatty acid *de novo* synthesis in plants occurs in the plastids of the seeds and the chloroplasts of green tissue (Ohlrogge et al., 1991). The first step is the generation of acetyl-coenzyme A (acetyl-CoA) by the plastidial pyruvate dehydrogenase complex. Acetyl-CoA is used as the central building block for the fatty acid production. Subsequently, acetyl-CoA is carboxylated to malonyl-CoA by acetyl-CoA carboxylase (ACCase; (Konishi et al., 1996)). The malonyl group is transferred by malonyl-CoA: ACP transacylase from CoA to acyl carrier protein (ACP) to form malonyl-ACP. From this point, the acyl groups are bound as thioester derivatives of ACP, and CoA is not involved in the later reactions. ACP, a small (8-10 kDa) and acidic protein, is the central protein in the fatty acid biosynthesis, since it carries the acyl chain during elongation. ACP navigates between all the enzymes involved in fatty acid synthesis to deliver the acyl chains (Byers and Gong, 2007). It contains a phosphopantetheine prosthetic group to which the growing acyl chain is attached as a thioester. The growing acyl chain is elongated by the stepwise addition of two carbon atoms via condensation with malonyl-ACP, accompanied with the release of CO_2. Each cycle of reactions includes a condensation, reduction, dehydration and a second reduction reaction. Acetyl-CoA and malonyl-ACP are condensed by the β-ketoacyl-ACP synthase III (KAS III) resulting in the formation of acetoacetyl-ACP. This is reduced by the β-ketoacyl-ACP reductase and dehydrated by the β-hydroxyacyl-ACP dehydrase. Additional reduction by the enoyl-ACP reductase results in butyryl-ACP. This cycle continues six more times for C16 fatty acids and seven more times for C18 fatty acids. A second condensing enzyme, KAS I, is responsible for producing chain lengths from six to 16 carbons. Beyond that, elongation of the C16 palmitoyl-ACP, to stearoyl-ACP, requires a separated condensing enzyme, KAS II. Thus, the primary product of plastidial fatty acid synthesis is palmitoyl-ACP (16:0-ACP), which has three fates: (i) the hydrolysis by acyl-ACP thioesterase, (ii) the elongation to stearoyl-ACP (18:0-ACP), which is subsequently converted into oleoyl-ACP (18:1-ACP) after the introduction of a *cis* double bond into the Δ9-position by the action of 18:0-ACP desaturase (Shanklin and Somerville, 1991), and (iii) the transfer of 16:0 from ACP to the *sn*-2 (stereochemical numbering) position of lysophosphatidic acid (LPA). Therefore, the ratio of C16 to C18 fatty acids in the membrane lipids is determined by the relative fluxes through these three reactions. Termination of the fatty acid synthesis at the C16 and C18 chain lengths occurs by the action of acyl-ACP thioesterases. The specificities of the different thioesterases regulate the ratio of C16 (16:0-ACP) to C18 (18:0-ACP and 18:1-ACP) fatty acids produced by fatty acid synthesis as well as the ratio of 18:1-ACP to 18:0-ACP. Thus, the major products of fatty acid synthesis in plants are 18:1-ACP and 16:0-ACP with very little 18:0-ACP produced.

Table 1.1: Major fatty acids in Arabidopsis. Values are given in mol % ± SD (n=12 for seeds; n=4 for leaves; n=9 for roots)(Lemieux et al., 1990). Dash, below the detection limit.

Fatty acid	mol %		
	seeds	leaves	roots
16:0	10.2±1,2	13.7±0,1	24.7±2.9
16:1	-	2.4±0.4	1.2±0.2
16:3	-	16.0±1.0	-
18:0	2.5±0.3	0.4±0.1	3.2±0.4
18:1	15.4±1.1	2.3±0.2	6.8±1.2
18:2	32.7±1.9	14.5±1.6	29.8±2.1
18:3	20.3±1.2	50.8±0.8	29.1±2.5
20:0	1.3±0.1	-	1.2±0.3
20:1	16.7±1.0	-	0.2±0.2
22:1	3.5±1.3	-	-

1.3.2 Membrane Glycerolipid Biosynthesis

1.3.2.1 Two Pathways for Membrane Lipid Synthesis

Glycerolipids of plant cells consist of two fatty acids esterified to the *sn*-1 and *sn*-2 positions of a glycerol backbone and a polar headgroup, which is attached to the *sn*-3 position. Glycerolipids of plant membranes comprise mostly the galactolipids, including monogalactosyldiacylglycerol (MGDG) and digalactosyldiacylglycerol (DGDG). Phospholipids (PL) such as phosphatidic acid (PA), phosphatidylserine (PS), phosphatidylcholine (PC), phosphatidylethanolamine (PE), phosphatidylglycerol (PG) and phosphatidylinositol (PI) are minor components of plant membranes in green tissues. Each class of glycerolipids is composed of many molecular species, since the different headgroups can be combined with a large number of fatty acids that vary in chain length and degree of desaturation. The fatty acid distribution in glycerolipids is not random. Different acyl groups are specifically found in the *sn*-1 or *sn*-2 positions of each lipid class (Heinz, 1977). Glycerolipids are predominantly synthesized in the chloroplast or at the endoplasmic reticulum (ER). Kinetics of ^{14}C-acetate incorporation in Arabidopsis revealed that there are two distinct pathways for glycerolipid biosynthesis, the prokaryotic and the eukaryotic pathway (Fig.: 1.7). Both lipid biosynthesis pathways operate in parallel (Roughan and Slack, 1982; Roughan, 1982), resulting in distinct structures of glycerolipids due to different substrate specificities of the enzymes involved in the acylation of glycerol-3-phosphate (G3P) and lysophosphatidic acid (LPA).

In many plants, acyl groups derived from plastidial fatty acid *de novo* synthesis can be directly incorporated into chloroplast lipids (prokaryotic pathway) or exported from the chloroplast and employed for lipid synthesis at the ER (eukaryotic pathway) (Browse et al., 1986). The prokaryotic pathway, located in the chloroplast envelope (Roughan and Slack, 1982) uses 18:1-ACP and 16:0-ACP as substrates predominantly. Lipids derived from the prokaryotic

pathway contain mostly C16 fatty acid esterified at the *sn*-2 position and C18 fatty acid at the *sn*-1 position of the glycerol backbone. The sequential acylation of G3P results in the synthesis of lysophosphatidic acid (LPA) and PA. PA is either converted into DAG by a phosphatidic acid phosphatase (PAP) or serves as a substrate for the synthesis of PG. DAG is the precursor for the synthesis of the major thylakoid glycolipids MGDG, DGDG, and sulfoquinovosyldiacylglycerol (SQDG) using UDP-galactose and UDP-sulfoquinovose, respectively (Douce and Joyard, 1990; Browse, 1991; Browse and Somerville, 1991). The glycerolipid biosynthesis by the eukaryotic pathway is initiated by the hydrolysis of 16:0-ACP and 18:1-ACP. The acyl groups are re-esterified to CoA and exported to the cytoplasm (Roughan and Slack, 1982). Acyl-CoA substrates are employed for the eukaryotic pathway, in which C18 fatty acids, with highly enriched 18:1 content, are positioned at *sn*-2 of G3P. Some 18:1 is incorporated into *sn*-2, while 16:0 is confined to *sn*-1 position (Frentzen, 1990). PA constituting one primary product of the prokaryotic, as well as the eukaryotic pathway, is the precursor for the PC, PE, PG, and PI synthesis. In the eukaryotic pathway, PA is converted into DAG or CDP-DAG. PC and PE are synthesized by combining DAG with the substrate CDP-choline or CDP-ethanolamine. Conversely, when CDP-DAG serves as a substrate, the reaction with myo-inositol and glycerol-phosphate results in the synthesis of PI and PG-phosphate. PG is produced from PG-phosphate in a subsequent phosphatase reaction.

Triacylglycerol (TAG) is the principal storage lipid in plants (Alvarez and Steinbüchel, 2002; Baud and Lepiniec, 2008) with fatty acids esterified at each of the three hydroxyl groups of the glycerol backbone. It is synthesized by the Kennedy pathway (Kennedy, 1961), which occurs in the ER (Ohlrogge and Browse, 1995). The Kennedy pathway involves four enzymatic steps with three acyl-CoA dependent acyltransferases, and a phosphatase. PA is formed after the stepwise acylation catalyzed by G3P-acyltransferase, and acyl-CoA lysophosphatidic acid acyltransferase (LPAAT), respectively. PAP further dephosphorylates it for generating DAG, which is subsequently acylated at *sn*-3 position by diacylglycerol acyltransferase (DGAT). There is an alternative pathway for the formation of TAG, which is independent of acyl-CoA donors, catalyzed by phospholipid-diacylglycerol acyltransferase (PDAT). PDAT transfers an acyl group from the *sn*-2 position of PC to the *sn*-3 position of DAG (Banas et al., 2000; Dahlqvist et al., 2000; Zhang et al., 2009). TAG massively accumulates during embryo development. In oilseed plants, a transient accumulation of starch in the course of embryogenesis is followed by the substantial synthesis and assembly of TAGs. In Arabidopsis seeds, TAG content increases from around 0.02 μg seed^{-1} in heart stage embryos to approximately 5 μg seed^{-1} in mature embryos. TAG can account up to 60 % of the cell volume in the cotyledons of mature embryos (Mansfield and Briarty, 1992). TAG accumulates in oil bodies, surrounded by a phospholipid monolayer, which contains oleosins, representing the primary type of proteins within these structures.

1.3.2.2 The Role of Thioesterases in Fatty Acid and Lipid Biosynthesis

The synthesis of eukaryotic lipids is initiated by acyl-ACP thioesterases, hydrolyzing the thioester bond between the acyl moiety and ACP of acyl-ACPs, releasing free fatty acids and ACP (Ohlrogge and Jaworski, 1997). The free fatty acids are re-esterified to acyl-CoA by the action of acyl-CoA synthetase located in the outer plastidial membrane (Koo et al., 2004) and exported from the chloroplast to the ER (Kim et al., 2013) (Fig.: 1.7). Thus, the acyl-ACP thioesterases determine to a large extent the chain length and degree of unsaturation of most plant fatty acids and are crucial for the regulation of the flux of acyl groups from plastidial fatty acid *de novo* synthesis into the eukaryotic lipid pathway. Therefore, their role in the regulation of lipid synthesis has been the focus of intense studies (Yuan et al., 1995; Eccleston and Ohlrogge, 1998; Salas and Ohlrogge, 2002).

There are two different types of acyl-ACP thioesterases, FatA and FatB with differences in amino acid sequences and substrate specificities (Dörmann et al., 1995; Jones et al., 1995). Both enzymes are found ubiquitously in plants. The FatA thioesterase shows the highest activity for oleoyl-ACP (18:1-ACP). The FATB enzymes can be divided into two functional groups FatB1 and FatB2 according to the chain length of their preferred substrate. FatB1 harbors broad substrate specificity for long-chain acyl groups (Hellyer et al., 1992; Dörmann et al., 1994; Salas and Ohlrogge, 2002; Sánchez-García et al., 2010). There are some plants that accumulate short or medium chain fatty acids in their seed oils (e.g. Cuphea, California Bay Laurel). These plants contain specialized FatB enzymes of the group 2, which hydrolyze short or medium chain acyl-ACPs (C8-C14 acyl-ACPs) (Voelker et al., 1992; Dehesh et al., 1996). The FatB1 thioesterases are active with palmitoyl-ACP (16:0-ACP), stearoyl-ACP (18:0-ACP), and oleoyl-ACP. They are widely distributed across the plant kingdom (Jones et al., 1995; Dörmann et al., 2000). In Arabidopsis there is one *FatB* gene (At1g08510), whose disruption leads to a reduction of palmitate by around 50 % in a variety of tissues, and of stearate by 30 % to 50 % in seeds and leaves, respectively. The Arabidopsis *fatB* mutant also shows a stunted growth, but the cause for this growth reduction is still unclear. The dwarf phenotype could be explained by increased rates of fatty acid *de novo* synthesis and degradation resulting in a futile cycle (Bonaventure et al., 2004), or by the shortage in palmitoyl-CoA for sphingolipid synthesis (Chen et al., 2006). Based on these data, it was concluded that about half of the saturated fatty acids in Arabidopsis are exported from the chloroplast by *FatB*. This contribution to the total flux of fatty acids for the leaf lipid formation is crucial for normal plant growth and maturation (Bonaventure et al., 2003).

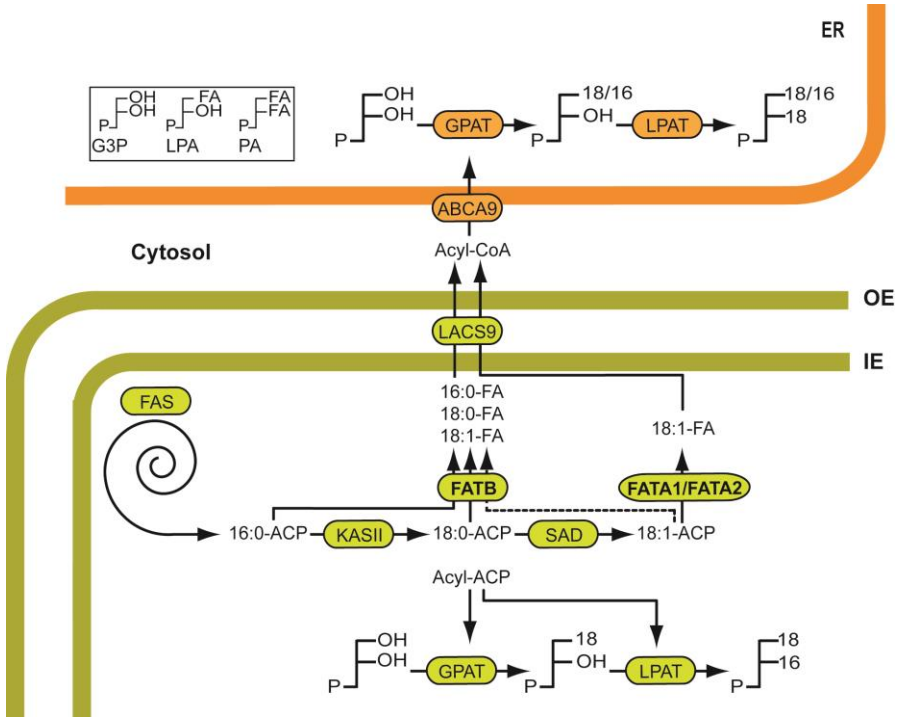

Figure 1.7: Acyl-ACP thioesterases in fatty acid biosynthesis, the prokaryotic and eukaryotic pathway. The fatty acid chain length after FAS *de novo* synthesis is determined by the action of acyl-ACP thioesterases. Fatty acids are employed for PA synthesis either via the prokaryotic or by the eukaryotic pathway of lipid biosynthesis occurring in the plastid or at the ER, respectively. OE, outer envelope; IE, inner envelope; LPAT, Lysophosphatidyl acyltransferase.

In addition to the FatB thioesterase, all plants contain a FatA thioesterase which is highly specific for 18:1-ACP (Jones et al., 1995; Salas and Ohlrogge, 2002). Arabidopsis contains two copies of *FatA* in its genome, *FatA1* (At3g25110) and *FatA2* (At4g13050) (Beisson et al., 2003), whose amino acid sequences are highly similar (74.3 % identity). A double mutant for *FatA1* and *FatA2* (*fatA1-1fatA2-1*) with T-DNA insertions in the promoter regions of the two *FatA* genes showed a reduced expression for the two genes. However, *FatA1* and *FatA2* transcripts were still detectable in the respective mutants, demonstrating that the two mutations do not represent null alleles. This partial reduction in *FatA1* and *FatA2* gene transcript abundance did not lead to any morphological changes of the mutant plants or of the reproductive organs, but to an altered oil content and fatty acid composition of the seeds. Thus, dry mature mutant seeds had decreased TAG content. The metabolic flow into seed oil was reduced in the developing seeds at different stages of seed formation in *fatA1-1fatA2-1* (Moreno-Pérez et al., 2012). This resulted in an increased linolenic acid (18:3) and erucic acid (22:1) content in the seed oil, similar as observed for the Arabidopsis mutant *wri1* (mutation in the transcription factor WRI1; (Focks and Benning, 1998). The alterations found in the double *fatA1-1fatA2-1* mutant were more similar to those of Arabidopsis mutants deficient in oil accumulation than the Arabidopsis *fatB* mutant line (Moreno-Pérez et al., 2012). However, the relevance of the *FatA1* and *FatA2* genes for lipid synthesis through the eukaryotic pathway could not be addressed due to the residual expression of the two genes in the double mutant.

1.3.3 Remodeling of the Plant Membrane in Response to Phosphate Starvation

Lipids are not only important structural membrane components, but also play crucial roles in the plant's ability to survive and adapt to environmental changes. Phosphate (inorganic phosphate, Pi) is an essential macronutrient for plant growth and development (Raghothama, 1999). Many soils around the world are characterized by low Pi availability, and its concentration is generally below that of many other nutrients (Barber et al., 1963). Even in fertile soils, available Pi rarely exceeds 10 µM (Bieleski, 1973) and most soils only contain around 2 µM of available Pi, which is several orders of magnitude lower than that in plant tissues (5-20 mM). In response to continuously low levels of available Pi in the rhizosphere, plants have developed mechanisms to cope with Pi starvation by acquiring and utilizing Pi from the environment and by remobilizing endogenous Pi from phosphorus-containing molecules such as phospholipids (PL).

Under Pi starvation, membrane PL, which constitute up to 1/3 of the organically bound P (Poirier et al., 1991) reserves in plants, are degraded (Fig.: 1.8) to release the Pi for other important cellular processes. These membrane PLs are replaced by non-phosphorus lipids to compensate for the loss of lipids in the membrane (Table 1.1). This replacement from phosphorus to non-phosphorus lipids in plants was first observed in the Arabidopsis *pho1* mutant, which carries a recessive mutation in the *PHO1* locus, leading to a leaf Pi concentration of approximately 5 % of that of the WT. However, the root Pi content and uptake remain unaltered, indicating a participation of *PHO1* in Pi loading into the xylem and the subsequent transport from the roots to the shoots (Poirier et al., 1991; Essigmann et al., 1998). The overall PL content in the leaf lipid extracts analyzed in this study was decreased while there was an increase in the glycoglycerolipids DGDG and SQDG (appendix). This phospholipid-to-galactolipid membrane lipid remodeling is a major strategy in plants to cope with Pi starvation. It includes the induction of the phospholipid degradation pathway and of the galactolipid biosynthetic pathway to adjust the internal Pi concentration during Pi deprivation. This conversion consists of the initial hydrolysis of the phosphorus-containing polar head group from PLs resulting in DAG, which is used as a substrate for the galactolipid biosynthesis (Härtel and Benning, 2000; Härtel et al., 2000, 2001).

1.3.3.1 Phospholipid Degradation by Phospholipases

Phospholipase C (PLC)

Phospholipid degradation catalyzed by PLC leads to the formation of DAG, the precursor for the galactolipid biosynthesis, plus a phosphorylated headgroup. In leaves the expression of the different PLC isoenzymes is strongly induced by Pi deprivation, implicating an involvement in PL turnover (Andersson et al., 2005; Nakamura et al., 2005; Gaude et al., 2008). PLCs in plants

can be divided into three groups according to substrate specificity and cellular function: (i) PC-PLCs or non-specific PLCs that hydrolyze PC and other phospholipids, (ii) PIP_2-PLCs which act on phosphoinositides and (iii) glycosylphosphatidylinositol (GPI)-PLCs that hydrolyze GPI anchors on proteins. Arabidopsis contains six genes (*NPC1-NPC6*) showing sequence similarities to bacterial non-specific phospholipases C (NPC), which are predicted to harbor putative PC-PLC enzyme activity. In Arabidopsis, expression of two of these genes (*NPC4, NPC5*) is strongly induced upon low Pi conditions (Nakamura et al., 2005; Gaude et al., 2008). The Arabidopsis *npc4* mutant has a severely reduced PLC activity under Pi starvation (Nakamura et al., 2005) while DGDG accumulation is not affected. In contrast, the *npc5-1* and *npc5-2* mutant lines show a reduced DGDG level compared to the WT, suggesting that NPC5 contributes to the conversion of PC into DAG (Gaude et al., 2008). The residual amount of DAG required for DGDG synthesis under Pi limitation might be derived from DAG *de novo* assembly or the PLD/PAP pathway of the PC hydrolysis described below.

Phospholipase D (PLD) and Phosphatidate Phosphatase (PAP)

PLDs catalyze the first step of the conversion of PLs into DAG by cleaving the terminal phosphodiester bond of PLs, resulting in the formation of PA and a free head group. PA can be further hydrolyzed by a PAP resulting in DAG formation (Nakamura et al., 2005). PLDs establish a ubiquitous family of phospholipases, divided into several subfamilies. Arabidopsis contains 12 *PLD* genes divided into five groups (3 *PLDα*, 2 *PLDβ*, 3 *PLDγ*, 1 *PLDδ*, 1 *PLDε*, 2 *PLDζ*), most of which are activated in response to Pi starvation and may have unique functions (Wang, 2002; Wang et al., 2004; Li et al., 2006). Expression of the two *PLDζ*s and particularly *PLDζ*2 is strongly induced upon Pi deficiency (Mission, 2005; Li et al., 2006). The altered lipid composition in response to Pi deprivation differs from leaves and roots, due to the diverse membrane structure. The involvement of *PLDζ*1 and *PLDζ*2 in membrane lipid remodeling is restricted to roots (Cruz-Ramírez et al., 2006; Li et al., 2006; Yamaryo, 2008; Yamaryo et al., 2008), which also mediate alterations in root structure in response to Pi deficiency (Cruz-Ramírez et al., 2006). In oat, about 70 mol % of root plasma membrane PLs are replaced by DGDG, and PLD was shown to play a predominant role in lipid remodeling during Pi deprivation (Andersson et al., 2005; Tjellström et al., 2008). An involvement of the other members of the PLD family in the degradation of phospholipids during Pi deplete conditions seems to be likely, since PLDα, PLDβ and PLDγ hydrolyze PC, PE and PG, but differ in their requirement for Ca^{2+} (Pappan et al., 1998).

PA can further be degraded by PAP, which catalyzes the dephosphorylation of PA, the product of the PLD reaction as well as of *de novo* glycerolipid assembly, releasing DAG and free Pi. Due to the predominant role of DAG in the galactolipid synthesis, PAP activity is crucial during membrane remodeling and Pi mobilization in Pi-starved plants (Nakamura, 2010). The PAP enzyme family is divided into PAP_1, comprising the soluble enzymes, and PAP_2, containing

the membrane bound enzymes (Carman and Han, 2006). Enzymes harboring PAP_2 activity are designated lipid phosphate phosphatases (LPPs) and are mainly involved in signaling. There are nine LPPs in Arabidopsis involved in stress responses (Pierrugues et al., 2001), abscisic acid signaling (Katagiri, 2005; Paradisa et al., 2011) and chloroplast lipid metabolism (Nakamura, 2010). In the yeast *Saccharomyces cerevisiae* a phosphatidate phosphohydrolase (PAH) belonging to PAP_1 regulates the cellular PA content and provides PA as substrate for membrane and storage lipids assembly (Carman, 2007; Eastmond, 2010; Eastmond et al., 2010) Arabidopsis contains two PAH enzymes, PAH1 and PAH2, (Nakamura et al., 2009; Eastmond, 2010; Eastmond et al., 2010). The Arabidopsis *pah1pah2* double mutant shows an increased PL content and a change in ER morphology associated with massive membrane proliferation (Eastmond et al., 2010). The double mutant plants also show severely impaired growth, and a decreased DGDG accumulation under Pi deprivation. These findings indicate that *PAH1* and *PAH2* are limiting for the eukaryotic pathway of the galactolipid synthesis, and crucial for membrane lipid remodeling under Pi deprivation (Nakamura et al., 2009).

Acyl hydrolases

Besides the hydrolysis via PLC and PLD/PAP, an alternative pathway for phospholipid hydrolysis exists in Arabidopsis. This pathway is mediated by lipid acyl hydrolases (LAH) comprising phospholipase A (PLA) and phospholipase B (PLB) enzymes. The PLA superfamily is divided into PLA_1 and PLA_2, which catalyze the hydrolysis of the acyl ester bond of membrane PLs at their *sn*-1 and *sn*-2 positions, yielding free fatty acids and lysophospholipids. Lysophospholipids are further hydrolyzed to glycerophosphodiesters by lysoPLA. PLAs in plants are suggested to be involved in the regulation of plant growth, root and pollen development, stress responses, and defense signaling (Chapman, 1998; Ryu, 2004; Rietz et al., 2010). Alternatively, sequential deacylation of glycerophospholipids at *sn*-1 and *sn*-2 positions can be catalyzed by PLB, which has both PLA and lysoPLA activities. The enzymatic products of PLA/lysoPLA and PLB are glycerophosphodiesters (GPD), substrates for glycerophosphodiester phosphodiesterases (GDPD). GDPD hydrolyzes a GPD to yield G3P and the corresponding alcohol, e.g. choline (PC) or ethanolamine (PE). G3P is the initial substrate for glycerolipid biosynthesis and is also crucial for the galactolipid synthesis. The involvement of LAH and GDPD in lipid remodeling under Pi deprivation remains unclear, since there are numerous *LAH* and *GDPD* genes in Arabidopsis, which await their characterization (Matos and Pham-Thi, 2009; Cheng et al., 2011).

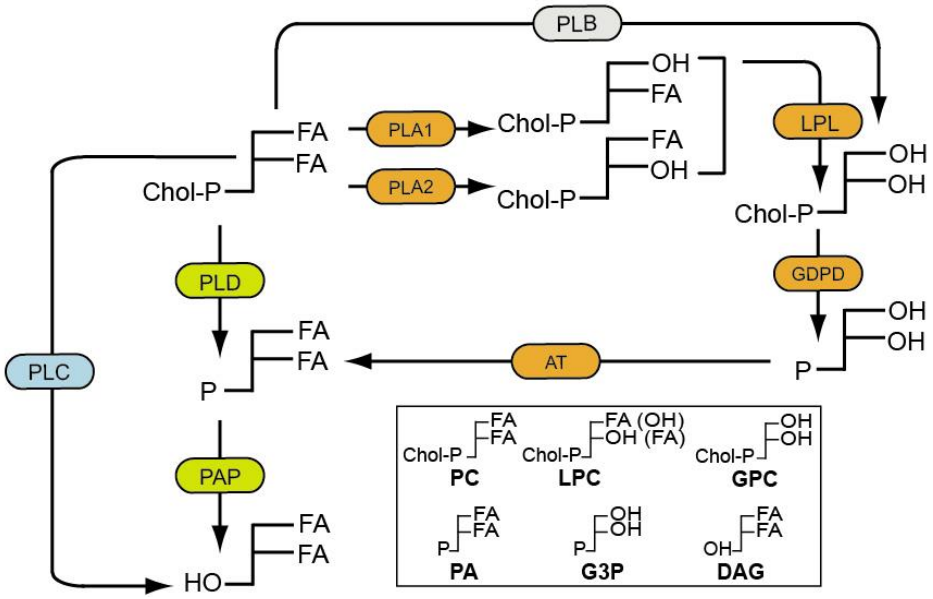

Figure 1.8: The hydrolysis of phosphatidylcholine (PC) by phospholipases C (PLC) and phospholipases D (PLD) produces diacylglycerol and phosphatidic acid, respectively. Deacylation by phospholipase A (PLA) and lysophospholipase (LPL), or by phospholipase B (PLB) results in the release of glycerol-3-phosphocholine, a substrate for glycerophosphodiester phosphodiesterases (GDPD), whose activity results in glycerol-3-phosphate (G3P) formation.

1.3.3.2 Glycerophosphodiester Phosphodiesterases in Arabidopsis

Glycerophosphodiester phosphodiesterases hydrolyze GPDs, phospholipid metabolites generated by PLA/LPL or PLB activity, between the phosphate and the amino alcohol group, thereby releasing G3P and the free amino alcohol. These enzymes are presumably involved in phospholipid degradation. The first *GDPD* gene (*GlpQ*) was isolated from the *glp* regulon in *Escherichia coli* (*E. coli*) (Larson et al., 1983). Enzyme activity of *glpQ* is dependent on divalent cations (Ca^{2+}) and the enzyme exhibits broad substrate specificity for different GPDs such as glycerophosphoethanolamine (GPE), glycerophosphocholine (GPC), and glycerophosphoglycerol (GPG), with similar activities for these substrates (Larson et al., 1983). In 2008, a second GDPD (*UgpQ*) was identified and characterized (Ohshima et al., 2008). UgpQ requires divalent cations such as Mg^{2+}, Mn^{2+} or Ca^{2+}. *S. cerevisiae* contains two homologs to *E. coli GlpQ*, YPL110c and YPL206c. While YPL206c (termed *GDE1*) is a PG specific PLC (Fernández-Murray and McMaster, 2005; Fisher et al., 2005; Šimočková et al., 2008), expression of YPL110c is induced under low Pi conditions and shows GDPD activity for GPC (Fisher et al., 2005). In the yeast *gde1*Δ mutant, the activity of choline hydrolysis from GPC, is greatly decreased. Furthermore, the WT strain is able to utilize GPC as the sole Pi source for growth in contrast to the *gde1*Δ mutant (Fisher et al., 2005). *GDPD* genes were also isolated from humans (Tommassen et al., 1991; Zheng et al., 2003; Fernández-Murray and McMaster, 2005). The *MIR16* (membrane interacting protein of RGS16) gene belongs to a family of GDPDs containing a putative catalytic domain comparable to the

mammalian phosphoinositide PLC domains. *MIR16* is specific for glycerophosphoinositols (GPI) (Zheng et al., 2003).

Up to now, little is known about the physiological significance of *GDPD* in plants. A plant derived *GDPD* with sequence similarity to *GlpQ* from *E. coli* was first characterized from carrots (Van Der Rest et al., 2004). This GDPD harbors activity towards different substrates including GPC and GPI. Arabidopsis contains 13 genes with sequence similarities to *GDPD*s from other organisms (Cheng et al., 2011). These genes are classified into two subfamily types, type-A (*AtGDPD1-6*) and type-B (*AtGDPDL1-7*), depending on the number of *GDPD* domains and the similarity of the conserved sequence motif within this domain (Fig.: 1.9) (Cheng et al., 2011). Type-A members contain one *GDPD* domain, with high conservation of the critical residues of the active site. *AtGDPD4-6* also include a membrane-spanning region at the N-terminus before the *GDPD* domain. Expression of most of the type-A members is induced under low Pi conditions, except *AtGDPD4.* Members of the GDPD subfamily type-B, which are induced by salt and osmotic stress, contain two *GDPD* domains and at least one transmembrane domain, but not all active site residues are conserved. Type B members are also designated "GDPD-like" (GDPDL). *AtGDPD1* (At3g02040) and *AtGDPDL1* (At1g66970) have been characterized as representatives of the two *GDPD* subfamilies (Cheng et al., 2011). Both enzymes show activities towards a broad range of GPDs with no differences in substrate preferences but depend on divalent cations. No alteration in the membrane lipid composition in P-deprived plants could be detected in the *Atgdpd1-1* mutant. However, a decrease in G3P content, Pi content, and seedling growth rate was measured under Pi starvation in *Atgdpd1-1* compared to WT (Cheng et al., 2011).

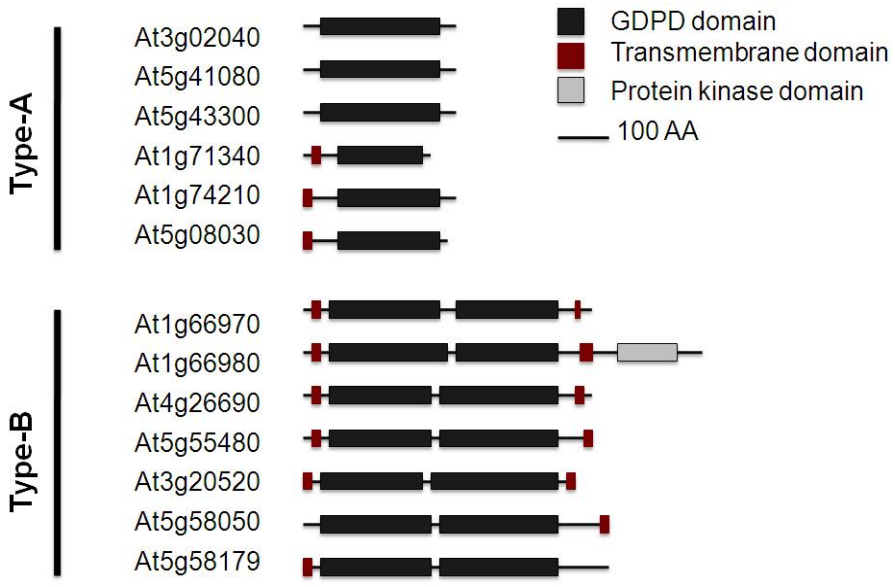

Figure 1.9: Organization of the glycerophosphodiester phosphodiesterase (GDPD) family in Arabidopsis. GDPD family can be divided into type-A and type-B subfamilies, according to the number of GDPD domains (modified after (Cheng et al., 2011)).

G3P consists of a glycerol backbone with an ester-linked phosphate group at *sn*-3 position. G3P and its metabolites are required for many biochemical processes in eukaryotes as well as prokaryotes (Brisson et al., 2001). The conversion of glycerol to G3P is a highly conserved process in a variety of organisms (Venugopal et al., 2009). In plants G3P fulfills a plethora of functions, e.g. it is a proposed regulator of plant defense signaling, an important component of diverse energy producing reactions and a crucial precursor for glycerolipid biosynthesis in the prokaryotic and eukaryotic pathway (Chanda et al., 2008; Venugopal et al., 2009). In plants, G3P can be synthesized via two metabolic pathways, by the glycerol kinase, or the reduction of dihydroxyacetone phosphate (DHAP) through G3P dehydrogenase (GPDH) (Shen et al., 2010). G3P is not only crucial for lipid biosynthesis in plants, but is also essential for maintaining homeostasis between the prokaryotic and eukaryotic pathway by regulating other metabolites, such as lipids and sugars (McKee and Hawke, 1979; Shen et al., 2010).

1.3.3.3 Biosynthesis of Non-Phosphorous Lipids and Lipid Balancing under Pi starvation

During Pi deprivation, DAG released by different phospholipases or derived from the Kennedy pathway, is converted into galactolipids or sulfolipid to compensate for the reduced phospholipid content (Härtel and Benning, 2000; Yu et al., 2002). MGDG is synthesized by the transfer of galactose from UDP-Gal onto DAG (Fig.: 1.10) (Miège et al., 1999). Arabidopsis contains three MGDG synthases, MGD1, MGD2 and MGD3 (Shimojima et al., 1997; Awai et al., 2001). MGDG synthesized under Pi depleted conditions is converted into DGDG, which is incorporated into plastidial and extraplastidial membranes when PLs are degraded. DGDG is synthesized by transferring galactose from UDP-Gal to MGDG (Kelly and Dörmann, 2002; Kelly et al., 2003). Arabidopsis contains two DGDG synthases, DGD1 and DGD2 (Kelly et al., 2003). The *Arabidopsis dgd1* mutant carries a single recessive mutation in the *DGD1* locus. The complete loss of DGD1 activity leads to a 90 % reduction of DGDG, stunted growth and reduced photosynthetic activity under Pi fertilization conditions (Dörmann et al., 1995). Besides DGDG, which shows the strongest increase during Pi deprivation, additional lipids are involved in the adaptation to Pi limitation For example, the anionic lipids SQDG and glucuronosyldiacylglycerol (GlcADG) accumulate to replace PLs inside the plastid (Yu et al., 2002; Okazaki et al., 2009). DGDG as a bilayer-forming lipid can replace the bilayer-forming lipids PC, and PI. The capacity of replacing the non-bilayer forming lipid PE by DGDG might be limited as a particular ratio of bilayer to non-bilayer lipids needs to be sustained for proper membrane functions. The anionic phospholipid PG is replaced by SQDG and probably by GlcADG in the photosynthetic membranes. This replacement mechanism is required to maintain the surface charge of thylakoid membranes (Frentzen, 2004), and occurs in a reciprocal manner. (Fig.: 1.10) (Okazaki et al., 2013).

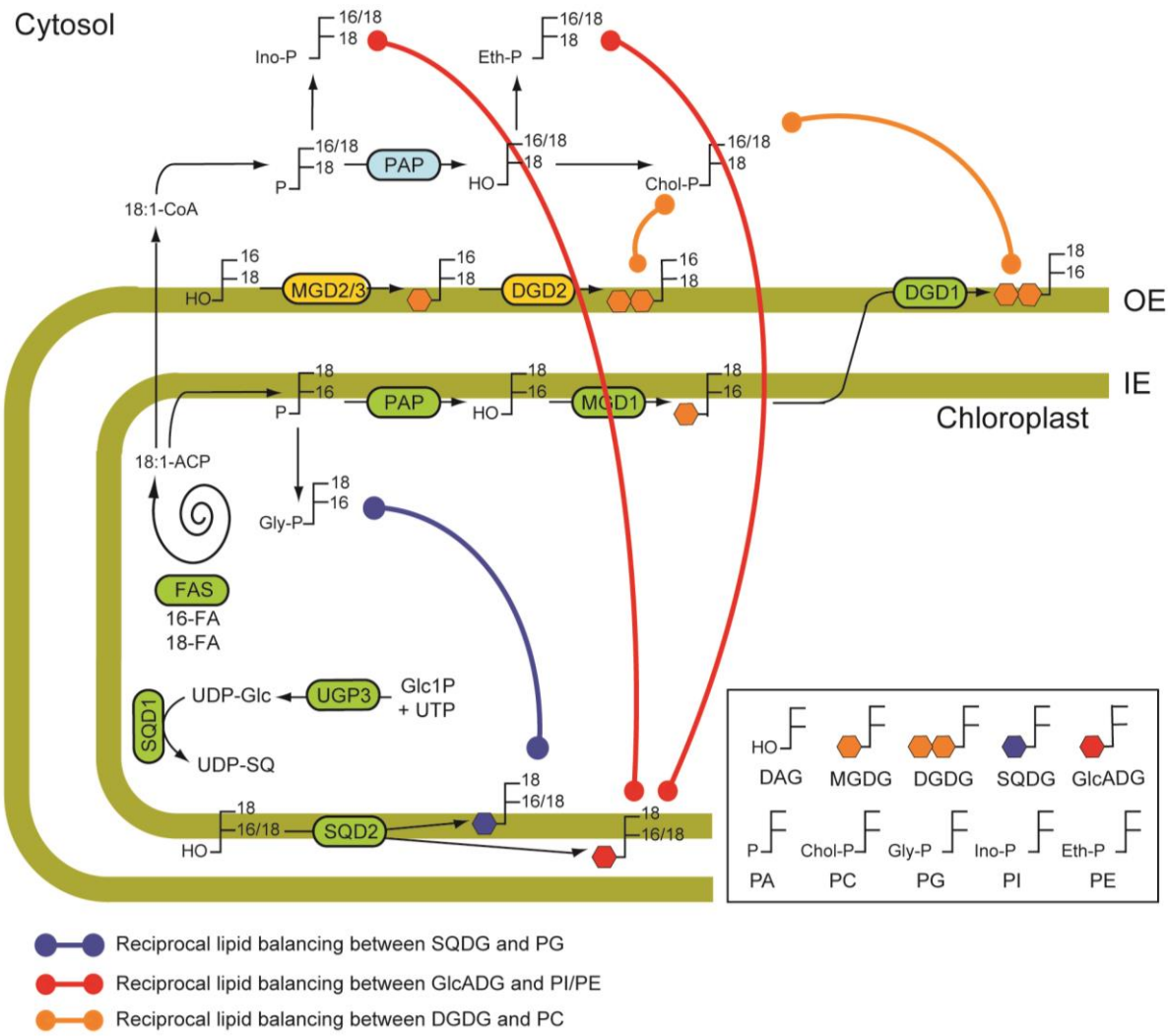

Figure 1.10: Scheme for the biosynthesis of different lipids and the balancing of glycolipids and phospholipids under Pi deprivation. Biosynthesis of the major plant glycerolipids is represented in a scheme modified from Okazaki and co-workers (2013), and Siebers and co-workers (2015). Enzymes depicted in orange are mainly active under Pi deprivation.

DGDG serves as a surrogate for PLs, especially in extraplastidial membranes, thus playing a prominent role during lipid remodeling under Pi deprivation. As mentioned above, the membrane remodeling differs in response to Pi deficiency between roots and leaves, which can be explained by the distinct membrane structure of these tissues. Due to the abundance of photosynthetic membranes, leaves contain high proportions of galactolipids, while roots are enriched in PLs. DGDG increases by approximately 2-fold in leaves and by around 8 to 10-fold in roots (Table 1.2) (Härtel and Benning, 2000; Härtel et al., 2001; Kelly et al., 2003; Li et al., 2006). However, the newly synthesized DGDG is not sufficient to substitute for the lack of phospholipids in roots, leading to a reduction in total lipid content by around 42 % (Li et al., 2006).

Table 1.2: Lipid content of Arabidopsis leaves and roots grown under Pi replete (+P) or depleted (-P) conditions. Values are given in mol % (Härtel and Benning, 2000). Dash below detection limit (<1 mol %).

	leaves		roots	
Lipid	+ P	- P	+ P	- P
MGDG	45	47	3	6
DGDG	12	26	2	17
SQDG	2	5	-	-
PG	8	5	4	4
PI	1	-	4	2
PS	-	-	1	2
PE	10	6	30	22
PC	22	11	56	47

1.4 Objectives

The goals of this thesis include the analysis of regulatory points of plant lipid biosynthesis, in particular the regulation of membrane lipid biosynthesis and of membrane lipid remodeling under Pi starvation. In the first part of the thesis, the enzymes catalyzing the initial committed step of the eukaryotic lipid biosynthesis pathway occurring in the plastid were characterized. Acyl-ACP thioesterases hydrolyze acyl-ACPs in the plastid, releasing free fatty acids. These free fatty acids are subsequently esterified to CoA and exported to the ER, serving as substrates for the eukaryotic lipid biosynthesis. The aim of this part was the analysis of the two acyl-ACP thioesterases of type A (FatA), FatA1 and FatA2, in Arabidopsis. To this end, T-DNA insertion lines for *FatA1* and *FatA2* and a double mutant were isolated. In contrast to previous studies, these new *fatA1-2* and *fatA2-2* mutant plants are complete null alleles providing for the first time the means to explore the role of FatA thioesterases in plant lipid metabolism. The characterization of the fatA single and double mutant plants includes the measurements of the glycerolipid and fatty acid composition by mass spectrometry and gas chromatography. Embryo development was found to be impaired in the *fatA1-2fatA2-2* double mutant, only reaching late heart to early torpedo stage. Double mutant embryos were analyzed morphologically and biochemically. Furthermore, FatA activity of the two Arabidopsis proteins can be measured after heterologous expression in the *E. coli fadD* mutant, lacking the acyl-CoA synthetase resulting in an accumulation of free fatty acids.

In the second part of the thesis, the regulation of the replacement of membrane phospholipids with non-phosphorous lipids during Pi depletion will be studied. Specific phospholipases hydrolyze phospholipids releasing lipid metabolites such as free fatty acids, lysophospholipids, diacylglycerol, phosphatidic acid and glycerophosphodiesters. In Arabidopsis, two genes (*GDPD5* and *GDPD6*), with sequence similarities to glycerophosphodiester phosphodiesterases (GDPD) from different organisms, are assumed to be involved in membrane lipid remodeling. Different Arabidopsis T-DNA insertion lines for *GDPD5*

and *GDPD6* and the respective *gdpd5gdpd6* double mutant plants were isolated and employed for abiotic stress experiments to characterize the roles of the different genes and metabolites. To this end, the WT and different mutant lines were exposed to Pi starvation conditions and measurements of glycerolipids and secondary metabolites were performed. GDPD activity of the two Arabidopsis proteins was measured by expression in *Nicotiana benthamiana* (*N. benthamiana*) in an enzyme-coupled spectrophotometric assay.

2 Materials and Methods

2.1 Materials

2.1.1 Equipment

Autoclave	Tuttnauer Systec, Kirchseeon-Buch (D)
Balance 770	Kern, Balingen-Frommern (D)
Balance PG503-S Delta Range	Mettler Toledo, Gießen (D)
Block heater SBH130D/3	Stuart, Bibby Scientific, Staffordshire (USA)
Binocular microscope SZX16	Olympus, Hamburg (D)
Camera DP7Z for microscope	Olympus, Hamburg (D)
Centrifuge 5810 R	Eppendorf, Hamburg (D)
Centrifuge 5417R	Eppendorf, Hamburg (D)
Gel caster, Mighty small II	GE Healthcare Europe GmbH, Freiburg (D)
Growing cabinet, Rumed	Rubarth Apparate GmbH (D)
Heating block	Bioer, Hangzhow (CHN)
Homogeniser Precellys®24	PeQlab, Erlangen (D)
Incubator, Kelvitron®t	Thermo Scientific Heraeus®, Waltham (USA)
Incubation shaker, Multitron 28570	INFORS, Einsbach (D)
Light microscope B H-2	Olympus, Hamburg (D)
Micro pulser electroporator	Bio-Rad Laboratories GmbH, München (D)
Microtome Leica RM 2155	Leica Instruments GmbH, Nussloch (D)
Mixer mill MM400	Retsch, Haan (D)
pH meter inoLab pH Level 1	WTW GmbH, Weilheim (D)
Photometer, Specord 205	Analytik Jena, Jena (D)
Running chamber for gel electrophoresis	Cti, Idstein (D)
Sample concentrator	Techne (Bibby Scientific), Stone (UK)
Semi-dry transfer cell Trans-BLOT SD	Bio-Rad Laboratories GmbH, München (D)
Spectrophotometer Nanodrop 1000	PeQlab, Erlangen (D)
Sterile bench model 1.8	Holten Lamin Air, Allerød (DK)
Thermocycler Tpersonal	Biometra, Göttingen (D)
Ultracentrifuge Optima L 90K	Beckman Coulter, Krefeld (D)
UV-transilluminator DP-001 T1A	Vilber Lourmat GmbH, Eberhardzell (D)
Vortex Cetromat® MV	Braun Biotech, Melsungen (D)
Water purification system ELIX® 35	Mercck Millipore, Merck KGaA, Darmstadt (D)
6530 Accurate-mass quadrupole time-of-flight (Q-TOF) LC/MS	Agilent, Böblingen (D)
7890 Gas chromatograph (GC) with flame ionization detector (FID)	Agilent, Böblingen (D)
7890 Gas chromatograph (GC) with mass spectrometer (MS)	Agilent, Böblingen (D)

2.1.2 Consumables

Coverslips, 24 mm x 60 mm	Marienfeld, Lauda Königshofen (D)
Glass pipettes	Brand, Wertheim (D)
Glass tubes, 8 mL	Fisher Scientific, Schwerte (D)
Glass tubes, 8 mL with 40 GL thread	Agilent, Böblingen (D)
Glass vials and inlets for sample analysis	Agilent, Böblingen (D)
Microliter pipette tips type 3 series 1700	Labomedic, Bonn (D)

Microscope slides, 76 x 26 x 1 mm	Marienfeld, Lauda Königshofen (D)
Petri dishes 94 x 16 mm	Greiner bio-One, Frickenhausen (D)
Petri dishes 145 x 20 mm	Greiner bio-One, Frickenhausen (D)
Pots for plant cultivation, 10 cm	Pöppelmann, Lohne (D)
Reaction tubes, 1.5 mL and 2 mL	Sarstedt, Nümbrecht (D)
Reaction tubes, 15 mL and 50 mL	Greiner bio-One Frickenhausen (D)
Screw caps with GL 14 threads	Agilent, Böblingen (D)
Soil, type 'Pikier'	Gebrüder Patzer, Sinntal-Jossa (D)
SPE silica columns, Strata Si-1 1 mL	Phenomenex, Aschaffenburg (D)
Sterile filters, 0.2 µm pore size	Schleicher und Schuell, Dassel (D)
Syringe, 30 mL, Luer Lock Tip	TERUMO EUROPE N.V., Leuven (B)
Teflon septa for GL 14 screw caps	Schmidlin, Neuheim (CH)
Tays for plant cultivation	Pöppelmann, Lohne (D)
Vacuum driven sterilefilter, 500 mL, 0.22 µm	Merck Millipore , Massachusetts (USA)
Vermiculite, grain size 2-3 mm	Rolfs, Siegburg (D)

2.1.3 Chemicals

Acetic acid	AppliChem, Darmstadt (D)
Acetone	Prolabo VWR, Darmstadt (D)
Agarose	PeQlab, Erlangen (D)
Ammonium acetate	Sigma-Aldrich, Taufkirchen (D)
Ammonium sulfate	Sigma-Aldrich, Taufkirchen (D)
Bacto agar	Duchefa Biochemie, Haarlem (NL)
Bacto peptone	Duchefa Biochemie, Haarlem (NL)
Barium hydroxide	Riedel-de Haën (Honeywell), Seelze (D)
Betaine hydrochloride	Sigma-Aldrich, Taufkirchen (D)
Boric acid	Grüssing, Filsum (D)
Butylated hydroxytoluene	Sigma-Aldrich, Taufkirchen (D)
Cadmium carbonate	Sigma-Aldrich, Taufkirchen (D)
Calcium chloride	Merck, Darmstadt (D)
Chloroform	Merck, Darmstadt (D)
Diethylether	Prolabo VWR, Darmstadt (D)
Dipotassiumhydrogenphosphate	AppliChem, Darmstadt (D)
Ethanol 99 %, technical grade with 1 % MEK	Hofmann
Ethanol, p.A.	Merck, Darmstadt (D)
Ethidium bromide	Serva, Heidelberg (D)
Ethylenediaminetetraacetic acid (EDTA)	Roth, Karlsruhe (D)
Formaldehyde	AppliChem, Darmstadt (D)
Formic acid	VWR, Darmstadt (D)
Gelrite	Duchefa Biochemie, Haarlem (NL)
Glutaraldehyde	Sigma-Aldrich, Taufkirchen (D)
Glycerol	AppliChem, Darmstadt (D)
Hexane	Merck, Darmstadt (D)
Iron-ethylenediaminetetraacetic acid (Fe-EDTA)	Sigma-Aldrich, Taufkirchen (D)
Isopropanol	AppliChem, Darmstadt (D)
Magnesium chloride	AppliChem, Darmstadt (D)
Magnesium sulfate	Duchefa Biochemie, Haarlem (NL)
β-Mercaptoethanol	Sigma-Aldrich, Taufkirchen (D)
Methanol	J.T. Baker, Phillipsburg (USA)
Methanolic hydrochloric acid (3N)	Sigma-Aldrich, Taufkirchen (D)
Methylene chloride	AppliChem, Darmstadt (D)
Molybdenumtrioxide ammoniumtetrahydrate	Sigma-Aldrich, Taufkirchen (D)

N-methyl-N-(trimethylsilyl)-trifluoroacetamide	AppliChem, Darmstadt (D)
3-(N-morpholino)propanesulfonic acid (MOPS)	AppliChem, Darmstadt (D)
ortho-Phthaldialdehyde (OPA)	Sigma-Aldrich, Taufkirchen (D)
Phosphoric acid	AppliChem, Darmstadt (D)
Potassium chloride	Merck, Darmstadt (D)
Potassium dihydrogenphosphate	Merck, Darmstadt (D)
Potassium hydroxide	Merck, Darmstadt (D)
Potassium nitrate	Grüssing, Filsum (D)
Pyridine	AppliChem, Darmstadt (D)
Sodium chloride	Duchefa Biochemie, Haarlem (NL)
Sodium hypochlorite	Roth, Karlsruhe (D)
Sorbitol	Duchefa Biochemie, Haarlem (NL)
Sucrose	Duchefa Biochemie, Haarlem (NL)
Technovit 3040	Heraeus Kulzer GmbH, Werheim (D)
Technovit 7100	Heraeus Kulzer GmbH, Werheim (D)
Tetrahydrofuran	Merck, Darmstadt (D)
Thionyl chloride	Fluka, Sigma-Aldrich, Saint-Louis (USA)
Toluene	Prolabo VWR, Darmstadt (D)
Toluidine blue	Sigma-Aldrich, Taufkirchen (D)
Tricine	Sigma-Aldrich, Taufkirchen (D)
Tris-(hydroxymethyl)-aminomethane	Duchefa Biochemie, Haarlem (NL)
Trizol®	Life Technologies (Invitrogen), Darmstadt (D)
Tryptone	AppliChem, Darmstadt (D)
Yeast Extract	Duchefa Biochemie, Haarlem (NL)

2.1.4 Kits and Enzymes

First Strand cDNA Synthesis Kit	Fermentas, St. Leon-Rot (D)
MinElute Gel Extraction Kit	Quiagen, Hilden (D)
Plant Total RNA Mini Kit	DNA Cloning Service, Hamburg (D)
Omniscript RT Kit	Quiagen, Hilden (D)
SuperScript III First Strand Synthesis Kit	Life Technologies (Invitrogen), Darmstadt (D)
NucleoSpin Plasmid preps	Machery-Nagel, Düren (D)
High-Speed Plasmid Mini Kit	DNA cloning service e.K., Hamburg (D)
pGEM-T Easy vector systems	Promega, Madison (USA)
CloneJET PCR Cloning Kit	Thermo Fisher Scientific, Karlsruhe (D)
TURBO DNA-free™ Kit	Thermo Fisher Scientific, Karlsruhe (D)
T_4 DNA Ligase	Fermentas, St. Leon-Rot (D)
DCS DNA Polymerase	DNA cloning service e.K., Hamburg (D)
Taq DNA Polymerase	Fermentas, St. Leon-Rot (D)
Pfu DNA polymerase	Thermo Fisher Scientific, Karlsruhe (D)
Paq 5000 hotstart PCR Master Mix	Agilent, Böblingen (D)
Phire® Hot Start II DNA Polymerase	Thermo Fisher Scientific, Karlsruhe (D)
Glycerol-3-phosphate dehydrogenase	Sigma-Aldrich, Taufkirchen (D)
Lysozym	Sigma-Aldrich, Taufkirchen (D)

Restriction endonucleases, buffers and deoxyribonucleotide triphosphates (dNTPs) were ordered from Thermo Fisher Scientific and New England Biolabs. The GeneRulerTM 1 kb DNA Ladder was ordered from Thermo Fisher Scientific. Primers for PCR analysis were ordered from Integrated DNA Technologies (IDT). The peqGold Protein Marker III was purchased from PEQLAB Biotechnologie GmbH. For histidine tag (His-tag) detection, the 'His DetectorTMWesternBlot Kit' from Kirkegaard & Perry Laboratories (KPL), Inc. was used.

2.1.5 Plants, Bacteria, and Fungi

Arabidopsis thaliana Columbia 0	ABRC, Columbus, USA
Nicotiana benthamiana	
Agrobacterium tumefaciens	
GV3101	Koncz und Schell (1986) Genotype: pMP90 (pTiC58ΔT-DNA)
Escherichia coli	
XL1-Blue	Stratagene, Agilent, Böblingen (D)
BL21(DE3)pLys	Novagen (Merck KGaA), Madison (USA)
fadD	JB Ohlrogge
Saccharomyces cerevisiae	
INVSc1	Life Technologies (Invitrogen), Darmstadt (D)
BY4741	EUROSCARF, Johann Wolfgang Goethe-University Frankfurt, Institute for Molecular Biosciences (D)
gdeΔ1(YPL110c)in BY4741	EUROSCARF, Johann Wolfgang Goethe-University Frankfurt, Institute for Molecular Biosciences (D)

Table 2.1: Arabidopsis mutants alleles used in this study

Mutant	Mutant line	Ecotype	Origin
fatA1-2	WiscDcLox357F07	Columbia-0	Krysan et al., 1999; Sussman et al., 2000
fatA2-2	GABI_822B01	Columbia-0	GABI-Kat genome center
gdpd5-1	GABI_346F05	Columbia-0	GABI-Kat genome center
gdpd5-2	FLAG_354D01	Columbia-0	SGAP INRA center
gdpd6-1	SALK_133368	Columbia-0	NASC stock center
gdpd6-2	GABI_502F08	Columbia-0	GABI-Kat genome center

2.1.6 Internal Standards for Lipid Quantification with Q-TOF MS/MS

di14:0-PC	Avanti, Alabaster (USA)
di20:0-PC	Avanti, Alabaster (USA)
di14:0-PE	Avanti, Alabaster (USA)
di20:0-PE	Avanti, Alabaster (USA)
di14:0-PG	Avanti, Alabaster (USA)
di20:0-PG	Avanti, Alabaster (USA)
di14:0-PA	Avanti, Alabaster (USA)
di20:0-PA	Avanti, Alabaster (USA)
di14:0-PS	Avanti, Alabaster (USA)
PI (soybean)	Sigma
MGDG (spinach)	Larodan, Malmö (S)
DGDG (spinach)	Larodan, Malmö (S)
SQDG (spinach)	Larodan, Malmö (S)
di-14:0-DAG	Larodan, Malmö (S)
di-14:1-DAG	Larodan, Malmö (S)
di-20-DAG	Larodan, Malmö (S)
di-20:1DAG	Larodan, Malmö (S)
tri-10:0-TAG	Larodan, Malmö (S)
tri-20:0-TAG	Larodan, Malmö (S)
tri-22:1-TAG	Larodan, Malmö (S)

Plasmids used for subcloning of PCR products as well as expression vectors are listed in Table 2.2. All PCR products were ligated into the subcloning vectors with blunt ends or 3' T-overhangs. Recombinant plasmids containing the prefix 'pG' and 'pJ' are derived from pGEM-T and pJet1.2, respectively.

Table 2.2: cloning vectors

Stock number	Vector	Selection marker	Reference
-	pGEM-T	Amp^R	Promega
-	pUC18	Amp^R	Yanish-Perron, 1989
-	pJET1.2	Amp^R	Thermo Fisher Scientific
460	pQE-80L	Amp^R	Qiagen
45	pBinGlyRed2+*UcFatB*	Kan	Edgar Cahoon (Department of Biochemistry, University of Nebraska-Lincoln, Nebraska, USA)
427	pLnD1cM1-DsRed	Sm/Sp	G. Hölzl, unpublished
57	pBinGlyRed1-*PHE1*	Kan	A. Fatihi *et al*., 2013
58	pBinGlyRed1-*FIE*	Kan	A. Fatihi *et al*., 2013
255	DsRed-NDgd1-pLW01	Amp^R	B. Kalisch, unpublished
	pLMsyn	Sm/Sp	G. Hölzl, unpublished
	p35iGCSAt-2		G. Hölzl, unpublished
73	pDR196	Amp^R, URA3	Rentsch *et al*., 1995

Table 2.3: Recombinant plasmids - cloning of PCR-products into different subcloning vectors.

Insert	Primer: forw. rev.	Template	Notes	Recombinant plasmid
FatA1	bn460 bn461	cDNA	heterologous expression (full length)	pG-*FatA1*-*Bam*HI/*Kpn*I
FatA2	bn462 bn463	cDNA	heterologous expression (full length)	pG-*FatA2*-*Bam*HI/*Kpn*I
FatA1	bn887 bn461	cDNA	heterologous expression w/o transit peptide	pG-*FatA1*oTP-*Bam*HI/*Kpn*I
FatA2	bn888 bn463	cDNA	heterologous expression w/o transit peptide	pG-*FatA2*oTP-*Bam*HI/*Kpn*I
FatA1	bn433 bn 434	genomic DNA	sense orientation	pG-sense-*FatA1*-*Eco*RI/*Sal*I
FatA1	bn435 bn436	genomic DNA	antisense orientation	pG-asense-*FatA1*-*Pst*I/*Bam*HI
FatA1	bn670 bn671	cDNA	35S construct with DsRed	pJ-*FatA1*-*Bcu*I/*Sal*I
FatA2	bn672 bn673	cDNA	35S construct with DsRed	pJ-*FatA2*-*Bcu*I/*Sal*I
FatB	bn1162 bn1163	cDNA	35S construct with DsRed	pJ-*FatB*-*Bgl*II/*Sal*I

Table 2.3 (continued)

Insert	Primer: forw. rev.	Template	Notes	Recombinant plasmid
UcFatB	bn1740 bn1741	plasmid	35S construct with DsRed	pJ-*UcFatB*-*Bcu*I/*Sal*I
FatA1	bn1350 bn1366	plasmid	glycinin construct with DsRed	pJ-*FatA1*-*Mlu*I/*Sal*I
FatB	bn1160 bn1161	plasmid	glycinin construct with DsRed	pG-*FatB*-*Mlu*I/*Xho*I
CMV	bn1658 bn1659	plasmid	CMV construct with DsRed	pJ-*CMV*-*Spe*I/*Sfi*I
proFatA1	bn1721 bn1722	genomic DNA	native promoter for overexpression with DsRed	pJ-pro*FatA1*-*Sfi*I-a/*Nhe*I
GDPD5oTMD	bn1182 bn467	cDNA	Heterologous expression w/o transmembrane domain	pG-*GDPD5*oTMD-*Bam*HI/*Kpn*I
GDPD5oTMD	bn1181 bn465	cDNA	heterologous expression w/o transmembrane domain	pG-*GDPD6*oTMD-*Bam*HI/*Kpn*I
GDPD5oTMD	bn1212 bn1221	plasmid	DsRed fusion construct	pG-*GDPD5*oTMD-*Xho*I/*Ase*I
GDPD5oTMD	bn1210 bn1220	plasmid	DsRed fusion construct	pG-*GDPD6*-oTMD-*Xho*I/*Ase*I
GDPD5	bn676 bn677	cDNA	35S construct with DsRed	pJ-*GDPD5*- *Bcu*I/*Sal*I
GDPD6	bn674 bn675	cDNA	35S construct with DsRed	pJ-*GDPD6*- *Bcu*I/*Sal*I
e*GFP*	bn1280 bn1281	plasmid	eGFP with ATG and stop codon (TAA)	pJ-e*GFP*-*Bam*HI/*Sal*I
GDPD5	bn1278 bn1279	plasmid	GDPD5 (w/o stop codon) N-terminal fused to eGFP	pJ-*GDPD5*-w/o stop-*Spe*I/*Bam*HI
GDPD6	bn1276 bn1277	plasmid	GDPD6 (w/o stop codon) N-terminal fused to eGFP	pJ-*GDPD6*-w/o stop-*Spe*I/*Bam*HI
GDPD5	bn451 bn452	genomic DNA	sense orientation	pG-sense-*GDPD5*-*Eco*RI/*Sal*I
GDPD5	bn453 bn454	genomic DNA	antisense orientation	pG-asense-*GDPD5*-*Pst*I/*Bam*HI
GDPD6	bn1548 bn1737	Genomic DNA	Full genomic construct including 5'-utr and 3'-utr bn1548-*Sfi*I-a (GGCCATGGCGGCC) bn1737-*Sfi*I-b (GGCCCTTAAGGCC)	pJ-utr*GDPD6*utr-*Sfi*I-a/*Sfi*I-b

Table 2.4: Vectors used for transformation and expression.

Subcloning vector(s)	Release of insert(s)	Expression vector (fragment ends)	Recombinant plasmid
pG-*FatA1*-*Bam*HI/*Kpn*I	*Bam*HI/*Kpn*I	pQE-80L (*Bam*HI/*Kpn*I)	pQ-*FatA1*
pG-*FatA2*-*Bam*HI/*Kpn*I	*Bam*HI/*Kpn*I	pQE-80L (*Bam*HI/*Kpn*I)	pQ-*FatA2*
pG-*FatA1*oTP-*Bam*HI/*Kpn*I	*Bam*HI/*Kpn*I	pQE-80L (*Bam*HI/*Kpn*I)	pQ-*FatA1*oTP
pG-*FatA2*oTP-*Bam*HI/*Kpn*I	*Bam*HI/*Kpn*I	pQE-80L (*Bam*HI/*Kpn*I)	pQ-*FatA2*oTP
pG-asense-*FatA1*-*Pst*I/*Bam*HI pG-sense-*FatA1*-*Eco*RI/*Sal*I	*Pst*I/*Bam*HI *Eco*RI/*Sal*I *Pst*I/*Eco*RI	pLnD1cM1-DsRed (*Bam*HI/*Sal*I)	pL-35S::RNAi-*FatA1*-DsRed
p35iGCSAt-2 pJ-*FatA1*-*Bcu*I/*Sal*I	*Bcu*I/*Sal*I	pL-35S::RNAi-*FatA1*-DsRed (*Bcu*I/*Sal*I)	pL-35S::*FatA1*-DsRed
pJ-*FatA2*-*Bcu*I/*Sal*I	*Bcu*I/*Sal*I	pL-35S::RNAi-*FatA1*-DsRed (*Bcu*I/*Sal*I)	pL-35S::*FatA2*-DsRed
pJ-*FatB*-*Bgl*II/*Sal*I	*Bgl*II/*Sal*I	pL-35S::RNAi-*FatA1*-DsRed (*Bam*HI/*Sal*I)	pL-35S::*FatB*-DsRed
pJ-UcFatB-*Sal*I/*Bcu*I	*Sal*I/*Bcu*I	pL-35S::*FatA1*-DsRed (*Sal*I/*Bcu*I)	pL-35S::*UcFatB*-DsRed
pJ-FatA1-*Mlu*I/*Sal*I	*Mlu*I/*Sal*I	pBinGlyRed1-*PHE1* (*Mlu*I/*Xho*I)	pBin-gly::*FatA1*-DsRed
pG-FatB-*Mlu*I/*Xho*I	*Mlu*I/*Xho*I	pBinGlyRed1-*PHE1* (*Mlu*I/*Xho*I)	pBin-gly::*FatB*-DsRed
pBinGlyRed2+*UcFatB*	XhoI/EcoRI	pBinGlyRed1-*FIE* (*Xho*I/*Eco*RI)	pBin-gly::*UcFatB*
pJ-*CMV Spe*I/*Sfi*I	*Spe*I/*Sfi*I	pL-*35S::FatA1*-DsRed (*Spe*I/*Sfi*I)	pL-*CMV::FatA1*-DsRed
pJ-pro*FatA1 Sfi*I-a/*Nhe*I	*Sfi*I/*Nhe*I	pL-*35S::FatA1*-DsRed (*Spe*I/*Sfi*I)	pL-pro*FatA1::FatA1*-DsRed
pJ-pro*FatA1 Sfi*I-a/*Nhe*I	*Sfi*I/*Nhe*I	pL-*35S::FatB*-DsRed (*Spe*I/*Sfi*I)	pL-pro*FtaA1::FatB*-DsRed
pJ-pro*FatA1 Sfi*I-a/*Nhe*I	*Sfi*I/*Nhe*I	pL-*35S::UcFatB*-DsRed (*Spe*I/*Sfi*I)	pL-pro*FatA1::UcFatB*-DsRed
pG-*GDPD5*oTMD *Bam*HI/*Kpn*I	*Bam*HI/*Kpn*I	pQE-80L (*Bam*HI/*Kpn*I)	pQ-*GDPD5*oTMD

Table 2.4 (continued)

Subcloning vector(s)	Release of insert(s)	Expression vector (fragment ends)	Recombinant plasmid
pG-*GDPD6*oTMD *Bam*HI/*Kpn*I	*Bam*HI/*Kpn*I	pQE-80L (*Bam*HI/*Kpn*I)	pQ-*GDPD6*oTMD
pG-*GDPD5*oTMD *Xho*I/*Ase*I	*Xho*I/*Ase*I	DsRed-NDgd1-pLW01 (*Nde*I/*Xho*I)	pLW01-*DsRed::GDPD5*oTMD
pG-*GDPD6*-oTMD *Xho*I/*Ase*I	*Xho*I/*Ase*I	DsRed-NDgd1-pLW01 (*Nde*I/*Xho*I)	pLW01-*DsRed::GDPD6*oTMD
pJ-*GDPD5*- *Bcu*I/*Sal*I	*Bcu*I/*Sal*I	pL-*35S::GDPD5*-RNAi-DsRed (*Bcu*I/*Sal*I)	pL-*35S::GDPD5*-DsRed
pJ-*GDPD6*- *Bcu*I/*Sal*I	*Bcu*I/*Sal*I	pL-*35S::GDPD5*-RNAi-DsRed (*Bcu*I/*Sal*I)	pL-*35S::GDPD6*-DsRed
pJ-*GDPD5*- *Bcu*I/*Sal*I	*Bcu*I/*Sal*I	pDR196 (*Bcu*I/*Sal*I)	pDRGDPD5
pJ-*GDPD6*- *Bcu*I/*Sal*I	*Bcu*I/*Sal*I	pDR196 (*Bcu*I/*Sal*I)	pDRGDPD6
pJ-*GDPD5*-w/o stop-*Bcu*I/*Bam*HI	*Bcu*I/*Bam*HI	pL-*GDPD6::eGFP* (*Bcu*I/*Sal*I)	pL-*GDPD5::eGFP*
pJ-e*GFP*-*Bam*HI/*Sal*I	*Bam*HI/*Sal*I *Bcu*I/*Bam*HI	pLMsyn (*Bcu*I/*Sal*I)	pL-*GDPD6::eGFP*
pJ-*GDPD*6-w/o stop-*Bcu*I/*Bam*HI			
pG-asense-*GDPD5*-*Pst*I/*Bam*HI	*Pst*I/*Bam*HI *Eco*RI/*Sal*I	pLnD1cM1-DsRed (*Bam*HI/*Sal*I)	pL-*35S::GDPD5*-RNAi-DsRed
pG-sense-*GDPD5*-*Eco*RI/*Sal*I	*Pst*I/*Eco*RI		
p35iGCSAt-2 pJ-utr*GDPD6*utr	*Sfi*I	pL-*35S::GDPD6*-DsRed	pL-utr*GDPD6*utr-DsRed

2.2 Methods

2.2.1 Techniques in Molecular Biology

2.2.1.1 Isolation of Genomic DNA from Arabidopsis Leaves

For genomic DNA extraction, fresh Arabidopsis leaf material was harvested and transferred into a 1.5 mL microcentrifuge tube containing five small ceramic beads. 1 mL CTAB extraction buffer was added and the leaves were immediately homogenized in the Precellys homogenizer at 6500 rpm for 45 sec. The tubes were incubated at 65 °C under vigorous shaking for 10 min. Subsequently, 400 µL chloroform was added to the sample and mixed thoroughly by vortexing. Phase separation was achieved by centrifugation at 1000 *x g* for 5 min. After transferring the aqueous phase (upper phase) into a fresh microcentrifuge tube, 700 µL ice-cold isopropanol was added and mixed by inverting the tubes ten times. The samples were placed at -20 °C for 10 minutes to precipitate the DNA. After centrifugation for 5 min at 10000 *x g* the DNA pellet was washed with 70 % (v/v) ethanol and centrifuged again for 3 min at 10000 *x g*. The supernatant was discarded and the DNA was almost completely dried. The DNA was resuspended in 50 µL ddH_2O containing 0.5 µL of RNaseA (10 µg/mL). Samples were incubated at room temperature (RT) for 15 min before analyzing quality and quantity of the isolated DNA using a spectrophotometer (NanoDrop) and stored at -20 °C.

CTAB extraction buffer

140 mM	Sorbitol
220 mM	Tris-HCl, pH 8
22 mM	EDTA
800 mM	NaCl
1 % (w/v)	Sarkosyl N-lauroylsarcosine
0.8 % (w/v)	CTAB

2.2.1.2 Polymerase Chain Reaction (PCR)

DNA fragments were amplified by polymerase chain reaction (PCR). PCR consists of three steps, denaturation of the double stranded DNA by heating to 94 °C, annealing of the primers (Integrated DNA Technologies (IDT)), and elongation of the sequence of interest by the heat stable *Taq* DNA polymerase. This cycle was repeated 25-40 times (Table 2.5). DNA fragments designated for cloning were amplified with the proof reading *Pfu* DNA polymerase, to minimize the error rate.

PCR reaction mixture

2.5 µL	10 x PCR buffer
0.75 µL	50 mM $MgCl_2$
0.5 µL	10 mM dNTP-mix (10 mM of each)
2.5 µL	Forward primer 10 pmol/µL
2.5 µL	Reverse primer 10 pmol/µL
10-500 ng	Template DNA
0.5 µL	DNA polymerase (5 units/µL)
ad 25 µL	ddH_2O

Total volume: 25 µL

For correct primer binding, the annealing temperature (T_a) had to be adjusted with respect to the length and nucleotide composition of the primers. T_a depends on the melting temperature (T_m) of the primers. In general T_a is 4 °C below the lowest T_m of the primers used. T_m was determined by adding 4 °C for each G and C nucleotide and 2 °C for T and A in the primer sequence.

Table 2.5: Standard PCR program

Temperature	Time	Cycle step	Cycle number
95 °C	3-5 min	Initial denaturation	1
94 °C	45 sec	Denaturation	
Tm – 4 °C	45 sec	Annealing	
72 °C	1 min/kb (*Taq*) 2 min/kb (*Pfu*)	Elongation	25-40
72 °C	10 min	Final extension	1
4 – 15 °C	Hold	Hold storage	-

2.2.1.3 PCR-Analysis of Arabidopsis T-DNA Insertion Mutants

Arabidopsis plants carrying T-DNA insertions were screened by PCR analysis, to identify mutant lines homozygous for the gene of interest. For this purpose one T-DNA primer (LBb1) and a locus specific primer (LP or RP) were used. Primers binding within the T-DNA insertion were chosen according to supplier's suggestion. Touchdown (TD) PCR was used for analysis. TD-PCR employs an initial annealing temperature above the calculated melting temperature of the primers. Then, the annealing temperature is progressively lowered to a more permissive temperature within successive cycles. This PCR method is particularly useful for templates that are difficult to amplify and was used to enhance specificity for screening T-DNA insertion lines (Table 2.6).

Table 2.6: Touchdown PCR program

Temperature	Time	Cycle step	Cycle number
95 °C	3-5 min	Initial denaturation	1
94 °C	45 sec	Denaturation	
Tm + 10 °C	45 sec	Annealing	10
72 °C	1 min/kb (*Taq*)	Elongation	
94 °C	45 sec	Denaturation	
Tm °C	45 sec	Annealing	15
72 °C	1 min/kb (*Taq*)	Elongation	
94 °C	45 sec	Denaturation	
Tm -10 °C	45 sec	Annealing	15
72 °C	1 min/kb (*Taq*)	Elongation	
72 °C	10 min	Final extension	1
4 – 15 °C	Hold	Hold storage	-

PCR analysis from Arabidoposis embryo tissue was performed using the Phire® Hot Start II DNA Polymerase (Thermo Fisher Scientific), which allows for the direct analysis of plant tissue without the need of a prior DNA extraction. The Phire® Hot Start II DNA Polymerase is specially engineered to contain a DNA-binding domain that enhances the processivity of the polymerase. It also exhibits extremely high resistance to many PCR inhibitors found in plants. For PCR reaction, the embryo was dissected from the surrounding endosperm and testa and placed into 8 µL of 1x TE buffer (pH 8.0). Samples were crushed with a pipette tip and incubated for 3 min at 50 °C. After brief centrifugation, 2 µL of the supernatant was used as a template in 20 µL PCR reaction.

Table 2.7: Touchdown PCR program for amplification of DNA from Arabidopsis embryo tissue using Phire HotStart Polymerase (Thermo Fisher Scientific).

Temperature	Time	Cycle step	Cycle number
98 °C	5 min	Initial denaturation	1
98 °C	5 sec	Denaturation	
65 °C	5 sec	Annealing	10
72 °C	20 sec/ 1 kb	Elongation	
98 °C	5 sec	Denaturation	
55 °C	5 sec	Annealing	20
72 °C	20 sec/ 1 kb	Elongation	
98 °C	5 sec	Denaturation	
45 °C	5 sec	Annealing	10
72 °C	20 sec/ 1 kb	Elongation	
72 °C	1 min	Final extension	1
4 – 15 °C	Hold	Hold storage	-

2.2.1.4 Colony-PCR

For colony PCR, a single *E. coli* colony was used as template. Plasmid DNA becomes accessible for PCR amplification because the cell wall and plasma membrane are disrupted by the initial denaturating step (Fuchs and Podda, 2005). The colony PCR was used to detect cloned fragments in vectors after ligation. Each colony chosen for colony PCR was transferred to a new LB plate containing the corresponding antibiotics before addition to the PCR reaction mixture. The PCR reaction mixture was set up as described, except that no extra DNA template was added. Colonies were analyzed using the normal PCR program and PCR products separated by agarose gel electrophoresis. Primers were chosen that amplify the insert plus flanking regions.

2.2.1.5 DNA Agarose Gel Electrophoresis

Agarose gel electrophoresis was employed for the analysis of PCR products and restriction enzyme fragments. Gels containing 1 % (w/v) of agarose in 1 x TAE buffer were used for the separation of DNA fragments. Ethidium bromide (EtBr) was added to the melted gel to a final concentration of 5 μg/mL prior to pouring. DNA samples were mixed with 1/5 volume of 6x loading dye. To estimate fragment size, the GeneRuler 1kb DNA ladder (Thermo Fisher Scientific) was used as molecular weight standard. DNA fragments were separated by applying an electric voltage of 100-120 V until the desired separation was achieved. EtBr DNA complexes were visualized under an UV transilluminator at 312 nm.

TAE buffer (5x)

200 mM	Tris base
200 mM	Glacial acetic acid
5 mM	EDTA, pH 8.0

Ethidium bromide stock solution 10 mg/mL (in deionized water)

6x Gel-loading buffer

10 mM	Tris-HCl, pH 7.6
60 % (v/v)	Glycerol
60 mM	EDTA (pH 8.0)
0.03 % (w/v)	Bromophenol blue

2.2.1.6 Purification of PCR Products and Restriction Fragments

Purification of PCR products after agarose gel electrophoresis was performed with a PCR clean-up Kit (DNA Cloning Service) according to the supplier's instructions. The purified DNA was stored at -20 °C or directly used.

2.2.1.7 Sequencing

Highly purified DNA was employed in order to obtain reasonable sequencing results. To this end, plasmid DNA was isolated using the plasmid extraction kit (DNA Cloning Service) and PCR products were purified from agarose gels as described above. Samples should have a minimum concentration of 100 ng/µL for plasmid DNA or 10 ng/µL for PCR products. Samples were prepared following the instructions and sent to LGC Genomics in Berlin. Sequencing results were assembled using the Laser Gene software (DNAStar).

2.2.1.8 RNA Extraction from Arabidopsis

Arabidopsis total RNA was extracted according to Chomczynski and Sacchi (1987). 50-100 mg of leaf material was harvested and transferred into a 2 mL microcentrifuge tube, containing two metal beads and immediately frozen in liquid nitrogen. The tissue was ground to a fine powder in the Mixer Mill homogenizer (Retsch) for 30 sec at 3000 rpm and subsequently stored in liquid nitrogen. 1 mL Trizol (Invitrogen) was added and the sample was incubated for 5 min at RT. 200 µL chloroform was added and vortexed thoroughly, before incubation for 3 min at RT. Phase separation was achieved by centrifugation for 15 min at 20000 *x g* at 4 °C. 500 µL of the aqueous upper phase was transferred to a fresh 1.5 mL microcentrifuge tube and precipitated with equal volumes of isopropanol for 10 min at RT. RNA was collectedd by centrifugation for 10 min at 20000 *x g* at 4 °C. The pellet was washed with 70 % (v/v) ethanol and again centrifuged at 20000 *x g* for 5 min at 4 °C. The pellet was air dried before resuspension in 30 µL nuclease free ddH_2O. The concentration was determined by absorbance measurement with the photometer (NanoDrop) and RNA was stored at -80 °C.

2.2.1.9 Quantification of Nucleic Acids

Nucleic acids were quantified spectrophotometrically (NanoDrop). Absorbance was measured at 260 nm (A_{260}) and 280 nm (A_{280}). An optical density of 1 corresponded to a concentration of 50 µg/mL double stranded DNA or 40 µg/mL of single stranded RNA. The ratio of the absorbance at 260 and 180 nm (A_{260}/A_{280}) was used to assess the purity of isolated nucleic acids. A DNA sample of high purity had a (A_{260}/A_{280}) ratio around 1.8 whereas it was around 2 for pure RNA.

2.2.1.10 RNA Gel Electrophoresis

RNA quality was confirmed using the NanoDrop photometer or by RNA gel electrophoresis. For cDNA synthesis, the amount of RNA had to be estimated by gel electrophoresis. For preparation of the formaldehyde gel, agarose was mixed with ddH_2O and heated in the microwave oven until the agarose was melted. After adding 10 x MOPS buffer the

mixture was cooled at RT for 5 min. Subsequently, the formaldehyde was added and the gel was immediately poured. When the gel was solidified after approximately 30 min, it was transferred into a gel chamber filled with RNA running buffer and formaldehyde.

1-3 µg of RNA were mixed with DEPC treated water to a final volume of 10 µL. This mixture was added to the same amount of RNA sample buffer and incubated at 65 °C for 10 min. After cooling on ice for 2 min, the RNA was loaded into the slots and separated in the formaldehyde gel by applying a voltage of 90 V for approximately 30 min. RNA was detected under UV light (λ=302 nm).

2.2.1.11 First Strand cDNA Synthesis and Reverse Transcription PCR (RT-PCR)

To analyze the gene expression level, semi-quantitative RT-PCR was employed. To this end, mRNA was isolated from different tissues and transcribed into cDNA using a first strand cDNA synthesis kit (Thermo Fisher Scientific or Invitrogen). RNA quality was determined spectrophotometrically (NanoDrop) and by formaldehyde gel electrophoresis. RNA gel electrophoresis was repeated until all samples showed ribosomal bands of comparable intensity. The RNA concentration estimated by these gels was subsequently used to calculate the amount of RNA for cDNA synthesis. cDNA was synthesized according to the supplier's instructions (Thermo Fisher Scientific or Invitrogen). Total RNA was reverse transcribed by Superscript II Reverse Transcriptase using oligo dT primers. To remove remaining RNA after cDNA synthesis, 1 µL of RNAse H was added and the sample was incubated at 37 °C for 20 min. cDNA was stored at -80 °C or directly used for subsequent PCR reaction.

RT-PCR was carried out with *Taq* polymerase using the standard PCR program described above. Gene specific primers for *FatA1*, *FatA2*, *GDPD5*, *GDPD6*, and for the housekeeping gene *actin* were used. DNA was amplified by 25 to 32 PCR cycles before analysis via agarose gel electrophoresis and EtBr staining. Signal intensities of the PCR products were compared for the estimation of gene expression levels.

RNA sample buffer

65 % (v/v)	Formamide
8 % (v/v)	Formaldehyde
1.3 %	1x MOPS, pH 8
54 µg/mL	EtBr

10 x MOPS buffer

0.2 M	MOPS
50 mM	Sodium acetate
10 mM	Na-EDTA

adjusted to pH 7 - pH 8 with NaOH

1.5 % (w/v) agarose gel

1.5 % (w/v)	Agarose
6 % (v/v)	Sodium acetate

in 1x MOPS, pH 8

RNA running buffer

10 % (v/v)	Formaldehyde

in 1x MOPS, pH 8

2.2.1.12 Enzymatic Modification Restriction Enzyme Digestion

Plasmid DNA was cleaved by restriction enzyme digestion, separated by agarose gel electrophoresis, gel purified and stored at -20 °C or directly processed.

A-tailing of Blunt-ended PCR Fragments

PCR products generated by *Pfu* polymerase enzyme have blunt ends due to 3'-5' exonuclease activity of the *Pfu* polymerase. An A nucleotide was added to the 3' end of the gel purified PCR product using dATP and *Taq* polymerase in order to enable TA-cloning into the pGEM-T- vector.

Template	16 µL
10 x buffer	2 µL
Taq polymerase	0.3 µL (2U/µL)
dATP	2 µL (0.2 mM final concentration)

After incubation for 15 min at 72 °C, *Taq* polymerase was inactivated by desalting the reaction mixture via dialysis on a microfilter.

Ligation

T4 DNA ligase, originating from the bacteriophage T4, catalyses the ligation of cohesive or blunt DNA ends by an ATP and Mg^{2+} dependent reaction. For optimal ligation efficiency the ratio of vector to insert should be 1:3 to 1:5. The concentration of vector to insert was determined by agarose gel electrophoresis containing EtBr. Vector and insert were loaded onto an agarose gel and the gel run briefly. Subsequently, the fluorescence of the vector and insert bands were compared and the DNA amounts calculated using the online gibthon ligation calculator tool (http://django.gibthon.org/tools/ligcalc/). A second possibility to determine the concentration of vector and insert was the absorbance measurement with the NanoDrop photometer. Calculation was performed as described above. A ligation reaction of 10 µL final volume was set

up by mixing the calculated amount of vector and insert with 1 µL 10 x ligation buffer containing ATP, and 0.2 to 0.5 µL T4 DNA ligase (10 U/µL). After adding ddH_2O to a final volume of 10 µL the reaction mixture was incubated for 30 min at RT or at 4 °C overnight. For subsequent transformation of *E. coli* by electroporation, the ligation mixture was desalted via dialysis on a microfilter.

2.2.2 *Saccharomyces cerevisiae* Techniques

2.2.2.1 Cultivation of *S. cerevisiae*

The cultivation of *S. cerevisiae* was carried out in liquid or agar-solidified CMdum medium (Ausubel et al., 1995) or complete YPD medium at 30 °C. To provide sufficient ventilation liquid cultures were shaken at 180-200 rpm. For selection of plasmid containing clones the cells were cultivated on agar-solidified selective medium depleted in uracil.

Dropout Powder

2.5 g	Adenine (hemisulfate)
1.2 g	L-arginine
6.0 g	L-aspartate
6.0 g	L-glutamate (sodium-salt)
1.8 g	L-lysine (HCl)
1.2 g	L-methionine
3.0 g	L-phenylalanine
22.5 g	L-serine
12.0 g	L-threonine
1.8 g	L-tyrosine
9.0 g	L-valine

(mixture was ground to a fine powder)

CMdum

1.16 g/L	Dropout powder
2 % (w/v)	Bacto-agar (Difco)
2 % (w/v)	Glucose
0.67 % (w/v)	YNB (yeast nitrogen base with ammonium Sulfate, without amino acids)
20 mg/L	Histidine
60 mg/L	Leucine
40 mg/L	Tryptophane
20 mg/L	Uracil

2.2.2.2 Generation and Transformation of Electrocompetent *S. cerevisiae* Cells

To generate electrocompetent *S. cerevisiae* cells, 2 mL YPD-media was inoculated overnight. Subsequently 500 mL YPD-medium containing 10 % (v/v) glycerol was inoculated

with 5 mL of the overnight culture and grown to an OD_{600} of 1.3-1.5 at 30 °C. To provide sufficient ventilation the culture was shaken at 180-200 rpm. The cells were centrifuged at 4000 *x g* for 10 min at 4 °C. After discarding the supernantant the cells were resuspended in 500 mL ice cold 1 mM ddH_2O. The centrifugation and the following wash step were repeated two times and the cells were eventually suspended in 20 mL ice cold sterile 1 M sorbitol and again centrifuged. The cells were resuspended in 0.5-1.0 mL 1 M sorbitol + 10 % (v/v) glycerol. Aliquots of 65 µL were shock-frozen in liquid nitrogen and stored at -80 °C.

For transformation of electrocompetent *S. cerevisiae* cells an aliquot was thawed on ice. Either 10 µL desalted ligation mixture or 1-2.5 µL plasmid DNA was added and the mixture was incubated on ice for 5 min. The cells were transferred to a pre-cooled 1 mm electroporation cuvette and an electric field pulse of 750 V was applied. The transformed cell were eluted in 800 µL ice cold 1 M sorbitol and kept on ice for 2 min. After centrifugation at 3000 *x g* the supernatant was discarded and the cells were eluted in 1 M sorbitol + 10 % (v/v) glycerol and plated out on agar-solidified selection medium. The cells were incubated for 2 days at 30 °C.

2.2.2.3 Functional Expression in *S. cerevisiae*

For the characterization of the enzymatic properties of the putative glycerophsophosdiester phosphodiesterases (GDPD) from Arabidopsis functional expression in *S. cerevisiae* INVSc1 cells was done. For this reason the pDR196-vector from Invitrogen (Hilden) was used. The different *S. cerevisiae* strains harboring the different putative *GDPD* genes were grown under the same conditions. In order to express a recombinant protein a 2 mL *S. cerevisiae* overnight culture was used to inoculate cMdum medium lacking uracil. Cell cultures were incubated to an OD_{600} at 2. The cells were collected by centrifugation at 4000 *x g* for 10 min. However, heterologous expression in *S. cerevisiae* INVSc1 did not lead to the expression of a functional protein (data not shown).

2.2.2.4 Complementation of *GDE1* in *S. cerevisiae*

For complementation of the *gde1*Δ loss-of-function mutant the yeast expression constructs pDRGDPD5 and pDRGDPD6 were introduced in competent *gde1*Δ *S. cerevisiae* cells. Strains were controlled by PCR analysis to verify integration. Strains harboring the expression constructs were pre-grown for several hours in medium lacking a Pi source (CMdum -P). Cells were harvested and suspended to equivalent cell densities of OD_{600} at 2 in sterile ddH_2O. Four 10-fold serial dilutions were made for each cell suspension. 5 µL of each cell suspension were spotted onto plates containing either no source of phosphate (-Pi), 200 µM KH_2PO_4, or 200 µM GPC. The plates were incubated for several days at 28 °C.

CMdum -P

1.16 g/L	Dropout powder
2% (w/v)	Bacto-agar (Difco)
2% (w/v)	Glucose
0.67% (w/v)	YNB (yeast nitrogen base with ammonium sulfate, lacking amino acids and any source of phosphate) (Formedium)
20 mg/L	Histidine
60 mg/L	Leucine
40 mg/L	Tryptophane
20 mg/L	Uracil

2.2.3 *Escherichia coli* Techniques

2.2.3.1 Cultivation of *E. coli*

E. coli were grown described by Sambrook (Sambrook et al., 1989) in liquid or agar-solidified LB media at 37 °C. To provide sufficient ventilation liquid cultures were shaken at 180 -200 rpm. For selection of plasmid containing clones, appropriate antibiotics were added to the cultures (Table 2.8). The antibiotics were stored as filter sterilized stock solutions at -20 °C.

Table 2.8 Used antibiotics for the selection of plasmid containing clones.

Antibiotics	Stock solution	Final concentration
Ampicillin (Amp)	100 mg/mL	100 µg/mL
Kanamycin (Kan)	50 mg/mL	25 µg/mL
Streptomycin (Strep)	25 mg/mL	25 µg/mL
Spectinomycin (Spec)	25 mg/mL	25 µg/mL

LB Medium	LB Broth (Duchefa)	2% (w/v), consisting of 1% (w/v) Trypton, 0.5% (w/v) Yeast Extract and 0.5% (w/v) NaCl
	Bacto Agar (Difco)	1.5% (w/v)
		The pH was adjusted to 7.5 before autoclaving.

Glycerol stocks were made with 0.5 mL of an *E. coli* overnight culture mixed with 0.5 mL 70 % (v/v) sterile glycerol and stored at -80 °C.

2.2.3.2 Generation and Transformation of Chemically Competent *E. coli* Cells

To generate chemically competent *E. coli* cells, 2 mL SOB-medium were inoculated and the cells grown overnight. Subsequently, 200 mL SOB-medium were inoculated with 1 mL of the overnight culture and grown to an OD_{600} of 0.5 at 37 °C. To provide sufficient ventilation the culture was shaken at 180 - 200 rpm. The cells were incubated on ice for 10 min before they were centrifuged at 4000 *x g* for 10 min at 4 °C. The cells were resuspended in 80 mL ice cold TB buffer and incubated on ice for 10 min. The cells were centrifuged again at 4000 *x g* for 10 min at 4 °C and resuspended in 8 mL TB buffer with 7% (v/v) DMSO. Subsequently, the cells were incubated on ice for 10 min and aliquots of 200 µL were shock-frozen in liquid nitrogen and stored at -80 °C.

SOB Medium

2% (w/v)	Bacto-Peptone (Difco)
0.5% (w/v)	Yeast Extract (Difco)
10 mM	NaCl
2.5 mM	KCl

$MgSO_4$ and $MgCl_2$ were added as filter sterilized solutions after autoclaving.

10 mM	$MgSO_4$
10 mM	$MgCl_2$

TB buffer

10 mM	PIPES	Adjust pH to 6.7 with KOH, filter sterilized and stored at 4 °C
55 mM	$MnCl_2$	
15 mM	$CaCl_2$	
250 mM	KCl	

For the transformation of chemically competent *E. coli* cells, an aliquot of the cells was thawed on ice. 10 µL ligation mixture or 1 µL plasmid DNA was added and the mixture was incubated on ice for 20 minutes. Subsequently, a heat shock at 42 °C was applied for 60 second followed by a 2 min incubation on ice. The cells were resuspended in 800 µL ice cold LB medium without antibiotics and allowed to regenerate at 37 °C for 40 min. After regeneration the cells were plated out on agar-solidified LB medium containing the appropriate antibiotics and incubated overnight at 37 °C.

2.2.3.3 Generation and Transformation of Electrocompetent *E. coli* Cells

To generate electrocompetent *E. coli* cells 2 mL SOB medium was inoculated and the cells grown overnight. Subsequently 200 mL SOB-medium was inoculated with 1 mL of the overnight culture and grown to an OD_{600} of 0.5 at 37 °C. To provide sufficient ventilation the culture was shaken at 180-200 rpm. The cells were incubated on ice for 30 min before they were centrifuged

at 4000 *x g* for 10 min at 4 °C. After discarding the supernatant the cells were resuspended in 400 mL ice cold 1 mM HEPES and incubated on ice for 10 min. The centrifugation and the following wash step were repeated three times and the cells were finally suspended in 2 mL ice cold sterile 10 % (v/v) glycerol. Aliquots of 50 µL were shock-frozen in liquid nitrogen and stored at -80 °C.

For transformation of electrocompetent *E. coli* cells, an aliquot of the cells was thawed on ice. 10 µL ligation mixture or 1 µL plasmid DNA was added and the mixture was incubated on ice for 5 min. The cells were transferred to a pre-cooled 1 mm electroporation cuvette and an electric field pulse of 1250 V was applied. The transformed cells were immediately transferred into 800 µL ice cold LB medium without antibiotics and kept on ice for 2 min. The cells were allowed to regenerate at 37 °C for 40 min and plated out on agar-solidified LB medium containing the appropriate antibiotic. The cells were grown overnight at 37 °C.

2.2.3.4 Isolation of Plasmid DNA from *E. coli*

The isolation of plasmid DNA from *E. coli* was performed with a plasmid preparation kit (High-Speed Plasmid Mini Kit, DNA Cloning Service) according to the supplier's instruction or via a modified method by Riggs & McLachlan (Riggs and McLachlan, 1986).

The isolation of plasmid DNA from *E. coli* by Riggs & McLachlan (Riggs and McLachlan, 1986) was performed by collecting the cells of a 2 mL *E. coli* overnight culture by centrifugation at 14000 *x g* for 1 min. The pellet was resuspended in 200 µL BF buffer with 10 µL 20 mg/mL lysozyme and incubated at RT for 1 min. The cells were incubated at 95 °C for 1 min and cell debris and genomic DNA were removed by centrifugation at 14000 *x g* for 20 min. The supernatant was transferred to a clean microcentrifuge tube and 400 µL IS mix was added. After inverting, the cells were incubated at -20 °C for 10 min to precipitate the plasmids. Plasmid DNA was collected by centrifugation at 14000 *x g* for 10 min. The precipitated plasmid DNA was washed with 75 % (v/v) ethanol and again centrifuged at 14000 *x g* for 5 min. The plasmid DNA was dried at 45 °C in the thermo block. The dried plasmids were dissolved in 100 µL ddH_2O with 1 µL RNAse A 10 mg/mL RNAse A in ddH_2O and stored at -20 °C.

BF Buffer

8 % (w/v)	sucrose
0.5 % (w/v)	Triton X-100
50 mM	EDTA, pH 8.0
10 mM	Tris-HCl, pH 8.0

Lysozyme solution

20 mg/mL	lysozyme

IS mix

400 µl	isopropanol
80 µL of a 5 M stock solution	ammonium acetate

2.2.3.5 Recombinant Protein Expression in *E. coli*

For the characterization of the enzymatic properties of the putative GDPDs and acyl-ACP thioesterases A (FatA1, FatA2) from Arabidopsis, the proteins were expressed in *E. coli* XL1-Blue or BL21(DE3)pLys cells. To this end, the pQE-vector system from Qiagen (Hilden, DE) was used. The different *E. coli* strains harboring the different putative *GDPD* or *FatA* cDNAs were grown in liquid LB medium. 2 mL of an *E. coli* overnight culture was used to inoculate a fresh culture of 50 mL LB medium containing the appropriate antibiotics. This culture was grown to an OD_{600} of 0.6 and protein expression was induced by adding 1 mM IPTG. The culture was further incubated at 16 °C, 28 °C, or 37 °C. Incubation at low temperatures was done to ensure correct folding of the recombinant proteins. For heterologous expression of *FatA1* and *FatA2* containing cells, cultures were incubated at 37 °C, and for *GDPD5* and *GDPD6* containing cells, cultures were incubated at 28 °C after induction with IPTG. Because no activity of the recombinant protein for *GDPD5* and *GDPD6* could be obtained at 28 °C, cells were incubated at 16 °C overnight. After 4 to 6 h of incubation at 28-37 °C or 12 h at 16 °C the cultures reached a density of OD_{600} of 1.2 to 1.5, and the cells were collected by centrifugation at 4000 *x g* for 10 min.

2.2.4 *Agrobacterium tumefaciens* Techniques

2.2.4.1 Cultivation of *A. tumefaciens*

The cultivation of *A. tumefaciens* was carried out in liquid or agar-solidified YEP-medium containing rifampicin at 28 °C. To provide sufficient ventilation liquid cultures were shaken at 180-200 rpm. For selection of plasmid containing clones appropriate antibiotics were added to the cultures (Table 2.9). The antibiotics were stored as filter sterilized stock solutions at -20 °C.

Table 2.9 Used antibiotics for the selection of plasmid containing clones.

Antibiotics	Stock solution	Final concentration
Rifampicin	20 mg/mL	80 µg/mL
Kanamycin (Kan)	50 mg/mL	50 µg/mL
Streptomycin (Strep)	300 mg/mL	300 µg/mL
Spectinomycin (Spec)	100 mg/mL	100 µg/mL

YEP medium

10 g	BD Bacto Peptone
10 g	Yeast Extract (Duchefa)
0.5% (w/v)	NaCl

2.2.4.2 Generation and Transformation of Electrocompetent Cells

To generate electrocompetent *A. tumefaciens* cells 5 mL YEP medium was inoculated and the cells were grown overnight. Subsequently, 200 mL YEP-medium containing rifampicin (80 mg L^{-1}) was inoculated with 1 mL of the overnight culture and grown to an OD_{600} of 0.7 at 28 °C. To provide sufficient ventilation the culture was shaken at 180-200 rpm. The cells were incubated on ice for 30 min before they were harvested by centrifugation at 4000 *x g* for 10 min at 4 °C. The cells were resuspended in 400 mL ice-cold ddH_20 and incubated on ice for 15 min. The centrifugation and the following wash step were repeated five times and the cells were finally suspended in 1 mL ice cold sterile 10 % (v/v) glycerol. Aliquots of 40 µL were shock-frozen in liquid nitrogen and stored at -80 °C.

For transformation of electrocompetent *A. tumefaciens* cells, an aliquot of the cells was thawed on ice. 2.5 µL plasmid DNA was added and the mixture was incubated on ice for 15 min. The cells were transferred to a pre-cooled 1 mm electroporation cuvette and an electric field pulse of 1250 V was applied. The transformed cells were immediately transferred to 800 µL ice cold YEP medium without antibiotics and kept on ice for 2 min. The cells were allowed to regenerate at 28 °C for 2 h and plated on agar-solidified YEP medium containing the appropriate antibiotic. The cells were grown for 2 days at 28 °C.

2.2.4.3 Glycerol Stocks

Glycerol stocks of plasmids clones were prepared by mixing 70 % sterile glycerol with the same volume of bacterial culture. The mixture was immediately shock-frozen in liquid nitrogen and stored at -80 °C.

2.2.5 Arabidopsis Techniques

2.2.5.1 Arabidopsis Seed Surface Sterilization

Before growing Arabidopsis on synthetic growth medium, the seeds must be surface sterilized. Arabidopsis seeds were placed into a 1.5 mL microcentrifuge tube and 1 mL of the sterilizing solution was added. The seeds were shaken for 15 min and centrifuged briefly to collect the seeds. The supernatant was removed under the laminar flow hood and the seeds were washed in 96 % (v/v) ethanol three times by inverting the tube. The seeds were washed five times with sterilized, double deionized water, air-dried under the laminar flow hood and kept sterile at 4 °C.

Sterilizing solution

21 mL	ddH_2O
4 mL	12 % NaOCl
25 mL	Ethanol 96 % (v/v)

2.2.5.2 Cultivation of Arabidopsis

Arabidopsis WT (different ecotypes) and mutant seeds (Table 2.1) were sown on soil supplemented with vermiculite (in a ratio of 3:1) in pots with a diameter of 10 cm. The soil was treated with nematodes to antagonize thrips infestation. Trays were covered with a transparent plastic hood and transferred into a growth chamber where the seeds were incubated at 8 h photoperiod, 160 µmol m^{-2} s^{-1} light, 22 °C, and 65 % humidity for germination. After reaching the four leaves stage the covers were removed and the seedlings were singularized.

2.2.5.3 Stable Transformation and Selection of Transgenic Seeds

Arabidopsis was transformed by the floral dip method according to Clough and Bent (1998). 5 Arabidopsis plants were grown in 10 cm diameter pots. Approximately one week after removing the first inflorescence shoot to induce the development of secondary bolts, the plants were transformed using *A. tumefaciens*. Two days before transformation a 2 mL *A. tumefaciens* culture was inoculated with a single colony carrying the respective binary vector and the cells grown overnight at 28 °C. Liquid cultures were shaken at 180-200 rpm. For selection of plasmid containing clones appropriate antibiotics were added (Table 2.9). The main culture of 100 mL YEP medium with corresponding antibiotics was inoculated with the preculture and incubated for 36 h. The cells were harvested by centrifugation at 4000 *x g* for 10 min at 18 °C and resuspended in 200 mL freshly prepared infiltration medium. For transformation, all green parts of the plant were dipped for about 15-30 sec in the bacterial solution and allowed to dry lying before being covered with a plastic hood to keep high humidity. After 24 h at RT in the dark, transformed plants were transferred to long day conditions into the phytochamber with 16 h photoperiod until seed set. Transgenic seeds carrying the red fluorescence marker (DsRed) were selected under the fluorescence microscope.

2.2.5.4 Manual Pollination

For crossing plants, emerging inflorescences were employed. Mature siliques, open flowers, and open buds were removed from the inflorescence of the pollen recipient plant. Afterwards the sepals, petals, and anthers were gently removed from a closed flower bud using fine forceps. The emasculated flower was manually pollinated with the pollen of a donator plant. The pollen was transferred by gentle touching the stigma of the recipient plant with the stamen of the pollen donator plant. The pollinated inflorescence were marked and covered with plastic foil for 3 to 4 days. Siliques from manually pollinated flowers were harvested prior to opening and kept at RT for further maturation.

2.2.5.5 Large-Scale Pollen Isolation from Arabidopsis

For the large-scale isolation of pollen grains from Arabidopsis a special collection tube attached to a vacuum cleaner was used. The collection tube consists of three different-sized meshes held together in sequence by three metal rings, which can be screwed together (Fig.: 2.1) for assembly instructions see (Johnson-Brousseau and McCormick, 2004). The collection tube was attached to a handheld vacuum cleaner. The pollen passed through the 60- and the 36-micron (µm) mesh and collected on the 6-micron mesh. Flower parts were trapped on the 60-micron mesh and debris, such as soil and vermiculite particles were trapped on the 36-micron mesh.

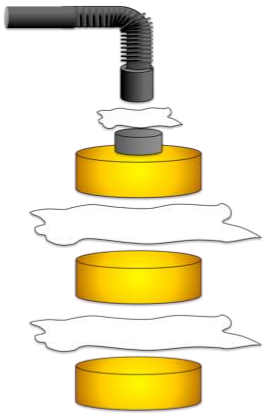

Figure 2.1: Collection tube for large-scale pollen isolation. The collection tube consists of three different-sized meshes held together in sequence by three metal rings, which can be screwed together.

2.2.5.6 Alexander Staining of Arabidopsis Pollen Grains

For the evaluation of pollen viability a modified method of the Alexander's staining was used (Alexander, 1969). Anthers just beginning to dehisce from the open flower were dissected under the binocular microscope and incubated for 1-3 h in 3 mL FPA50 solution for fixation. Subsequently, the anthers were placed onto a microscope slide and covered with a drop of Alexander's staining solution. After 15 min of incubation at RT the excess staining solution was removed using a paper towel and a coverslip was placed onto the sample. Pollen grains were observed under the light microscope.

Alexander staining solution

Ethanol 95 % (v/v)	10 mL
Malachite-green (1 % (w/v) in 95 % (v/v) ethanol)	1 mL
Fuchsine acid (1 % (w/v) in ddH_2O)	5 mL
Orange G (1 % (w/v) in ddH_2O)	0.5 mL
Phenol	5 g
Chloral hydrate	5 g
Acetic acid	2 mL
Glycerol	25 mL
ddH_20	50 mL

2.2.5.7 Embryo Isolation from Arabidopsis

In Arabidopsis, the embryo is surounded by the maternal seed coat and develops within the endosperm. Thus, the isolation of 'clean' embryos at early stage of the development is technically challenging because of potential contaminations with the surrounding tissue. Embryos at late heart to early torpedo stage were either manually dissected or isolated based on

density gradient centrifugation. For manual dissection of Arabidopsis embryos, fine syringes and forceps were used. The developing siliques were opened and the seeds impaired in their development were removed under the binocular microscope. The developing embryos at late heart to early torpedo stage were dissected using two syringes. Attention should be paid to the adhesiveness of the embryo to the surrounding tissues, contamination can adulterate subsequent analyses. To avoid desiccation, the isolated embryos were immediately transferred into ddH_2O or solvent for lipid isolation. Approximately 30 embryos were collected for lipid and nucleic acid isolation. To obtain larger numbers of developing embryos more rapidly, an isolation technique based on density gradient centrifugation was performed according to Perry and Wang (Perry and Wang, 2003). To this end, approximately 400 immature seeds, containing the embryos to be analyzed, were colleced on a microsope slide in a few drops of MC buffer. Then a second microscope slide was placed on top of the seeds and gently pressed downward with slight rotation, causing the seed coats to rupture. The emerged embryos and the seed coats were collected in MC buffer and kept on ice. The embryo/seed coat mixture was concentrated in a microcentrifuge tube by centrifugation for 10 sec at 14000 *x g*. The mixture was resuspended in buffer to isolate embryos. Approximately 0.6 mL of the embryo/seed coat suspension was layered onto 1 mL 50 % Percoll cushion in MC buffer. After centrifugation at 800 *x g* for 10 min at RT, the pellet was enriched in embryos, while the seed coats remained near the top of the Percoll cushion. To avoid cross contamination the fractions were collected and concentrated by a brief centrifugation for 10 sec at 14000 *x g.* The pellet was resuspended in 1 mL MC buffer, layered onto 50 % Percoll solution, and centrifuged for 10 min at 800 *x g.* The supernatant and the loose material were discarded and the compact cell pellet consisting nearly completely of embryos were washed two times in phosphate buffer and employed for further analyses.

MC buffer

Potassium phosphate pH 7.0	10 mM
NaCl	50 mM
Sucrose	0.1 M

10x 0.1 M PBS buffer (1 L)

Na_2HPO_4	14.4 g
KH_2PO_4	2.4 g
NaCl	80 g
KCl	2 g

2.2.5.8 Labeling of Arabidopsis Siliques

Opening flowers of WT and mutant plants grown in the growth chamber were tagged every second day until the siliques from the earliest tagged flowers turned brown. All tagged siliques were harvested in the following intervals: 2, 4, 6, 8, 10, 12, 14, and 16 days, and after more than 3 weeks (mature dehydrated seeds). While harvesting, the siliques were kept in a microcentrifuge tube on ice until ready for dehydration and sectioning.

2.2.6 *Nicotiana benthamiana* Techniques

2.2.6.1 Cultivation of *N. benthamiana* and Transient Expression

N. benthamiana plants were grown in 10 cm diameter plastic pots on soil/vermiculite (2:1), at 22 °C with 60 % humidity and 12 h light and 12 h dark photoperiod of 160 µmol m^{-2} s^{-1} light in a growth chamber. After four weeks the plants had the optimal developmental stage for agroinfiltration, with four to five fully developed true leaves and visible flower buds. For transient expression by agroinfiltration, *A. tumefaciens* GV3101 cells harboring the desired plasmid were grown to an OD_{600} at 0.8 to 1.0 as described above (see 2.2.4.1). After harvesting, the cells were adjusted to equivalent cell density of OD_{600} 0.5 in infiltration medium containing acetosyringone for the induction of *vir* genes. The expression constructs were co-infiltrated with a second *A. tumefaciens* strain carrying the p19 suppressor from tomato bushy stunt virus. P19 expresses a viral suppressor protein that prevents the onset of post-transcriptional gene silencing in the infiltrated tissue and allows high level protein expression (Voinnet et al., 2000). Each cell culture, harboring the desired expression constructs, was mixed with the same amount p19 cell culture and incubated for 2 h at RT in the dark. Infiltration was done by injecting the cell suspension with a 6 mL needleless syringe into the stomata on the abaxial side of the leaves. Four to seven days after infiltration, leaf samples were collected and analyzed.

Infiltration medium

20 mM	Citric acid
2 % (w/v)	Sucrose
100 µM	Acetosyringon (500 mM stock in DMSO)
	pH 5.2 (NaOH)

2.2.7 Biochemical Methods

2.2.7.1 Isolation of Recombinant Proteins from *E. coli*

For heterologous expression of *GDPD5* and *GDPD6* in *E. coli*, ElectroSHOX competent cells (Biolone) were transformed with the expression constructs pQGDPD5oTMD, pQGDPD6oTMD, DsRed-GDPD5oTMD-pLW01, or DsRed-GDPD6oTMD-pLW01, and the corresponding empty vector control. Recombinant cells were cultivated in 100 mL LB medium containing the

appropriate antibiotics at 37 °C and 180-200 rpm. After reaching an OD_{600} of 0.4 to 0.6, protein expression was induced by adding IPTG to a final concentration of 0.1 mM. Subsequently cultures were grown at 16 °C and 180-200 rpm to an OD_{600} of 1.2. Cells were harvested by centrifugation at 4000 *x g* for 15 min at 4 °C. Cells were resuspended in lysis buffer and incubated on ice for 1 h. Then the cells were homogenized in the Precellys for 30 sec at 6500 rpm. This homogenization step was applied six times. After each homogenization step, the samples were cooled on ice for 5 min to prevent heat degradation of the proteins. To separate the supernatant from the cell walls and debris, the samples were centrifuged at 4000 *x g* for 15 min at 4 °C. The supernatant was transferred into fresh tubes and the pellet was resuspended in 1 mL assay buffer. Protein concentration was determined by the BCA assay. Equal amounts of proteins were used in each assay.

Lysis buffer

Tris HCl, pH 7.5	50 mM
$MgCl_2$	5 mM
Lysozyme	10 mg/mL

Assay buffer

Tris HCl, pH 7.5	50 mM
$MgCL_2$	5 mM
$CaCl_2$	5 mM

2.2.7.2 Sodium Dodecyl Sulfate Polyacrylamide Gel Electrophoresis (SDS PAGE)

The discontinuous gel system (SDS-PAGE) was used for the separation of proteins according to their molecular weight (Laemmli, 1970). A molecular weight marker (PeqGold Protein Marker III Prestained, PEQLAB) was used for the identification of the proteins. SDS-PAGE gels were poured according to Sambrook (Sambrook et al., 1989). The glass plates were assembled according to the manufacturer's instruction (GE Healtcare Europe GmbH). The acrylamide gels started to polymerize after adding TEMED and APS. For producing the resolving gel, the acrylamide solution was poured into the gap between the glass plates and overlayed with 1 mL of isopropanol. After the polymerization was complete, the overlay was poured off and the top of the gel washed several times with ddH_2O. The liquid was completely removed from the top of the gel with the edge of a paper towel. The stacking gel was poured directly onto the surface of the polymerized resolving gel and a clean teflon comb was inserted immediately into the stacking gel solution. Protein samples were mixed with Laemmli SDS sample loading buffer and incubated for 5 min at 95 °C. After a 2 min centrifugation at 14000 *x g* the samples were loaded onto the polymerized SDS-PAGE gels and separated in Tris glycine electrophoresis

buffer. Electrophoresis was started with 25 mA. When the samples reached the the resolving gel, the current was increased to 35 mA. The gel was stained with Coomassie Brilliant Blue R250. To this end, the gel was incubated in the staining solution, heated in the microwave oven for approximately 1 min and incubated at RT for 5 min under gentle agitation. The gel was destained in destaining solution by heating the gel again in the microwave oven for approximately 1 min and gentle agitation at RT for 5 min until the background was clear. Alternatively, the proteins were transferred from the gel to a nitrocellulose membrane (Western blotting).

4x Laemmli SDS sample loading buffer

200 mM	Tris-HCl (pH 6.8)
400 mM	Dithiothreitol (DTT)
8 % (v/v)	Sodium dodecyl sulfate (SDS)
0.4 % (w/v)	Bromophenol blue
40 % (v/v)	Glycerol

pH was adjusted to 6.8 with HCl

Stacking gel 4 %

2.66 mL	Acrylamide stock solution (30% acrylamide, 0.8% bisacrylamide)
5 mL	4 x Stacking gel buffer (Tris-HCl, pH 6.8, 0.5 M)
0.2 mL	SDS solution (100 mg/mL, in ddH_2O)
12 mL	ddH_2O
10 µL	Tetramethylethylenediamine (TEMED)
0.2 mL	Ammonium persulfate (APS) solution (100 mg/mL in ddH_2O)

Resolving gel 10 %

17 mL	Acrylamide stock solution (30 % acrylamide, 0.8 % bisacrylamide)
12.5 mL	Tris-HCl (pH 8.8) [1.5 M]
0.5 mL	SDS-solution (100 mg/mL, in ddH_2O)
20 mL	ddH_2O
20 µL	TEMED
0.3 mL	APS solution (100 mg/mL in ddH_2O)

5 x Tris glycine electrophoresis buffer

125 mM	Tris
960 mM	Glycine
0.5% (w/v)	SDS

Staining solution

500 mL	Ethanol 95% (v/v)
70 mL	Acetic acid
428 mL	ddH_2O
2.52 g	Coomassie brilliant blue R250

Destaining solution

100 mL	Glycerol
150 mL	Acetic acid
1750 mL	ddH_2O

2.2.7.3 Western Blotting

For western blot analysis the proteins from SDS PAGE gels were transferred onto nitrocellulose membranes according to Towbin (Towbin et al., 1979) by semi-dry blotting in Towbin-transfer-buffer. For His-tag detection, the His Detector™WesternBlot Kit AP Colorimetric (KPL) was used according to the supplier's instructions.

Towbin-transfer-buffer

25 mM	Tris
192 mM	Glycine
20 %	Methanol
0.1 % (w/v)	SDS

2.2.7.4 Isolation of Proteins from *Nicotiana benthamiana*

Total protein extracts from *N. benthamiana* leaves were prepared as follows. Up to 10 g leaf material was homogenized in a mixer (Philips HR 2870/50 Minimixer) by mashing the sample 6 times for 3 seconds in extraction buffer containing 1 mM DTT and 1 mM phenylmethanesulfonyl fluoride (PMSF). Between the homogenization steps samples were cooled on ice for 2 min each. The homogenate was filtered through a layer of miracloth and centrifuged at 600 *x g* for 10 min at 4 °C. The supernatant containing the total proteins was centrifuged at 42000 *x g* for 2 h at 4 °C. The pellet was suspended in 2 mL suspension buffer, and the suspension was used for microsomal protein extraction. The supernatant was employed for soluble protein analysis. The protein concentration was photometrically determined by the BCA assay and protein concentration adjusted. After addition of 15 % (v/v) glycerol samples were stored at - 80 °C for several weeks.

Extraction buffer

50 mM	Tris-HCl, pH 8,0
150 mM	NaCl
5 mM	$CaCl_2$
1 mM	DTT
1 mM	PMSF

Suspension buffer

50 mM	HEPES-NaOH pH 7.4
5 mM	$CaCl_2$

2.2.7.5 Protein Quantification by BCA Assay

The BCA assay is used for determining the total concentration of protein in a solution (Smith et al., 1985). It combines the protein-dependent biuret reaction and the selective colorimetric detection of the resulting cuprous cation by bicinchoninic acid (BCA). The chelation of two molecules of BCA with one cuprous ion forms the purple colored reaction product. This complex is water-soluble and exhibits a linear absorbance at 562 nm or 550 nm over a broad range of protein concentrations.

25 µL of protein sample were mixed with 200 µL BCA-reagent. This mixture was incubated for 30 min at 37 °C and chilled on ice for 2 min. The samples were centrifuged for 5 min at 10000 *x g* and the protein concentration was determined by measuring the absorbance at a wavelength of 550 nm. Based on the absorbance of a defined standard curve with bovine serum albumin (BSA) the protein concentration in the samples could be measured.

BCA-reagent

98% (v/v)	Bicinchoninic acid (BCA)
2% (v/v)	$CuSO_4$ [4% (w/v)]

2.2.7.6 Synthesis of Glycerophosphodiesters by Mild Alkaline Hydrolysis

The synthesis of GPDs from phospholipids by mild alkaline hydrolysis was performed according to Clarke and Dawson (Clarke and Dawson, 1981). Approximately 10 mg of different phospholipids (PC, PE, PI, PS and PG from egg yolk) dissolved in 1 mL chloroform/methanol [1:1] was transferred into a glass vial with teflon-lined screw cap. An aliquot of 10 µL was used for determining the fatty acid content to calculate the exact phospholipid concentration of the sample by FAME analysis (see 2.2.8.6). To synthesize GPDs from PLs, the fatty acids need to be cleaved off by mild alkaline hydrolysis without affecting the headgroup-phosphate-glycerol bonds. For alkaline hydrolysis the lipids were dried under a stream of air and subsequently dissolved in 1 mL 33 % methylamine solution in ethanol/water [7:3 v/v] and incubated at 50 °C for 1 h. The methylamine was removed by drying under a stream of air and the GPDs dissolved in 500 µL methanol/water [7:3 v/v]. 1 mL hexane (with 1 % acetic acid fatty acid protonation) was added and the sample was vortexed thoroughly. After centrifugation at 1000 *x g* for 3 min the hexane phase was removed and the residual phase extracted once more with 1 mL hexane (without acetic acid). After removing the hexane phase the methanol/water phase, containing the deacylated GPDs, was dried and dissolved in a small defined volume of methanol/water

[1:1]. The exact amount of GPDs in the sample was calculated in nmol from the FAME measurement (see below) by dividing the amount of FAME by two.

2.2.7.7 Enzyme-Coupled Spectrophotometric Assay for Determining GDPD Activity

The GDPD activity assay was performed as described by Ohshima (Ohshima et al., 2008). The enzyme activity was examined by an enzyme-coupled spectrophotometric assay, measuring the amount of G3P generated by GDPD activity. The reaction mixture, containing 0.25 to 5 mg total protein extracted from *E. coli* cultures or *N. benthamiana* leaf material dissolved in suspension buffer (see 2.2.7.4) was filled up to a total volume of 1 mL with hydrazine-glycine assay buffer containing different GPDs (GPC, glycerophosphoethanolamine (GPE), glycerophosphoinositol (GPI), glycerophosphoserine (GPS), and glycerophosphoglycerol (GPG), synthesized as described in 2.2.7.6) as substrates. After incubation for 15 to 60 min at 30 °C the proteins were inactivated by incubating the reaction mixture for 5 min at 95 °C. Debris was removed by centrifugation for 2 min at 11000 *x g*, and 500 µL of the supernatant was used for the photometric detection of GDPD activity. To this end, 500 µL GDPD assay reaction mixture was added to 500 µL 0.2 M hydrazine-glycine buffer (working stock) containing NAD and mixed thoroughly. This mixture was transferred into a spectrophotometer-cuvette and absorbance at 340 nm was measured according to Wei and co-workers (Wei et al., 2004). 10 U GDPH (Sigma) eluted in hydrazine-glycine buffer (working stock) without NAD were added and the G3P concentration was calculated from the absorbance change. The amount of G3P can be measured by the NAD dependent conversion of G3P into DHAP catalyzed by GPDH. This reaction is accompanied with the reduction of NAD to NADH which can be measured via the absorbance change at 340 nm.

Hydrazine-glycine buffer (stock solution)

5.2 g (w/v)	Hydrazin sulfate salt
7.5 g (w/v)	Glycine
0.2 g (w/v)	EDTA

Dissolve in 30 mL ddH_2O and adjust pH to 6 with KOH. Fill up to a final volume of 50 mL with ddH_2O. Can be stored at 4 °C for several weeks.

Hydrazine-glycine buffer (working stock)

15 mL	Hydrazine-glycine buffer stock solution (pH 9.0 with KOH, filled up to a final volume of 20 mL with ddH_2O).
2 mM	NAD

Working solution had to be prepared freshly.

2.2.8 Analytical Techniques for Lipid Quantification

2.2.8.1 Extraction of Lipids from Plant Material

The extraction of lipids from plant material for Q-TOF MS analysis is based on the common procedure described by Bligh and Dyer (Bligh and Dyer, 1959) with slight modifications. To minimize contamination, only glass and teflon ware was used and washed with chloroform prior to use. Furthermore, 0.01 % (w/v) butylated hydroxytoluene was added to all HPLC or GC grade solvents as antioxidant (Welti et al., 2002).

Plant tissue (~ 25 to 100 mg wet weight) was harvested and placed into a 50 mL glass vial with a teflon-lined screw cap conatining 1 mL water. To avoid degradation by lipases the tissue was boiled for 20 min. Total lipids were extracted in two steps. Lipid-extract A: The plant tissue was transferred to a 6 mL glass vial and 4 mL of chloroform/methanol/formic acid [1:1:0.1] was added. The sample was vortexed and incubated under continuous shaking for 15 min at RT. Formic acid was added to the solvent to prevent lipid degradation by lipases during lipid isolation (Browse et al., 1986). The lipid-extract A was harvested and transferred to another vial and evaporated under a stream of air. Lipid-extract B: 4 mL of chloroform/methanol [2:1] was added to the residue of the first extraction A and subsequently vortexed and incubated for 10 min at RT under continuous shaking. The lipid-extract B was then combined with lipid extract A and 2 mL of 1 M KCl/0.2 M H_3PO_4 was added before the mixture was shaken vigorously. Phase separation was achieved by centrifugation at 1500 *x g* for 10 min. Afterwards the total lipids were harvested from the lower organic phase and dried under a stream of air. The dried lipids were dissolved in chloroform or Q-TOF running buffer (chloroform/methanol/300 mM ammonium acetate [300:665:35]) and measured immediately or stored at -20 °C.

2.2.8.2 Extraction of Lipids from Arabidopsis Seeds

Arabidopsis seeds (10 – 20) were harvested, placed into a microcentrifuge tube, and frozen in liquid nitrogen. The samples were ground to a fine powder using ceramic balls in the Precellys homogenizer. The samples were not allowed to thaw during homogenization. 500 µL diethylether/methanol [2:1] and 50 µL of internal standard mixture, containing 1 nmol of each TAG standard, was added to the sample and vortexed thoroughly. Phase separation was achieved by adding 250 µL of 1 M KCl/0.2 M H_3PO_4 and centrifugation for 5 min at 5000 *x g*. The upper organic phase was transferred into a fresh 6 mL glass vial with teflon-lined screw cap. Extraction was repeated two more times by adding 500 µL diethylether. After combining the organic phases, the solvent was evaporated under a stream of air and the lipids were dissolved

in chloroform or Q-TOF running buffer (chloroform/methanol/300 mM ammonium acetate [300:665:35]) and measured immediately or stored at -20 °C.

2.2.8.3 Extraction of Lipids from Cell Cultures for Fatty Acid Analysis

Extraction of lipids from cell cultures was carried out in all cases from cells in liquid culture and cell pellets at cell density OD_{600} of 1.2 without boiling the samples prior to extraction. For lipid isolation from *E. coli*, two volumes of chloroform were added to the culture and shaken vigorously. Phase separation was achieved by centrifugation at 1500 *x g* for 10 min. Total lipids were harvested from the lower organic phase and transferred into a fresh glass vial. Extraction was repeated two more times. After combining the organic phases, the solvent was evaporated under a stream of air and lipids were dissolved in a defined volume of chloroform. Neutral lipid fractions were obtained by solid phase extraction (see 2.2.8.4) and employed for fatty acid methyl ester synthesis (see 2.2.8.6) or stored at -20 °C.

2.2.8.4 Solid Phase Extraction of Lipid Extracts

Lipid extracts were fractionated based on their polarity by solid phase extraction on 100 mg Strata silica columns equilibrated with chloroform. Non-polar lipids were eluted with 4 mL of chloroform and secondly glycolipids were eluted with 4 mL of acetone/isopropanol [1:1]. Finally, the polar lipid fraction, including phospholipids, was eluted by applying 4 mL of methanol. The polar lipids in methanol were evaporated under a stream of air and dissolved in 1 mL Q-TOF solvent [chloroform/methanol/300 mM ammonium acetate [300:665:35] (Welti et al., 2002)]. Thus, an extract highly enriched in phospholipids was obtained, which showed reduced ion suppression during Q-TOF MS/MS analysis.

2.2.8.5 Analysis of Lipids by Q-TOF MS/MS

Q-TOF MS/MS represents a method for the non-destructive identification and quantification of intact glycerolipids and thus provides information about the molecular species composition of the different glycerolipid classes. Mass spectrometric methods require the ionization of molecules in an ion source. For Q-TOF analysis the lipids are directly infused via a nano-capillary infusion chip (HPLC chip) and are ionized by nanospray ionization. Ions are subsequently transferred into the mass analyzer and separated according to their *m/z* in the quadrupole. Ions of a specific *m/z* value are selected and characteristic fragment ions are generated by collision-induced dissociation in the MS/MS mode. In the time-of-flight analyzer, ions are accelerated, separated, and detected at the photomultiplier plate. The quantification of the different lipids was based on precursor ion or neutral loss scanning in relation to internal standards of known concentrations. For each lipid class at least two different internal standards

were selected, which were absent from the sample. For quantitative analysis, an aliquot of 10 µL lipid extract and 10 µL of phospho- and galactolipid standard mix (0.1 nmol di14:0-PC and di20:0-PC, 0.1 nmol di14:0-PE and di20:0-PE PE, 0.1 nmol di14:0-PG and di20:0-PG, 0.07 nmol di14:0-PA and di20:0-PA, 0.014 nmol di14:0-PS, 0.15 nmol 34:0-PI, 0.07 nmol 34:0-MGDG and 0.05 nmol 36:0-MGDG, 0.1 nmol 34:0-DGDG and 0.2 nmol 36:0-DGDG, 0.2 nmol 34:0-SQDG) in chloroform/methanol [2:1] was mixed with Q-TOF solvent to a final volume of 100 µL (Gasulla et al., 2013). 34:0-PI, as well as MGDG and DGDG standards were obtained after catalytic hydrogenation of PI, MGDG and DGDG from biological sources according to Buseman and co-workers (Buseman et al., 2006) (Helga Peisker, IMBIO Institute). For DAG and TAG analysis 10 µL of a DAG/TAG standard mix in chloroform-methanol [2:1] containing 1 nmol each of di14:0, di14:1, di20:0 and di21:0 or tri10:0, tri11:1, tri20:0 and tri22:1, respectively, were used.

2.2.8.6 Synthesis of Fatty Acid Methyl Esters and Analysis by GC

For fatty acid methyl ester (FAME) analysis by gas chromatography (GC) was done according to Browse and co-workers (Browse et al., 1986). Fatty acid methyl esters were synthesized by incubating the sample in 1 mL 1 N methanolic HCl for 20 min at 80 °C. In case of seed samples, 2 h of incubation in 2 N methanolic HCl at 80 °C was done. After cooling, 1 mL 0.9 % NaCl and 1 mL hexane was added and the mixture was shaken vigorously. Phase separation was achieved by centrifugation at 1000 *x g* for 3 min. The hexane phase containing the FAMEs was directly measured in the GC with flame ionization detector (GC-FID). For quantification, an internal standard (100 µL of pentadecanoic acid, 50 µg/mL in methanol) was used.

2.2.8.7 G3P Extraction and Measurement with a Photometer or by GC-MS

Isolation of G3P from different plant tissues grown on soil or synthetic growth medium was carried out using TCA (trichloroacetic acid) or chloroform/methanol extraction. Extraction with TCA was done as described by (Jelitto et al., 1992) Jelitto and co-workers (1992). Leave material (~ 25 to 50 mg wet weight) growing on 2 MS medium or soil was harvested, frozen in liquid nitrogen, and homogenized to a fine powder using the Precellys. A 1.5-mL aliquot of pre-cooled 16 % (w/v) TCA in diethylether was added to the sample. Subsequently the sample was inverted and incubated for 15 min on dry ice. After adding 0.8 mL of 16 % (w/v) TCA in ddH_2O and 5 mM EGTA, the sample was further homogenized, warmed to 4 °C, and left on ice for 3 h. The sample was centrifuged for 5 min at 15000 *x g* and 4 °C. The upper aqueous phase was transferred to a new microcentrifuge tube. To remove the TCA, the samples were washed four times with 1.0 mL of diethylether. Phase separation was achieved by centrifugation for 5 min at 15000 *x g*. The aqueous phase was then neutralized by the stepwise addition of 5 M KOH/1 M

triethanolamine. G3P content was measured enzymatically using GPDH as described above (2.2.7.7) or by the GC-MS-based method (see below).

For the extraction using chloroform/methanol, plant tissue (~ 25 to 50 mg wet weight) was harvested, frozen in liquid nitrogen and ground to a fine powder in the mixer Mill (Retsch) for 30 sec at 6500 rpm. 1 mL chloroform/methanol [1:2] and 10 nmol internal sorbitol standard was added to the samples and subsequently vortexed. After an incubation of 5 min at RT samples were centrifuged for 5 min at 10000 *x g*. The supernatant was collected and transferred to a fresh glass vial. Samples were dried under a stream of air and dissolved in 60 µL BSTFA (N,O-Bis(trimethylsilyl)trifluoroacetamide) + 60 µL pyridine, or in 80 µL MSTFA (N-Methyl-N-(trimethylsilyl) trifluoroacetamide)(without pyridine). Samples were derivatized for 40 min at 70 °C and measured by GC-MS. Trimethylsilylated G3P and sorbitol were analyzed according to the retention time and mass spectra obtained from the National Institute of Standards and Technology (NIST) library. The NIST mass spectral library is a collection of electron ionization (EI) and MS/MS mass spectra, with chemical and GC data. The software can be used to identify unknown spectra. Identification and quantification of G3P and sorbitol were based on the single ion monitoring of selected characteristic ions. For the identification of G3P the characteristic 299.1 m/z ion was used, while sorbitol was identified and quantified by screening for the 319.2 m/z ion.

Internal standard: 0.5 mM sorbitol (100 mM dissolved in ddH_2O, diluted to 0.5 mM in methanol)

Parameters of the GC-MS

GC:	7890A Agilent
MS:	5975C inert XL MSD Agilent
Software:	MSD ChemStation (Agilent)
Column:	HP-5MS
Length:	30 m
Diameter:	0.53 mm
Coating thickness:	0.20 µm
Carrier gas:	Helium
Flow rate:	2 mL/min
Injection:	1 µL, Split 1:10

Temperature program

Oven ramp	**Oven temperature**	**Run time**
Initialization	140 °C	2 min
10 °C/min	to 250 °C	4 min
20 °C/min	to 100 °C	-

2.2.9 Microscopy

2.2.9.1 Fluorescence Microscopy

Seeds were screened for DsRed expression via fluorescence microscopy using the Olympus binocular microscope (SZX16) with a DsRed emission filter (557-563 nm excitation, and 579-582 emission) and photos taken with an Olympus digital camera (DP7Z) for microscope. Images were processed using Photoshop CS (Adobe).

2.2.9.2 Brightfield Microscopy

2.2.9.2.1 Embedding of Arabidopsis Tissue in Glycolmethacrylate

Different plant organs like green Arabidopsis seeds at different developmental stages and Arabidopsis pistils were employed for section cuttings with the microtome. To this end, samples were embedded in glycolmethacrylate resin (Technovit 7100). Plant organs were picked under the binocular and 10 to 15 seeds or 2-3 pistils were placed in 1 mL fixative solution and incubated for 1-2 h under vaccum at RT. After removing the fixative solution, fresh fixative solution was added and samples were kept under vaccum at 4 °C overnight. Following fixation, the samples were washed twice with 1x phosphate buffered saline (PBS) buffer, pH 8.0, and subsequently dehydrated. A series of dehydration was applied as indicated below:

30 % ethanol	15 min
50 % ethanol	30 min
70 % ethanol	30 min
80 % ethanol	1 h
90 % ethanol	1 h
100 % ethanol	2x 1 h

Subsequently, the samples were pre-infiltrated by incubation for 2 h at RT in a mixture of 100 % ethanol and base liquid Technovit 7100 mixed in equal volume parts. After discarding the pre-infiltration solution, 1 mL of solution A was added to the sample, shaken vigorously for 1 min, and incubated for up to 24 h at RT on a rotary shaker at 120 rpm. Following incubation, solution A was discarded and replaced by 1 mL of solution B. The specimens were placed in embedding cassettes of the Histoform S and, within 5 min, the samples were positioned in the filled cavities. The plastic was cured at RT for about 2 h before the plastic blocks were ready for further processing. To fasten the glycolmethacrylate blocks in the microtome, specimen adapters were mounted on top of the resin blocks by fixing the adapters with the fast curing Technovit 3040, as described in the users instructions (Heraeus Kulzer GmbH). After approximately 30 min, the mounted plastic blocks were removed from the molding tray cavities and ready for sectioning.

10x 0.1 M PBS buffer (1 L)

Na_2HPO_4	14.4 g
KH_2PO_4	2.4 g
NaCl	80 g
KCl	2 g

After dissolving the salts, the pH was adjusted to 8.0 using HCl and the buffer filled to a final volume of 1 L with ddH_2O. After autoclaving or filter sterilization the buffer can be stored at RT.

Fixative solution

4 % (v/v)	Paraformaldehyde
0.2 % (v/v)	Glutaraldehyde in 0.1 M PBS buffer, pH 8.0

The glutaraldehyde solution takes several hours to dissolve.

Solution A (infiltration solution)

1 g	Hardener I
100 mL	Technovit 7100

Solution is mixed thoroughly for 1 min at RT and can then be stored for 4 weeks at 4 °C.

Solution B (embedding solution)

Solution A and the hardener II is mixed thoroughly in a ratio of [15:1] for 1 min at RT and immediately poured into the mold cavities.

2.2.9.2.1.1 Preparing and Staining of Semi-Thin Sections

For the preparation of semi-thin sections the sample embedded in plastic resin was serially sectioned at a thickness of 30 μm with a rotating microtome (Leica RM 2155) using a steel histoknife until the sample was reached. Sample sections had a thickness of 1-4 μm. To avoid fractures in the sections, the plastic block was slightly moistered with ddH_2O water before section cutting. Sections were prepared with an average speed of 2 mm/sec for the microtome specimen holder, which correspond to 0.5 % of the maximum cutting speed on the Leica RM 2155 microtome. The sections were collected using fine forceps and strechted at RT in ddH_20 on a microscope slide. 1-2 drops of 0.05 % toluidine blue in 1 % sodium borate were placed onto the sections and placed on a heating plate for 10 min at 42 °C. After incubation the sections were rinsed with a gentle stream of ddH_2O to wash off excess stain. The washed slide was again placed onto the 42 °C warm heating plate after the water was carefully removed from the sections with a paper towel. The sections were kept on the heating plate until the sections were completely

dry. Following tuloidine blue staining, sections were analyzed by brightfield microscopy using the Olympus light microscope (BH-2). Images were taken with a digital Olympus camera (DP7Z) for microscope.

2.2.9.3 Electron Microscopy of Arabidopsis Pollen Grains

Scanning electron microscopy and transmission electron microscopy of Arabidopsis pollen grains was done by Michael Melzer from the Leibniz Institute of Plant Genetics and Crop Plant Research (IPK) Gatersleben (Germany).

3 Results

3.1 Molecular and Biochemical Characterization of Acyl-ACP Thioesterases in Arabidopsis

One of the goals of this work was the analysis of regulatory points of plant lipid biosynthesis, in particular the regulation of membrane lipid biosynthesis. Studies of the present work focused on the two acyl-ACP thioesterases A, *FatA1* (At3g25110) and *FatA2* (At4g13050), in Arabidopsis.

3.1.1 Amino Acid Sequences of Acyl-ACP Thioesterases from Different Organisms

Arabidopsis *FatA1* and *FatA2* share 74.3 % identity on amino acid level. The FatA enzymes are highly conserved between different plant species and it is believed that they serve as the general housekeeping thioesterase responsible for the export of most C18:1 fatty acids from plastids. A phylogenetic tree was generated for plant acyl-ACP thioesterases based on their deduced amino acid sequences (Fig.: 3.1). Arabidopsis thioesterases can be organized into the FatA or FatB thioesterase group, very closely related with those from *Camelina sativa*, *Arabidopsis lyrata*, *Capsella rubella*, *Brassica napus*, and *Brassica rapa.* All of these species belong to the Brassicaceae family.

In silico studies using the subcellular localization prediction program WOLF PSort (Horton et al., 2007) were used to predict the putative transit peptide and to choose the cleavage site. Gly-50 and Arg-43 were the best candidates to represent the N-terminal amino acid of the mature AtFatA1 and AtFatA2 protein, corresponding to a signal peptide of 49 and 42 amino acids residues, respectively (Fig.: 3.1 B). FatA1 and FatA2 are predicted to be chloroplast localized by WOLF PSort (Table 3.1).

Table 3.1: Predicted subcellular localization of FatA1 and FatA2 based on their amino acid sequences sequences using WoLF PSORT. chlo: chloroplast, nucl: nucleus, mito: mitochondrium, cyto: cytosol. RC: reliability class, whereat a high RC value indicates high prediction reliability.

Name	AGI	Amino acids	Subcellular compartment: RC
FatA1	At3g25110	1-362	chlo:12, nucl:1
FatA2	At4g13050	1-367	chlo; 6, mito: 4, cyto: 3

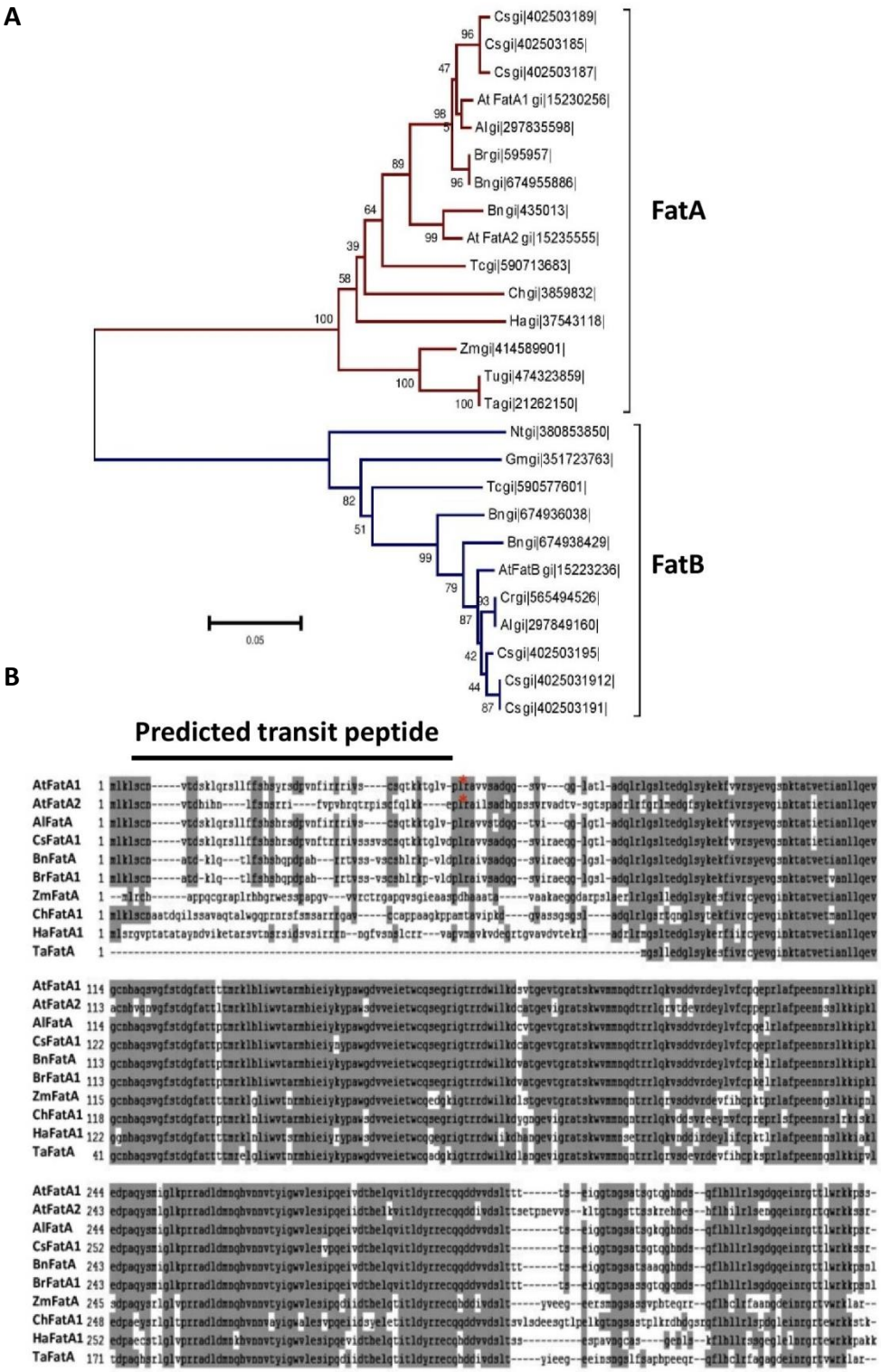

Figure 3.1: Phylogenetic tree and amino acid comparison for different plant acyl-ACP Thioesterases. (A) Phylogenetic tree showing the sequence relationships between acyl-ACP thioesterase proteins from different organism. The phylogenetic tree was derived from the amino acid sequence comparison using CloneManager Scoring Matrix: Blosum62 by the Neighbor-joining method. At, *Arabidopsis thaliana*; Al, *Arabidopsis lyrata*, Cr, *Capsella rubella*; Cs, *Camelina sativa*; Bn, *Brassica napus*; Tc, *Theobroma cacao*; Gm, *Glycine max*; Nt, *Nicotiana tabacum*; Br, *Brassica rapa*; Tu, *Triticum urartu*; Zm, *Zea mays*; Ta, *Triticum aestivum*; Ha, *Helianthus annuus*. **(B)** Alignment of the deduced amino acid sequences of the acyl-ACP thiosterase A enzymes. *Arabidopsis thaliana* (AtFatA1, AtFatA2), *Arabidopsis lyrata* (AlFatA), *Camelina sativa* (CsFatA1), *Brassica napus* (BnFatA), *Brassica rapa* (BrFatA1), *Zea mays* (ZmFatA), *Cuphea hookeriana* (ChFatA1), *Helianthus annuus* (HaFatA1), *Triticum aestivum* (TaFatA). The cleavage sites of the predicted transit peptide for AtFatA1 and AtFatA2 is marked by red asteriks. The alignment was derived from the amino acid sequence comparison using CloneManager Scoring Matrix: Blosum62. Prediction was done using WOLF PSort (Horton et al., 2007).

3.1.2 Expression of *FatA1* and *FatA2* in *E. coli* and Biochemical Characterization

The *E. coli fadD* (Kameda and Nunn, 1981) mutant was transformed with the expression construct pQFatA1oTP or pQFatA2oTP, lacking the predicted FatA transit peptide (Fig.: 3.2 B), and the corresponding empty vector as control.

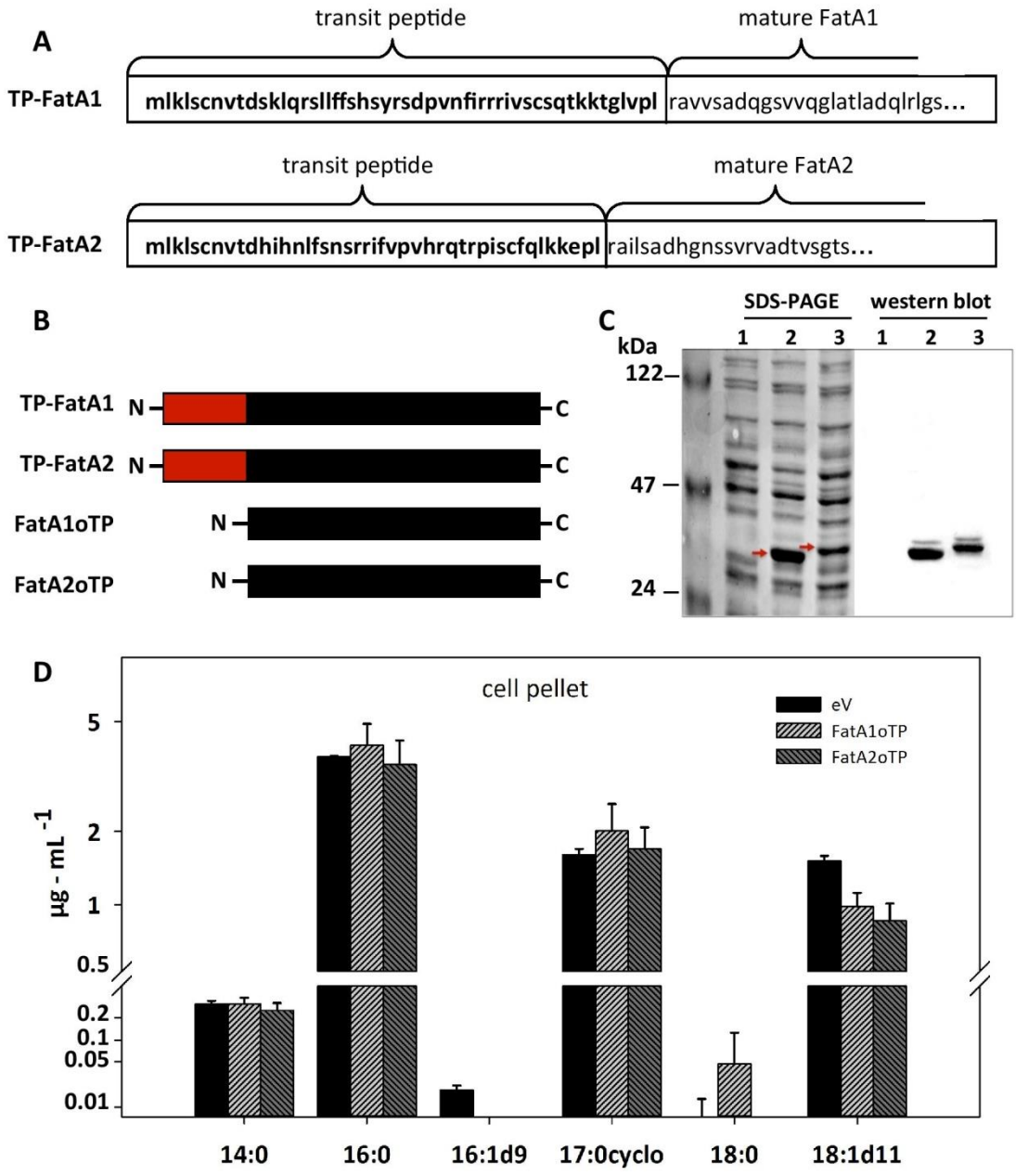

Figure 3.2: Heterologous expression of *FatA1* and *FatA2* cDNA in the *E. coli fadD* mutant. (A) Amino acid sequences of putative FatA1 and FatA2 transit peptides. **(B)** Schematics of the *FatA1* and *FatA2* constructs used for *E. coli* expression. Red boxes represent the transit peptide, black boxes the mature FatA proteins. TP, transit peptide; oTP, without transit peptide. **(C)** SDS PAGE and Western blot of recombinant protein after heterologous expression of *FatA1* and *FatA2* without transit peptide in the *E. coli fadD* mutant. Strong bands at 35 kDa and 37 kDa were obtained for the two proteins, indicated by the red arrows, while no signal was detected for the empty vector control. 1, empty vector control; 2, pQFatA1oTP; 3, pQFatA2oTP. **(D)** Total fatty acid composition (µg) of the cell pellet after recombinant expression of *FatA1*, *FatA2*, without transit peptide, and the corresponding empty vector control in the *E. coli fadD* mutant. *FatA1* and *FatA2* expressing *fadD* cells show no major alterations compared to the empty vector control. Data present means and standard deviations of five independent determinations.

The expression of the FatA1 and FatA2 proteins without putative transit peptide was intended to optimize expression levels of the recombinant proteins, and avoid potential negative effects of the transit peptide on enzyme activity. Indeed, expression of full-length thioesterase constructs of pQFatA1 and pQFatA2 in *E. coli* did not lead to protein accumulation with enzymatic activity (data not shown).

The FadD enzyme catalyzes the conversion of fatty acids into acyl-CoA thioesters in *E. coli*. A mutation in *fadD* abolishes the formation of acyl-CoA leading to an accumulation of free fatty acids (Kameda and Nunn, 1981; Weimar et al., 2002). Transformed *E. coli fadD* cells harboring the *FatA1* or *FatA2* expression constructs as well as the empty vector were grown and cells were harvested. Strong bands at 35 kDa for the recombinant FatA1oTP protein and at 37 kDa for FatA2oTP were obtained in the cell pellet fraction after SDS-PAGE and western blot analysis, (Fig.: 3.2 C). The thioesterase specificities of Arabidopsis FatA1 and FatA2 were measured by analyzing the fatty acid composition of the cell pellet and the liquid medium of recombinant *E. coli* cultures. Total lipids from the cell pellet and culture supernatant were extracted with chloroform/methanol and fatty acids were converted into their methyl esters for quantification via GC-FID. No major alterations in total fatty acid composition were found in the cell pellet (Fig.: 3.2 D) or the supernatant compared to the empty vector control (data not shown).

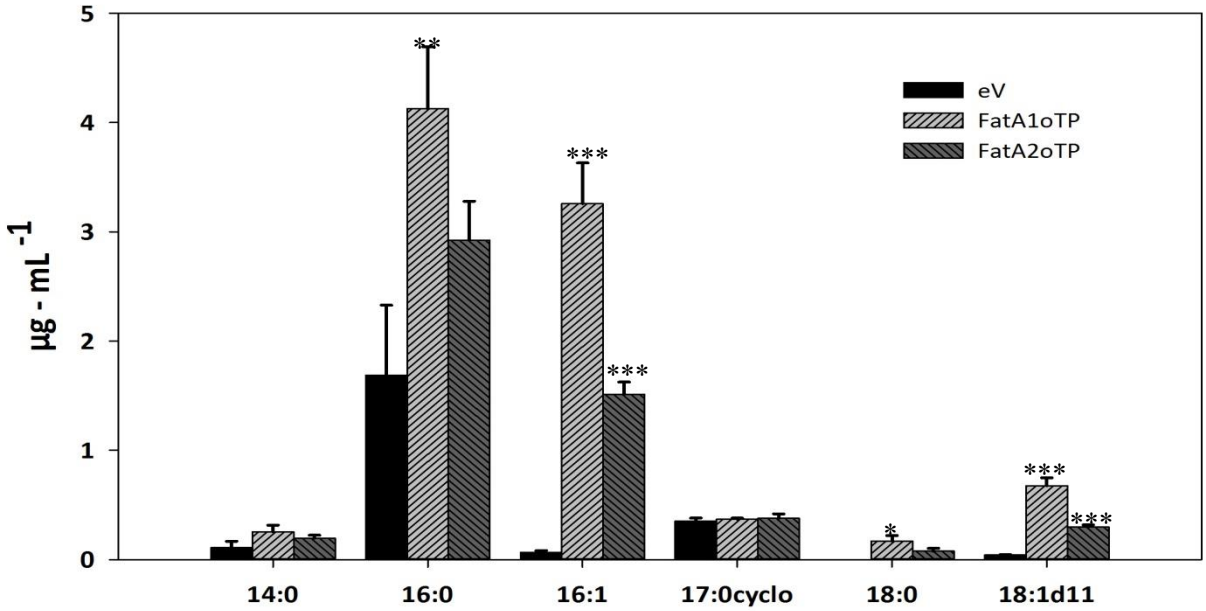

Figure 3.3: Fatty acid composition (µg) of the neutral lipid fraction. Fatty acid composition of neutral lipids (mostly free fatty acids) after recombinant expression of *FatA1*, *FatA2*, and the corresponding empty vector control in *E. coli fadD* mutant. Lipids were isolated from the cell pellet and a neutral lipid fraction, containing free fatty acids was obtained by solid phase extraction. Fatty acids were measured by GC of methyl esters. Data present means and standard deviations of five independent determinations. Asterisks indicate values that are significantly different from the control (according to Student's t test, Welch correction, $P<0.05$ (∗); $P<0.01$ (∗∗); $P<0.005$ (∗∗∗)).

Because the fatty acid composition of total lipids of *FatA* expressing *E. coli* cells was not different from the control, lipids isolated from *E. coli* cultures expressing FatA1oTP or FatA2oTP, were fractionated into polar and neutral lipids by solid phase extraction. The neutral lipid fraction, containing mostly free fatty acids, was harvested and fatty acids were quantified by GC-FID. The fatty acid composition of the neutral lipid fraction extracted from the supernatant (medium) of recombinant *FatA1* and *FatA2 E. coli fadD* cells did not show any differences compared to the empty vector control (data not shown). In contrast, the fatty acid composition isolated from the neutral lipids of the cell pellet showed a strong accumulation of 16:0, $16:1^{\Delta 9}$, and $18:1^{\Delta 11}$ fatty acids (Fig.: 3.3). The amount of $16:1^{\Delta 9}$ was increased by around 45 fold for FatA1oTP and 21 fold for FatA2oTP, while $18:1^{\Delta 11}$ fatty acids showed an increase by approximately 15 fold for FatA1oTP and around 6.5 fold for FatA2oTP as compared for the empty vector control (Fig.: 3.3). Beside $16:1^{\Delta 9}$ and $18:1^{\Delta 11}$, the amount of 16:0 fatty acids were also increased in recombinant *E. coli fadD* strains compared to the empty vector control. These three types of fatty acids made up the major components of the *FatA1* and *FatA2* expressing *fadD* cells. In addition, comparable amounts of myristic acid (14:0), cis-methylene-9,10-hexadecanoic acid (17:0cyclo), and trace amounts of stearic acid (18:0) were found in the recombinant *E. coli* strains.

3.1.3 Tissue Specific Expression of Acyl-ACP Thioesterases A in Arabidopsis

Expression levels of the Arabidopsis acyl-ACP thioesterases *FatA1* and *FatA2* were determined by semi-quantitative RT-PCR in different plant tissues (Fig.: 3.4 B). RT-PCR was done with RNA isolated from Arabidopsis WT root, leaf, stem, flower, and silique tissue at 5 days after flowering (DAF) using primers for *FatA1*, *FatA2*, and for the housekeeping gene *actin*. The results indicate that *FatA1 and FatA2* mRNA is present in all organs, with strong variation in expression levels. Expression level of *FatA1* was overall higher than for *FatA2*. RT-PCR products of the two genes showed high abundance in siliques 5 DAF as compared to the other tissues. (Fig.: 3.4 B). The data obtained by RT-PCR correspond to the expression pattern retrieved from the database Genevestigator, which showed that *FatA1* and *FatA2* are strongly expressed in early torpedo stage embryos (Hruz et al., 2008) (Fig.: 3.4 A).

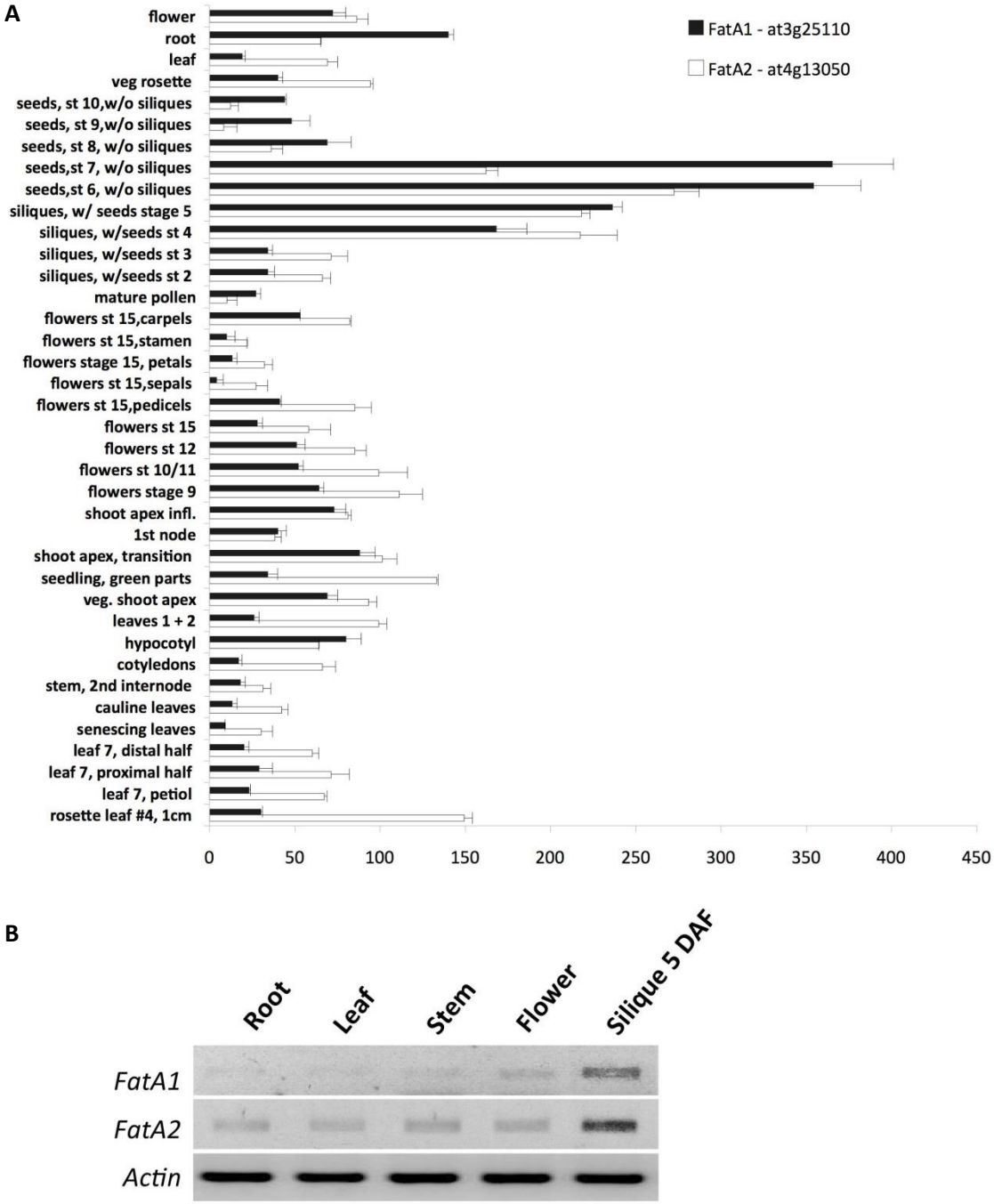

Figure 3.4: Transcript abundance of FatA1 and FatA2 in Arabidopsis. (A) *In silico* gene expression analysis of Arabidopsis *FatA1* and *FatA2* using the database Genevestigator. **(B)** Gene expression analysis of the acyl-ACP thioesterases *FatA1, FatA2* in Arabidopsis. RNA was isolated from different tissues and semi-quantitative RT-PCR performed with gene specific primers for *FatA1*, *FatA2*, and for *actin*. The PCR products were separated on an agarose gel and stained with EtBr.

3.1.4 Functional Analysis of *FatA1* and *FatA2* in Arabidopsis

To identify the function of FatA1 and FatA2, Arabidopsis mutant plants with altered activity of the *FatA1* and *FatA2* genes were obtained from stock centers (T-DNA insertion lines) or generated by plant transformation (overexpression and RNAi lines). *FatA1* is composed of 7

exons with a 1086 bp coding sequence, which is located to chromosome 3. The *FatA2* gene comprising 6 exons and 5 introns is located to chromosome 4. The FatA2 coding sequence encompasses 1101 bp. The genomic sequences, including exons and introns of *FatA1* and *FatA2* are 2.2 kb long, as predicted by The Arabidopsis Information Resource (TAIR) database. The predicted protein (including the putative transit peptide) derived from *FatA1* is 362 and from *FatA2*, 367 amino acids long, with a calculated mass of 40.8 and 42.2 kDa, respectively.

3.1.4.1 Isolation of Null Mutants for *FatA1* and *FatA2*

To investigate the contribution by FatA1 and FatA2 to acyl-ACP hydrolysis in Arabidopsis, two independent T-DNA insertion lines were obtained. The relative positions of T-DNA insertions, the intron/exon structure of the *FatA1* and *FatA2* genes, as well as the position of primers are indicated in Figure 3.5 A.

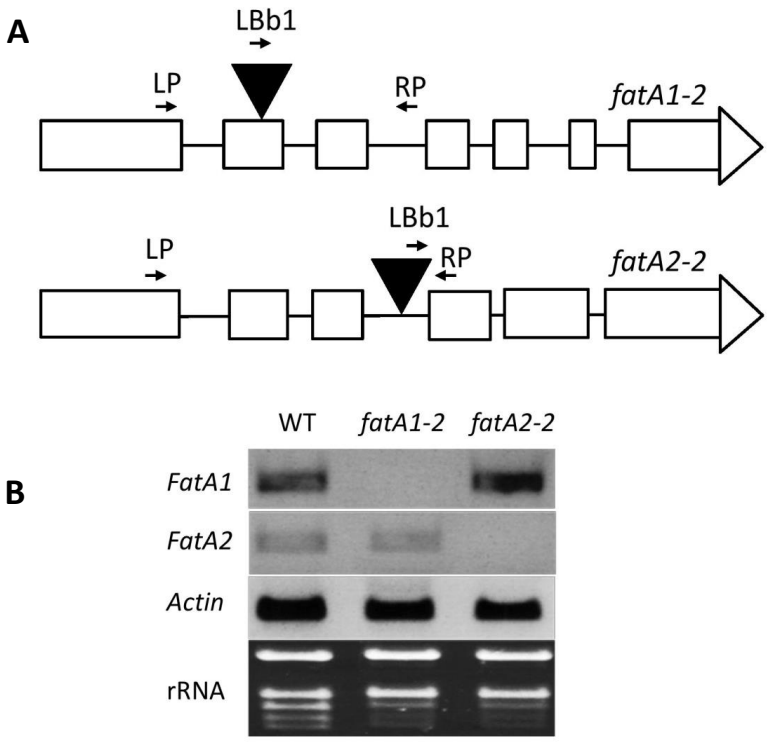

Figure 3.5: Isolaion of null mutants for *FatA1* and *FatA2*. (A) Schematic structure of the Arabidopsis *fatA1-2* and *fatA2-2* genes carrying the T-DNA insertions indicated by the triangles. The insertions in the *FatA1* and *FatA2* genes are located at positions 497 and 793 bp counting from the ATG translational start, respectively. **(B)** Expression analysis by semi-quantitative RT-PCR of Arabidopsis WT Col-0, *fatA1-2*, and *fatA2-2* plants. The PCR products were separated on an agarose gel and stained with EtBr. Total RNA was separated on a denaturing agarose gel and stained with EtBr.

Primers used for semi-quantitative RT-PCR are given in Table 3.2. PCR analysis with WT and homozygous T-DNA plants resulted in the amplification of only a gene-specific fragment or a gene/T-DNA insertion fragment, respectively. While PCR with DNA from heterozygous plants resulted in the amplification of both fragments. For the isolation of null mutants, primers RP and LP were designed to amplify a segment of specific size from the WT *FatA1* or *FatA2* allele,

whereas primers RP and LBb1 were designed to amplify segments of a defined size of the *FatA1*::T-DNA and *FatA2*::T-DNA alleles (Fig.: 3.5). Selected homozygous *fatA1-2* and *fatA2-2* plants were analyzed by semi-quantitative RT-PCR (Fig.: 3.5 B). RT-PCR analysis revealed that *fatA1-2* and *fatA2-2* mutants did not show residual gene expression for *FatA1* and *FatA2*, when primers were used that span the insertion site.

Table 3.2: Primers used for semi-quantitative RT-PCR.

Mutant	RP	LP	LBb1	T-DNA line
fatA1-2	PD687	PD686	PD188	WiscDcLox357F07
fatA2-2	PD649	PD648	bn142	GABI_822B01

3.1.4.2 Biochemical Characterization of *fatA1-2* and *fatA2-2* Mutants

The growth of homozygous *fatA1-2* and *fatA2-2* plants was indistinguishable from WT Col-0 (data not shown). As the two genes are highly expressed in seeds, the total fatty acid composition of the seeds was analyzed. 5 to 10 seeds for each line were employed for the FAME reaction and fatty acid composition was analyzed by GC. Seeds of the *fatA1-2* mutant show an elevated level of long to very long chain fatty acids. The amounts of 18:3, and 22:1 fatty acids are significantly increased, while the amount of $18:1^{\Delta 9}$ fatty acids is decreased by about 33 % compared Col-0 seeds. The *fatA2-2* mutant seeds show a fatty acid composition comparable to WT Col-0 (Fig.3.6).

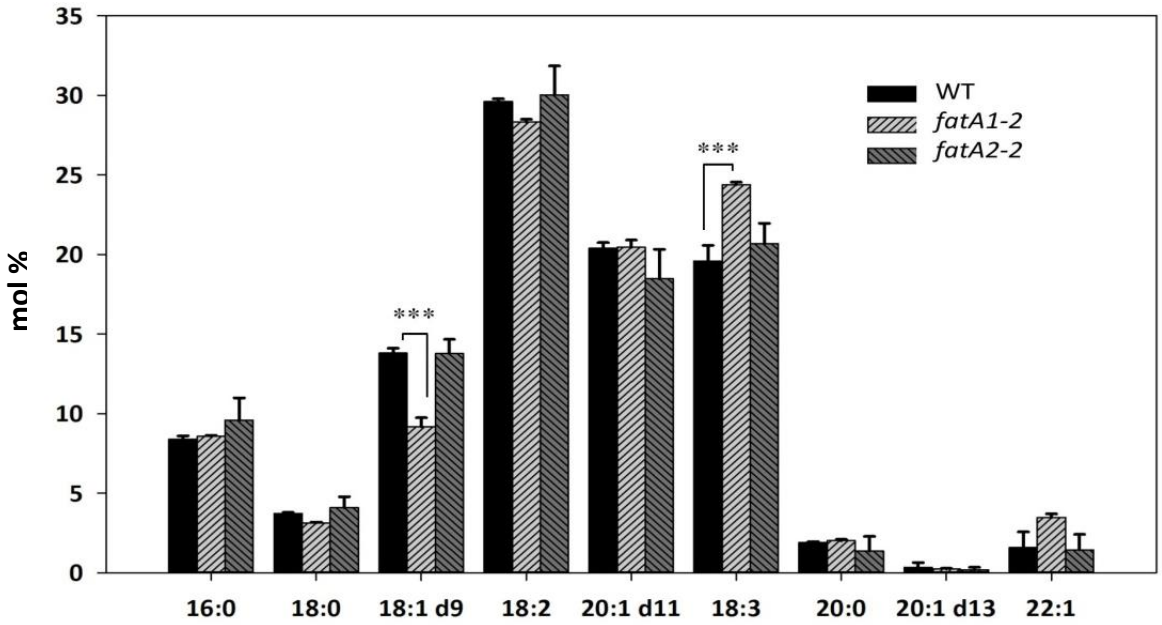

Figure 3.6: Fatty acid composition (mol %) of Arabidopsis WT, *fatA1-2*$^{-/-}$ and *fatA2-2*$^{-/-}$ mutant seeds. Data present means and standard deviations of four independent determinations. Asterisks indicate values that are significantly different from the control (according to Student's t test, Welch correction, $P<0.05$ (∗); $P<0.01$ (∗∗); $P<0.005$ (∗∗∗)).

The total fatty acid content of *fatA1-2* mutant seeds showed a decrease by about 20 %, while it remained unaltered in the *fatA2-2* mutant seeds (Fig.: 3.7 A). In order to assess the impact of the loss of *FatA1* or *FatA2* expression on the metabolic flux into storage oil, the DAG and TAG contents were determined in dry seeds of *fatA1-2* and *fatA2-2* mutants by Q-TOF MS/MS. Q-TOF MS/MS analysis revealed that the loss of *FatA1* or *FatA2* expression in Arabidopsis had a strong impact on seed TAG molecular species composition (Fig.: 3.7 C). Analysis of the molecular species composition of TAG showed a significant decrease in 18:3, 18:2, and 18:1 containing molecular species, and a concomitant increase in 22:1 and 20:1 molecular species (Fig.: 3.7 C). The total DAG content (Fig.: 3.7 B) and molecular species composition of the two single mutants was similar to WT seeds (data not shown).

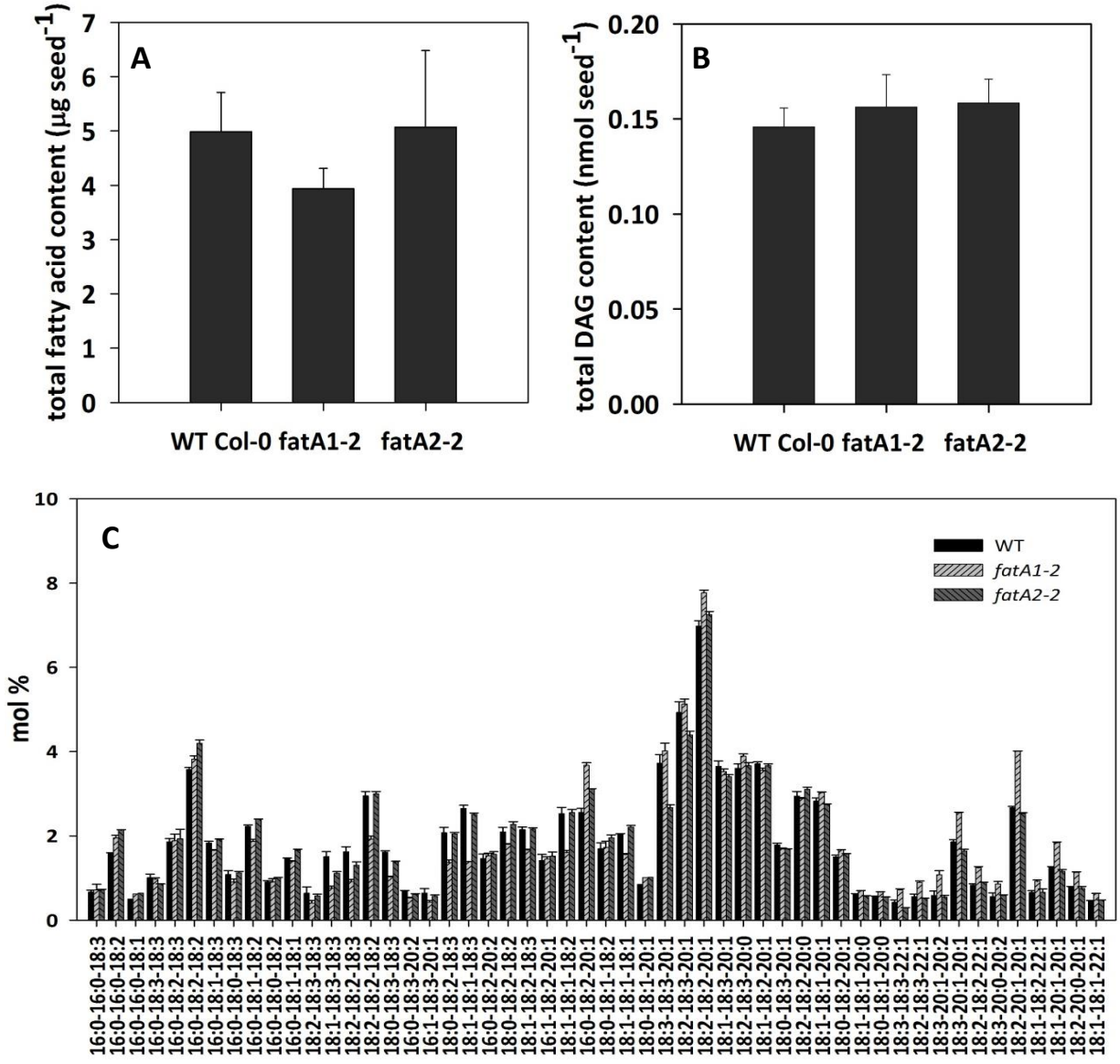

Figure 3.7: Lipid contents in seeds from Arabidopsis Col-0, *fatA1-2*, and *fatA2-2* mutants. (A) Total fatty acids measured by GC of methyl esters. **(B)** Total diacylglycerols (DAG). (C) Triacylglycerols (TAG) molecular species composition (mol %). For B and C lipids were extracted with diethylether/methanol and analyzed by Q-TOF MS/MS. Data present means and standard deviations of four independent determinations. Asterisks indicate values significantly different from the control (according to Student's t test, Welch correction, $P<0.05$ (∗); $P<0.01$ (∗∗)).

3.1.4.3 Molecular and Morphological Characterization of *fatA1-2 fatA2-2*

The fact that growth of the mutant plants was similar to WT was probably caused by functional redundancy of *FatA1* and *FatA2*. Therefore, the two single mutants were crossed (Svetlichnyy, 2007). *FatA1* and *FatA2* reside on different chromosomes, so plants harboring both T-DNA insertions were readily obtained. After several rounds of self-pollination and PCR-screening, only heterozygous/homozygous *fatA1-2*$^{+/-}$*fatA2-2*$^{-/-}$ or homozygous/heterozygous *fatA1-2*$^{-/-}$*fatA2-2*$^{+/-}$ mutants could be recovered, which was confirmed by PCR-analysis (Svetlichnyy, 2007). These results were confirmed in the present work (data not shown). According to Mendelian genetics, the progeny of a selfed *fatA1-2*$^{+/-}$*fatA2-2*$^{-/-}$ plant is expected to show a segregation ratio of 1:2:1 for *fatA1-2*$^{+/+}$*fatA2-2*$^{-/-}$: *fatA1-2*$^{+/-}$*fatA2-2*$^{-/-}$: *fatA1-2*$^{-/-}$*fatA2-2*$^{-/-}$. However, the observed segregation ratio was about 2:1:0 in the progeny of *fatA1-2*$^{+/-}$*fatA2-2*$^{-/-}$ (Fig.: 3.8). The same results were obtained after analysis of the progenies of *fatA1-2*$^{-/-}$*fatA2-2*$^{-/+}$ (data not shown).

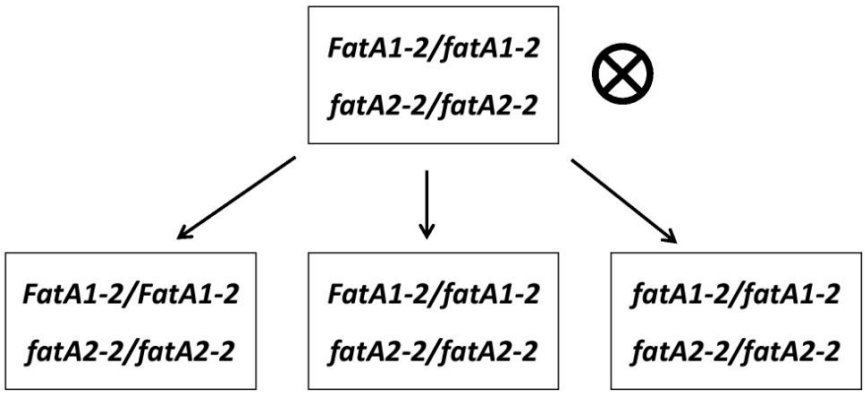

Theoretical ratio	1	2	1
Observed ratio (numbers)	327	158	0
Observed ratio (%)	67.5	32.5	0
Observed ratio	2	1	0

Figure 3.8: Segregation of *fatA1-2*$^{+/-}$*fatA2-2*$^{-/-}$ after self-pollination. Progeny was tested by PCR analysis.

3.1.4.4 Pollen Viability of *fatA1-2fatA2-2* Double Mutants

To assess pollen viability of heterozygous/homozygous *fatA1-2*$^{+/-}$*fatA2-2*$^{-/-}$ and homozygous/heterozygous *fatA1-2*$^{-/-}$*fatA2-2*$^{+/-}$ mutant plants, the pollen was stained according to Alexander (Alexander, 1969). Alexander staining turns viable pollen pink, whereas the non-viable pollen grains remain green or colorless (Fig.: 3.9).

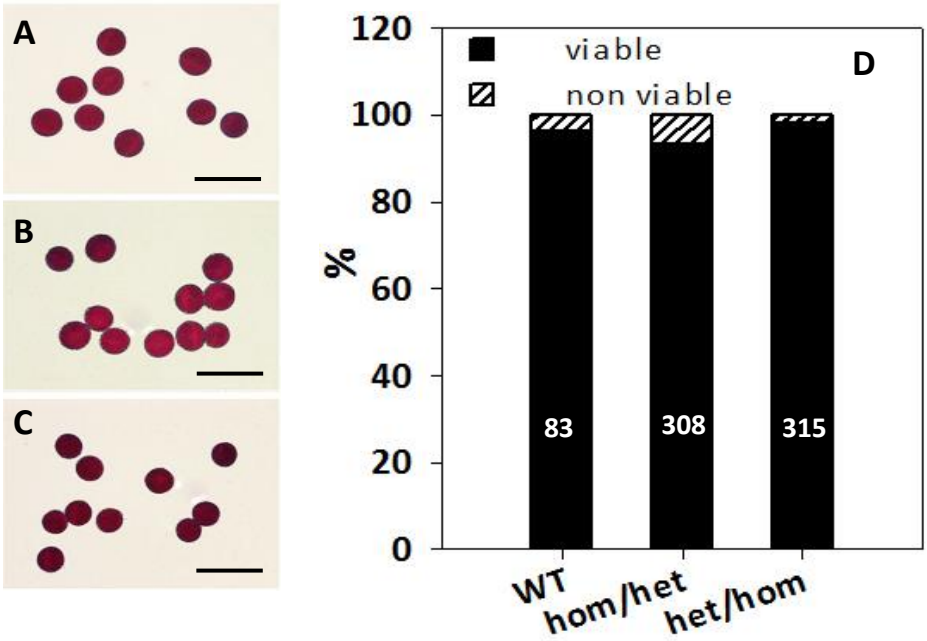

Figure 3.9: Ratio (%) of viable to non-viable pollen in WT and *fatA1-2fatA2-2* (hom/het - het/hom) anthers assessed by Alexander staining. (A) Pollen from WT Col-0 anther. **(B)** Pollen from *fatA1-2$^{-/-}$fatA2-2$^{+/-}$* anther **(C)** Pollen from *fatA1-2$^{+/-}$fatA2-2$^{-/-}$* anther. Pollen viability (purple-colored cytoplasm of pollen grains) is not significantly reduced in the *fatA1-2$^{+/-}$fatA2-2$^{-/-}$ or fatA1-2$^{-/-}$fatA2-1$^{+/-}$* mutant lines compared to WT Col-0. Scale bars 200 = µm. **(D)** Histogram showing the average number of viable pollen per anther in %. Numbers in bars correspond to numbers of analyzed pollen grains.

Both *fatA1-2$^{+/-}$fatA2-2$^{-/-}$* and *fatA1-2$^{-/-}$fatA2-2$^{+/-}$* double mutant lines were employed for pollen viability test. Mature pollen from WT plant showed approximately 4 % non-viable pollen. Based on the counting of viable and non-viable pollen no significant reduction in viability was found for *fatA1-2$^{+/-}$fatA2-2$^{-/-}$* and only a slight reduction in *fatA1-2$^{-/-}$fatA2-2$^{+/-}$* mutants in comparison to WT Col-0, indicating that the two mutations do not affect male gametogenesis (Fig.: 3.9). The high expression levels of *FatA1* and *FatA2* genes in siliques approximately 5 DAF suggested that these genes might play an essential role in the embryo development. The morphological characterization of the siliques of F1 plants derived from the cross of *fatA1-2* and *fatA2-2* confirmed the presence of abnormal F2 seeds (Fig.: 3.10 A). The F2 seeds were classified as normal or abnormal on the basis of morphological appearance. The ratio of normal seeds to abnormal seeds is approximately 3:1 (Fig.: 3.10 B). The fact that no double homozygous *fatA1-2$^{-/-}$fatA2-2$^{-/-}$* plants could be obtained and that 25 % of *fatA1-2$^{+/-}$fatA2-2$^{-/-}$* seeds were developing abnormal and were aborted in an early stage of the development, suggested that the simultaneous loss of the two *FatA* genes in Arabidopsis was embryo lethal and that the abnormal seeds might represent the missing double homozygous mutant seeds. For further analysis, the *fatA1-2$^{+/-}$fatA2-2$^{-/-}$* mutant line was selected.

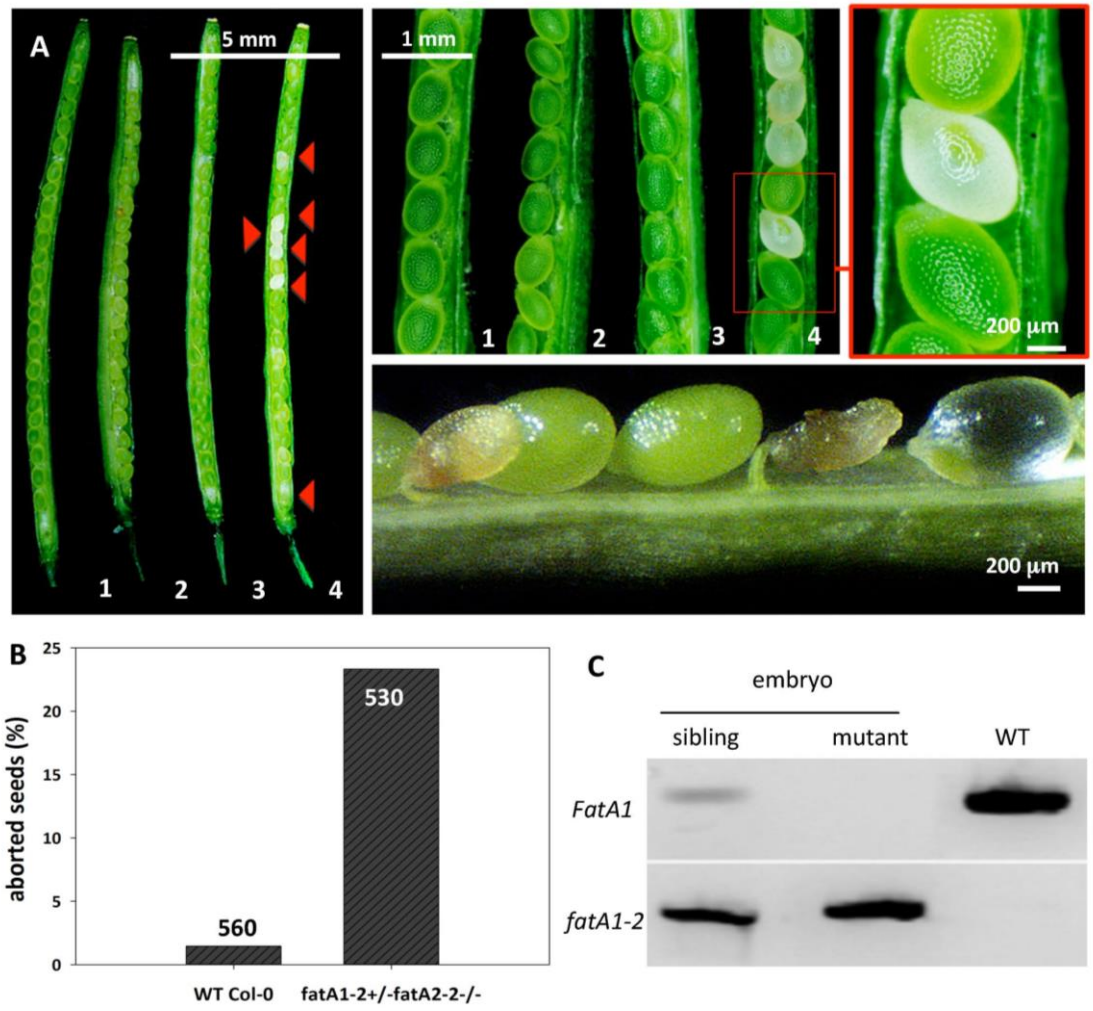

Figure 3.10: Morphological and molecular characterization of developing *fatA1-2*$^{+/-}$*fatA2-2*$^{-/-}$ seeds. (A) Siliques of *fatA1-2*$^{+/-}$*fatA2-2*$^{-/-}$ double mutant plants contained seeds, which were aborted in an early developmental stage. The single mutant lines did not show any alterations in seed development compared to WT. 1, WT Col-0; 2, *fatA1-2*; 3, *fatA2-2*; 4, *fatA1-2*$^{+/-}$*fatA2-2*$^{-/-}$. **(B)** Ratio (%) of intact to aborted seeds in *fatA1-2*$^{+/-}$*fatA2-2*$^{-/-}$ double mutants. Numbers on top of bars correspond to numbers of analyzed seeds. **(C)** Molecular analysis of genomic DNA isolated from aborted embryos from *fatA1-2*$^{+/-}$*fatA2-2*$^{-/-}$ siliques by PCR. Aborted embryos represented null mutants for the *FatA1 or FatA2* genes. The PCR bands depicted in the upper panel are specific for a *FatA1* genomic WT fragment, the lower lane for the *fatA1-2* mutation. Purified genomic WT DNA was used as control. The PCR products were separated on an agarose gel and stained with EtBr.

To confirm that the embryos in the abnormal seeds represent the double homozygous progeny of *fatA1-2*$^{+/-}$*fatA2-2*$^{-/-}$, on the genotype of the *FatA1* gene was analyzed by single-embryo PCR of genomic DNA. To this end, the embryos were cleanly dissected by the separation of the surrounding endosperm tissue and testa. PCR was performed using the Phire® Hot Start II DNA Polymerase (Thermo Fisher Scientific), which allows for the direct analysis of plant tissue. The single-embryo PCR was carried out with two primer pairs, LP and RP for the WT copy of the *FatA1* gene, and LBb1 and RP for the insertion of the *fatA1-2* mutation. Results from morphologically abnormal embryo and normal embryo revealed that the embryo from abnormal seeds was homozygous for the *fatA1-2* mutant gene, while the normally developing sibling embryos contained homozygous WT *FatA1* alleles (data not shown) or were heterozygous (*fatA1-2*$^{+/-}$) (Fig.: 3.10 C).

3.1.4.5 Histological Analysis of *fatA1-2$^{-/-}$fatA2-2$^{-/-}$* Double Mutant Embryos

The aborted seeds from *fatA1-2$^{+/-}$fatA2-2$^{-/-}$* siliques contained homozygous *fatA1-2$^{-/-}$fatA2-2$^{-/-}$* embryos, as shown above by PCR analysis. To investigate the developmental abnormalities associated with the homozygous *fatA1-2$^{-/-}$fatA2-2$^{-/-}$* mutations, developing seeds were examined by light microscopy after semi-thin sectioning(Fig.: 3.11).

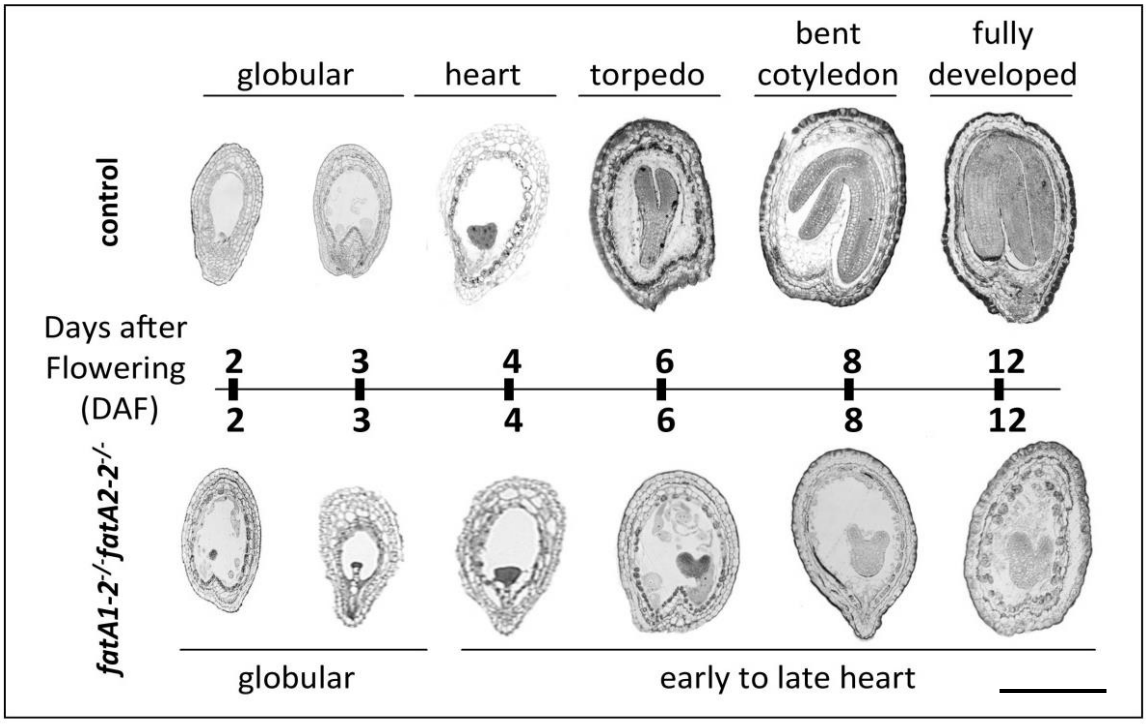

Figure 3.11: Histological analysis of developing embryos. Semi-thin-cross-sections through Arabidopsis mutant and control sibling embryos at different developmental stages. Toluidine blue staining of *fatA1-2$^{-/-}$fatA2-2$^{-/-}$* embryos revealed that the development was arrested at late heart stage when WT sibling embryos reached maturity in the same silique, DAF, days after flowering. Scale bar = 200 µm.

For histological analysis, flowers of *fatA1-2$^{+/-}$fatA2-2$^{-/-}$* mutants were tagged on the day of anthesis and siliques were collected at 2, 3, 4, 6, 8, and 12 DAF. Morphologically abnormal seeds harboring *fatA1-2$^{-/-}$fatA2-2$^{-/-}$* embryos were harvested, embedded in Technovit 7100 resin, cut into semi-thin sections and stained with toluidine blue. Analysis by brightfield microscopy revealed that *fatA1-2$^{-/-}$fatA2-2$^{-/-}$* embryo development was arrested at late heart to early torpedo stage (Fig.: 3.11). Morphologically abnormal seeds were compared with seeds of normal appearance from the same silique, further referred to as mutant sibling embryos. Mutant sibling embryos, either heterozygous (*fatA1-2$^{-/+}$*) or WT (*fatA1-2$^{+/+}$*) for the *FatA1* locus, reached the stage of a fully developed embryo within 12 DAF. The *fatA1-2$^{-/-}$fatA2-2$^{-/-}$* embryo development was indistinguishable from the sibling embryos until 4 to 5 DAF. After reaching late heart to early torpedo stage the *fatA1-2$^{-/-}$fatA2-2$^{-/-}$* embryo development was arrested until early abortion of the seed (Fig.: 3.11). While normal developing sibling embryos reached the

cotyledon stage approximately 6 DAF, the *fatA1-2*$^{-/-}$*fatA2-2*$^{-/-}$ embryo from the same silique reached the heart stage around 4 DAF. The same results were obtained by comparing embryos from abnormal seeds at 8 and 12 DAF to normal developing sibling embryos from the same silique. None of the analyzed *fatA1-2*$^{-/-}$*fatA2-2*$^{-/-}$ embryos progressed beyond the late heart to early torpedo stage of development.

3.1.4.6 Arabidopsis Embryo Lipid Content and Composition

Gas chromatography of methyl esters was employed to analyze the impact of the *fatA1-2*$^{-/-}$*fatA2-2*$^{-/-}$ mutations on the fatty pattern in comparison to WT embryos of either the same age or the same developmental stage. The fatty acid composition of WT embryos at different developmental stages, i.e. heart and torpedo stage as well as fully developed embryos was determined. To this end, lipids were extracted from embryo tissue, using 30 embryos for extraction of heart to torpedo stage embryos and 5 fully developed WT embryos. In the course of WT embryo development fatty acid composition changed from mostly medium (C12-C14) /long chain fatty acids (C16-C18) at heart stage to very long chain fatty acids (C20 and longer) in the fully developed embryo (Fig.: 3.12 A). In WT heart stage embryos, the saturated fatty acids palmitate (16:0) and stearate (18:0) made up the major components accounting for 30 % and 22 % of the total fatty acid content, respectively. The fatty acid profiles changed during embryo development. Torpedo stage embryos showed a shift from mostly saturated fatty acids to unsaturated fatty acids, comprising 18 % oleate (18:1) and 28 % linoleate (18:2). In the fully developed embryos, the polyunsaturated long chain fatty acids linoleate (18:2) and α-linolenate (18:3) were the major components with around 25 % and 24 %, respectively. There were also high amounts of gadoleate (20:1) accounting for approximately 20 % of the total fatty acids. Heart stage *fatA1-2*$^{-/-}$*fatA2-2*$^{-/-}$ embryos were compared to heart stage WT embryos and fully developed mutant sibling embryos collected from the same silique. Heart stage embryos of the *fatA1-2*$^{-/-}$*fatA2-2*$^{-/-}$ double mutant had an elevated level of long to very long chain fatty acids compared to heart stage WT embryos (Fig.: 3.12 B). In contrast, the amount of 16:1 and 18:0 fatty acids was drastically decreased in *fatA1-2*$^{-/-}$*fatA2-2*$^{-/-}$ embryos by about 70 % and 60 %, respectively. Contrary, the heart stage *fatA1-2*$^{-/-}$*fatA2-2*$^{-/-}$ embryos show a fatty acid pattern similar to torpedo stage in WT embryos. The fatty acid profiles of fully developed embryos of mutant siblings collected from the same silique were different compared to the double homozygous mutant embryos. The major fatty acids are mono- and polyunsaturated C18 fatty acids, with 30 % linoleate.

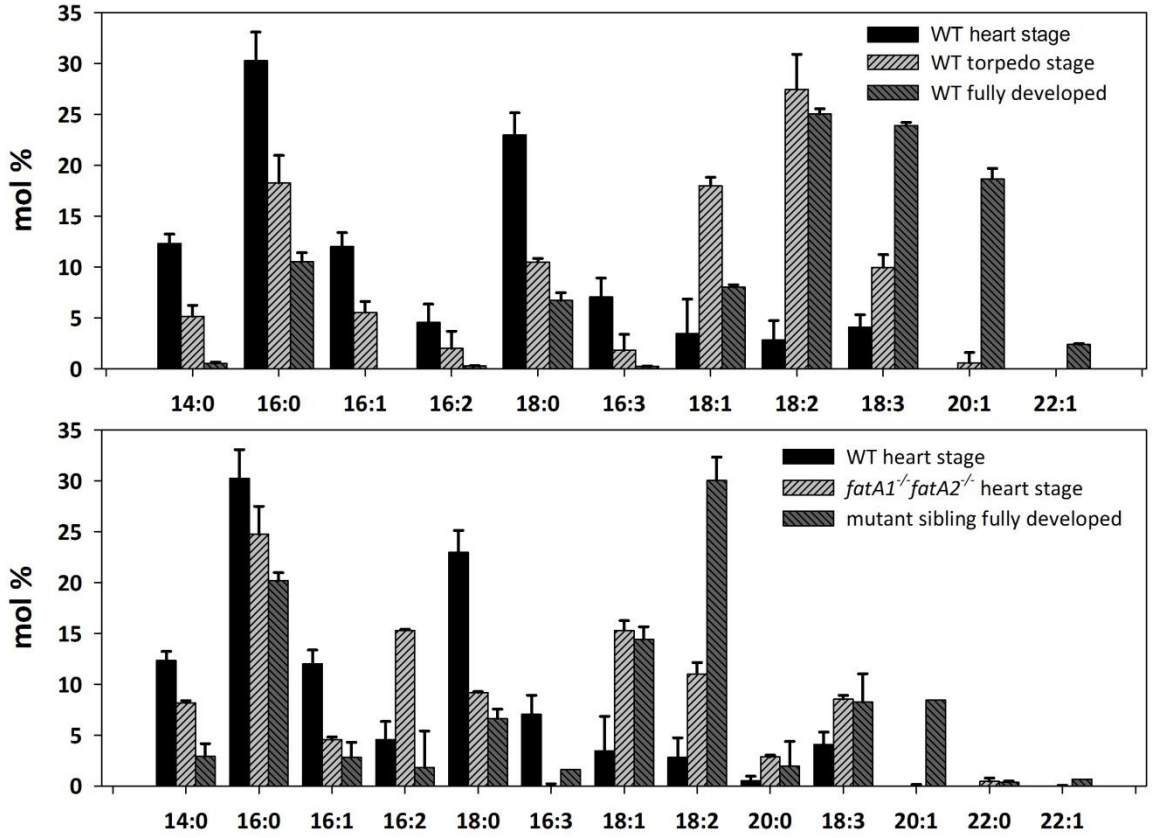

Figure 3.12: Fatty acid composition of Arabidopsis WT and *fatA1-2*$^{-/-}$*fatA2-2*$^{-/-}$ mutant embryos. (A) Fatty acid composition of WT embryos at different developmental stages. **(B)** Fatty acid composition of *fatA1-2*$^{-/-}$*fatA2-2*$^{-/-}$ embryos (heart stage) compared to WT (heart stage) and mature mutant sibling embryos isolated at the same age (fully developed stage). *fatA1-2*$^{-/-}$*fatA2-2*$^{-/-}$ embryos show a fatty acid pattern comparable to torpedo stage in WT embryos. Data present means and standard deviations of five independent determinations.

The glycerolipid composition of *fatA1-2*$^{-/-}$*fatA2-2*$^{-/-}$ embryos was determined by Q-TOF mass spectrometry. Arabidopsis Col-0 and the *fatA1-2*$^{-/-}$*fatA2-2*$^{-/-}$ embryos at heart stage were employed for lipid extraction using chloroform/methanol. Glycerolipids, comprising diacylglycerol and triacylglycerol as well as phospho- and glycolipids, were determined by Q-TOF MS/MS analysis. The contents of most phospholipids and glycolipids of WT Col-0 and *fatA1-2*$^{-/-}$*fatA2-2*$^{-/-}$ heart stage embryos were overall comparable with differences in total DGDG and SQDG content. The total amount of DGDG was significantly decreased by about 34 %, while the total SQDG content was increased by about 42 % in *fatA1-2*$^{-/-}$*fatA2-2*$^{-/-}$ embryos (Fig.: 3.13). The molecular species composition of SQDG was not altered compared to the WT (data not shown). In DGDG 16:0 and 18:2 containing molecular species were more abundant in the mutant embryos, while the content of 18:1 containing species were slightly decreased (data not shown).

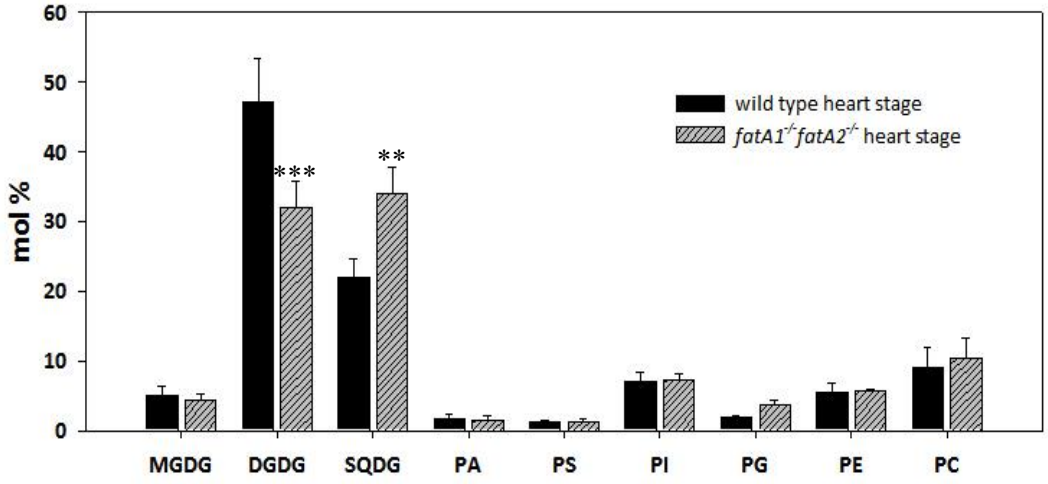

Figure 3.13: Phospho- and glycolipid content (mol %) in Arabidopsis embryos. Lipids from Arabidopsis WT and *fatA1-2*$^{-/-}$*fatA2-2*$^{-/-}$ heart stage embryos were analyzed by Q-TOF MS/MS. Data represent means and standard deviations of five independent determinations. Asterisks indicate values significantly different from the control (Student's t test, Welch correction, $P<0.05$ (∗); $P<0.01$ (∗∗); $P<0.005$ (∗∗∗)).

PE is exclusively synthesized outside the plastid. Hence, fatty acids incorporated into PE must be derived from the plastid after acyl-ACP hydrolysis by FatA or FatB activity. Therefore, PE can be employed as marker lipid to determine the export of fatty acids from the plastid. Accordingly, the PE content and its fatty acid composition was determined in WT and *fatA1-2*$^{-/-}$ *fatA2-2*$^{-/-}$ mutant embryos to analyze the incorporation of fatty acids from the plastids into PE. The total amount of PE is not altered compared to WT heart stage embryos. However, analysis of the PE molecular species composition in Arabidopsis WT embryos and *fatA1-2*$^{-/-}$*fatA2-2*$^{-/-}$ embryos at heart stage by Q-TOF MS/MS revealed an increase in 34:3 (16:0-18:3), and 36:6 (18:3-18:3) molecular species and a decrease in 36:4 (18:2-18:2) in *fatA1-2*$^{-/-}$*fatA2-2*$^{-/-}$ embryos (Fig.: 3.14).

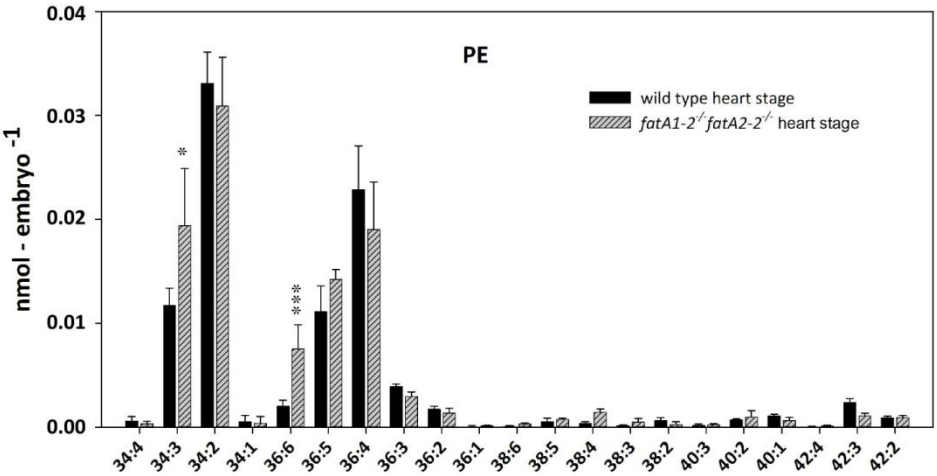

Figure 3.14: Phosphatidylethanolamine (PE) content (nmol - embryo^{-1}) in Arabidopsis embryos. Lipids from WT and *fatA1-2*$^{-/-}$*fatA2-2*$^{+/-}$ heart stage embryos were extracted with chloroform/methanol and analyzed by Q-TOF MS/MS. Data represent means and standard deviations of five individual determinations. Asterisks indicate values significantly different from the control (Student's t test, Welch correction, $P<0.05$ (∗); $P<0.01$ (∗∗); $P<0.005$ (∗∗∗)).

DAG is the main precursor for different glycerolipids, comprising galactolipids as well as PC and PE or TAG formation. To assess the impact of the loss of function of the two *FatA* genes on the metabolic flux into oil synthesis, the TAG and DAG contents were determined in developing WT Col-0 and *fatA1-2*$^{-/-}$*fatA2-2*$^{-/-}$ heart stage embryos (Fig.: 3.15). The total DAG and TAG contents were significantly increased in the *fatA1-2*$^{-/-}$*fatA2-2*$^{-/-}$ mutant line, while the molecular species composition was slightly different from Col-0 embryos. The differences in DAG species composition between the two embryos were mainly observed in molecular species containing 18:0, because all molecular species of DAGs that were decreased contained one or two 18:0 residues. By contrast, DAG species containing 16:1 or 18:1 acyl moieties were more abundant in the *fatA1-2*$^{-/-}$*fatA2-2*$^{-/-}$ mutant embryos. This tendency could also be observed for the TAG molecular species (appendix).

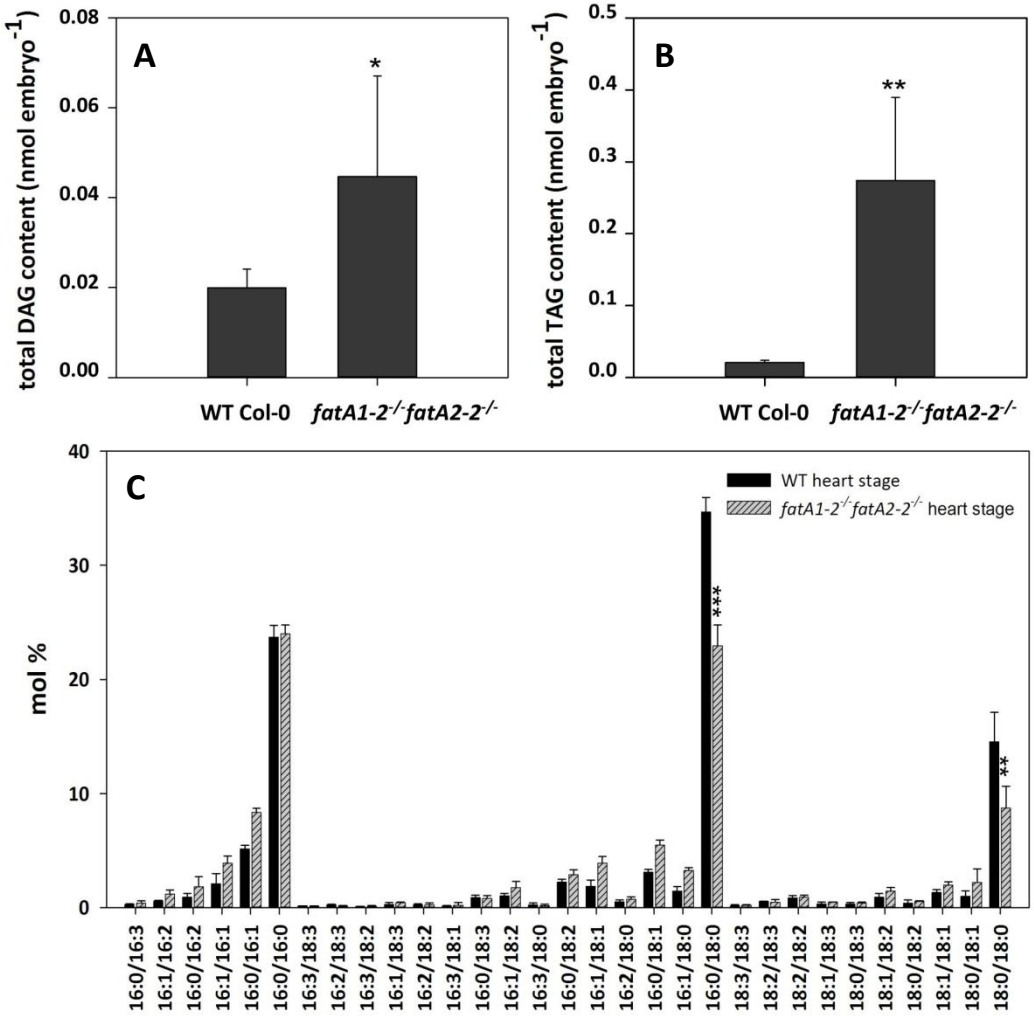

Figure 3.15: Lipid composition in Arabidopsis Col-0 and *fatA1-2*$^{-/-}$*fatA2-2*$^{-/-}$ heart stage embryos. (A) Total diacylglycerol (DAG) content. **(B)** Total triacylglycerol (TAG) content. **(C)** Diacylglycerol species composition (mol %) from WT and *fatA1-2*$^{-/-}$*fatA2-2*$^{-/-}$ heart stage embryos. Lipids were extracted with chloroform/methanol and analyzed by Q-TOF MS/MS. Data present means and standard deviations of five independent determinations. Asterisks indicate values significantly different from the control (according to Student's t test, Welch correction, $P<0.05$ (∗); $P<0.01$ (∗∗)).

Taken together, the total DAG and TAG contents were increased, and the fatty acid composition of the DAG molecular species in the *fatA1-2*$^{-/-}$*fatA2-2*$^{-/-}$ mutant embryos showed an elevated level in 18:1 and 16:1 fatty acids, while the content of 18:0 fatty acids was decreased. The fatty acid composition of the TAG molecular species remained mostly unaltered.

3.1.4.7 Reduction of FatA1 Transcription by RNAi in the *fatA2-2* Mutant

The homozygous single mutant lines for *fatA1-2* and *fatA2-2* did not show any alterations on the morphological level, and only minor differences in seed fatty acid composition, while the seed TAG content was significant reduced compared to WT. Because the analysis of the *fatA1-2*$^{+/-}$ *fatA2-2*$^{-/-}$ double mutant lines did not result in the identification of viable double homozygous mutant plants, downregulation by RNAi was employed.

3.1.4.7.1 Downregulation of *FatA1* Expression in *fatA2-2* Mutant Plants by RNAi

For RNAi Expression a modified pLH9000 vector (see Table 2.2), containing a 300 bp long *FatA1*-specific gene fragment in sense and antisense orientation, which shared no significant similarity with any other region in the Arabidopsis genome, was generated. Subsequently, the pL-*35S::FatA1*-RNAi-DsRed RNAi construct (Fig.: 3.16 A) was introduced into homozygous *fatA2-2*$^{-/-}$ mutants by *Agrobacterium* mediated transformation. Transgenic T_1 seeds were selected using the red fluorescence marker protein.

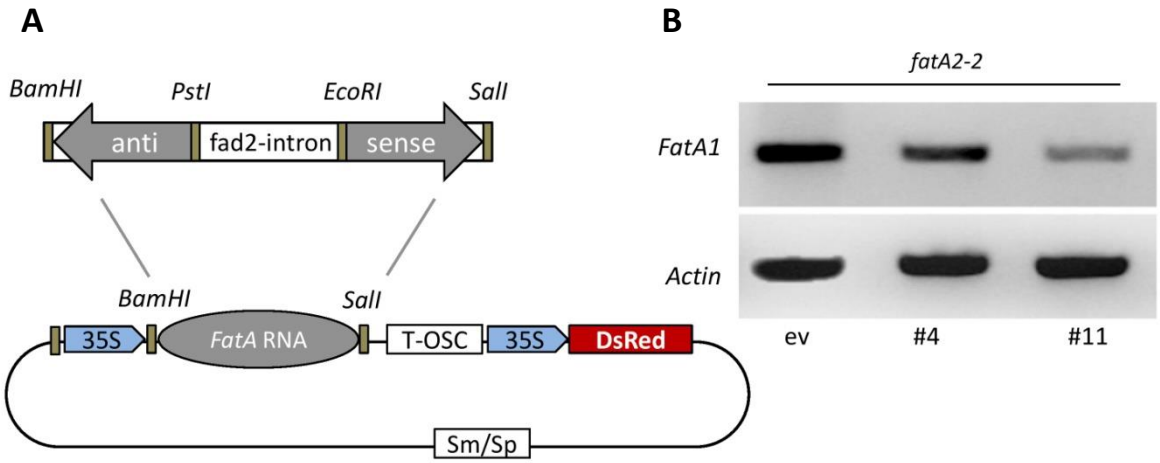

Figure 3.16: RNAi based downregulation of *FatA1* in *fatA2-2* mutant. (A) RNAi construct for *FatA1* transferred into the Arabidopsis *fatA2-2* mutant (B) Semi-quantitative RT-PCR analysis of FatA1-RNAi *fatA2-2*$^{-/-}$ plants. PCR analysis was performed using gene specific primers for *FatA1* and for *actin*. The PCR products were separated on an agarose gel and stained with EtBr.

Expression levels of *FatA1* in T_1 plants were determined by semi-quantitative RT-PCR (Fig.: 3.16 B). For this purpose, RNA was isolated from green siliques of Arabidopsis empty vector control and *fatA2-2*$^{-/-}$ mutants transformed with pL-*35S::FatA1*-RNAi-DsRed. RT-PCR was performed

with gene specific primers for *FatA1*, and the housekeeping gene *actin*. Thus, RNAi lines #4 and #11 were selected with a reduced transcription activity for *FatA1*, when compared to the empty vector control. RNAi line #11 showed a more severe reduction in *FatA1* transcript level than RNAi line #4 (Fig.: 3.16 B).

3.1.4.7.2 Characterization of Seed Lipids in *FatA1* RNAi *fatA2-2* Lines

In order to assess changes in seed lipid composition in the RNAi lines, 20 seeds, positive for the DsRed selection marker, of each line were employed for lipid extraction and FAME reaction. The analyzed RNAi lines did not show any alterations in seed lipid composition (data not shown), and only slight differences in the fatty acid pattern compared to WT control (Fig.: 3.17). While 16:0, 18:0, and 18:2 fatty acids were slightly decreased, the proportion of $18:1^{\Delta 9}$ is increased. The RNAi plants exhibited total fatty acid content similar to Arabidopsis control line (data not shown).

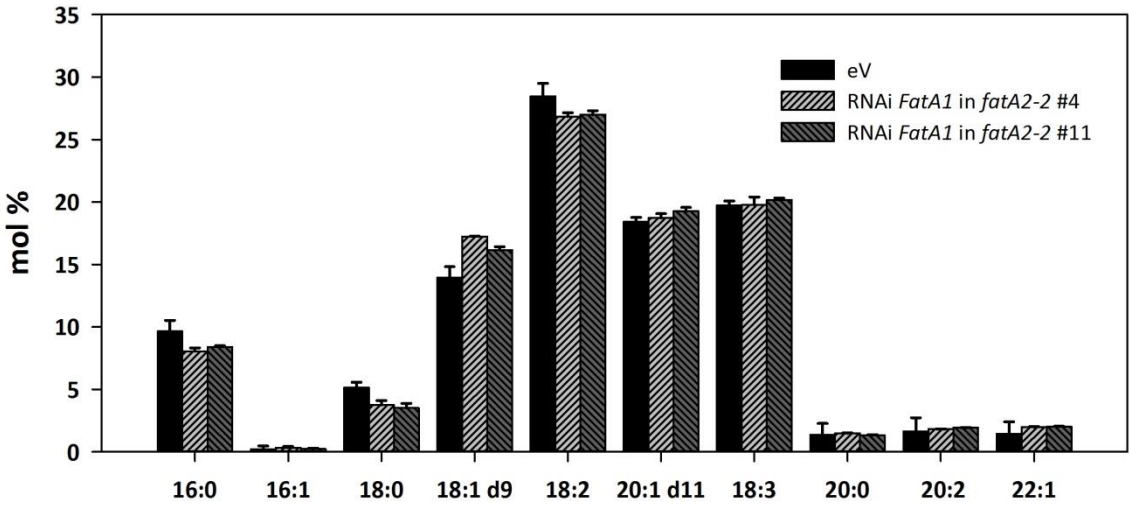

Figure 3.17: Fatty acid composition (mol %) of RNAi pants. Fatty acids of Arabidopsis WT and RNAi *FatA1* plants with *fatA2-2* background were isolated from seeds with chloroform/methanol extraction and analyzed by GC-FID. Data represent means and standard deviations of at least four independent determinations.

The analysis of TAG and DAG levels did not reveal alterations in molecular species composition in the seeds of RNAi lines (data not shown). Taken together, RNAi-based downregulation of *FatA1* in *fatA2-2*$^{-/-}$ mutant seeds had no detectable effect on seed lipid compostion. *FatA1* RNAi *fatA2-2*$^{-/-}$ plants did not show an increase in the number of aberrant seeds or a reduction in pollen viability (data not shown). This might be explained by the insufficient reduction in *FatA1* gene expression caused by RNA interference. The residual *FatA1* gene expression might be sufficient to provide enough enzymatic activity for normal growth and lipid biosynthesis.

3.1.4.8 Ectopic Expression of *FatA1* and *FatA2* in Arabidopsis

Gain-of-function lines can be used to analyze the function of genetically or functionally redundant genes, which can be members of the same gene families or whose function can be compensated for by alternative regulatory pathways. Overexpression of a gene driven by a strong promoter can result in gain-of-function phenotypes. In the strategy of this work full-length cDNA clones were used.

3.1.4.8.1 Analysis of Overexpression Lines for *FatA1* and *FatA2*

To further define the function of Arabidopsis *FatA1* and *FatA2*, *35S::FatA1* and *35S::FatA2* overexpression constructs were generated. To this end, *FatA1* and *FatA2* cDNAs were cloned in sense orientation, under the control of the 35S promoter and transformed into *A. tumefaciens* GV3101 cells. After transformation of Arabidopsis plants with the overexpression constructs, the T_1 seeds were selected using the red fluorescence marker protein. To select plants with increased expression of *FatA1* and *FatA2*, semi-quantitative RT-PCR was performed on siliques of T_1 plants. All analyzed transgenic plants showed an elevated level of *FatA1* and *FatA2* transcription in siliques in comparison to the empty vector control (Fig.: 3.18).

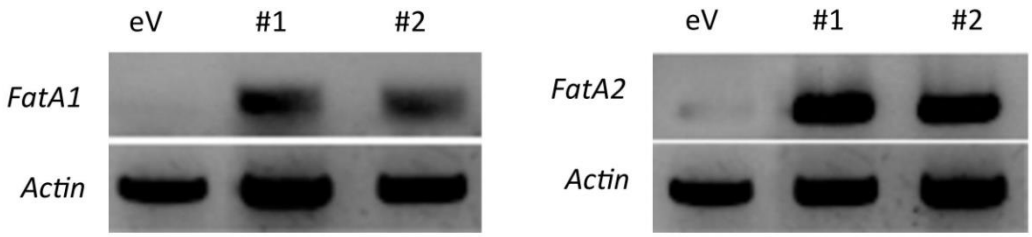

Figure 3.18: Semi-quantitative RT-PCR of Arabidopsis overexpression plants. RNA of the empty vector control (eV), *35S::FatA1* (*FatA1*), and *35S::FatA2* (*FatA2*) overexpression plants (#1 and #2) was extracted from siliques and RT-PCR was performed using gene specific primers for *FatA1*, *FatA2* and for *actin*. The PCR products were separated on an agarose gel and stained with EtBr.

3.1.4.8.2 Characterization of Seed Lipids in *FatA* Overexpression Lines

For fatty acid analysis of the *FatA1* and *FatA2* overexpression lines, 10-20 seeds of each line were employed for lipid extraction and FAME reaction. Total lipids were dissolved in 500 µL chloroform/methanol [2:1] and 375 µL of the extract were used for lipid quantification via Q-TOF MS/MS. The remaining extract was used for FAME synthesis and GC analysis. The overexpression lines did not show any differences in seed lipid composition or fatty acid pattern compared to the empty vector control (Fig.: 3.19). Only slight alterations in the overexpression *FatA2* #2 line were detected, showing increased levels in 16:0 and 18:0 fatty acids and a reduction in $20:1^{\Delta 11}$ fatty acids (Fig.: 3.19 B). Measurement of total DAG and TAG content as well as molecular species composition in the overexpression lines did not reveal alterations in

comparison to the empty vector control (data not shown). In summary, the seeds of overexpression lines were overall comparable to the control line on the morphological as well as the biochemical level. Therefore, increased *FatA1* or *FatA2* expression did not lead to a shift in the metabolic flux into oil in seeds. Furthermore, seed development of *FatA1* or *FatA2* overexpressing lines was not altered.

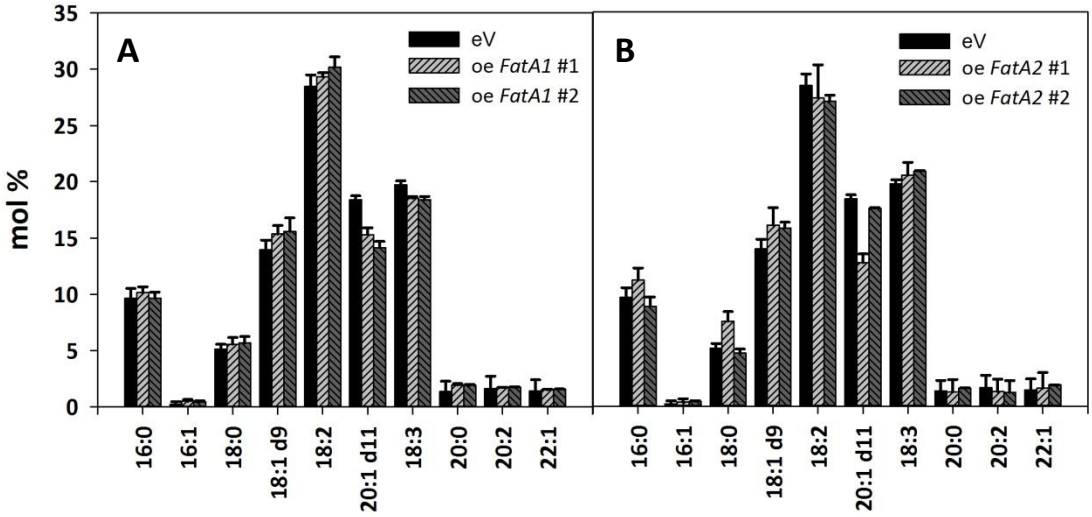

Figure 3.19: Seed total fatty acid composition of Arabidopsis overexpression lines. Lipids of Arabidopsis WT and *FatA1* (A) and *FatA2* overexpression lines (B) were isolated from dry seeds with chloroform/methanol and after transmethlyation, the fatty acid methyl esters were analyzed by GC. Data present means and standard deviations of at least four independent determinations.

3.1.4.9 Ectopic Expression of Different Acyl-ACP Thioesterases in *fatA1-2$^{+/-}$fatA2-2$^{-/-}$* Mutant Plants for Functional Complementation

The *fatA1-2$^{-/-}$fatA2-2$^{-/-}$* embryo development did not progress beyond late heart to early torpedo stage and embryos were aborted prematurely. In an attempt to restore FatA function during embryo development, the cDNA of Arabidopsis *FatA1* WT was introduced into the *fatA1-2$^{+/-}$fatA2-2$^{-/-}$* mutant line. Another approach included the rescue of the embryo lethal phenotype by the overexpression of the Arabidopsis *FatB* cDNA under the control of different promoters or the ectopic expression of the 12:0-ACP thioesterase from *Umbellularia californica* (UcFatB) in the *fatA1-2$^{+/-}$fatA2-2$^{-/-}$* mutant line.

3.1.4.9.1 Generation of Cloning Constructs for the Expression of Different Acyl-ACP Thioesterases

To corroborate if the embryo lethal phenotype caused by the *fatA1-2$^{-/-}$fatA2-2$^{-/-}$* mutation is caused by the loss of both *FatA* genes in Arabidopsis, overexpression constructs harboring acyl-ACP thioesterases with distinct substrate specificities from different organisms were introduced into Arabidopsis *fatA1-2$^{-/+}$fatA2-2$^{-/-}$* mutant plants (Table 3.3). The cDNAs were under the control of the 35S, glycinin, CvMV, or the native Arabidopsis *FatA1* promoter region (Table 3.4).

Table 3.3: Promoters used for functional complementation of *fatA1-2*$^{-/-}$*fatA2-2*$^{-/-}$ by the expression of acyl-ACP thioesterases with differences in substrate specificities.

Promoter	Expression type	Tissue
35S	constitutive	all tissues
glycinin	transient (mid seed maturity)	seed, embryo
CvMV	constitutive	all tissues
native *FatA1*	transient (early seed maturity)	seed, embryo

Table 3.4: Overexpression constructs used for complementation of *fatA1-2*$^{-/-}$*fatA2-2*$^{-/-}$ embryos

Gene	Organism	Substrate specificity	Expression construct	Promoter
FatA1	*Arabidopsis thaliana*	18:1-ACP	pL-*35S::FatA1*-DsRed	35S
FatB	*Arabidopsis thaliana*	16:0-ACP, 18:1-ACP	pL-35S::FatB-DsRed	35S
UcFatB	*Umbellularia californica*	12:0-ACP	pL-*35S::UcFatB*-DsRed	35S
FatA1	*Arabidopsis thaliana*	18:1-ACP	pBin-*gly::FatA1*-DsRed	glycinin
FatB	*Arabidopsis thaliana*	16:0-ACP, 18:1-ACP	pBin-*gly::FatB*-DsRed	glycinin
UcFatB	*Umbellularia californica*	12:0-ACP	pBin-*gly::UcFatB*-DsRed	glycinin
FatA1	*Arabidopsis thaliana*	18:1-ACP	pL-*CvMV::FatA1*-DsRed	CvMV
FatA1	*Arabidopsis thaliana*	18:1-ACP	pL-*proFatA1::FatA1*-DsRed	native *FatA1*
FatB	*Arabidopsis thaliana*	16:0-ACP, 18:1-ACP	pL-*proFatA1::FatB*-DsRed	native *FatA1*
UcFatB	*Umbellularia californica*	12:0-ACP	pL-*proFatA1::UcFatB*-DsRed	native *FatA1*

For cloning of the *FatA1* promoter, the sequence between stop codon of the 5' flanking gene to the start codon of *FatA1* (Fig.: 3.20) was introduced into pL-*35S::FatA1*-DsRed, replacing the 35S promoter, resulting in pL-*proFatA1::FatA1*-DsRed. Arabidopsis *fatA1-2*$^{-/+}$*fatA2-2*$^{-/-}$ mutant plants were transformed by agroinfiltration. Transgenic seeds were identified by their red fluorescence due to the DsRed marker gene in the overexpression constructs.

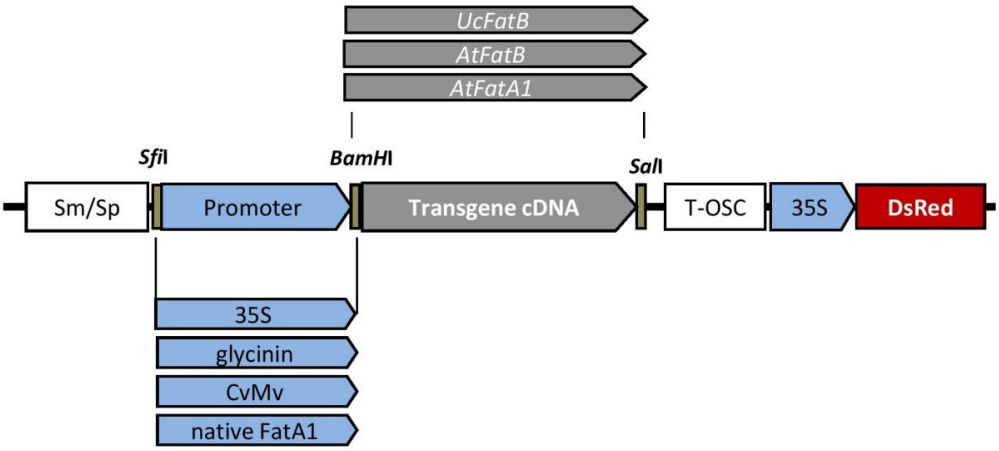

Figure 3.20: Diagram of constructs used for complementation. Complementation attempt of the embryo lethal *fatA1-2*$^{-/-}$*fatA2-2*$^{-/-}$ phenotype. The cDNAs were either under the control of the 35S, glycinin, CvMV, or the native FatA1 promoter.

3.1.4.9.2 Analysis of *fatA1-2$^{+/-}$fatA2-2$^{-/-}$* Mutants Expressing Acyl-ACP Thioesterases

Mutant plants expressing different acyl-ACP thioesterases were generated as described above and analyzed by PCR genotyping. *FatA1*, *FatB*, and *UcFatB* cDNAs under the control of the 35S promoter were introduced into *fatA1-2$^{+/-}$fatA2-2$^{-/-}$* mutant plants by agroinfiltration. Subsequently, around 300 plants of the T_0 to T_3 generation from over 15 independently transformed *fatA1-2$^{+/-}$fatA2-2$^{-/-}$* plants were tested by PCR analysis (data not shown). The expression of *FatA1*, *FatB*, and *UcFatB* cDNAs did not lead to a complementation of the embryo lethal phenotype of *fatA1-2$^{-/-}$fatA2-2$^{-/-}$*. A segregation still lacking the double homozygous genotype was observed in all cases. The same results were obtained after testing plants transformed with the *FatA1*, *FatB*, and *UcFatB* cDNAs under the control of the glycinin promoter or the *CvMV::FatA1* construct (data not shown).

Dry seed analysis of the *fatA1-2$^{+/-}$fatA2-2$^{-/-}$* mutant line harboring the *35S::FatA1* construct under the fluorescent binocular microscope revealed differences in shape and size compared to seeds of the WT control Col-0 (Fig.: 3.21).

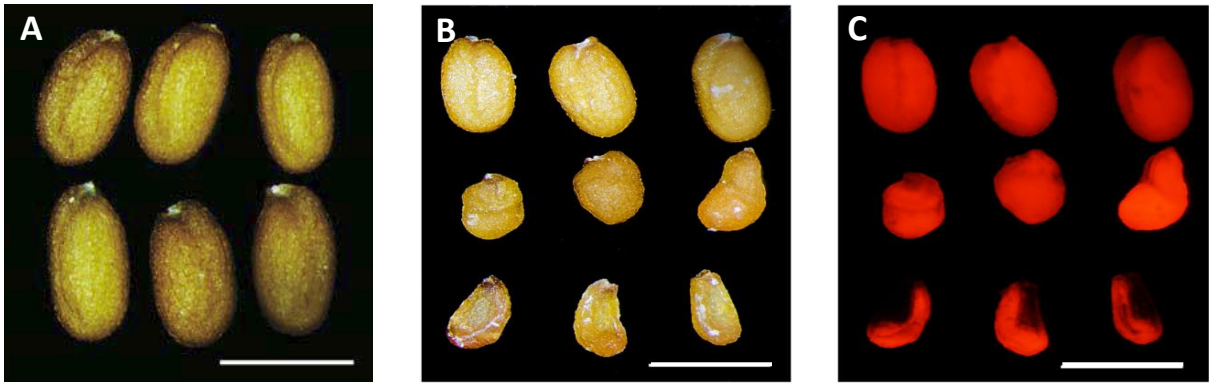

Figure 3.21: Microscopic analysis of Arabidopsis seeds expressing the *35S::FatA1* construct. (A) Bright field microscopy of dry Arabidopsis Col-0 seeds. **(B)** Bright field microscopy of dry *fatA1-2$^{+/-}$fatA2-2$^{-/-}$* mutant seeds expressing the *35S::FatA1* construct. The mutant line contained seeds comparable to Arabidopsis Col-0 (first lane), smaller and deformed seeds (second lane), and seeds harboring embryos arrested at late torpedo stage with a shriveled surface (third lane). **(C)** Mutant seeds showing red fluorescence of the DsRed marker after excitation with green light. Scale bars = 500 μm.

They segregated into three classes, WT like seeds, small and deformed seeds, and the third class of seeds contained embryos arrested at late torpedo stage with a shriveled surface. While the WT like seeds and the small/deformed seeds showed a germination rate comparable to WT (presumed genotypes *fatA1-2$^{+/-}$fatA2-2$^{-/-}$*, or *fatA1-2$^{+/+}$fatA2-2$^{-/-}$*), the seeds with arrested embryos were not able to germinate either on soil or synthetic growth medium (presumed genotype *fatA1-2$^{-/-}$fatA2-2$^{-/-}$*). The same results were obtained after analyzing the seeds of *fatA1-2$^{+/-}$fatA2-2$^{-/-}$* mutant plants transformed with the other acyl-ACP thioesterases under the control of different promoters listed in table 3.4 (data not shown).

Complementation approaches via the ectopic expression of different acyl-ACP thioesterases cDNAs under the control of either the 35S-, glycinin-, or CvMV-promoter (Table 3.4) did not lead to the identification of double homozygous *fatA1-2*$^{-/-}$*fatA2-2*$^{-/-}$ mutants in the progeny of *fatA1-2*$^{+/-}$*fatA2-2*$^{-/-}$ plants. On this account expression constructs were made under the control of the native promoter region of Arabidopsis *FatA1* and introduced into *fatA1-2*$^{+/-}$ *fatA2-2*$^{-/-}$ mutant plants by agroinfiltration. However, in the T_0 to T_3 generation no double homozygous *fatA1-2*$^{-/-}$*fatA2-2*$^{-/-}$ mutant plants could be dectected.

Glycerophosphodiester Phosphodiesterase

3.2 Biochemical and Molecular Characterization of GDPDs in Arabidopsis

In this study two *GDPD* genes, *GDPD5* and *GDPD6*, were characterized, with respect to their potential contribution to membrane lipid remodeling under Pi starvation in Arabidopsis.

3.2.1 Nucleic acid and Amino Acid Sequences of GDPDs from Different Organisms

The *GDPD5* gene comprises 8 exons and 7 introns, the full length genomic sequence is approximately 2628 bp long (including promoter and terminator sequences), and located to chromosome 1. The predicted coding sequence encompasses 1179 bp. The *GDPD6* gene comprising 7 exons and 6 introns, the full length genomic sequence is 1751 bp long (including promoter and terminator sequences), and located to chromosome 5. The predicted coding sequence encompasses 1119 bp. Sequence datasets were obtained from the TAIR database (http://www.Arabidopsis.org). Nucleotide sequences of *GDPD5* and *GDPD6* share 79 % identity (appendix). The first *GDPD* gene (*GlpQ*) was isolated from the *glp* regulon in *E. coli* (Larson et al., 1983). Since then, a high number of GDPDs have been characterized from different organisms including bacteria, fungi, plants, mammals, and human (Fig.: 3.22 B) (Tommassen et al., 1991; Zheng et al., 2003; Fernández-Murray and McMaster, 2005). Arabidopsis contains a family of GDPD with 6 sequences and a related gene family (GDPD like, GDPL) with 7 members (Cheng et al., 2011). Of the 6 GDPD family members, two proteins (*GDPD6*, At5g08030 and *GDPD5*, At1g71340) are highly related, and are the closest plant orthologs to the GDPD proteins from *E. coli* (glpQ) and man (MIR16). These two sequences share 74.5 % identity on amino acid level, and show an identity of 21-24 % and 16-17 % to glpQ and MIR16, respectively (Fig.: 3.22 A). GDPD4 (At1g71340) shows weaker similarity to glpQ and MIR16 and is more related to *E. coli* ugpQ, while the other three plant proteins (GDPD1, GDPD2, GDPD3) are even further diverse. Arabidopsis *GDPD4-6* also include a membrane-spanning region at the N-terminus before the *GDPD* domain.

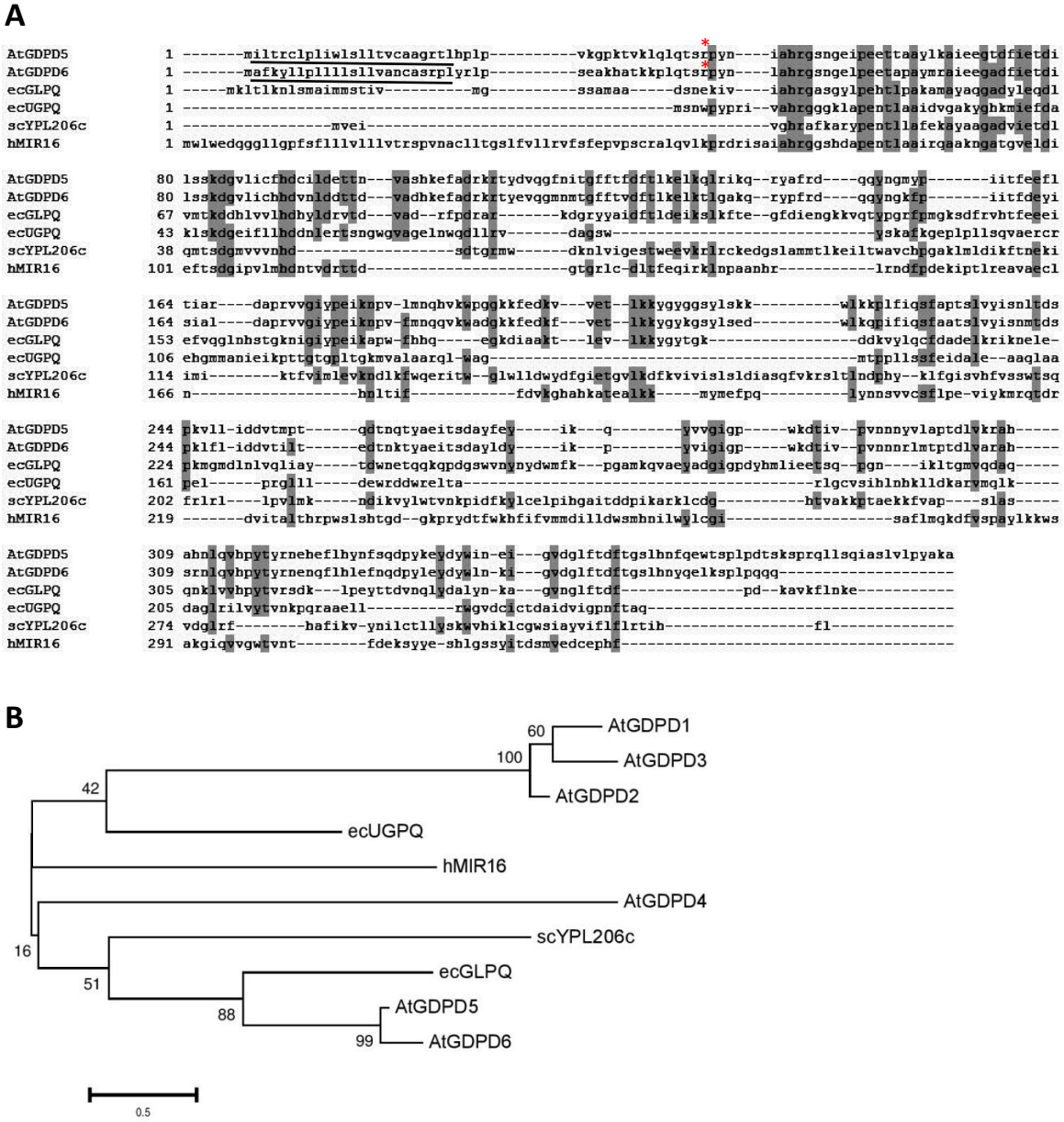

Figure 3.22: Multiple amino acid sequence alignment of GDPDs of plants, bacteria, yeast, and human. (A) Alignment of the deduced amino acid sequences of glycerophosphodiester phosphodiesterases from *Arabidopsis thaliana* (AtGDPD5, AtGDPD6), *Escherichia coli* (ecGLPQ, ecUDPQ), *Saccharomyces cerevisiae* (scYPL206e), and human (hMIR16). The predicted transemembrane domains for GDPD5 and GDPD6 are underlined and the cleavage sites for heterologous expression in *E. coli* are marked by red asteriks. The alignment was derived from the amino acid sequences comparison using CloneManager Scoring Matrix: Blosum62. **(B)** Unrooted phylogenetic tree showing the sequence relationships between glycerophosphodiester phosphodiesterase proteins from different organisms. The phylogenetic tree was derived from the amino acid sequences comparison using CloneManager Scoring Matrix: Blosum62 by the Neighbor-joining method. At, *Arabidopsis thaliana;* ec, *Escherichia coli;* sc, *Saccharomyces cerevisiae;* h, human.

3.2.2 Heterologous Expression of *GDPD5* and *GDPD6*

3.2.2.1 Expression of *GDPD5* and *GDPD6* in *E. coli*

For heterologous expression of *GDPD5* and *GDPD6*, the expression construct pQGDPD5oTMD or pQGDPD6oTMD, lacking the predicted GDPD transmembrane domain and the corresponding empty vector were introduced into *E. coli*. The removal of the putative

transmembrane domain by omitting 40 amino acids at the N-terminus (Fig.: 3.22 A) was intended to increase solubility of the recombinant proteins. *E. coli* cells harboring the *GDPD5* or *GDPD6* cDNAs as well as the empty vector were grown in LB medium at 37 °C to an OD_{600} at 0.8 and expression was induced with IPTG. Afterwards the cells were grown at 28 °C to an OD_{600} between 1.2 and 1.4, and harvested. Cells were ruptured, and soluble (supernatant) and insoluble (membrane pellet) protein fractions separated by centrifugation. Recombinant proteins could not be detected in the pellet fraction or in the supernatant containing the soluble protein fraction by SDS-page (data not shown). However, western blot analysis revealed recombinant protein bands in the pellet fraction but not in the supernatant. Strong bands for GDPD5 and GDPD6 were detected in Western blots while there was no signal in the empty vector control (Fig.: 3.23 A). Therefore, GDPD5 and GDPD6 were found to accumulate mostly as insoluble protein, presumably in the membranes or in inclusion bodies.

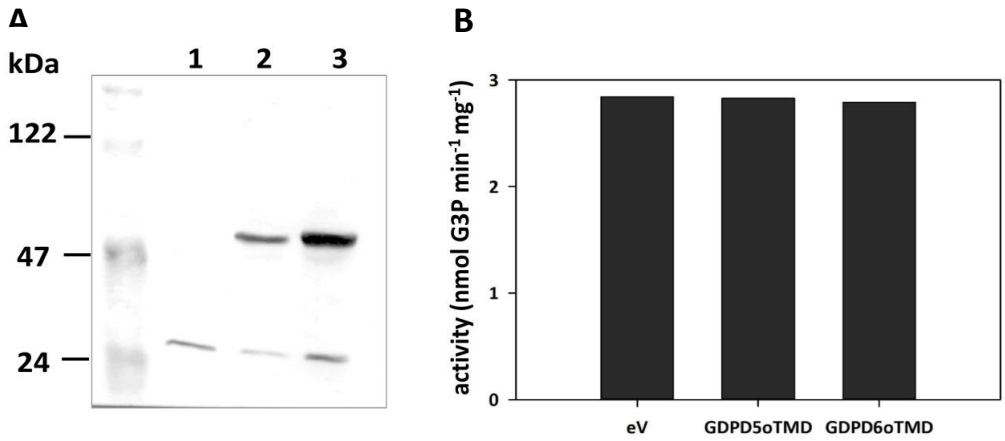

Figure 3.23: Expression of *GDPD5* and *GDPD6* in *E. coli*. (A) Western blot analysis of the crude protein extract from *E. coli* transformed with pQGDPD5oTMD and pQGDPD6oTMD, lacking the GDPD transmembrane domain, and the corresponding empty vector control. 1, empty vector; 2, GDPD5oTMD; 3, GDPD6oTMD. **(B)** Enzyme activity of GDPD5 and GDPD6 heterologously expressed in *E. coli*. Insoluble protein extracts (2 mg protein) from recombinant *E. coli* cells expressing Arabidopsis *GDPD5*, *GDPD6* (without N-terminal transmembrane domain), and the empty vector control were incubated with GPC for 60 min at 30 °C. G3P content was measured by an enzyme coupled spectrophotometric reaction using GPDH. No differences in GDPD activity could be detected compared to the empty vector control.

Enzyme activity of GDPD5 and GDPD6 was determined via an enzyme coupled spectrophotometric assay using GPDH. The empty vector control and the recombinant *GDPD5* and *GDPD6* strains showed comparable enzyme activity, most probably derived from *E. coli* GlpQ and UgpQ enzymes. Approximately 3 nmol min^{-1} mg^{-1} protein G3P was synthesized for each strain during the reaction (Fig.: 3.23 B).

3.2.2.2 Expression of *GDPD5* and *GDPD6* DsRed-Fusion Constructs in *E. coli*

Another strategy to avoid the accumulation of insoluble proteins was the expression of *GDPD5* or *GDPD6* DsRed-fusion constructs to increase solubility of the recombinant proteins. *E.*

coli cells were transformed with the expression constructs pLW01-DsRed-GDPD5oTMD and pLW01-DsRed-GDPD6oTMD, lacking the transmembrane domain, and the empty vector (Fig. 3.24 A). While the fusion with the highly soluble DsRed protein was anticipated to increase the solubility, the recombinant DsRed-GDPD fusion proteins could not be detected by Western blot analysis in the soluble protein fraction (data not shown). In contrast, the recombinant GDPD5 and GDPD6 DsRed fusion proteins were only detectable in the insoluble membrane protein fraction (data not shown). Enzyme activities of the insoluble membrane fractions were comparable to the empty vector control. The activity was ca. 2 nmol of G3P min^{-1} mg^{-1} of membrane protein (Fig.: 3.24 B).

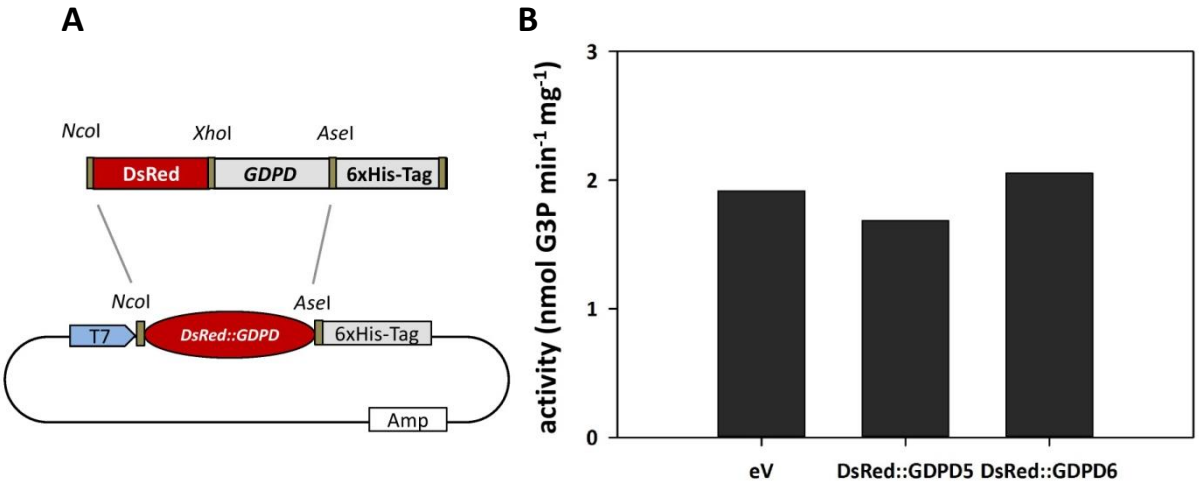

Figure 3.24: Enzyme activity of GDPD5 and GDPD6 DsRed fusion proteins heterologously expressed in *E. coli*. **(A)** DsRed fusion construct used to transform *E. coli* BL21Lys cells. The constructs harbor an N-terminal DsRed sequence in translational fusion with the GDPD5 or GDPD6 sequence lacking the N-terminal putative transmembrane domain. **(B)** Glycerophosphodiester phosphodiesterase activities. Enzyme assays with insoluble protein fractions (2 mg protein) from recombinant *E. coli* cells expressing Arabidopsis GDPD5, GDPD6 DsRed fusion proteins, and the corresponding empty vector were done by incubation with GPC for 60 min at 30 °C. G3P content was measured by an enzyme coupled spectrophotometric reaction using GPDH. No differences in G3P production could be detected compared to the empty vector control.

3.2.2.3 Transient Expression of *GDPD5* and *GDPD6* in *N. benthamiana*

Because recombinant GDPD5 or GDPD6 proteins were inactive after heterologous expression in *E. coli*, a plant expression system was used. The transient expression of cDNAs using agroinfiltration is a fast and simple method to study protein function (Kapila et al., 1997; Rossi et al., 1993). To this end, expression constructs under the control of the CaMV 35S-promoter (pL-*35S::GDPD5*-DsRed and pL-*35S::GDPD6*-DsRed) were introduced into *N. benthamiana* leaves by agroinfiltration. The empty vector was used as control. The proteins of the leaves were extracted at six days post infiltration (6 dpi) and protein concentration was measured by BCA analysis. Expression levels were estimated using the DsRed marker protein (Fig.: 3.25). Highest red fluorescent signal in *N. benthamiana* leaves was detected at 6 dpi. Only areas showing a bright red fluorescence signal were employed for protein extraction.

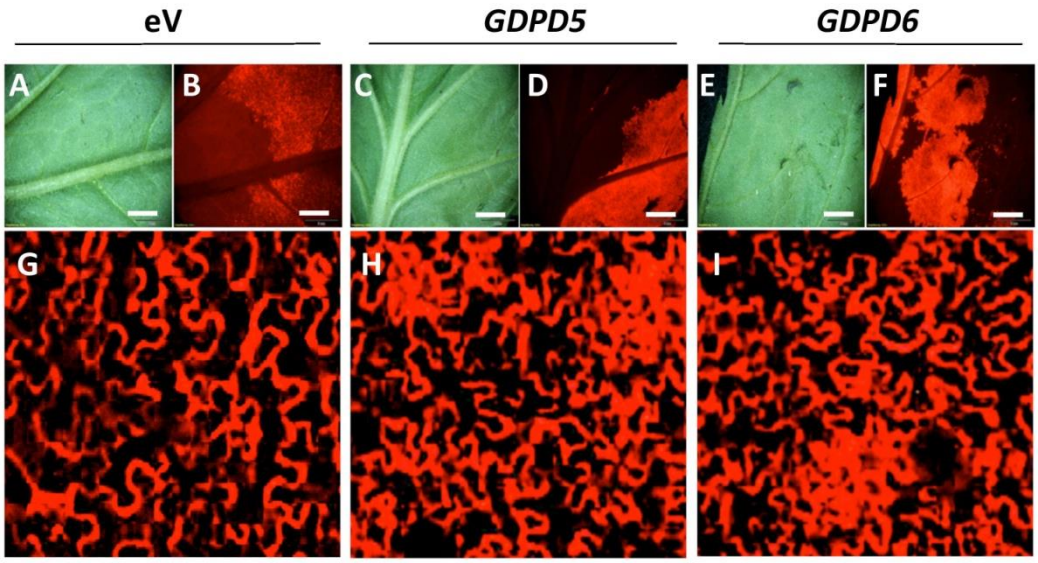

Figure 3.25: Transient expression of *GDPD5* and *GDPD6* in *N. benthamiana*. Arabidopsis *GDPD5* and *GDPD6* (full-length cDNAs including the N-terminal putative transmembrane domains) under the control of the 35S promoter were transiently expressed in *N. benthamiana* by Agrobacterium-mediated transformation. Proteins were isolated at highest level of DsRed expression after 6 days of incubation. **(A, C, E)** Bright field and **(B, D, F)** fluorescent microscopy of the empty vector control, *GDPD5*, and *GDPD6 constructs*, respectively. *A. tumefaciens* infiltrated parts show DsRed expression and were employed for protein isolation. (G-I) Enlargements of the area with DsRed expressing epidermal cells of the empty vector control, *GDPD5*, and *GDPD6*, respectively. Scale bars = 2 mm. G-I optical zoom function using Adobe Photoshop.

Enzyme activities of *GDPD5* and *GDPD6* were analyzed via an enzyme coupled spectrophotometric assay using GPDH. The calibration curve of G3P measured spectrophotometrically was linear over a range from 2 to 8 mM with a square correlation coefficient (R^2) of 0.98290, indicating a good fit to the regression line (Fig.: 3.26).

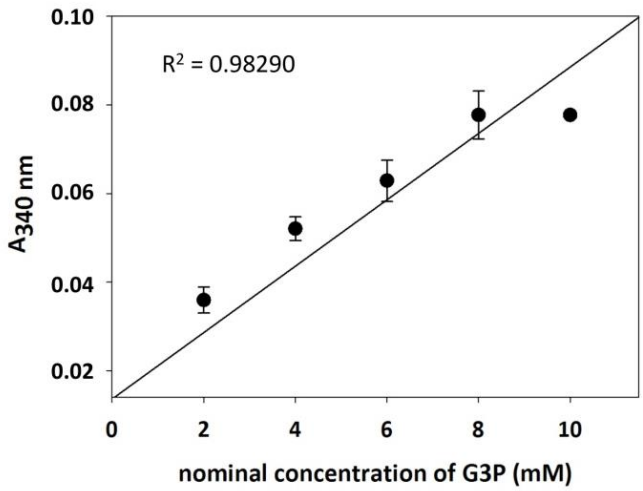

Fig. 3.26: Nominal concentrations of G3P measured by spectrophotometric method. The absorbance change using different concentrations of G3P was measured by an enzyme-coupled spectrophotometric reaction using 10 U GPDH (Sigma) dissolved in hydrazine-glycine buffer without NAD. R^2, square correlation coefficient. Data present means and standard deviation of three independent determinations.

The activity of the transiently expressed GDPD5 and GDPD6 proteins was up to 20 fold higher compared to the empty vector control (Table: 3.5). Therefore, the two GDPD proteins can be expressed in *N. benthamiana* leaves in an active form.

Different parameters were tested for optimal assay conditions. First, the dependence of GDPD5 and GDPD6 enzyme activity on divalent cations was analyzed. To this end, the assay was performed with 1 mg of *N. benthamiana* leaf membrane protein fraction in the presence of Mg^{2+}, Ca^{2+}, and without divalent cations using GPC as substrate. Incubation was done for 45 min at 30 °C. GDPD5 and GDPD6 enzyme activities were shown to be independent from divalent cations, because the activities of GDPD5 and GDPD6 were comparable in the presence of Mg^{2+}, Ca^{2+}, or the complete absence of Mg^{2+} or Ca^{2+} (Table: 3.5).

Table 3.5: Transient expression of *GDPD5* and *GDPD6* in *N. benthamiana* revealed glycerophosphodiester phosphodiesterase activity independent from divalent cations. Data present means and standard deviations of five independent determinations.

		Activity (nmol • min^{-1} • mg^{-1})		
Enzyme	**Substrate**	**Mg^{2+}**	**Ca^{2+}**	**w/o**
control	GPC	**0.092** ± 0.017	**0.043** ± 0.016	**0.068** ± 0.030
GDPD5	GPC	**1.087** ± 0.036	**0.970** ± 0.048	**0.869** ± 0.090
GDPD6	GPC	**0.682** ± 0.020	**0.764** ± 0.027	**0.580** ± 0.012

Next, different protein concentrations as well as incubation times were tested using GPC as substrate (Fig.: 3.27). Highest substrate conversion of approximately 1.7 nmol per min for GDPD5 and 1.2 for GDPD6 was obtained using 1 to 2 mg of membrane protein fraction from *N. benthamiana*. The time course experiment for the GDPD enzyme reaction is important for the determination of the appropriate incubation time. 2 mg enzyme and 0.5 mM substrate were incubated for various times at 30 °C. The enzyme activity was found to be linear up to a 45 min incubation time (Fig.: 3.27 B).

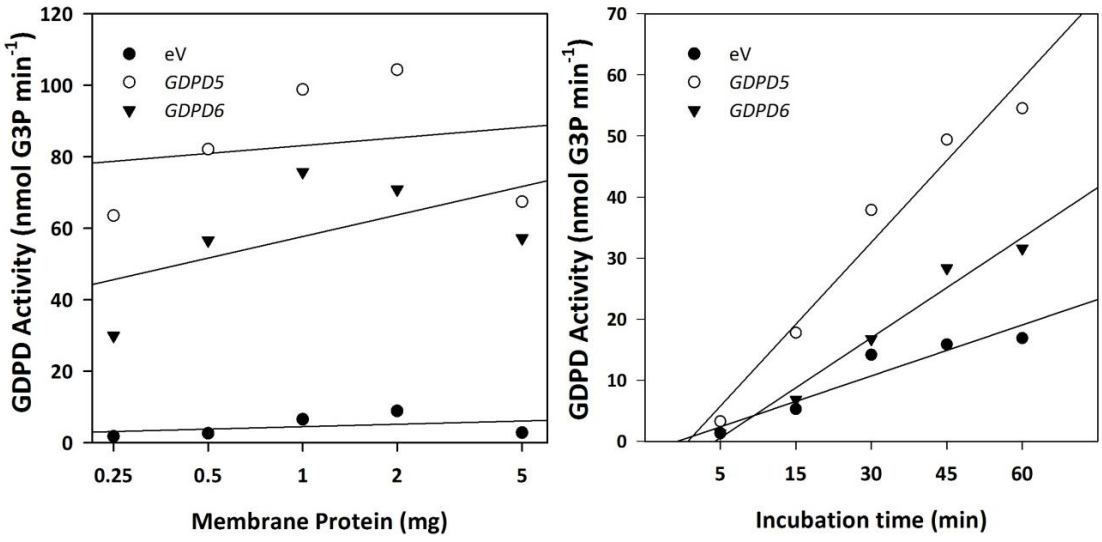

Figure 3.27: Assay conditions for optimal enzyme activity of GDPD5 and GDPD6 after transient expression in *N. benthamiana.* (A) Variation in protein concentrations between 0 mg to 5 mg mL^{-1} reaction. **(B)** Incubation times between 5 min to 60 min at 30 °C and 2 mg of protein were tested.

With regard to the assay sensitivity, the incubation time selected should be in the linear portion of the time course curve with sufficiently high signal Enzyme activity is generally higher when substrate concentration is not limited. Thus, an incubation time of 45 min at 30 °C was selected as optimal assay conditions when 0.5 mM GPC was used as substrate.

To assess substrate specificities of Arabidopsis GDPD5 and GDPD6, enzyme assays were perfomed using different GPCs, including GPC, GPE, GPI, GPS, and GPG (Fig.: 3.28). Substrates were obtained by hydrolyzing the respective phospholipids after mild alkaline hydrolysis. The assay was perfomed using a Mg^{2+} as well as Ca^{2+} containing assay buffer, 1 mg of the *N. benthamiana* membrane protein fraction, and an incubation time of 45 min. As shown in Fig. 3.28, GDPD5 and GDPD6 exhibit preference for GPC and GPE. Approximately 0.25 nmol and 1.8 nmol G3P min^{-1} mg^{-1} protein from GPC hydrolyzation was formed by GDPD5 and GDPD6, respectively. This was approximately 30 % above the levels of GPE hydrolyzation.

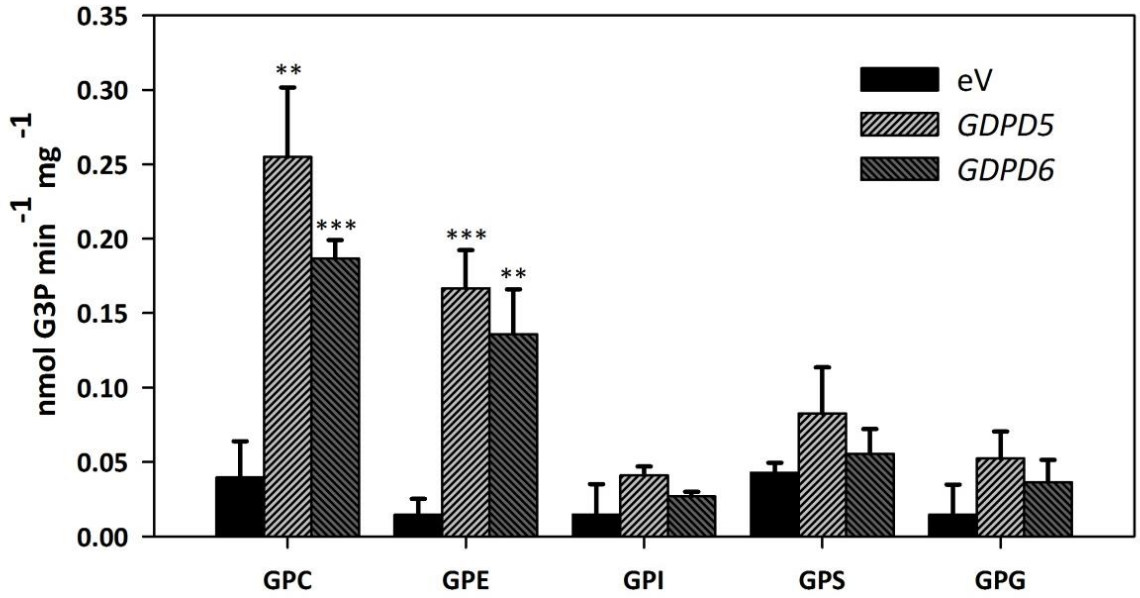

Figure 3.28: Substrate specificities of GDPD5 and GDPD6 after transient expression in *N. benthamiana*. Enzyme activities were measured using five different substrates, GPC, GPE, GPI, GPS and GPG (glycerophosphocholine, -ethanolamine, -inositol, -serine, -glycerol, respectively). GDPD5 and GDPD6 exhibit preference for GPC and GPE. Data present means and standard deviations of five independent determinations. Asterisks indicate values that are significantly different from the control (according to Student's t test, Welch correction, $P<0.05$ (∗); $P<0.01$ (∗∗); $P<0.005$ (∗∗∗)).

3.2.2.4 Protein Complementation Assay for *GDE1* in *S. cerevisiae*

Arabidopsis *GDPD5* and *GDPD6* were heterologous expressed in the *gde1*Δ *S. cerevisiae mutant*. *GDE1*, representing the sole glycerophosphodiester phosphodiesterase in yeast, is required for the utilization of GPC as its unique source of phosphate. The WT strain of *S.*

cerevisiae is able to use GPC as sole phosphate source but deletion of *GDE1* repealed that ability. Different yeast *gde1*Δ mutant strains harboring the yeast overexpression constructs pDRGDPD5 or pDRGDPD6, or the corresponding empty vector control, were grown in medium lacking a phosphate source, harvested and resuspended in water. Serial dilutions were made for each cell suspension and spotted onto plates containing either no source of phosphate, 200 μM KH_2PO_4 or 200 μM GPC. All strains tested were not able to utilize GPC as sole source of phosphate. It was expected that the *gde1*Δ mutant would not be able to grow on media lacking either KH_2PO_4 or GPC, while the WT as well as the *gde1*Δ mutant complemented with either *GDPD5* or *GDPD6* from Arabidopsis would be able to utilize GPC as phosphate source (Fig.: 3.29). The lack of growth of any of the strains might be due to the growth conditions, lacking uracil (selection marker) and phosphate. For optimal results different growth conditions should be applied.

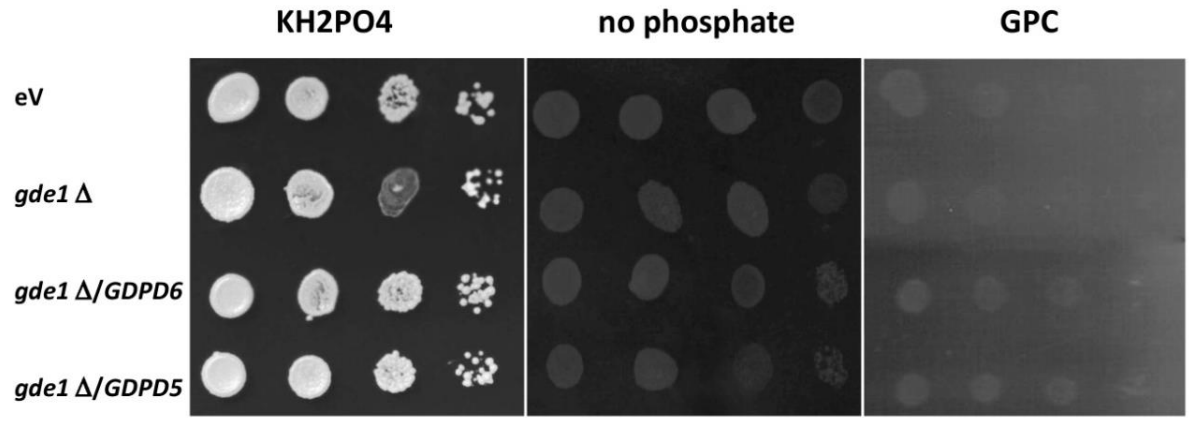

Figure 3.29: Protein complementation assay for GDPD in *S. cerevisiae*. Strains pre-grown for several hours in medium lacking a phosphate source were harvested and suspended to equivalent cell densities in water. Three 10-fold serial dilutions were made for each cell suspension and spotted onto plates containing no source of phosphate, 200 μM KH_2PO_4 or 200 μM GPC.

3.2.3 Subcellular Localization of GDPD5 and GDPD6 Proteins

In silico studies using the subcellular localization program WOLF PSort Horton (Horton et al., 2007) revealed that GDPD5 is predicted to be extracellular or located to the cell wall, followed by prediction of mitochondrial and nuclear localization, while targeting to the extracellular space was predicted for GDPD6 (Table 3.6).

Table 3.6: Predicted subcellular localization of GDPD5 and GDPD6 based on their N-terminal sequences using WoLF PSORT. chlo: chloroplast, vacu: vacuole, E.R.: endoplasmic reticulum, nucl: nucleus, mito: mitochondrium, extr: extracellular/cell wall, RC: reliability class, whereat a low RC value indicates a high prediction reliability.

Name	AGI	Amino acids	Subcellular compartment: RC
GDPD5	At1g74210	1-392	chlo: 5.0, vacu: 3.0, E.R.: 2.0, nucl: 1.0, mito: 1.0, extr: 1.0

GDPD6	At5g08030	1-372	vacu: 5.0, chlo: 4.0, nucl: 2.0, extr: 2.0

Subcellular localization of the Arabidopsis GDPD5 and GDPD6 proteins was examined by transient expression of enhanced green fluorescent protein (eGFP) fusion constructs, generated by fusing *GDPD5* and *GDPD6* full-length cDNA sequences in frame with a *eGFP* reporter sequence (*GDPD5-eGFP* and *GDPD6-eGFP*), in *N. benthamiana*. Infiltrated plants were examined at 5 dpi by fluorescent confocal laser-scanning microscopy to monitor eGFP expression. The subcellular accumulation for the GDPD5 and GDPD6 proteins N-terminally fused to the eGFP protein were compared with the localization of the ER-DsRed fusion protein (ER-control). Co-localization with the ER-control indicates that GDPD5 and GDPD6 are associated with the ER (Fig.: 3.30).

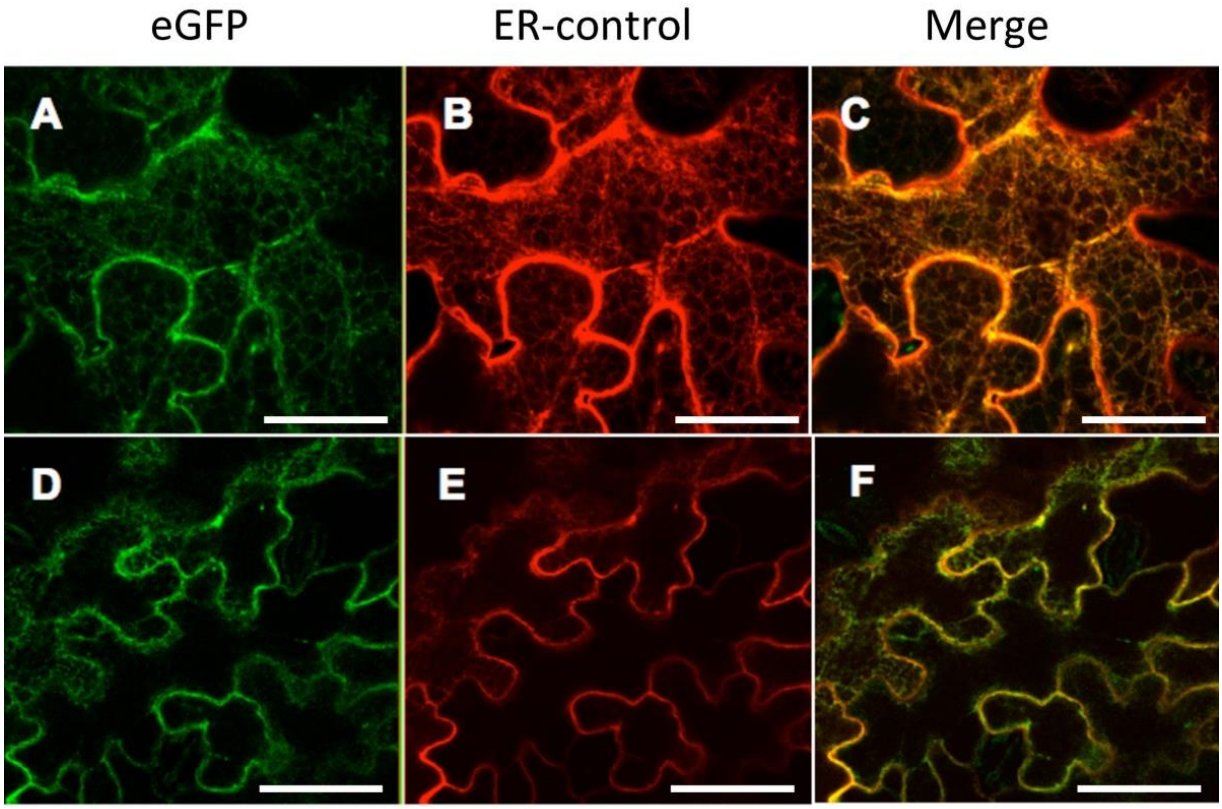

Figure 3.30: Subcellular localization of Arabidopsis GDPD5 and GDPD6 proteins. *N. benthamiana* leaves were infiltrated with *A. tumefaciens* containing a binary vector with expression constructs harboring the full-length GDPD5 and GDPD6 proteins N-terminal fused to eGFP. The green fluorescent signals of GDPD5 and GDPD6 co-localize with the red fluorescent signals of the ER-marker construct (merge). **(A-F)** Confocal analysis of sections showing transformed epidermal cells. **(A)** *GDPD5-GFP*; **(B)** ER-control; **(C)** merge; **(D)** *GDPD6-GFP*; **(E)** ER-control; **(F)** merge. (A-C) GDPD5; (D-F) GDPD6. Scale bars = 50 μm.

3.2.4 Isolation of Null Mutants for *GDPD5* and *GDPD6*

In order to understand *in vivo* functions of the *GDPD* genes, T-DNA tagged Arabidopsis plants (Sussman et al., 2000) with disruption of the *GDPD5* (At5g08030, ecotype Columbia-0) or *GDPD6* (At1g74210, ecotype Columbia-0) genes were employed (Table 3.7).

Table 3.7: Different Arabidopsis T-DNA insertion lines used for the characterization of *GDPD5* and *GDPD6*.

Gene	T-DNA line	Notation	Origin
At1g74210, *GDPD5*	GABI_346F05	*gdpd5-1*	GABI-Kat genome center
At1g74210, *GDPD5*	FLAG_354D01	*gdpd5-2*	SGAP INRA center
At5g08030, *GDPD6*	SALK_133368	*gdpd6-1*	NASC stock center
At5g08030, *GDPD6*	GABI_502F08	*gdpd6-2*	GABI-Kat genome center

The lines GABI_502F08 and GABI_346F05 were obtained from the GABI-Kat genome center at the University of Bielefeld (Bernd Weishaar (Rosso et al., 2003)). The SALK_133368 line was obtained from the NASC stock center and the FLAG_354D01 line from the SGAP INRA center (Versailles, France). For the isolation of null mutants, primers RP and LP (Table 3.8) were designed to amplify a segment of specific size from the WT *GDPD5* or *GDPD6* allele, whereas primers RP and LBb1 were designed to amplify segments of a defined size of the *GDPD5*::T-DNA and *GDPD6*::T-DNA alleles (Fig.: 3.31). The positions of T-DNA insertions and the intron/exon structure of the *GDPD5* and *GDPD6* genes are indicated in figure 3.31/3.32.

Table 3.8: Primers used for the PCR amplification of T-DNA insertion lines of *GDPD5* and *GDPD6*.

Mutant	RP	LP	LBb1	T-DNA line
gdpd5-1	bn122	bn123	bn142	GABI_346F05
gdpd5-2	bn208	bn207	bn212	FLAG_354D01
gdpd6-1	bn210	bn209	bn078	SALK_133368
gdpd6-2	bn288	bn287	bn142	GABI_502F08

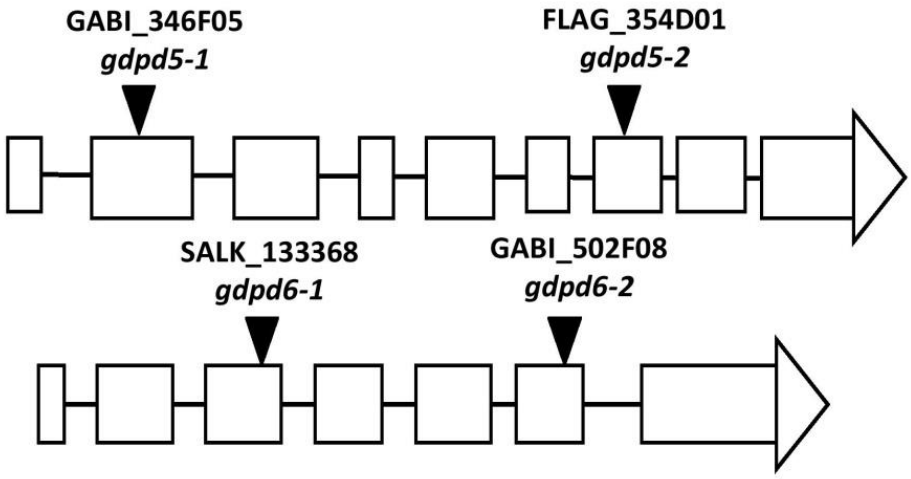

Figure 3.31: Schematic structure of the Arabidopsis *gdpd5* and *gdpd6* mutant genes. The T-DNA insertions between the start and the stop codon are indicated by the triangles. The insertions in the *GDPD5* gene are located at 830 and 1974 bp, and the *GDPD6* gene at position 455 bp and 1288 bp counting from the translational start codon. Boxes and lines depict exons and introns, respectively. The sequence is shown between translational start and stop codons.

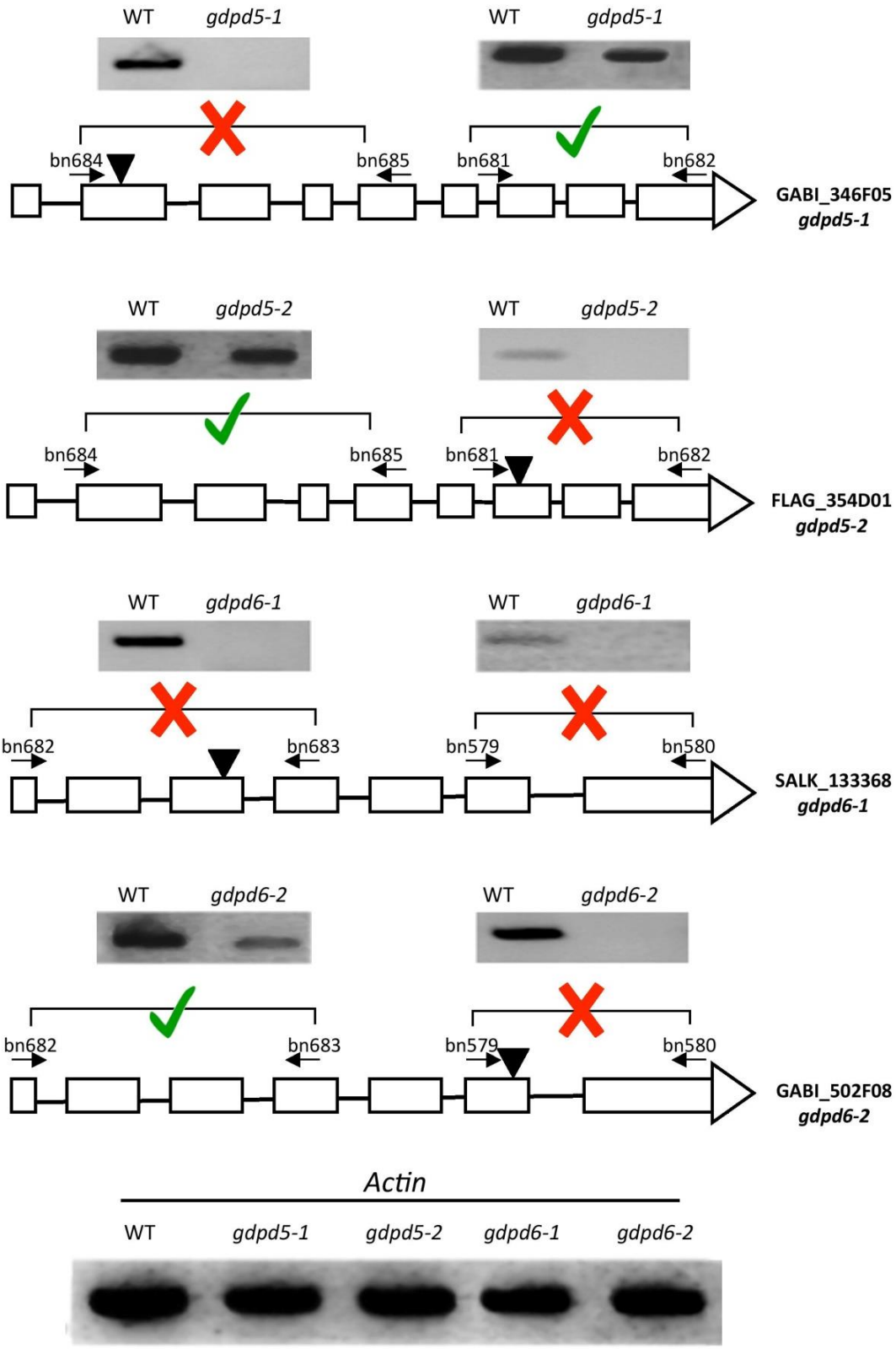

Figure 3.32: Transcriptional analysis of Arabidopsis mutants for *GDPD5* and *GDPD6*. Total RNA was isolated from flowers and employed for cDNA synthesis. Expression analysis by semi-quantitative RT-PCR of Arabidopsis WT Col-0, *gdpd5-1*, *gdpd5-2*, *gdpd6-1* and *gdpd6-2* plants using gene specific primers for *GDPD5*, *GDPD6* and for *actin*. The RT-PCR products were separated on an agarose gel and stained with EtBr. For all four mutant alleles, no transcript was detected when primers were used that span the insertion sites. In this regard the four lines represent null alleles. No further transcript was found for *gdpd6-1* when using primers downstream of the insertion site. However, RT-PCR products were obtained for primer pairs 5' to the insertion in *gdpd5-2* and *gpdp6-2*, and for a primer pair 3' to the insertion in *gpdp5-1*.

A three primer system was used for genotyping. Segregating plants were screened by PCR with genomic DNA isolated from leave material. PCR fragments harboring genomic sequences flanking T-DNA insertions were sequenced. Homozygous *gdpd5* mutant plants containing T-DNA insertions in the second exon at position C^{830} and in the seventh exon at position A^{1974} (counting the genomic sequence from start codon) of the *GDPD5* gene were identified. Furthermore, *gdpd6* mutant plants harboring insertions in the third exon at position G^{455} and in the sixth exon at T^{1288} (counting from start codon) were found for the *GDPD6* gene. In the progeny of heterozygous *GDPD5* and *GDPD6* T-DNA insertion lines, a segregation ratio of 3:1 was observed in accordance with Mendelian inheritance. To test whether the T-DNA insertions affect *GDPD5* and *GDPD6* expression, RNA from mutant and WT flowers were isolated and RT-PCR was performed using gene specific primers (Table 3.9). No transcript was detected by semi-quantitative RT-PCR analysis in each single mutant line when using primer pairs spanning the insertion sites, while residual expression was found for *gdpd5-1*, *gdpd5-2*, and *gdpd6-2* with primer pairs localizing 5' or 3' to the insertion sites (Fig.: 3.32). A *GDPD5* transcript was detected for the *gdpd5-1* allele downstream from the insertion site, but the transcript was less abundant than for the WT *GDPD5* gene. The residual expression of the *gdpd5-1* allele might be caused by promoter activity derived from T-DNA. For *gdpd5-2* and *gdpd6-2* alleles, transcripts were detected upstream the insertion site. The presence of these RT-PCR products were most likely due to residual expression of truncated mRNA sequences based on the endogenous GDPD5 or GDPD6 promoters.

Table 3.9: Primers used for semi-quantitative RT-PCR.

Mutant allele	forward primer.	reverse primer	T-DNA line
gdpd5-1	bn684	bn685	GABI_346F05
gdpd5-2	bn581	bn582	FLAG_354D01
gdpd6-1	bn682	bn683	SALK_133368
gdpd6-2	bn579	bn580	GABI_502F08

3.2.5 Characterization of *GDPD5* and *GDPD6* T-DNA Insertion Lines

The homozygous single mutant lines for *GDPD5* and *GDPD6* were comparable in growth and morphology to Arabidopsis Col-0 WT plants when grown on soil. The number and viability of the seeds were also comparable between control Col-0 and the single mutants.

3.2.5.1 Lipid Analysis of Arabidopsis *gdpd5* and *gpdp6* Single Mutants

One goal of this work was to analyze a possible involvement of *GDPD* in Arabidopsis lipid remodeling under Pi starvation. Therefore, different Arabidopsis *GDPD* T-DNA insertion lines were grown on synthetic growth medium for two weeks and subsequently transferred onto medium with or without Pi. Leaves and roots of these plants were harvested and employed for Q-TOF MS/MS analysis. Lipid composition of the different *gdpd* T-DNA insertion lines did not differ in comparison to the WT (Fig.: 3.33). Furthermore, no differences between *gdpd* mutants and WT with regard to molecular species composition of the phospholipids and galactolipids were observed (data not shown).

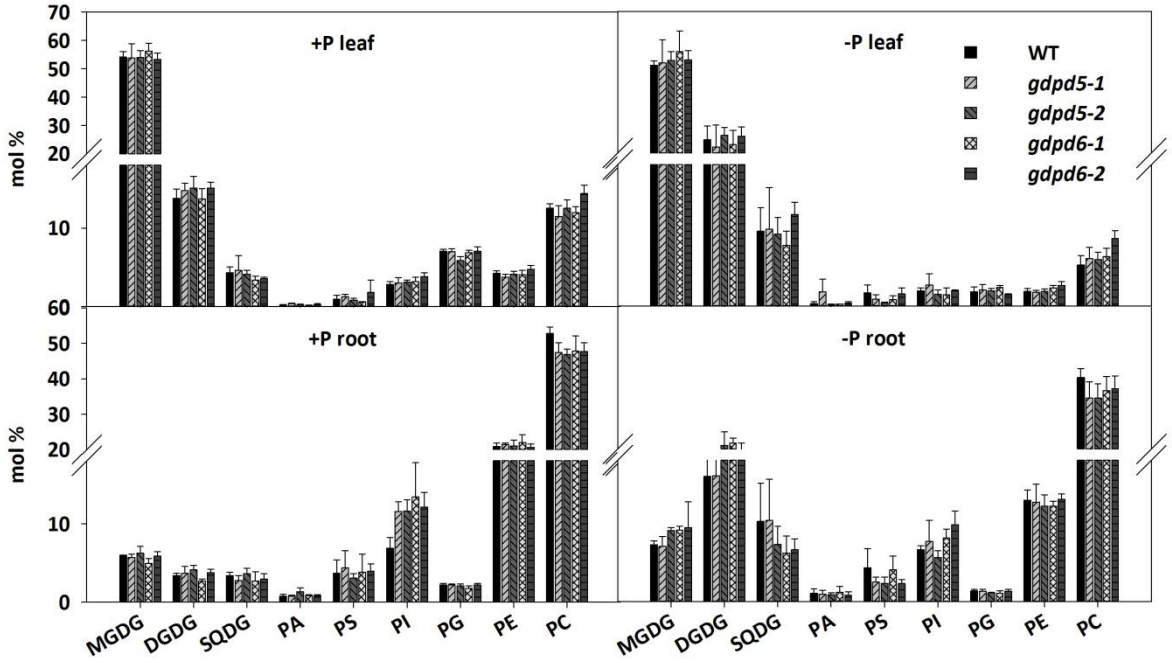

Figure 3.33: Glycerolipid composition of Arabidopsis leaf and root tissues under Pi plus and minus conditions. Glycerolipids were examined in the different *GDPD5* and *GDPD6* T-DNA insertion lines and in the control Col-0 line. Lipids were extracted by chloroform/methanol and analyzed by Q-TOF MS/MS. Data present means and standard deviations of five independent determinations.

All lines showed a reduction in phospholipid levels with the concomitant increase in SQDG and DGDG during Pi deprivation. The DGDG content was increased from 15 mol % to approximately 25 mol % in leaves and from around 3 mol % to 18 mol % in roots under Pi-depleted conditions. The phospholipid content was decreased under Pi starvation especially for PE and PC (Fig.: 3.33). Other genes presumably involved in lipid remodeling upon Pi starvation were analyzed in this study (appendix). Glycerolipid as well as DAG compositions were measured in Arabidopsis WT (different ecotypes), as well as *dgd1*, *npc5-1*, *npc5-2*, and *pho1npc5-2* T-DNA insertion lines. The *dgd1* mutant lacks 90 % of the DGDG content in leaves under Pi-repleted conditions. Under Pi-depleted conditions the amount of DGDG in leaves was increased, but not to the same extend as seen in the WT control. The *pho1* mutant showed an overall

decreased PL content in the leaf lipid extracts while there was an increase in the glycoglycerolipids DGDG and SQDG (appendix).

In conclusion, Pi deprivation resulted in a strong reduction of phospholipid contents in leaves and in roots of Arabidopsis. This decrease was compensated for by a strong accumulation of DGDG and SQDG, consistent with the literature (Härtel et al., 2000, 2001). The phospholipid and galactolipid levels of the different *GDPD5* and *GDPD6* T-DNA insertion mutants were comparable to WT under both Pi-replete and -deplete conditions (Fig.: 3.33). The effects seen in plants defective in genes associated with membranbe lipid remodeling under Pi starvation like *pho1* and *dgd1* were not seen in the different *gdpd* mutants analyzed in this study.

3.2.5.2 Determination of G3P

Glycerophosphodiester phosphodiesterases (GDPD) hydrolyze glycerophosphodiester resulting in the release of G3P. To assess whether the loss of *GDPD5* or *GDPD6* function in the mutant plants has an impact on metabolism, G3P levels were determined. To this end, a novel extraction and quantification method was established and validated by comparison with a published method. In the literature, different methods for the extraction and quantification of G3P from plant tissue are reported. For example, G3P quantification has previously been conducted after TCA extraction, based on an enzyme-coupled spectrophotometric reaction (Cheng et al., 2011). The novel method for the isolation and the quantification reported in this study includes chloroform/methanol extraction, silylation of G3P with MSTFA or BSTFA and subsequent measurement by GC-MS. In the following, advantages and disadvantages of the two different methods, with regard to reproducibility, precision and limits of detection, are shown.

3.2.5.2.1 Isolation of G3P from Plant Material

The isolation of G3P using TCA extraction is characterized by a relatively laborious and time-consuming procedure (Fig.: 3.34). The TCA extraction and enzyme-linked quantification with a photometer of a single sample by this procedure took approximately 5 h and up to 30 samples could be extracted at once. On the other hand, the isolation of G3P with chloroform/methanol is simple and fast. Extraction with chloroform/methanol, silylation and analysis by GC-MS of a single sample took around 1:15 h. Due to the simplified extraction procedure, large sample sets could be extracted at once. Similarities and differences between the two extraction methods using TCA or chloroform/methanol are depicted in Figure 3.35. G3P was extracted from leaves of Arabidopsis WT grown under normal conditions, with TCA or with chloroform/methanol. G3P levels were subsequently quantified using the GC-based method. Both extraction procedures resulted in G3P contents between 1.2 to 1.4 nmol per mg fresh weight in Arabidopsis WT leaf.

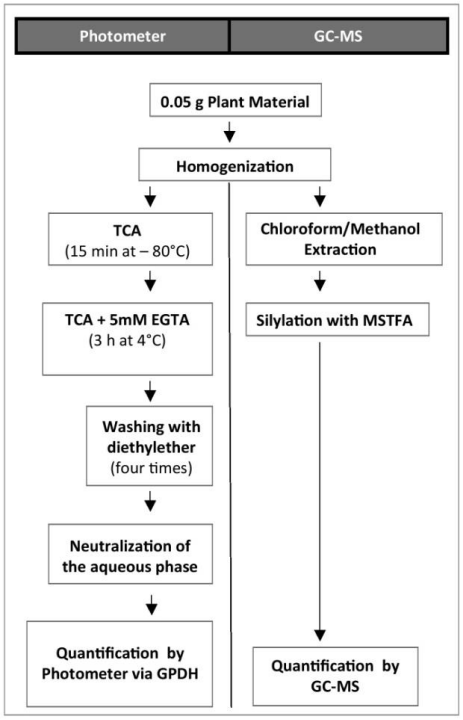

Figure 3.34: Methods for G3P extraction and quantification using the photometer or by GC-MS. The traditional method for quantification of G3P from plant tissue requires TCA extraction and quantification via an enzyme-coupled spectrophotometric reaction. The method for the quantification of G3P, developed in this study, includes chloroform/methanol extraction and silylation with MSTFA prior to GC-MS measurement.

The precision of the relative standard deviation (RSD %) was around 43 % when G3P was extracted with TCA. Isolation using chloroform/methanol and subsequent quantification was much more precise, with around 15 % (RSD). As the two extraction methods resulted in the detection of comparable amounts of G3P, but precision (Table 3.10) and the extraction/quantification time were superior for the chloroform/methanol extraction, G3P was isolated with chloroform/methanol and quantified by GC-MS in this work.

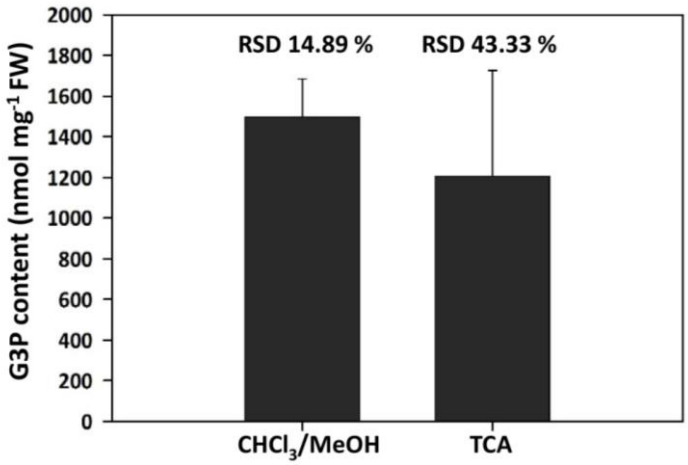

Figure 3.35: G3P content in Arabidopsis WT leaves grown under normal conditions. G3P was extracted with chloroform/methanol or TCA and quantified by GC-MS. RSD, relative standard deviation. Data present means and standard deviations of at least three independent determinations.

3.2.5.2.2 Spectrophotometric Determination of G3P

The NAD dependent conversion of G3P to DHAP catalyzed by GPDH can be measured by the absorbance change at 340 nm in the spectrophotometer taking account of the Beer-Lambert's law ($A=\varepsilon_\lambda * b * c$) (Fig.: 3.36).

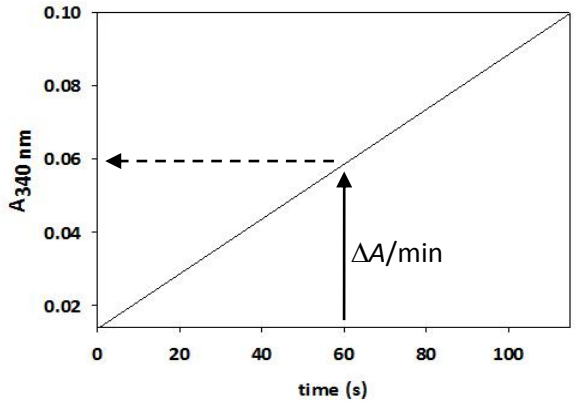

A = measured absorbance

t = time (s)

ε_λ = wavelength-dependent molar extinction coefficient (M^{-1} cm^{-1})

b = path length of the cuvette (cm)

c = analyte concentration (mol L^{-1})

Figure 3.36: Use of spectroscopy in enzyme assays. Continuous assay of a dehydrogenase producing NADH+ H^+. The rate is calculated from ε_{NADH} and the ΔA_{340} per min (dashed arrow).

For each nmol of G3P present in the sample an equivalent amount of NAD is reduced to NADH by GPDH. The nmol amount of G3P can therefore be calculated using the extinction coefficient for NADH according to the equation:

$$\frac{\Delta E_{340}}{\varepsilon_\lambda} \times \frac{a}{1000} \times \frac{1000}{x} = \text{Enzyme units (per cm}^3\text{ reaction mixture)}$$

ΔE = total absorbance change at 340 nm

ε_λ = molar extinction coefficient for NADH at 340 nm (6.3×10^3 M^{-1} cm^{-1})

a = total volume (cm^3) of the reaction mixture in the cuvette of 1 cm light path

x = volume (mm^3) of test solution added to the reaction mixture

The precision of the method was determined by calculating the RSD while recovery was evaluated through the comparison between the measured and nominal concentrations of G3P in a dilution series of G3P standard (%). The results obtained for spectrophotometric determination of G3P in standard solutions are shown in Table 3.10. Good accuracy was obtained in the range from 5 to 100 nmol of G3P mL^{-1} reaction mixture. Concentrations above 100 nmol G3P mL^{-1} reaction mixture resulted in a drastic reduction in recovery. Only 50 % and 30 % of the nominal concentration could be recovered for 500 and 1000 nmol of G3P mL^{-1} reaction mixture, respectively (Table 3.10).

Table 3.10: Assay validation results for G3P analyzed in an enzyme-coupled spectrophotometric reaction. The absorbance at 340 nm was measured according to Wei and co-workers (Wei et al., 2004), using 10 U GPDH (Sigma) eluted in hydrazine-glycine buffer without NAD. Reaction was carried out at RT. SD, standard deviation; RSD, relative standard deviation. Data present means and standard deviation of three independent measurements.

Assay validation results							
Nominal concentration [nmol mL^{-1}]	5	10	20	50	100	500	1000
Means (measured) [nmol mL^{-1}]	4,63	8,59	18,37	47,36	86,94	268,60	327,06
SD [nmol mL^{-1}]	0,10	0,40	1,22	1,28	0,81	34,37	9,94
Precision (RSD %)	2,25	4,66	6,62	2,70	0,93	12,80	3,04
Recovery (%)	92,70	85,95	91,85	94,72	86,94	53,72	32,71

The precision of the G3P content determination using the enzyme-coupled spectrophotometric reaction was in the range of 0.93-12.80 (RSD %) for concentrations of G3P between 5 - 1000 nmol mL^{-1} reaction mixture. Limit of detection (LOQ) was 5 nmol mL^{-1} reaction mixture, which was also the lowest standard concentration used (Fig.: 3.37).

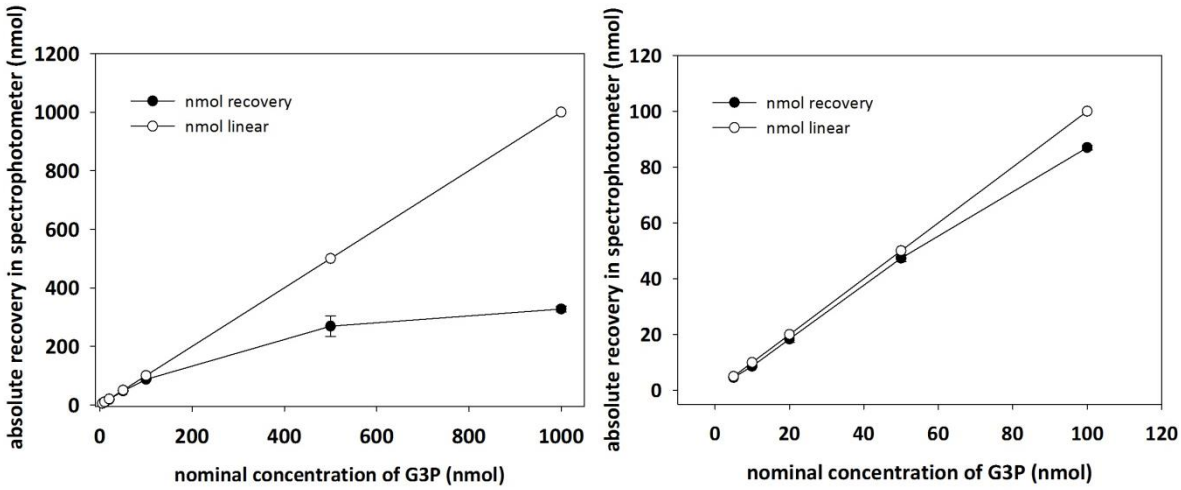

Figure 3.37: Absolute recovery of G3P by spectrophotometric determination. G3P concentration was measured by an enzyme-coupled spectrophotometric reaction using different nominal standard concentrations of G3P in hydrazine-glycine buffer containing 1 mM NAD, with 10 U GPDH (Sigma) dissolved in hydrazine-glycine buffer. Data present means and standard deviations of three independent measurements.

3.2.5.2.3 Determination of G3P by Gas Chromatography

As for the enyzmatic/photometric quantification, precision and recovery of the GC method were determined by analysis of replicates (n=3) of G3P standards with known concentrations. RSD was in the range of 15 to 21 % and recovery was between 97 to 99 % (Table 3.11). These results demonstrated acceptable precision and recovery of the GC-MS method. The limit of detection was around 1 nmol G3P. The quantification of G3P by GC-MS depends on the availability of a suitable internal standard. To this end, sorbitol and oleyl alcohol were tested as internal standards. These two alcohols are absent or of low abundance in plants.

Because the polarity of sorbitol is closer to that of G3P, oleyl alcohol was dropped as a potential internal standard. The quantification based on such standards requires careful measurement and calculation of correction factors, as the response factors for the analyte (G3P) and the internal standard (sorbitol) are presumably different. For the quantification of G3P levels in different plant tissues by GC-MS analysis, a correction factor was determined by employing G3P and sorbitol in an equimolar mixture for GC-MS measurement. For sorbitol a correction factor of 2.01 was determined by peak area measurements of the total ion count (TIC) signal of G3P and sorbitol and subsequent adjustment of the data. The correction factor for sorbitol, which was determined prior to the measurement, provided the means for a very precise and reliable G3P quantification.

Table 3.11: Assay validation results for G3P analyzed by the GC-MS method in comparison to the spectrophotometric measurement. Mean value of measured concentration, SD, standard deviation; RSD, relative standard deviation. Data present means and standard deviation of three independent determinations. Values for the photometric determination are taken from Table 3.10.

Glycerol-3-Phosphate recovery				
Detection method	GC-MS		Photometer	
Nominal concentration [nmol mL-1]	10	100	10	100
Mean[nmol mL-1]	9.70	98,44	8,59	86,94
SD [nmol mL-1]	2.05	16,11	0,40	0,81
Precision (RSD %)	21.08	15.86	4,66	0,93
Recovery (%)	**97.05**	**98.88**	**85.95**	**86.94**

The GC-MS-based method for G3P quantification is a reliable alternative to the photometric procedure. The sample preparation by chloroform/methanol extraction is simple and takes only a fraction of the time required for TCA extraction. The quantification by spectrophotometer or by GC-MS each have each advantages and disadvantages. Both methods require a comparable amount of plant tissue in the range between 25 to 50 mg (fresh weight). The main disadvantage of the GC-MS-based method is the necessity to derivatize the samples prior to the measurement, because G3P has to be converted into a volative compound. It turned out that the age and quality of the MSTFA or BSTFA reagents was critical to obtain reliable results. This might be due to degradation by water (moisture). For GC-MS, the analyte was dissolved in derivatizing reagent (MSTFA or BSTFA) and injected. Attempts to replace MSTFA or BSTFA with hexane as solvent strongly affected analyte stability. As a consequence, injection of MSTFA into the GC column resulted in the derivatization of the stationary phase of the column. Thus, care had to be taken and the column had to be frequently shortened at the injector side. On the other hand, the GC-MS based method allows an increased analytical sensitivity over the spectrophotometric method.

3.2.5.3 G3P Measurement of Leaves from *GDPD5* and *GDPD6* T-DNA Insertion Lines

The G3P content was measured in the different Arabidopsis *GDPD5* and *GDPD6* T-DNA insertion lines via GC-MS. To this end, Arabidopsis WT and the different *gdpd5* and *gdpd6* single mutant lines were grown on synthetic medium with or without Pi. Leaf tissues were harvested and fresh weights were determined prior to freezing in liquid nitrogen. G3P was extracted with chloroform/methanol as described above, and measured by GC-MS. Except *gdpd5-1* the amount of G3P was comparable among the single mutant lines and the WT control in leaves under Pi-replete conditions (Fig.: 3.38). The *gdpd5-1* mutant showed an increase in G3P content of approximately 20 % under normal growth conditions. Under Pi starvation, G3P levels in Arabidopsis leaves were strongly decreased in all lines as compared to Pi-replete conditions. The amounts of G3P in WT and in *gdpd5-1* were similar, while G3P was reduced in *gdpd5-2*, *gdpd6-1*, and *gdpd6-2* by about 30 % and 45 % for *gdpd6-2*, respectively. The amount of G3P was reduced by a factor of 10 in leaves under minus Pi conditions. Under Pi-repleted conditions around 1500 to 2000 nmol g^{-1} FW can be found in leaf material, while under Pi starvation the amount declined to around 180 nmol g^{-1} FW in Arabidopsis. The same trend could be observed in WT roots grown under plus or minus Pi conditions (appendix).

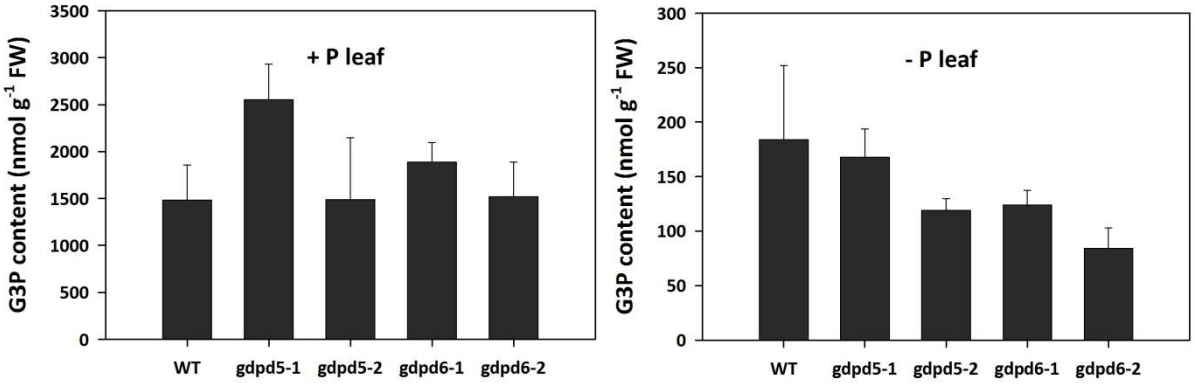

Figure 3.38: G3P content in Arabidopsis leaves grown on Pi plus or minus conditions. Plants were grown on synthetic medium with or without Pi. G3P was isolated by chloroform/methanol extraction and analyzed by GC-MS. Data present means and standard deviations of four independent determinations.

3.2.6 Molecular and Morphological Characterization of *GDPD5* and *GDPD6* Double Mutant Plants

The different *gdpd5* and *gdpd6* T-DNA insertion lines did not show any visible growth differences on soil (data not shown). At this point crosses of the homozygous single mutant lines were done. *GDPD5* and *GDPD6* reside on different chromosomes, so plants harboring both T-DNA insertions were readily obtained. After several rounds of self-pollination and PCR-screening of the progeny, only double heterozygous *gdpd5-1*$^{+/-}$*gdpd6-1*$^{+/-}$ (GABI_346F05 x SALK_133368) mutants could be recovered, while double homozygous mutant lines for *gdpd5-1*

$^{-/-}$*gdpd6-2*$^{-/-}$, (GABI_502F08 x GABI_346F05), *gdpd5-2*$^{-/-}$*gdpd6-1*$^{+/-}$ (FLAG_354D01 x SALK_133368), and *gdpd5-2*$^{-/-}$*gdpd6-2*$^{-/-}$ (FLAG_354_D01 x GABI_502F08) mutants were obtained (Table 3.12), as confirmed by PCR-analysis. A segregation ratio following the Mendelian inheritance was observed for the *gdpd5-1gdpd6-2*, *gdpd5-2gdpd6-1*, and *gdpd5-2gdpd6-1* crosses (data not shown).

Table 3.12: Arabidopsis *gdpd5* and *gdpd6* double mutants, recovered after crossing of the different single mutant lines.

mutant	*GDPD5*	*GDPD6*	T-DNA lines
gdpd5-1gdpd6-1	heterozygous	heterozygous	GABI_346F05 x SALK_133368
gdpd5-1gdpd6-2	homozygous	homozygous	GABI_502F08 x GABI_346F05
gdpd5-2gdpd6-1	homozygous	homozygous	FLAG_354D01 x SALK_133368
gdpd5-2gdpd6-2	homozygous	homozygous	FLAG_354_D01 x GABI_502F08

3.2.6.1 Crossing of *gdpd5-1* and *gdpd6-1*

Growth of *gdpd5-1*$^{+/-}$*gdpd6-1*$^{+/-}$ double heterozygous plants was indistinguishable from WT (data not shown). After several rounds of self-pollination and PCR-screening only double heterozygous *gdpd5-1*$^{+/-}$*gdpd6-1*$^{+/-}$ mutants were recovered, as confirmed by PCR-analysis (Fig.: 3.39 E).

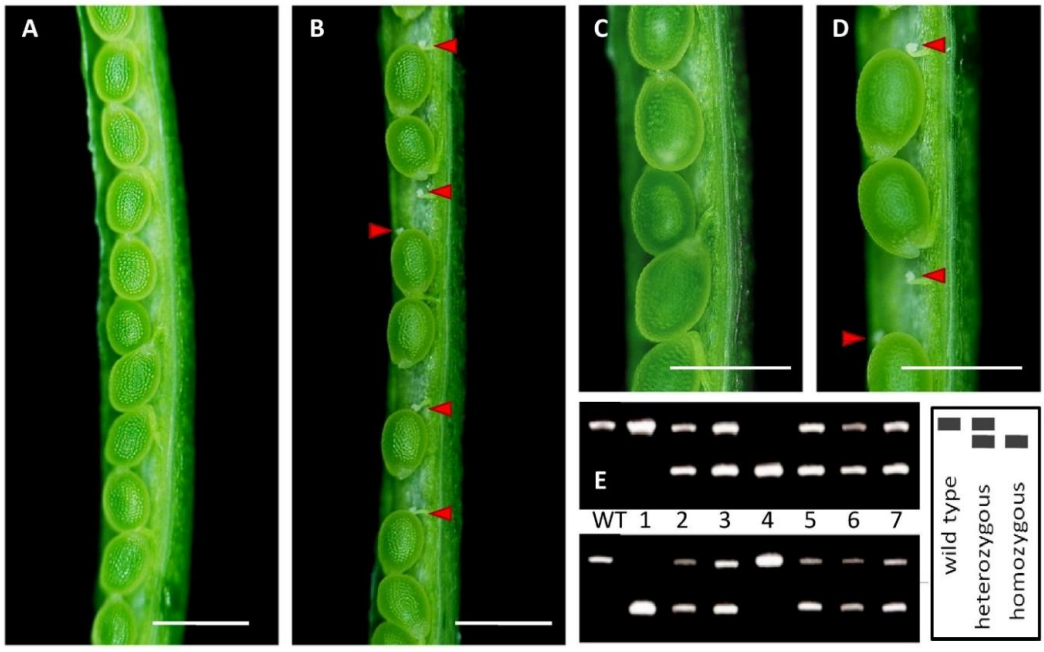

Figure 3.39: Morphological characterization of developing *gdpd5-1*$^{+/-}$*gdpd6-1*$^{+/-}$ seeds. Siliques of a *gdpd5-1*$^{+/-}$*gdpd6-1*$^{+/-}$ double mutant plant show ovules, which are not fertilized (red arrow heads). (A, C) WT Col-0; (B, D) *gdpd5-1*$^{+/-}$*gdpd6-1*$^{+/-}$. (E) Genotyping of the F1 progeny of the *gdpd5-1*$^{+/-}$*gdpd6-1*$^{+/-}$ mutant by PCR analysis. Numbers indicate individual F1 plants. Plants 2, 3, 5, 6 and 7 were double heterozygous, while plants 1, and 4 were WT/homozygous. Scale bars = 1 mm.

The double heterozygous individuals showed a high percentage of non-fertilized ovules, dispersed randomly from the top to the base of the siliques. Hence the average number of seeds per silique was decreased, compared to the WT segregants (Fig.: 3.39).

Table 3.13: Analysis of the dihybrid crosses of *gdpd5* and *gdpdD6* T-DNA insertion lines. The F1 double heterozygous plants are selfed to produce a F2 generation. **(A)** The Punnett square is shown for the F2 segregation of the cross *gpdp5-1* x *gpdp6-1*. A, *GDPD5-1*; a, *gdpd5-1*; B, *GDPG6-1*; b, *gdpd6-1*. Gametophyte combinations that are lethal are crossed out in the Punnett square. **(B)** Segregation ratio of F2 progeny determined by PCR analysis. Genotypes being either double homozygous (aabb), or homozygous/heterozygous (Aabb or aaBb) could not be detected after testing approximately 230 plants.

A

Gametes		Pollen			
		AB	Ab	aB	ab
Ovule	AB	AABB	AABb	AaBB	AaBb
	Ab	AABb	AAbb	AbBb	~~Aabb~~
	aB	AaBB	AaBb	aaBB	~~aaBb~~
	ab	AaBb	~~Aabb~~	~~aaBb~~	~~aabb~~

B

F2 Theoretical ratio	F2 Measured ratio	
1/16 AABB (6.25 %)	**0/16 AABB (0%)**	viable
2/16 AABb (12.5 %)	**2/16 AABb (15.27 %)**	
2/16 AaBB (12.5 %)	**2.5/ 16 AaBB (15.69 %)**	
4/16 AaBb (25 %)	**9/16 AaBb (53.42 %)**	
1/16 aaBB (6.25 %)	**1/16 aaBB (7.26 %)**	
1/16 AAbb (6.25 %)	**1.5/16 AAbb (8.36 %)**	
2/16 Aabb (12.5 %)	**0/16 Aabb (0 %)**	non-viable
2/16 aaBb (12.5 %)	**0/16 aaBb (0 %)**	
1/16 aabb (6.25 %)	**0/16 aabb (0 %)**	

3.2.6.2 Gametophyte Analysis of *gdpd5-1$^{+/-}$gdpd6-1$^{+/-}$* Mutants

After screening approximately 230 plants of the F2 generation from a *gdpd5-1$^{+/-}$gdpd6-1$^{+/-}$* cross, no double homozygous (*gdpd5-1$^{-/-}$gdpd6-1$^{-/-}$*) or heterozygous/homozygous (*gdpd5-1$^{+/-}$gdpd6-1$^{-/-}$*) mutant plants were obtained. To assess whether the absence of *gdpd5-1$^{-/-}$gdpd6-1$^{-/-}$* or *gdpd5-1$^{+/-}$gdpd6-1$^{-/-}$* or *gdpd5-1$^{-/-}$gdpd6-1$^{+/-}$* plants is the consequence of an abnormal male or female gamete development, reciprocal crosses of *gdpd5-1$^{+/-}$gdpd6-1$^{+/-}$* and WT were done. PCR analysis of the F1 progeny of this cross revealed a severe male transmission defect (Table 3.14). A reduced male fertility was observed when the *gdpd5-1$^{+/-}$gdpd6-1$^{+/-}$* plant was used as the pollen donor. The numbers of heterozygous plants in the F1 progeny of this cross demonstrated

that transmission of the *gdpd5-1gdpd6-1* haplotype through the male gametophyte, but not the female gametophyte, was specifically affected.

Table 3.14: Reciprocal cross of the *gdpd5-1$^{+/-}$gdpd6-1$^{+/-}$* mutant to WT revealed that the *gdpd5-1gdpd6-1* mutation could not be transduced through the pollen. Parent genotypes were confirmed by PCR and by determining the segragation ratio of the progeny.

parent		progeny
pollen donor	**pollen acceptor**	**transmission efficiency (mutant/total)**
gdpd5-1$^{+/-}$gdpd6-1$^{+/-}$	WT Col-0	0 %
WT Col-0	*gdpd5-1$^{+/-}$gdpd6-1$^{+/-}$*	20 %

3.2.6.2.1 Analysis of *gdpd5-1$^{+/-}$gdpd6-1$^{+/-}$* Pollen

Because a transmission defect through the male gametes was observed, the pollen viability was analyzed using the Alexander staining method (Alexander, 1969). The analysis of the single mutant plants revealed pollen viability comparable to the WT (appendix). Analysis of *gdpd5-1$^{+/-}$gdpd6-1$^{+/-}$* pollen grains showed that approximately 50 % of the pollen was non-viable (as judged by green staining), while anthers of Col-0 plants contained only approximately 1 % non-viable pollen (Fig.: 3.40).

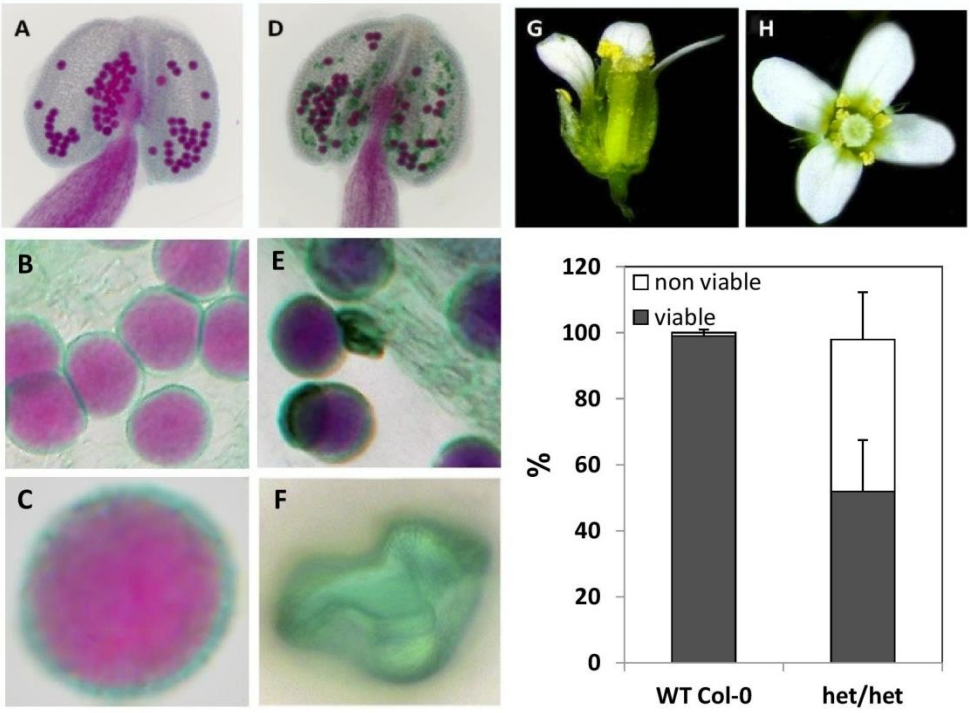

Figure 3.40: Viability test of pollen from WT and *gdpd5-1$^{+/-}$gdpd6-1$^{+/-}$* anthers. Microscopical analysis after Alexander staining revealed that approx. 50 % of *gdpd5-1$^{+/-}$gdpd6-1$^{+/-}$* pollen was non-viable. **(A-C)** Pollen viability of WT, and **(D-F)** *gdpd5-1$^{+/-}$gdpd6-1$^{+/-}$* anthers assessed by Alexander staining method. **(I)** The number of viable pollen (viable pollen show purple-coloured cytoplasm of pollen grains) of *gdpd5-1$^{+/-}$gdpd6-1$^{+/-}$* was reduced by about 50 % compared to WT. Non-viable pollen lack the purple colour of the cytosol and appear mostly green. Pollen was isolated from flowers at stage 14 **(G, H)** according to Alvarez-Buylla and co-workers (Alvarez-Buylla et al., 2010).

Comparative histological structure analysis of Arabidopsis anthers revealed an abnormal pollen development. For histological analysis, flowers pre-anthesis of Col-0 and *gdpd5-1*$^{+/-}$ *gdpd6-1*$^{+/-}$ mutant plants were collected and semi-thin sections were stained with toluidine blue and analyzed by brightfield microscopy. The *gdpd5-1*$^{+/-}$*gdpd6-1*$^{+/-}$ mutant showed impaired pollen development. In Arabidopsis, anther development can be divided into 14 well-defined stages by morphological characteristics (Sanders et al., 1999). The anthers analyzed in this work were harvested between stages 9 to 10 of development. At stage 7 the callose walls surrounding the tetrads degenerate and the microspores are released. At stages 8 and 9, the microspores generate an exine wall and become vacuolated before the degeneration of the tapetum is initiated at stage 10. Pollen development of *gdpd5-1*$^{+/-}$*gdpd6-1*$^{+/-}$ mutant anthers at stage 9 to 10 was impaired showing high number of abnormal microspores when microspore polarization started (Fig.: 3.41 D-H).

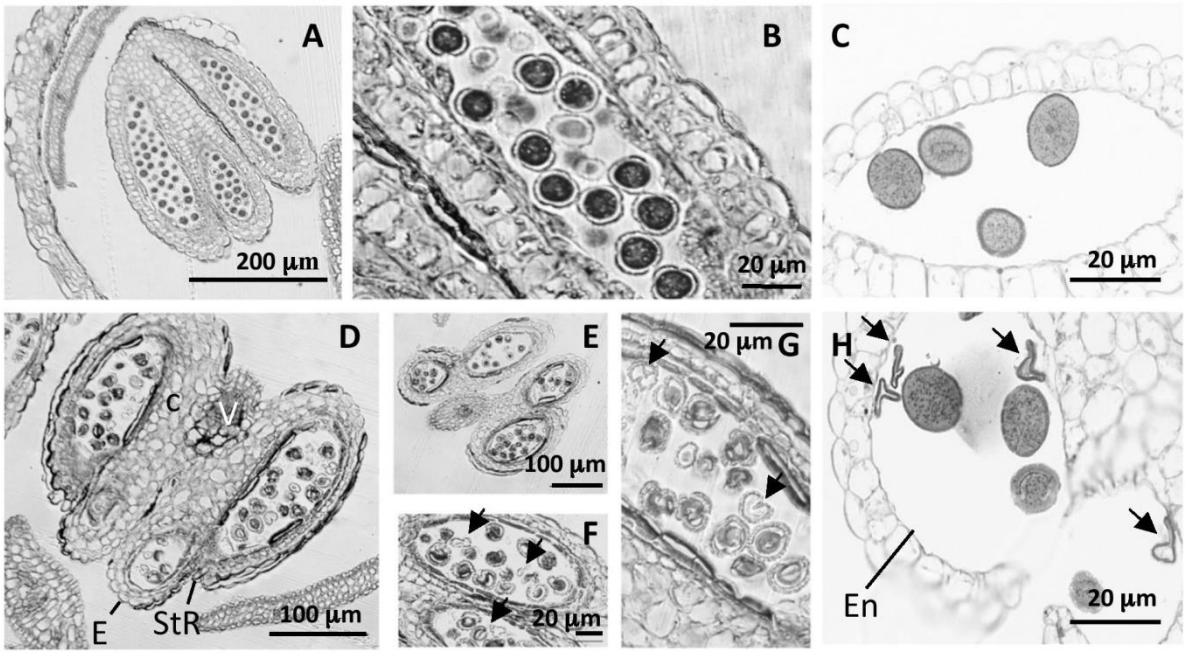

Figure 3.41: Comparison of histological structures of Arabidopsis anthers. (A, B, D, E, F, G) Semi-thin cross-sections through Arabidopsis WT **(A-C)**, and *gdpd5-1*$^{+/-}$*gdpd6-1*$^{+/-}$ **(D-H)** anthers at stage 7 to 8. **(A-C)** Anthers from *gdpd5-1*$^{+/-}$*gdpd6-1*$^{+/-}$ mutant anthers, showing a high number of abnormal microspores. Stage classification of anther development according to Sanders and co-workers (1999). **(A, B)** 1 µm semi-thin sections of Arabidopsis WT and *gdpd5-1*$^{+/-}$*gdpd6-1*$^{+/-}$ **(D-G)**. Mature pollen grains stained with toluidine blue and observed by light microscopy. **(C, H)** transmission electron (TEM) microscopy (Azur II – Methylene blue – Borax stain) of pollen grains of Arabidopsis WT Col-0 **(C)** and *gdpd5-1*$^{+/-}$*gdpd6-1*$^{+/-}$ mutant **(H)** pollen grains. Abnormal pollen grains (distorted and invaginated) are marked with arrows. V, vascular bundle; c, connective En, endothecial cell layer; E, epidermal cell layer; StR, stomium region.

Around half of the *gdpd5-1*$^{+/-}$*gdpd6-1*$^{+/-}$ microspores were condensed and less stained, lacking the nucleus, whereas numerous dark stained evenly distributed microspores existed in normal developing anthers of the Col-0 plant (Fig.: 3.41 A-C). The tapetal cells were normally developed in *gdpd5-1*$^{+/-}$*gdpd6-1*$^{+/-}$ mutant anthers compared to WT. All anthers of the *gdpd5-1*$^{+/-}$ *gdpd6-1*$^{+/-}$ mutant plants contained abnormal non-viable pollen grains, thus displaying partial male sterility. In fully developed anthers at stage 12 (Fig.: 3.41 H) the tapetum already

underwent cellular degradation and rupture of the septum below the tapetum. At this stage the pollen grains were released from the anthers. Anther cell development of *gdpd5-1*$^{+/-}$*gdpd6-1*$^{+/-}$ mutants was comparable to Arabidopsis WT Col-0 (Fig.: 3.41). The difference in morphology between WT pollen and pollen from *gdpd5-1*$^{+/-}$*gdpd6-1*$^{+/-}$ mutant plants are even more evident when analyzed by electron microscopy (Fig.: 3.42 C, H; Fig. 3.42).

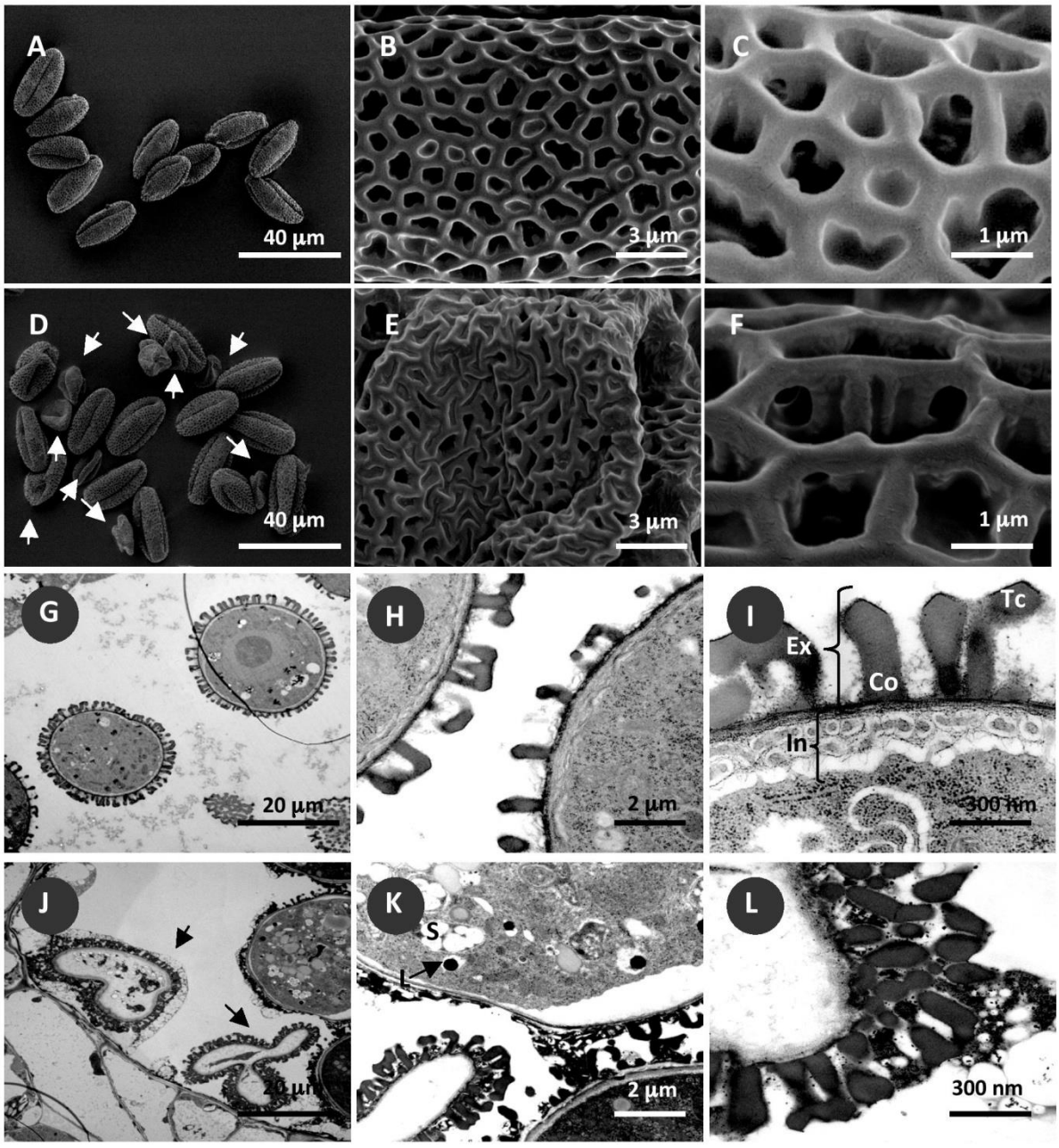

Figure 3.42: SEM and TEM of mutant pollen. Scanning electron microscopy **(SEM, A-F)** and transmission electron microscopy **(TEM, E-H)** microscopy (Azur II – Methylene blue – Borax stain) of pollen grains of Arabidopsis WT Col-0 **(A-C, G-I)** and *gpde1*$^{+/-}$*gpde2*$^{+/-}$ mutant **(D-F, J-L)** pollen grains. Anthers of *gpde1*$^{+/-}$*gpde2*$^{+/-}$ plants showed high numbers of strongly deformed pollen grains. In, intine; L, lipid body; S, starch grain; Tc, tectum; Co, columnelle, Ex, exine.

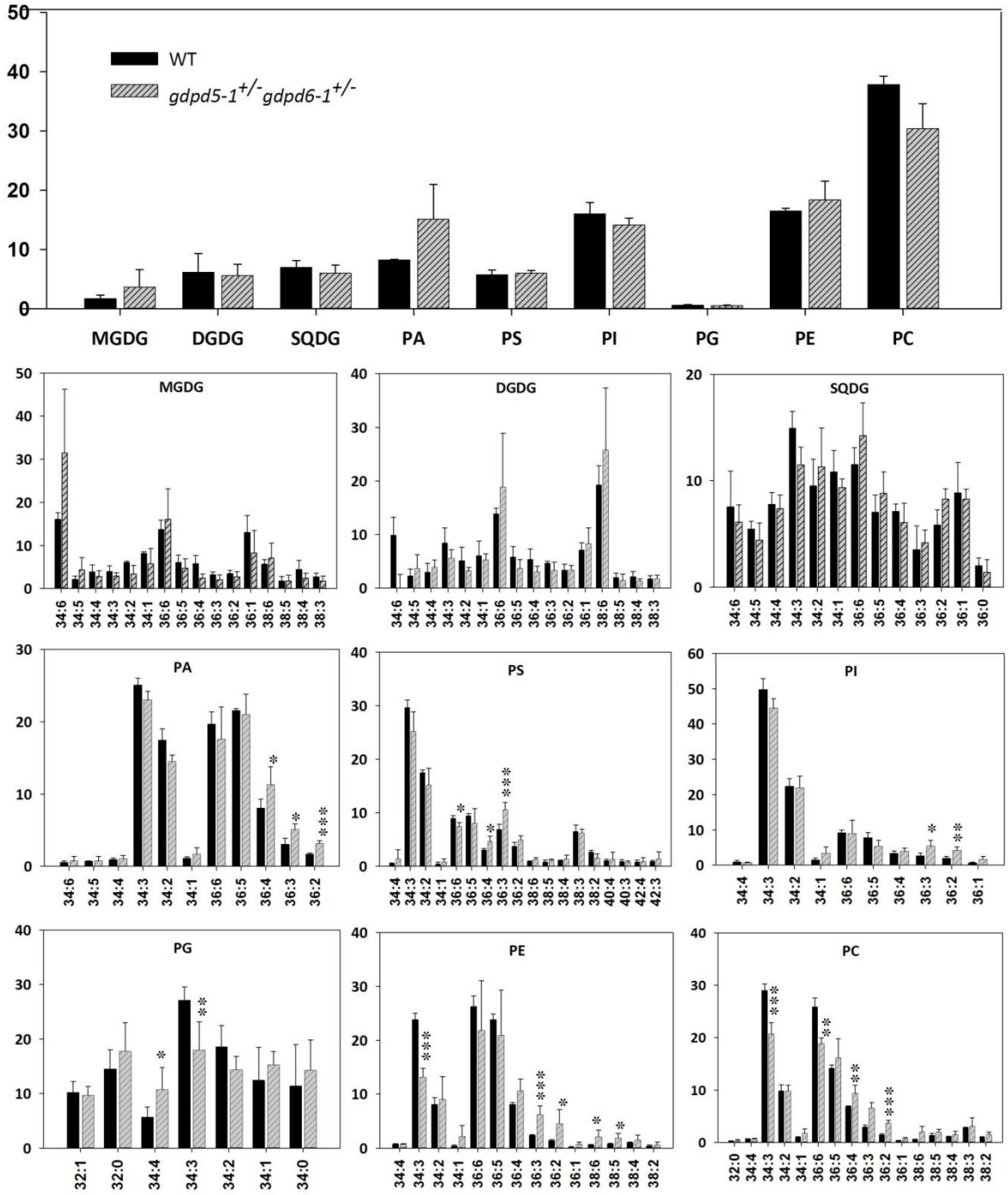

Figure 3.43: Analysis of *gdpd5-1⁺/⁻gdpd6-1⁺/⁻* pollen grains. Total glycerolipid content and molecular species composition (mol %) in Arabidopsis WT and *gdpd5-1⁺/⁻gdpd6-1⁺/⁻* pollen grains. Plants were grown on soil until anthesis before sampling. Pollen was collected by using a modified vacuum cleaner for large-scale pollen isolation. Lipids were extracted by chloroform/methanol extraction and analyzed by Q-TOF MS/MS. Data represent means and standard deviations of five independent determinations. Asteriks indicate values that are significantly different from the control (according to Student's t test, Welch correction, $P<0.05$ (∗); $P<0.01$ (∗∗); $P<0.005$ (∗∗∗)).

SEM and TEM analyses of the pollen grains were done by Michael Melzer at the Leibniz Institute of Plant Genetics and Crop Plant Research (IPK) in Gatersleben. Scanning electron microscopy revealed that pollen grains from *gdpd5-1⁺/⁻gdpd6-1⁺/⁻* lines were partially less turgescent, resulting in a distorted and invaginated morphology, which indicates a reduced

amount of intracellular material or turgor (Fig.: 3.42 A-D). Differences are also evident in cross sections analyzed under the transmission electron microscope. While exine and intine layers were comparable between WT and *gdpd5-1*$^{+/-}$*gdpd6-1*$^{+/-}$ mutant pollen grains, the microspores in the mutant line were partially shrunken and disintegrated due to autolysis (Fig.: 3.42 D, E). The mutant pollen grains showed varying degrees of damage and could be grouped into two classes (moderate and strong). Moderately affected mutant pollen still had intracellular structures, but showed large areas severely affected by autolysis, and fewer lipid bodies. In agreement with the observations made by light microscopy, a considerable proportion of mutant pollen grains were collapsed, showing a highly reduced amount of intracellular material (Fig.: 3.42 J). Despite the severity of the damage in the vegetative cells, the exine layer of these pollen grains was still fully comparable to the WT, as confirmed by scanning electron microscopy (Fig.: 3.42 D-F). The glycerolipid composition of pollen from *gdpd5-1*$^{+/-}$*gdpd6-1*$^{+/-}$ plants was determined by Q-TOF mass spectrometry (Fig. 3.43).

Arabidopsis Col-0 and *gdpd5-1*$^{+/-}$*gdpd6-1*$^{+/-}$ mature pollen grains were employed for analysis. Large-scale pollen isolation was done using a collecting tube consisting of different segments separated by meshes of defined pore sizes, attached to a vacuum cleaner (Fig.: 2.1). Lipids were extracted by chloroform/methanol and glycerolipids were determined by Q-TOF MS/MS analysis. Glycerolipid composition of *gdpd5-1*$^{+/-}$*gdpd6-1*$^{+/-}$ pollen grains was similar to WT pollen grains. Only slight differences in PA levels were detectable. Pollen collected from the *gdpd5-1*$^{+/-}$*gdpd6-1*$^{+/-}$ mutant showed an increase in PA levels of approximately 30 % compared to the WT control, while PC was decreased by around 20 %. The molecular species composition of phospholipids showed significant decreases in PC34:3, PE34:3, PI34:3 as well as PC36:6 (Fig.: 3.43). In contrast, the levels of PC36:4, 36:3, 36:2, and 38:6 as well as PI36:3, 36:2, and 36:1 were upregulated in pollen grains of the *gdpd5-1*$^{+/-}$*gdpd6-1*$^{+/-}$ mutant line compared to WT (Fig. 3.43).

3.2.6.2.2 Structural Analysis of *gdpd5-1*$^{+/-}$*gdpd6-1*$^{+/-}$ Pistils

Around 45 % of the pollen grains of double heterozygous Arabidopsis *gdpd5-1*$^{+/-}$*gdpd6-1*$^{+/-}$ plants were non-viable. To confirm that the development of the female gametophyte is not impaired, comparative histological analyses were performed (Fig.: 3.44).

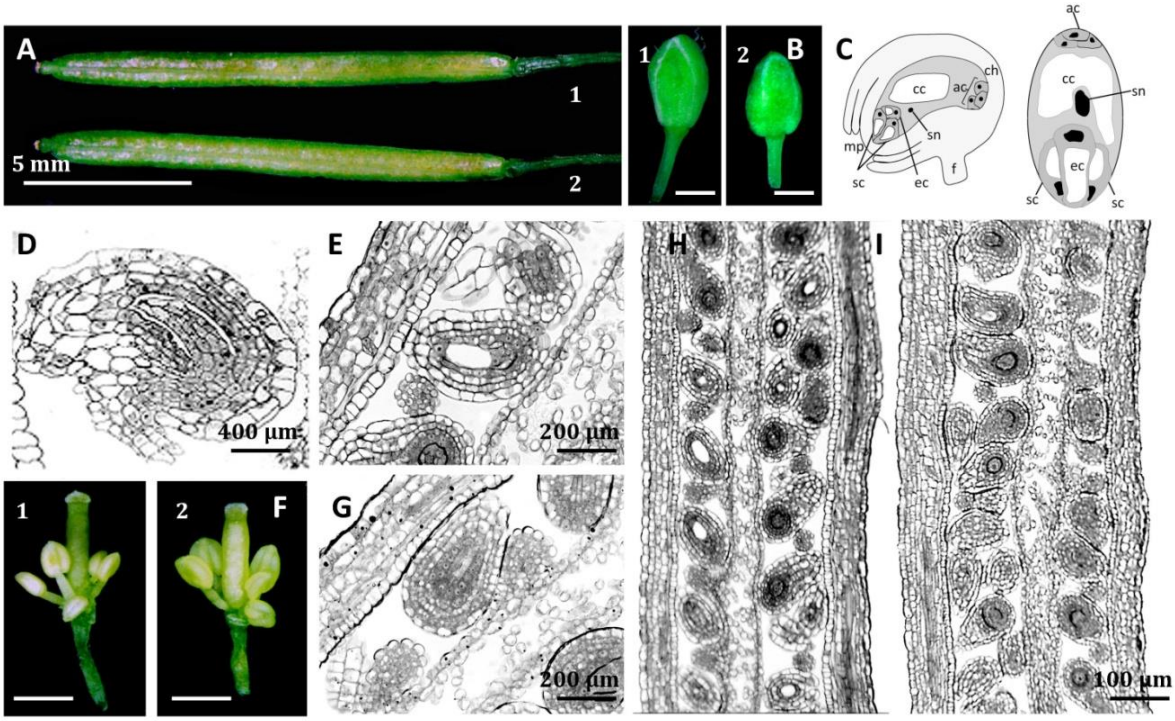

Figure 3.44: Histological analyses of Arabidopsis pistil sections. (A, B, F) Morphological characterization of Arabidopsis siliques, closed buds, and emasculated flowers, respectively. 1, WT Col-0; 2, *gdpd5-1*$^{+/-}$*gdpd6-1*$^{+/-}$. **(D, E, G, H, I)** Semi-thin-cross-sections through Arabidopsis *gdpd5-1*$^{+/-}$*gdpd6-1*$^{+/-}$ gynoecium compared to WT. Toluidine blue staining of the sections revealed that ovary and ovule development are not affected in *gdpd5-1*$^{+/-}$*gdpd6-1*$^{+/-}$ compared to WT. **(D, E, H)** WT Col-0; **(G, I)** *gdpd5-1*$^{+/-}$*gdpd6-1*$^{+/-}$. ac, antipodal cells; cc, central cell; ch, chalazal region of the ovule; ec, egg cell; f, funiculus; mp, micropyle; sc, synergid cell; sn, secondary nucleus. Scale bars = 1 mm.

To this end, pistils at pre-anthesis stage of *gdpd5-1*$^{+/-}$*gdpd6-1*$^{+/-}$ and WT plants were employed for sectioning and toluidine blue staining. Observation by brightfield microscopy revealed that pistils of *gdpd5-1*$^{+/-}$*gdpd6-1*$^{+/-}$ plants did not show any differences in structure and size compared to WT at the same developmental stage (Fig.: 3.44). Embryo sac development was comparable to the WT at all stages. Together with the results of the reciprocal crosses described before, an involvement of *GDPD5* and *GDPD6* in female gametophyte development can be excluded.

3.2.7 Downregulation of *GDPD5* Gene Expression Employing RNAi

As described in chapter 3.2.6.1, it was impossible to obtain double homozygous plants in 230 F2 plants of the *gdpp5-1* x *gdpd6-1* cross. To obtain plants with downregulated expression of the two genes, *GDPD5* expression was reduced by RNA interference in the *gdpd6-1* background. To this end, a modified pLH9000 vector (Table 2.2/2.3), containing a 300 bp long *GDPD5*-specific gene fragment in sense and antisense orientation, which shared no significant similarity with any other region in the Arabidopsis genome, was generated (Fig.: 3.45 A).

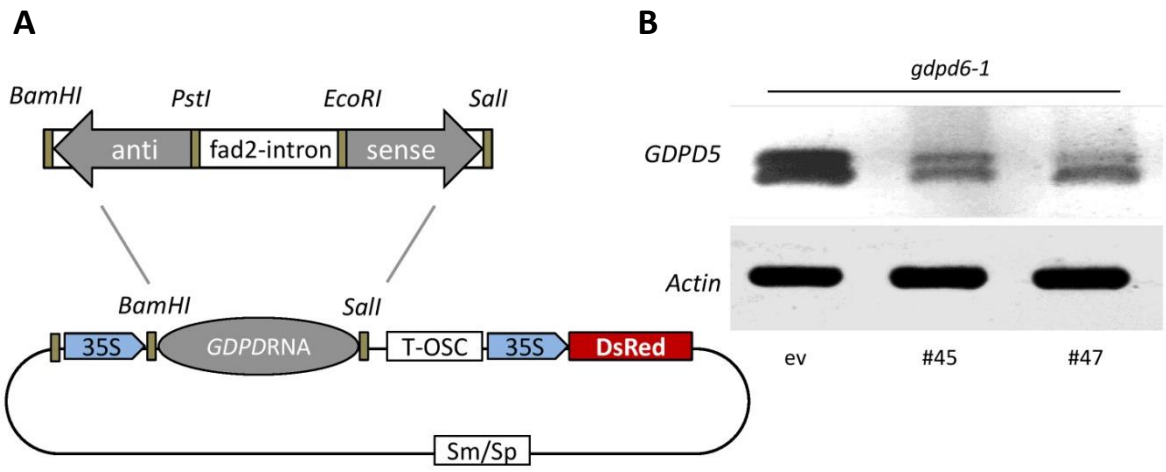

Figure 3.45: Downregulation of *GDPD5* by RNA interference. (A) RNAi construct for *GDPD5* used to transform Arabidopsis *gdpd6-1* mutant. **(B)** Semi-quantitative RT-PCR analysis of *GDPD5*-RNAi *gdpd6-1* plants. Total RNA was isolated from flowers and employed for RT-PCR analysis using gene specific primers for *GDPD* and *actin*. The PCR products were separated on an agarose gel and stained with EtBr.

The pL-*35S::GDPD5*-RNAi-DsRed RNAi construct was introduced into the homozygous *gdpd6-1* mutant by *Agrobacterium* mediated transformation. The F1 seeds were selected for transgenic events using the red fluorescence marker protein, Expression levels in flowers of F1 plants were determined by semi-quantitative RT-PCR (Fig.: 3.45 B). RNA was isolated from flowers of Arabidopsis *gdpd6-1* mutant plants transformed with empty vector or with the *GDPD5* RNAi construct (Fig.: 3.45 A). RT-PCR was performed with specific primers for *GDPD5* and *actin*. Analysis by RT-PCR resulted in the identification of RNAi lines #45 and #47 (*gdpd6-1* background) with reduced transcription levels for *GDPD5* when compared to the empty vector control (Fig.: 3.45 B).

3.2.7.1 Characterization of *GDPD5 gdpd6-1* RNAi Lines

Because a transmission defect through the male gametes in the *gdpd5-1*$^{+/-}$*gdpd6-1*$^{+/-}$ mutant line combined with a reduced pollen viability of about 50 % was observed, the pollen viability of the *GDPD5 gdpd6-1* RNAi Lines was assessed, too. Analysis by Alexander staining revealed that around 25 % of the pollen grains of the *GDPD5::RNAi gdpd6-1* lines #45 and #47 were non-viable (Fig.: 3.46 A). In order to assess changes in the G3P content in the RNAi lines, approximately 50 mg leaf material (fresh weight) of plants grown on soil was employed for G3P extraction with chloroform/methanol and quantification by GC-MS. The RNAi lines did not show any alterations in G3P content when grown under Pi plus condition compared to Arabidopsis empty vector control (Fig.: 3.46 C).

A

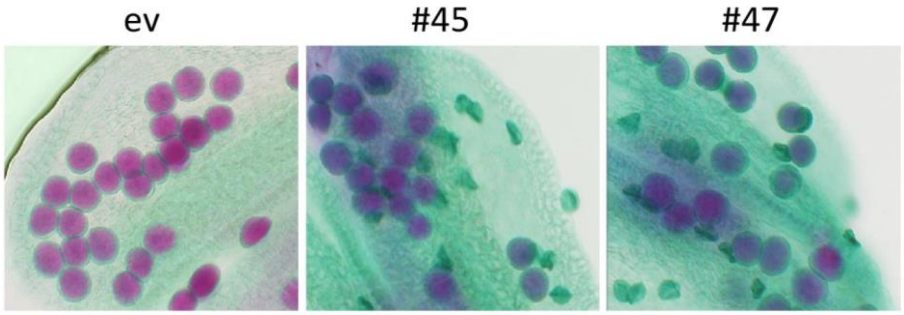

B

Pollen viability of RNAi lines

Pollen	eV		RNAi #45		RNAi #47	
	Numbers		Numbers		Numbers	
Total	**1896**	**100 %**	**1085**	**100 %**	**1622**	**100 %**
Viable	11868	99 %	798	74 %	1142	70 %
Non-viable	18	1 %	287	26 %	480	30 %

C

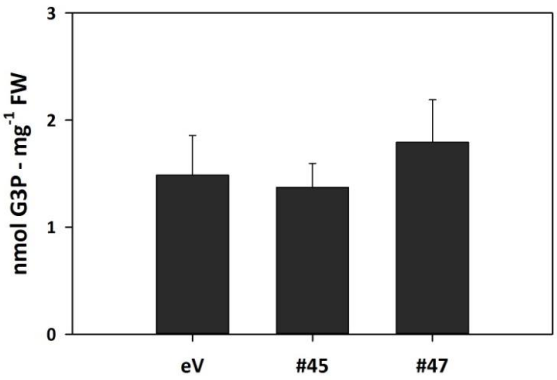

Figure 3.46: Viability test of pollen from WT and RNAi *GDPD5* plants with *gdpd6-1* background. (A) Alexander staining of the empty vector control (eV), RNAi line #45, and RNAi line #47 pollen grains. **(B)** Pollen viability rates determined by Alexander staining. **(C)** G3P content in Arabidopsis leaf from the empty vector control (eV), RNAi line #45, and RNAi line #47 grown on soil.

Taken together, RNAi-based downregulation of *GDPD5* in *gdpd6-1* mutant plants affected pollen viability as observed for the double heterozygous *gdpd5-1*$^{+/-}$*gdpd6-1*$^{+/-}$ mutant line. Approximately 25 % of the pollen grains of *GDPD5* RNAi plants #45 and #47 were non-viable (Fig.: 3.46 A, B). When plants were grown on soil, no differences in G3P levels in leaves compared to the empty vector control could be detected.

3.2.8 Ectopic Overexpression of *GDPD5* and *GDPD6* in Arabidopsis

3.2.8.1 Generation of Overexpression Constructs for *GDPD5* and *GDPD6*

To further study the function of Arabidopsis *GDPD5* and *GDPD6*, *35S::GDPD5* and *35S::GDPD6* overexpression constructs were generated. To this end, *GDPD5* and *GDPD6* full-length cDNAs were cloned in sense orientation, under the control of the 35S promoter and transformed into *A. tumefaciens* GV3101. After transformation of Arabidopsis plants with the

overexpression constructs, the F1 seeds were selected for transgenic events using the red fluorescence marker protein. To select plants with increased expression of *GDPD5* and *GDPD6*, semi-quantitative RT-PCR was performed on leaves of T_1 plants using primers specific for *GDPD5*, *GDPD6* and *actin*. All analyzed transgenic plant lines showed an elevated level of *GDPD5* and *GDPD6* transcription in leaves in comparison to the empty vector control (Fig.: 3.47).

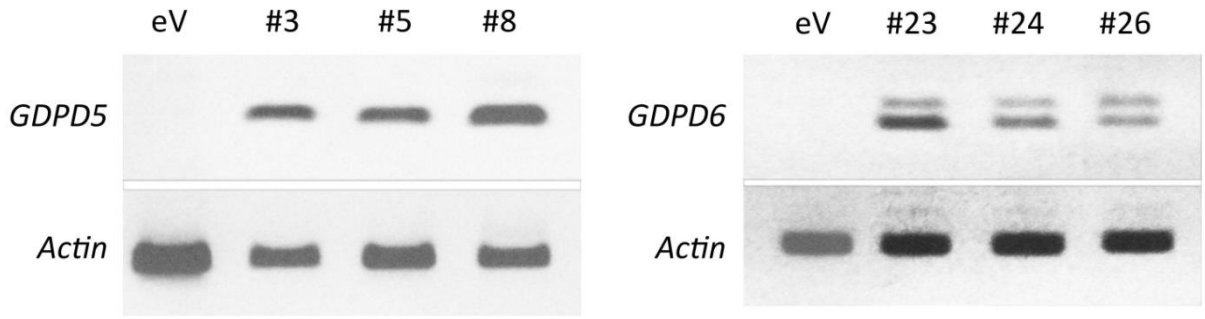

Figure 3.47: RT-PCR of GDPD overexpression lines. Semi-quantitative RT-PCR analysis of Arabidopsis empty vector control (eV), *35S::GDPD5* (#3, #5, and #8), and *35S::GDPD6* overexpression plants (#23, #24, and #26). RNA was extracted from leaf tissue and RT-PCR was performed using gene specific primers for *GDPD5*, *GDPD6,* and for *actin*. The PCR products were separated on an agarose gel and stained with EtBr.

3.2.8.2 Characterization of Glycerolipid Content in *GDPD5* and *GDPD6* Overexpression Lines

For lipid quantification by Q-TOF MS/MS analysis of the *GDPD5* and *GDPD6* overexpression lines, ~50 mg leaf material (fresh weight) of plants grown with or without Pi was employed. The overexpression lines did not show any differences in glycerolipid contents or molecular species composition (data not shown) compared to the empty vector control. Therefore, the overexpression lines were overall comparable to the control line on the morphological level and in the glycerolipid composition. The increased *GDPD* expression did not lead to alterations in the glycerolipid content under Pi-repleted or Pi-depleted conditions in Arabidopsis.

3.2.8.3 Ectopic Expression of *GDPD6* in *gdpd5-1$^{+/-}$gdpd6-1$^{+/-}$* Plants

Constructs harboring the *GDPD6* full length genomic DNA under the control of the CMV 35S promoter or the *GDPD6* native promoter were introduced into *gdpd5-1$^{+/-}$gdpd6-1$^{+/-}$* plants for a complementation experiment. After transformation by agroinfiltration, the transgenic seeds were identified by the DsRed selection marker. After testing approximately 500 plants of the T_0 to T_3 generation by PCR analysis, a segregation pattern still lacking the double homozygous mutant genotype was observed (data not shown). Only heterozygous/homozygous mutant plants could be recovered. Therefore, the ectopic expression of *GDPD6* under the control

of the 35S promoter did not lead to a full complementation of the lethal phenotype. However, heterozygous/homozygous *gdpd5-1*$^{+/-}$*gdpd6-1*$^{-/-}$ plants could be found, which were absent in the progeny of double heterozygous *gdpd5-1*$^{+/-}$*gdpd6-1*$^{+/-}$ plants without ectopic expressed *35S::GDPD6* construct. Due to the inability of the CMV 35S construct to fully complement the lethal phenotype, resulting in viable, complemented double homozygous plants, a complementation construct with *GDPD6* genomic DNA under the control of the *GDPD6* native promoter region was made. To this end, the complete genomic region between the stop codon of the 5' flanking gene to the start codon of the 3' flanking gene (Fig. 3.48) was amplified by PCR from genomic DNA and introduced into pL-*35S::GDPD6*-DsRed, replacing the 35S promoter and the *GDPD6* cDNA. This construct (pL-utr-GDPD6-utr-DsRed), harbors the 5' and 3' non-transcribed region and the genomic sequence of *GDPD6*. After transformation by agroinfiltration, the transgenic seeds were identified by the DsRed selection marker and the plants tested by PCR analysis. After screening approximately 250 plants of the T_0 to T_3 generation no complemented double homozygous *gdpd5-1*$^{-/-}$*gdpd5-2*$^{-/-}$ mutant plants were obtained in the progeny.

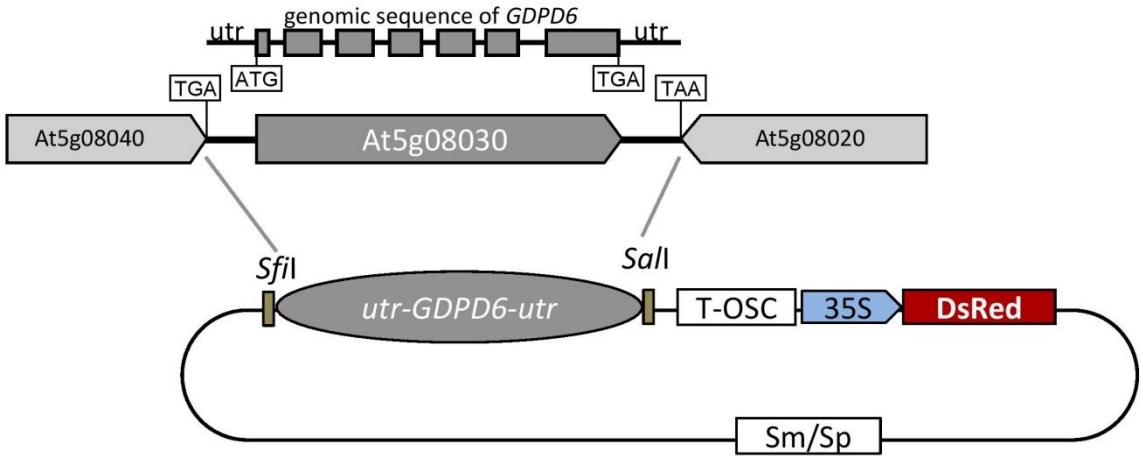

Figure 3.48: Complementation constructs for *gdpd5-1*$^{+/-}$*gdpd6-1*$^{+/-}$ mutant. Diagram of the construct used for the complementation experiment of the pollen lethal *gdpd5-1*$^{+/-}$*gdpd6-1*$^{+/-}$ phenotype. The full genomic *GDPD6* sequence was introduced into the *gdpd5-1*$^{+/-}$*gdpd6-1*$^{+/-}$ mutant.

4 Discussion

Lipids are major constituents of all biological membranes and play crucial roles in the plant's ability to survive and adapt to environmental changes. Plants are capable of changing their membrane composition as a response to abiotic or biotic stress conditions such as Pi deprivation. Pi is an essential macronutrient for plant growth and development (Raghothama, 1999). Many soils around the world are characterized by low Pi availability (Vance et al., 2003; Fang et al., 2009). In response to continuously low levels of Pi, different organisms such as non-photsynthetic bacteria, cyanobacteria, and plants have developed mechanisms to cope with Pi starvation by the utilization of endogenous Pi from phosphorus-containing molecules like phospholipids. In the present work, the regulation of membrane lipid biosynthesis and the remodeling under Pi deprivation in Arabidopsis were analyzed.

4.1 Characterization of Arabidopsis *FatA1* and *FatA2*

The first part of this work focused on the characterization of the two isoforms of acyl-ACP thioesterases A, which catalyze the first committed step of the eukaryotic lipid biosynthesis pathway. Acyl-ACP thioesterases hydrolyze acyl-ACPs in the plastid, releasing free fatty acids and ACP. Free fatty acids are subsequently esterified to CoA and exported to the ER, serving as substrates for the eukaryotic lipid biosynthesis.

4.1.1 The *FatA1* and *FatA2* Genes Encode Proteins with Acyl-ACP Thioesterase Activity

The acyl-ACP thioesterase family shows diversity in enzymatic function. Thioesterases represent the major determinants of the chain length and level of saturated fatty acids. Therefore, thioesterases contribute to the regulation of the fatty acid composition. To address the question of enzyme function and substrate specificity of Arabidopsis *FatA1* and *FatA2*, the cDNAs were heterologously expressed in *E. coli.* Previously, the expression of plant acyl-ACP thioesterases resulted in strong alterations in the fatty acid profiles in *E. coli* membranes as well as in the culture supernatant (Voelker and Davies, 1994; Huynh et al., 2002; Jha et al., 2006). The *E. coli fadD* mutant lacks the acyl-CoA synthetase FadD. FadD mediates the transport of fatty acids from the periplasm to the cytosol and harbors acyl-CoA ester synthesis activity (Weimar et al., 2002). It also uses free fatty acids derived from membrane lipids. Acyl-CoAs can then be degraded via the β-oxidation pathway. Consequently, the *fadD* disruption mutant accumulates free fatty acids in the cytosol (Pech-Canul et al., 2011)(Fig.: 4.1).

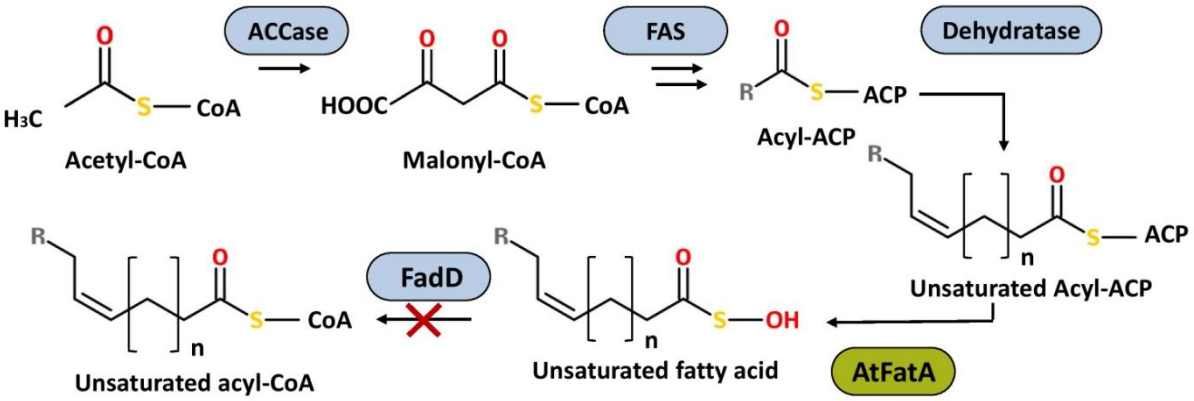

Figure 4.1: Biosynthetic pathway of free monounsaturated fatty acids in this study. Arabidopsis *FatA* was introduced into *E. coli fadD* mutant. ACCase, acetyl-CoA carboxylase; FAS, fatty acid synthase; AtFatA, Arabidopsis acyl-ACP thioesterase; FadD, acyl-CoA synthetase.

Sequence analysis demonstrated that the Arabidopsis *FatA* genes encode proteins related to acyl-ACP thioesterases of the family A. Type A and Type B thioesterases can be distinguished with regard to sequence similarity, and show different substrate specificities for chain lengths and degree of fatty acid desaturation. In plants, full-length coding sequences of type A acyl-ACP thioesterases show highest specificity towards the hydrolysis of $18{:}1^{\Delta 9}$-ACP. Initially, the complete coding sequences for *FatA1* and *FatA2* were heterologously expressed in the *E. coli fadD* mutant. SDS gel electrophoresis and Western blot analysis of the total proteins from recombinant FatA strains revealed both FatA cDNAs to be expressed in *E. coli*. However, the expression did not result in the change of fatty acid composition in the recombinant strains, presumably due to the presence of the predicted transit peptides. After the removal of the predicted N-terminal targeting sequence of 50 and 43 amino acids for FatA1 and FatA2 in new constructs, respectively, functional proteins were obtained after expression in *E. coli*. No changes in fatty acid composition were detectable in *E. coli* total lipid extracts. After solid phase extraction and subsequent analysis of the neutral lipid fraction containing mostly free fatty acids, an accumulation of 16:0, $16{:}1^{\Delta 9}$, and $18{:}1^{\Delta 11}$ fatty acids was observed in the *E. coli* cell pellet. It is known that FatA enzymes from other plants are specific for oleoyl-ACP ($18{:}1^{\Delta 9}$-ACP) (Serrano-Vega et al., 2005; Sanchez-Garcia et al., 2010). Therefore, the accumulation of C16 saturated fatty acids as well as $16{:}1^{\Delta 9}$ in transformed *E. coli* cells was unexpected. This substrate preference of *FatA1* and *FatA2* when expressed heterologously in *E. coli* may be explained by the differences in *E. coli* fatty acid synthesis and composition compared to plants. The palmitoyl-ACP (16:0-ACP) pool is much larger in *E. coli* than in plants (Ohlrogge et al., 1995; Rock and Jackowski, 1982). Therefore substrate availability in *E. coli* is distinct from that *in planta*. Although there is much more 16:0-ACP available in *E. coli*, free palmitoleic acid ($16{:}1^{\Delta 9}$) levels were similar to free palmitic acid levels in the recombinant *FatA1* and *FatA2* expressing cells. This can be explained by the fact that Arabidopsis *FatA1* and *FatA2* prefer unsaturated rather

than saturated acyl-ACPs. Unlike plants, *E. coli* only contains cis-palmitoleic acid ($16:1^{\Delta 9}$) and cis-vaccenic acid ($18:1^{\Delta 11}$) as unsaturated fatty acids. Oleoyl-ACP ($18:1^{\Delta 9}$-ACP), which is the endogenous substrate for Arabidopsis FatA , appears only in trace amounts in *E. coli*. Free *cis*-vaccenate levels are much higher in the recombinant strains compared to the empty vector control. The amount of $18:1^{\Delta 11}$ fatty acid is below that of $16:1^{\Delta 9}$ in the recombinant *E. coli* strains and therefore seems to be a worse substrate for FatA in *E. coli*. This might be due to the position of the double bond. This finding points to a preference of Arabidopsis *FatA* for monounsaturated fatty acids and also for the double bond position at Δ9. This data was partially confirmed by Cao and co-workers (2014). In a biotechnological approach, they expressed Arabidopsis *FatA1* heterologously in the *E. coli fadD* mutant to release free unsaturated fatty acids. Because the expression of *FatA1* per se did not result in an increase of the *cis*-vaccenate level, they simultaneously overexpressed the native acyl-CoA carboxylase (ACCase) and Arabidopsis fatty acid desaturase *SSI2* in the *FatA1* overexpressing *fadD* mutant. This resulted in a considerable increase in monounsaturated fatty acid levels comprising $16:1^{\Delta 9}$ and $18:1^{\Delta 11}$ (Cao et al., 2014).

4.1.2 Characterization of the Arabidopsis *fatA1-2 and fatA2-2* Mutants

4.1.2.1 *fatA1-2* Single Mutant Seeds Showed Increased Levels of 18:3 and 22:1 Fatty Acids

T-DNA insertion mutants for the *FatA1* and *FatA2* genes have been studied previously (Moreno-Pérez et al., 2012). Moreno-Pérez and co-workers (2012) analyzed the physiology and biochemistry of the two mutants, *fatA1-1* and *fatA2-1*, harboring insertions in their promoter regions, with intact coding regions. They also generated a *fatA1-1fatA2-1* double mutant, which did not differ in growth rate, number of leaves, or the number or viability of the seeds compared to Arabidopsis Col-0. The single mutant lines as well as the double mutant still showed residual expression of *FatA1* and *FatA2* as analyzed by Q-RT-PCR. The focus of the study by Moreno-Pérez and co-workers (2012) was the oil (TAG) accumulation in the developing *fatA1-1fatA2-1* seeds, which was decreased at different seed development stages (Moreno-Pérez et al., 2012). In the present work, two Arabidopsis *FatA* mutant alleles were employed, with insertions located in exons between start and stop codon. These mutants represent null alleles as revealed by the absence of *FatA1 and FatA2* expression, when analyzed by semi-quantitative RT-PCR using primers binding 5' and 3' of the insertion site. Different morphological and biochemical aspects of the two mutants were analyzed. The homozygous single mutant lines *fatA1-2* and *fatA2-2* used in this study were comparable in growth and morphology to Arabidopsis Col-0 WT plants. The number and viability of the seeds were also comparable between control Col-0 and the single mutants. Hence, the insertions did not interfere with the synthesis of lipids necessary for the vegetative development of the plant. Mutants were analyzed for biochemically aspects,

especially for fatty acid composition and oil accumulation in the developing seeds, since this was the plant tissue that most actively synthesized lipids.

The *fatA1-2* single mutant seeds showed a reduction in $18:1^{\Delta 9}$ content by about 33 mol % with a concomitant increase in 18:3 and 22:1 compared to WT Col-0 total fatty acids. This increase in the proportion of 18:3 and 22:1 accompanied by the decrease in $18:1^{\Delta 9}$ was also seen in the double homozygous *fatA1-1fatA2-1* mutant line analyzed by Moreno-Perez et al (2012), but not in the *fatA1-1* or *fatA2-1* single mutants. This shift in fatty acid composition may be explained by the relative activities of different enzymes involved in fatty acid synthesis. In the homozygous *fatA1-1fatA2-1* double mutant, the flux through each enzymatic step of fatty acid biosynthesis was estimated by means of the amount of fatty acids measured and values were compared to a control line (Moreno-Perez et al., 2012). In the double mutant, the flux of acyl groups through ketoacyl-ACP synthase II (KASII) and stearoyl-ACP desaturase (SAD) were comparable to the control, whereas flux through linoleate desaturase and fatty acid elongase activities were higher. This suggests a general downregulation of some enzymatic activities involved in fatty acid synthesis caused by the decrease in *FatA*1 and *FatA2* expression. Consequently, this resulted in increased proportions of linolenic and erucic acid at the expense of their precursors, as shown for the *fatA1-1fatA2-1* mutant analyzed by Moreno-Perez (2012) and the *fatA1-2* single mutant line studied in the present work. However, the fatty acid composition of the *fatA2-2* null mutant was comparable to Arabidopsis WT. This data agrees with the results obtained after heterologous expression of *FatA1* and *FatA2* in the *E. coli fadD* mutant. In addition, *FatA1* expression levels were overall higher than the expression levels of *FatA2* in different Arabidopsis tissues. *FatA1* and *FatA2* share 74.3 % identity on amino acid level and 84 % on nucleotide sequence. The data suggests that *FatA1* and *FatA2* are homologous genes sharing functional redundancy. Therefore, the residual *FatA1* enzyme activity in the *fatA2-2* mutant presumably was able to compensate for the loss of *FatA2* while *FatA2* was not able to completely compensate the *FatA1* loss of function due to its lower expression level.

In plant seeds, acyl-ACP thioesterases are the primary biochemical determinants of the fatty acid composition of storage lipids because they terminate the acyl chain elongation of fatty acid biosynthesis. Thus, the loss of *FatA1* in the *fatA1-2* mutant caused a reduced total fatty acid content in dry seeds, as well as, a shift in TAG molecular species composition, showing a decrease of 18:1, 18:2, and 18:3 fatty acids and a concomitant increase in 20:1 and 22:1 containing molecular species, while content and composition of other neutral lipids like DAG were not affected. A similar effect has previously been reported for the Arabidopsis *wri1* mutant (reduced expression of the transcription factor WRI1, Focks and Benning, 1998), showing a decrease in TAG content by 80 %. The fatty acid composition in the *wri1* mutant seeds was comparable to the fatty acid composition of the *fatA1-1fatA2-1* double mutant analyzed by Moreno-Perez and co-workers (2012). Moreover, the *fatA1-2* single mutant line studied in this

work, showed increased levels of linolenic and erucic acid and a decrease in oleic and linoleic acid (Focks and Benning, 1998; Moreno-Perez et al., 2012). The *wri1* mutant had a reduced TAG content due to an embryonic deficiency in the conversion of sucrose to precursors for the TAG biosynthesis. *WRI1* is an AP2-type transcription factor essential for the accumulation of TAGs in Arabidopsis seeds. The overexpression of *WRI1* resulted in induced expression of different genes involved in fatty acid synthesis in plastids. Potential DNA-binding motifs (AW-box) for *WRII* in both *FatA* promoter regions indicate an involvement of WRI1 in the regulation of the transcription of the *FatA* genes (Maeo et al., 2009). The AW-box [CnTnG](n)(7)[CG] can notably be found in promoters of fatty acid biosynthesis genes. WRI1 binds directly to the AW-box, and mutation of it abolishes WRI-mediated transcriptional activation *in vitro* (Maeo et al., 2009). *WRI1* did not activate the expression of genes involved in TAG synthesis like *TAG1* (diacylglycerol acyltransferase, DGAT1). This data indicates, that in addition to *WRI1*, other transcription factors are required for the activation of genes involved in assembly and storage of TAG (Focks and Benning, 1998; Maeo et al., 2009). This suggests that transcription of the *FatA* genes is affected in the *wri1* mutant. For *FatA1*, a significant decrease of mRNA accumulation in early-maturing seeds of the triple *wri1wri3wri4* mutant was shown by To and co-workers (To et al., 2012), showing an involvement of WRI1 in the regulation of the transcription of *FatA1*. Amongst others, *KASII* and *SAD*, encoding enzymes involved in fatty acid biosynthesis, belong to the genes affected by the *wri1* mutation. It is believed that a reduction in the rate of glycolysis may induce a downregulation in the fatty acid biosynthesis pathway.

4.1.2.2 Embryo Development of *fatA1-2*$^{-/-}$*fatA2-2*$^{-/-}$ Mutant seeds is Aborted at the Late Heart to Early Torpedo Stage

The absence of double homozygous *fatA1-2*$^{-/-}$*fatA2-2*$^{-/-}$ plants in the progeny of heterozygous/homozygous *fatA1-2*$^{-/-}$*fatA2-2*$^{-/+}$ plants and the 3:1 segregation of viable to aborted seeds in the siliques of *fatA1-2*$^{-/-}$*fatA2-2*$^{-/+}$ mutant plants suggested that *FatA1* and *FatA2* are essential for Arabidopsis embryo development. After crossing heterozygous *fatA1-2*$^{-/+}$ and *fataA2-2*$^{-/+}$ single mutants, no double homozygous mutants were obtained in the progeny, but heterozygous/homozygous *fatA1-2*$^{-/-}$*fatA2-2*$^{-/+}$ or *fatA1-2*$^{-/+}$*fatA2-2*$^{-/-}$ plants were recovered. Both lines showed the 3:1 segregation ratio of viable to aborted seeds and no double homozygous plants were observed in the progeny. The embryo development of the aborted seeds in the two lines was arrested at the late heart to early torpedo stage, and PCR analysis revealed these embryos carry homozygous mutations for the two *fatA* genes. Pollen viability in the two lines was unchanged compared to Arabidopsis WT pollen as revealed by Alexander staining. These results indicate that the two genes are functionally redundant and that one WT allele of *FatA1* or *FatA2* is sufficient to maintain proper embryo development in heterozygous/homozygous mutant plants. This hypothesis is corroborated by the results obtained after heterologous

expression in *E. coli*, demonstrating *FatA1* and *FatA2* share the same enzymatic function, and by the overlapping gene expression patterns in different Arabidopsis tissues.

To monitor possible changes on the levels of lipids, double homozygous embryos were analyzed. Initially, the fatty acid compositions in Arabidopsis WT embryos at the heart stage, torpedo stage, and in the fully developed embryo were determined by GC. During embryo development in Arabidopsis WT, the content of long and very long chain fatty acids and the degree of desaturation are increased. In heart stage embryos, palmitate (16:0) and stearate (18:0) together accounted for approximately 50 % of the total fatty acids, while in the fully developed embryos, the unsaturated fatty acids made up around 75 %. The fatty acid profiles of double homozygous heart stage mutant embryos were compared to regular developing mutant sibling embryos from the same silique (*fatA1-1*$^{+/-}$*/fatA2-2*$^{-/-}$ or *FatA1-2+/+/fatA2-2*$^{-/-}$) and WT embryos at different stages. The double mutant embryos showed a fatty acid composition comparable to WT torpedo stage embryos. The differences in fatty acid composition between the embryos of the *fatA1-2*$^{-/-}$*fatA2-2*$^{-/-}$ *double* mutant and the heart stage WT control line mainly concerned the degree of desaturation of C18 fatty acids and the chain length, which was increased. The unsaturated C18 fatty acids were more abundant in the double mutant embryos. Taking into consideration Arabidopsis *FatA* substrate specificity, *FatA* deficiency is expected to affect the ratio between C16 and longer fatty acids due to the specificity of the remaining FatB thioesterase. The loss of *FatA* function while the activity of FatB remained constant is expected to result in a reduced content of oleic acid in glycerolipids and increased levels of C16 fatty acids. However, the levels of C18 fatty acids were increased, and the proportion of palmitic acid was even slightly reduced when comparing heart stage double mutant and WT embryos, in contrast to the Arabidopsis *fatB* mutant. The fatB mutant exhibited a drastic decrease in palmitic acid levels in all plant tissues and alterations in the relative C16 fatty acid content in the seed oil (Bonaventure et al., 2003). Moreno-Pérez and co workers (2012) found differences in desaturation of C18 fatty acids between mature, dry seeds of the *fatA1-1fatA2-1* double mutant and WT. The *fatA1-1fatA2-1* double mutant showed elevated erucic acid and linolenic acid levels and a decrease in oleic acid in seed oil. The total amount of oil was also significantly decreased. These changes in the fatty acid composition of the *fatA1-1fatA2-1* double mutant were not found to be related to the *de novo* synthesis but rather to the subsequent steps of fatty acid modification. The changes were, therefore, not a direct consequence of the reduced *FatA1 and FatA2* activities but due to a metabolic response of the plant to the changes caused by the mutations (Moreno-Pérez et al., 2012).

To assess the contribution of *FatA1* and *FatA2* to the metabolic flux into oil, the DAG and TAG contents were determined in the double homozygous *fatA1-2*$^{-/-}$*fatA2-2*$^{-/-}$ mutant embryos at heart stage. The total amount of DAG and TAG was significantly increased in the double mutant embryos compared to WT heart stage embryos. While the DAG content was increased

approximately 2.2 fold, the TAG levels were 5 fold as high as the TAG levels in the control embryos. There was also a substantial increase in 16:1 and 18:1 containing molecular species of DAG, while 18:0 containing species were significantly decreased compared to WT heart stage embryos. This tendency was also observed in the TAG molecular species. The elevated levels in DAG and TAG content were unexpected but most probably caused by the difference in age of the control line. The mutant embryos in the siliques of *fatA1-2*$^{+/-}$*fatA2-2*$^{-/-}$ plants were only distinguishable from the normally developing sibling embryos when these were fully developed, because the mutant embryos did not progress beyond the late heart stage. Differentiation was possible around 12 days after flowering. Until this point of development, the lipid accumulation in the normal developing sibling embryos proceeded, and the fatty acid composition changed while the mutant embryos were morphologically arrested at heart stage. Biochemically, the mutant embryos were most similar to torpedo or early cotyledon stage embryos of WT. Hence, WT embryos at heart stage were selected as a second control next to mutant sibling embryos for fatty acid analysis. However, the WT embryos at heart stage were much younger than the mutant embryos arrested at heart stage. WT heart stage embryos were collected approximately four days after flowering while the double mutant "heart stage" embryos were isolated around 12 days after flowering, when differentiation between normal mutant sibling seeds and *fatA1-2*$^{-/-}$ *fatA2-2*$^{-/-}$ seeds was possible. The control seeds for fatty acid analysis used in this study were either on the same developmental stage but younger, or they were about the same age, being fully developed, which made a comparison on the biochemical level difficult. Analysis of the mutant embryos implicates a progress until torpedo to early cotyledon stage on the biochemical level. Morphologically, the mutant embryos did not progress beyond the heart stage. TAG content massively accumulates during embryo development. The fact that fatty acid composition in *fatA1-2*$^{-/-}$*fatA2-2*$^{-/-}$ embryos is more comparable to torpedo stage WT embryos, while morphologically arrested at heart stage, may explain the elevated levels TAG content in *fatA1-2*$^{-/-}$ *fatA2-2*$^{-/-}$ embryos compared to WT heart stage embryos.

Arabidopsis green embryos are photosynthetically active. The total glycerolipid content, as well as lipid molecular species composition of Arabidopsis *fatA1-2*$^{-/-}$*fatA2-2*$^{-/-}$ embryos, was most comparable to the heart stage WT embryos with changes in DGDG and SQDG content. The mutant embryos exhibited a decrease of DGDG content by about 34 % with the concomitant increase of SQDG levels of approximately 42 % compared to heart stage WT embryos. While no alterations in SQDG molecular species were detected, DGDG showed increased levels of 16:0 and 18:2 containing molecular species and a lower abundance in 18:1 containing molecular species. Molecular species composition of PE was analyzed. PE is synthesized extraplastidially, thus, C18 fatty acids incorporated into PE have previously been exported out of the plastid. Hence, PE can be employed as marker lipid, providing information about the amount of exported 18:1 fatty acids. Molecular species composition of PE in *fatA1-2*$^{-/-}$*fatA2-2*$^{-/-}$ embryos was comparable to

those of the WT heart stage embryos. Equal amounts of 18:1 fatty acids and desaturation products (18:2, 18:3) were still incorporated into PE, implying that the export of 18:1 from the plastid was still active and were probably due to the remaining enzymatic function of FatB in the *fatA1-2*$^{-/-}$*fatA2-2*$^{-/-}$ embryos. Differences in 18:3 and 16:0 fatty acid contents were more prominent. FatB exhibits activity towards 16:0-ACP and 18:1-ACP, but the 18:1-ACP activity is lower than that with 16:0-ACP (Dörmann et al., 1995). The 18:1-ACP thioesterase activity of FatB is presumably responsible for the residual export of 18:1 fatty acids. Export of 18:1 fatty acids outside the plastid by FatB activity appears to be sufficient to promote proper embryo development until the late heart stage in the *fatA1-2*$^{-/-}$*fatA2-2*$^{-/-}$ mutant. At this point, lipid export from the chloroplast drastically increases at the onset of TAG synthesis and assembly in developing seeds (Fig.: 4.2).

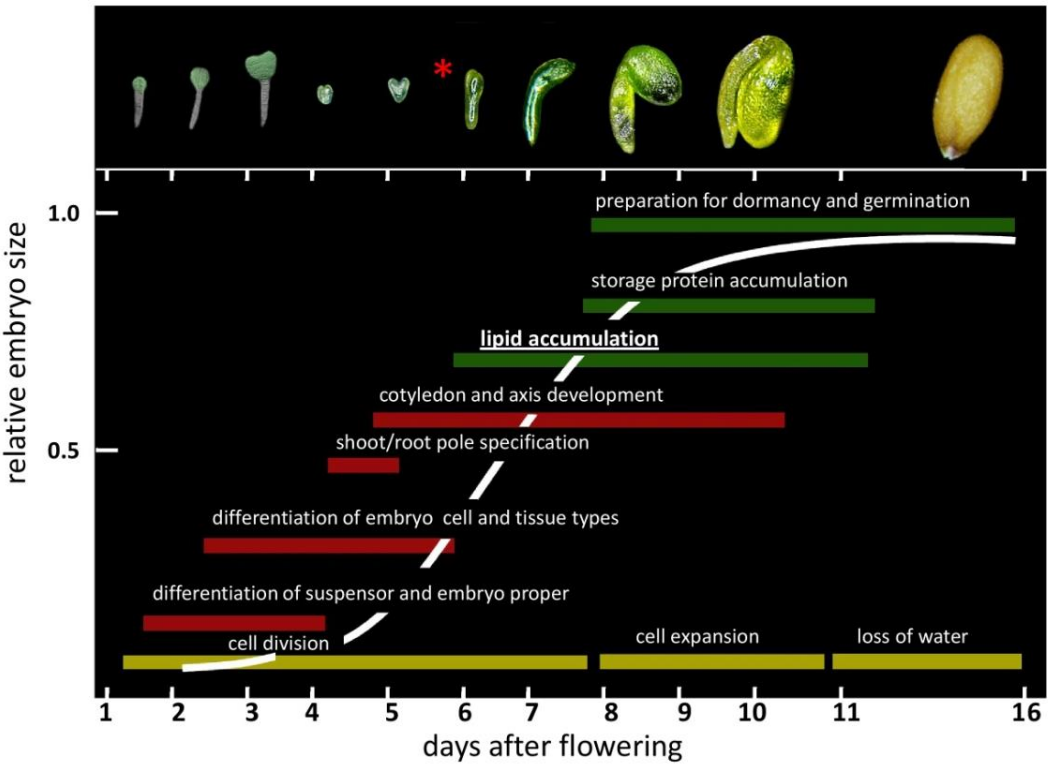

Figure 4.2 Different phases of embryogenesis in Arabidopsis. The embryo undergoes three phases of embryogenesis, i.e. morphogenesis, where the cell division takes place, cell expansion and the preparation of dormancy. Lipid accumulation begins at late heart to early torpedo stage and ends with the preparation for dormancy by the embryo losing water. The red asterisk marks the developmental stage, when *fatA1-2*$^{-/-}$*fatA2-2*$^{-/-}$ embryo development is arrested. Pictures are not to scale. Modified after Kunst, Plant Bio-Industrial Oils Workshop Presentation.

Taken together, the difference in fatty acid composition between *fatA1-2*$^{-/-}$*fatA2-2*$^{-/-}$ loss-of-function mutant embryos and the WT heart stage embryos mainly concerned the degree of desaturation of C18 fatty acids and the decrease in the amounts of unsaturated fatty acids. There is also an increase in TAG content. All differences found in the *fatA1-2*$^{-/-}$*fatA2-2*$^{-/-}$ double mutant embryos were rather minor. This may be due to the remaining FatB activity in these embryos,

which was apparently able to provide sufficient 18:1 fatty acids up to the heart stage of embryo development. In conclusion, the results show that a heterozygous/homozygous *fatA1-2*$^{-/-}$*fatA2-2*$^{-/-}$ embryo can provide sufficient oleic acid to support oil accumulation and embryo development up to late heart stage. Though beyond that point, the export of 18:1 fatty acids from the plastid becomes insufficient for proper development. There are two possible explanations, namely a feedback inhibition of the plastidic ACCase involved in fatty acid *de novo* synthesis by 18:1-ACP, or the lack of 18:1 fatty acids outside the plastid for lipid biosynthesis. One possibility is that a block of 18:1-ACP hydrolysis and the subsequent export from the plastid causes the accumulation of 18:1-ACP, which has been shown to act as an allosteric regulator (Heath and Rock, 1995), targeting the plastidic ACCase in *Brassica napus* (Andre et al., 2012). ACCase catalyzes the carboxylation of acetyl-CoA to malonyl-CoA. Subsequently, the malonyl group is transferred from CoA to ACP. Malonyl-ACP is the elongation unit during plastidiyl fatty acid synthesis. Accumulation of 18:1-ACP induces a rapid feedback inhibition of the plastidic ACCase, which was shown to be reversible after the decrease of 18:1-ACP to a normal level (Andre et al., 2012). This was analyzed by feeding oleic acid-Tween esters to *B. napus* suspension cell cultures. Previous studies revealed the crucial role of the *de novo* fatty acid synthesis during embryo development in Arabidopsis. The Arabidopsis T-DNA insertion mutant *kasI*, lacking the ß-ketoacyl-ACP synthase I (KASI), which catalyzes the elongation from C4 to C16, showed reduced fatty acid levels and a disrupted embryo development before the globular stage (Wu and Xue, 2010). These results indicate a possible involvement of the *FatA1 and FatA2* genes in early embryo development by 18:1-ACP dependent regulation of fatty acid synthesis in the chloroplast. In analogy with Arabidiopsis, it has been shown that the primary mechanism regulating fatty acid biosynthesis in *E. coli* is controlled by a feedback inhibition of acetyl-CoA carboxylase caused by long-chain acyl ACPs (Davis et al., 2001).

A second possible explanation for the embryo lethal phenotype in the Arabidopsis *fatA1-2*$^{-/-}$*fatA2-2*$^{-/-}$ mutant might be the lack of 18:1 fatty acids exported from the plastid. 18:1 esterified to coenzyme A is elongated and desaturated by different enzymes at the endoplasmic reticulum. In Arabidopsis, the most abundant fatty acids are 18:1, 18:2 and 18:3 (Lemieux et al., 1990). 18:1 is further processed to 18:2 and 18:3 fatty acids by desaturases or elongated to very long chain fatty acids by elongases. In many plants, 18:2 and 18:3 account for more than 70 % of the fatty acids in leaf cells, and 55 to 70 % in non-photosynthetic tissues such as roots (Harwood, 1980). The *fatA1-2*$^{-/-}$*fatA2-2*$^{-/-}$ embryo development is arrested at the late heart to early torpedo stage, when the lipid accumulation sharply increases (Fig.: 4.2). The severe lack of 18:1 fatty acids outside the plastid may affect a different biochemical processes. 18:1 fatty acids are amongst others required for (i) the phospholipid synthesis. Phospholipids, as well as, eukaryotic galactolipids contain high proportions of 18:1, 18:2, and 18:3 fatty acids. Hence, the export of 18:1 fatty acid from the plastid is essential for membrane formation in extra and intraplastial

membranes. (ii) In plant signaling, 18:3 is a key precursor for jasmonic acid synthesis, which is critical for embryo and pollen development. For (iii) storage lipid accumulation in the developing embryos, mainly 18:1, 18:2, 18:3 and 20:1 fatty acids are required (Fig.: 4.3). Very long chain fatty acids (VLCFA) are synthesized at the ER by the sequential addition of 2-carbon moieties to C18 fatty acids. They are generally important for cuticle wax formation (Fig.: 4.3). It has been shown that the *acc1* mutant, affected in the cytosolic acetyl-CoA carboxylase 1 (ACCase1), is entirely deprived of VLCFAs and impaired in embryo morphogenesis, because it is embryo lethal (Baud et al., 2003; Baud et al., 2004). ACCase1 catalyses the formation of malonyl-CoA from acetyl-CoA and bicarbonate. The loss of ACCase1 activity leads to a lack of malonyl-CoA, crucial for VLCFA synthesis. Therefore, it is possible that embryos lacking large amounts of C18 fatty acids outside the plastid are impeded in fatty acid elongation at the ER and therefore in VLCFA synthesis.

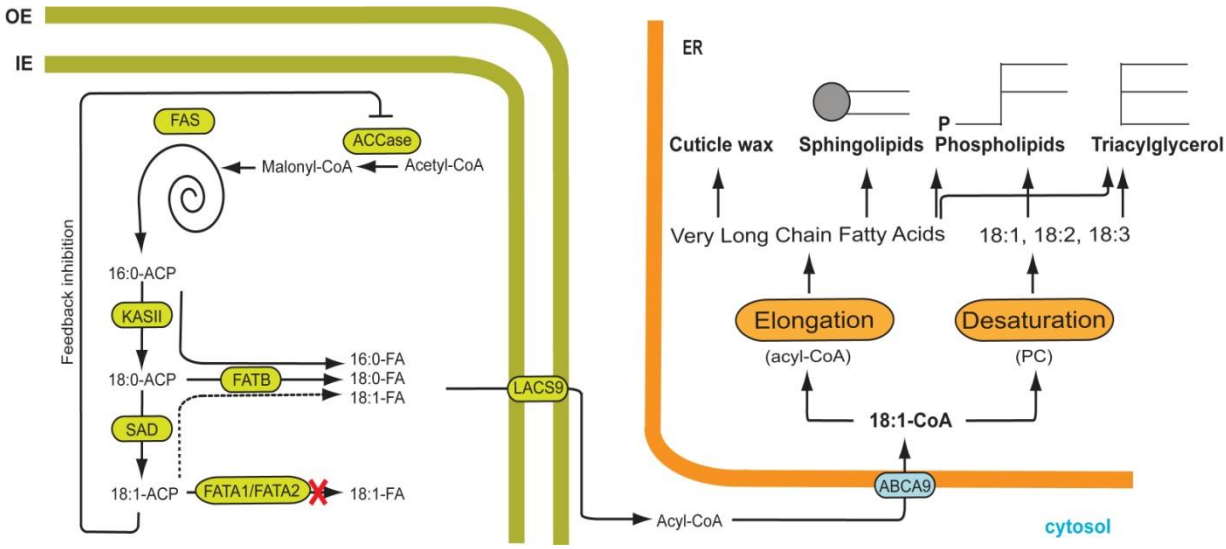

Figure 4.3: Mode of Action. Schematic presentation of putative metabolic responses to the loss of *FatA1* and *FatA2* activities in Arabidopsis. The loss of *FatA1* and *FatA2* activities lead to an accumulation of 18:1-ACP in the plastid, which was shown to negatively regulate ACCase activity. The export of 18:1 fatty acid is also drastically diminished, resulting in a lack of substrate for fatty acid elongation and desaturation, crucial for a multitude of reactions and processes at the ER.

4.1.3 The Expression of Different Acyl-ACP Thioesterases Did Not Rescue the Embryo Lethal Phenotype

Plants are not able to take up free fatty acids from their surrounding. In cell culture, plant cells are able to uptake exogenous fatty acids in form of Tween-fatty acid esters (Tween-18:1), as shown by different experiments with *Nicotiana tabacum*, and *Glycine max* (Terzaghi, 1986; Shintani and Ohlrogge, 1995). The complete loss of Arabidopsis *FatA1* and *FatA2* activity causes an early abortion of heart-staged embryos. Former approaches to chemically complement the *fatA1-2*$^{-/-}$*fatA2-2*$^{-/-}$ phenotype by Tween-80 (C18:1 fatty acids) supplementation to the growth

medium when growing seedlings on synthetic growth medium, or by direct application onto or into the siliques of *fatA1-2$^{-/-}$fatA2-2$^{-/-}$ plants*, were not successful (Svetlichnyy, 2007).

To assess if the embryo lethal phenotype is truly caused by the loss of *FatA* function, complementation experiments using acyl-ACP thioesterases (FatA or FatB) from Arabidopsis and *Umbellularia californica* with specificities for different acyl-ACPs under the control of the 35S, CvMV, glycinin, or the Arabidopsis *FatA1* promoter region in all possible combinations were performed. The transfer of all of these acyl-ACP thioesterase constructs into *fatA1-2$^{+/-}$fatA2-2$^{-/-}$* did not rescue the aborted embryos. In no case, complemented plants with the genotype *fatA1-2$^{-/-}$fatA2-2$^{-/-}$* were observed in the progeny. There are several possible explanations for the failure to complement the embryo lethal phenotype; (i) the promoters used for the different complementation constructs are silent during the critical stage of embryo development (heart stage), (ii) for the FatB constructs, the fatty acid export, mediated by FatB thioesterase activity from Arabidopsis and *U. californica,* is not sufficient to compensate for the loss of both *FatA* genes in Arabidopsis, or (iii) alterations in the sequence context upstream of the AUG initiation codon might affect expression of the transgene.

The expression pattern of *FatA1* and *FatA2* derived from *in silico* studies and semi-quantitative RT-PCR revealed that the two genes are highly expressed in siliques approximately 5 days after flowering, when embryo development reaches late heart stage in Arabidopsis. It is possible that the 35S, CvMV or glycinin promoters used for complementation experiments of the into *fatA1-2$^{+/-}$fatA2-2$^{-/-}$* double mutant, were silent, when FatA activity becomes significant in Arabidopsis. Considering the expression analysis of *FatA1* and *FatA2,* a promoter active during embryo development before late heart to torpedo stage is necessary for complementation analysis.

The first constructs (Arabidopsis *FatA1* and *FatB* cDNA, as well as, *U. californica UcFatB* cDNA) employed for complementing the embryo lethal phenotype were under the control of the cauliflower mosaic virus 35S (35S-CaMV) promoter. The 35S promoter is one of the most widely used general-purpose constitutive promoters, causing high levels of gene expression in dicot plants. It is known to be silent during microspore and pollen development (Twell et al., 1989, Mascarenhas and Hamilton, 1992, Wilkinson et al., 1997). The 35S promoter was also silent during early sporophytic divisions and remained inactive up to the mid-cotyledonary stage of embryonic microspores, in which the male gametes are induced to form embryos in cell culture (Bohanec, 2009; Seguí-Simarro, 2010). The haploid embryos produced by microspore embryogenesis are able to germinate and grow into mature but sterile plants (Soriano et al., 2013). It is suggested that microspore embryogenesis is equivalent to zygotic embryogenesis at the gene expression level (Custers et al., 2001). Other analyses revealed the 35S promoter to be silent in young zygotic embryos (Custers et al., 1999). The 35S promoter activity was analyzed in *B. napus* embryos from 5-cell to mid-cotyledon stage expressing a transgenic 35S-CaMV-

promoter-driven GUS construct. The 35S promoter appeared to be silent up to the mid-cotyledonary embryo stage (Custers et al., 1999). These findings suggest that the constitutive 35S promoter might be inactive at early embryo development in Arabidopsis, too. Another reason for the inability of the 35S constructs to restore *FatA1* function may be a silencing effect from the T-DNA insertion in the mutants. The 35S promoter is present in the T-DNA insertions of the SALK, FLAG, GABI, and WISCOSLOX collections (Daxinger et al., 2007; Daxinger et al., 2008). Transgene expression in commonly used T-DNA insertion lines can result in the silencing of constructs harboring the CaMV 35S promoter. Gene expression may be silenced by epistatic *trans*-inactivation. The non-reciprocal interaction that occurs between homologous transgenes present at ectopic chromosomal locations results in the inactivation of one transgene locus in the presence of the second one. Active transgenes can also become silent and methylated when brought into the presence of an unlinked homologous transgene. This can affect any transgene that is expressed under the control of the same promoter, independent of the coding sequence being expressed (Vaucheret, 1993; Matzke et al., 1994). The 35S constructs used for complementation contained at least two 35S promoter sequences, regulating the expression of the cDNA and the DsRed marker sequence. A failure rate up to 50 % in the F1 generation as shown in previous studies (Daxinger et al., 2007) indicates that a possible gene silencing, mediated by 35S promoter homology between transgene and T-DNA insertion used for mutagenesis, might be a problem in tagged lines from different collections.

To avoid this unwanted silencing effect, complementation constructs under the control of the promoter from the cassava vein mosaic virus (CvMV), a plant pararetrovirus from the Caulimoviridae family, were generated. The CvMV-promoter confers almost constitutive gene expression in all plant tissues (Verdaguer et al., 1998). A complementation construct of the CVMV promoter with the *FatA1* cDNA was introduced into *fatA1-2*$^{+/-}$*fatA2-2*$^{-/-}$mutant plants, but the progeny obtained after self-pollination still lacked complemented double homozygous *fatA1-2*$^{-/-}$*fatA2-2*$^{-/-}$ mutant plants. An additional approach for complementation was the use of the glycinin promoter from soybean (*Glycine max*), which specifically regulates the expression of transgenes in embryos and cotyledons of transgenic plants (Nielsen, 1989; Sims and Goldberg, 1989; Ding et al., 2006). The glycinin promoter is active during the mid to late phase but repressed during the early stage of embryogenesis (Nielsen, 1989; Fait et al., 2006). The expression of Arabidopsis *FatA1* and *FatB,* as well as, *U. californica UcFatB* cDNA under the control of the glycinin promoter did not lead to the complementation of the embryo lethal phenotype of the *fatA1-2*$^{-/-}$*fatA2-2*$^{-/-}$mutant. This might be due to restricted activity at late stage of embryo development.

Because ectopic expression of the different acyl-ACP-thioesterases under the control of the heterologous 35S, CvMV, and glycinin promoter did not rescue the embryo lethal phenotype of *fatA1-2*$^{-/-}$*fatA2-2*$^{-/-}$ mutants, complementation constructs under the control of the *FatA1* native

promoter region were generated. To this end, the 5'-flanking promoter region of the *FatA1* gene from Arabidopsis was employed for regulating the expression of Arabidopsis *FatA1, FatB,* and *U. californica UcFatB* cDNA. For the cloning of the *FatA1* promoter region, the sequence spanning from the stop codon of the (5') flanking gene to the start codon of the *FatA1* gene was employed. However, after stable transformation of Arabidopsis *fatA1-2*$^{+/-}$*fatA2-2*$^{-/-}$ no complemented double homozygous mutants were found in the progeny. Hence this construct also failed in complementation.

Acyl-ACP thioesterase activity is highly specific among the different organisms and acyl-ACP thioesterase families. Therefore, the ectopic expression of *UcFatB* or *FatB* might not be sufficient for complementing the embryo lethal phenotype. *UcFatB* is specific for the hydrolysis of 12:0-ACP, and plays a critical role in medium chain fatty acid production (Pollard et al., 1991; Voelker et al., 1992), whereas *FatB* from Arabidopsis shows highest activity for 16:0-ACP (Dörmann et al., 1995). The naturally occurring amount of C12 and C16 fatty acids in seeds is very low compared to C18 fatty acids (Lemieux et al., 1990). 18:2 fatty acids, derived from 18:1, accounts for approximately 30 % of total fatty acid content in Arabidopsis seeds, whereas 16:0 fatty acids and its derivatives making up around 10 % of the total fatty acid content (Lemieux et al., 1990). 12:0 fatty acids accumulate only in trace amounts in Arabidopsis seed tissue, due to the rapid elongation during fatty acid *de novo* synthesis.

The 5'-untranslated region (5'-UTR) just upstream of the start codon plays a crucial role in determining the translational efficiency of plant genes (Kim et al., 2013). In eukaryotes, the Kozak sequence A/GCCACCAUGG, located within a short 5'-UTR region, regulates translation of the mRNA (Nakagawa et al., 2008; Kozak, 1987). The sequence context in the -1 to -21 region of the 5'-UTR was conserved in different plant species. Studies by Kim and co-workers revealed a great variety in translational efficiency of 25 tested Arabidopsis genes, with a difference of up to 200-fold between the strongest 5'-UTR and the weakest 5'-UTR (Kim et al., 2013). After analyzing 3643 different plant genes, the consensus sequence, AAAA/CAAUGGC, for the translational initiation site was obtained (Kanoria and Burma, 2012). This sequence was not fully conserved in the complementation constructs under the control of the 35S, CvMV, glycinin or native FatA1 promoter used in this study. In these constructs, the promoter sequence ends immediately 5' of the start codon of the coding regions of Arabidopsis *FatA1*, *FatB,* and *U. californica UcFatB*. However, mRNA sequences harboring a partial Kozak sequence can also be translated. It is possible that the translation efficiency is suppressed to a level not sufficient for functional complementation of the *fatA1-2*$^{-/-}$*fatA2-2*$^{-/-}$ mutant. For optimal results constructs preceded by a Kozak sequence 5' of the start codon or a full length genomic sequence construct of *FatA1* gene should be used for complementation.

For overexpression the full length cDNA of *FatA1* and *FatA*2 under the control of the 35S promoter was introduced into WT by Agroinfiltration. The seeds of overexpression lines were

overall comparable to the control line on the morphological as well as the biochemical level. Therefore, increased *FatA1* or *FatA2* expression did not lead to a shift in the metabolic flux into oil in seeds. Furthermore, seed development of *FatA1* or *FatA2* overexpressing lines with WT background was not altered. *FatA1* and *FatA2* transcript levels were most abundant in early embryogenesis. A possible shift in the fatty acid pattern might be adjusted during seed development. This hypothesis is in line with data obtained by Moreno-Peréz and co. workers (Moreno-Pérez et al., 2012). The total fatty acid content and composition of a *fatA1-1fatA2-1* double mutant green cotyledon stage embryos were different, from the WT but at later stages of the development, fatty acid accumulation reached similar levels and the distribution was more similar to WT (Moreno-Pérez et al., 2012). It is likely that expression of *FatA1* or *FatA2* was already sufficient in the WT and that ectopic overexpression did not have any biochemical effect.

4.2 Characterization of Arabidopsis *GDPD5* and *GDPD6*

The second aim was the analysis of regulatory points of plant lipid biosynthesis, in particular membrane lipid remodeling under Pi starvation. The possible involvement of Arabidopsis *GDPD5* and *GDPD6* in membrane lipid remodeling was studied using a reverse genetic approach in combination with biochemical analyses. Under Pi deprived conditions, a fraction of the phospholipids, which constitute up to 1/3 of organically bound Pi reserves in plants, is degraded to release the phosphate, and replaced by non-phosphorous. Phospholipids are the major constituents of extraplastidial plant membranes. The exact functions of the individual phospholipids are still unknown, since they can be replaced up to a certain amount by non-phosphorous lipids with comparable characteristics. The functional integrity of the plant membrane remains intact despite the changes in lipid order and composition under Pi deficiency. Thus, it might be speculated that at least a fraction of the phospholipids in the plant membranes serves as a reservoir for the phosphate mobilization during Pi limitation. For the degradation upon Pi deprivation, specific phospholipases hydrolyze phospholipids, releasing lipid metabolites such as free fatty acids, lysophospholipids, diacylglycerol, and phosphatidic acid. In yeast and animals, glycerophosphodiesters derived from phospholipids, are produced after deacylation by phospholipase B (PLB) activity. In plants, fatty acid moieties of polar lipids are removed by lipid acyl hydrolases (LAH) specific for plants. In an alternative pathway, glycerophosphodiesters can also be generated by the combined activity of phosphilipases A, PLA_1, and PLA_2, on phospholipids (Wang et al., 2012). In Arabidopsis, the possible involvement of the two genes, *GDPD5* and *GDPD6,* in membrane lipid remodeling upon Pi deprivation by hydrolyzing glycerophosphodiester, releasing G3P, which is the initial substrate for glycerolipid biosynthesis, was analyzed in this study. *GDPD5* and *GDPD6* show sequence similarities to glycerophosphodiester phosphodiesterases from other organisms like the human *MIR16* gene, which belong to a large evolutionarily conserved family of GDPDs, harboring GDPD activity

towards glycerophosphoinositol (Zheng et al., 2003), as well as GDPDs from plants (Van Der Rest et al., 2004), bacteria (Larson et al., 1983; Ohshima et al., 2008), and yeast (Fisher et al., 2005). Arabidopsis *GDPD5* and *GDPD6* share high similarities with the *E. coli* Ca^{2+} dependent periplasmic GlpQ (Van Der Rest et al., 2004). Phylogenetic analysis revealed that *GDPD5* and *GDPD6* are grouped with GlpQ and enzyme assays showed that the enzyme activity towards different glycerophosphodiester is similar. Enzyme activity assays with recombinant GDPD5 and GDPD6 proteins purified from *N. benthamiana* revealed that both enzymes hydrolyze different glycerophosphodiesters, including GPC, GPE, GPI, GPS, and GPG into G3P and the corresponding alcohol, showing preference for GPC and GPE. The broad substrate specificities of GDPD5 and GDPD6 are analogous with that of GDPD enzymes from other organisms and with *GDPD1* from Arabidopsis, which hydrolyzes GPG, GPC, and GPE, without substrate preference (Cheng et al., 2011). Although Arabidopsis GDPD5 and GDPD6 are most similar to GlpQ from *E. coli* as shown by phylogenetic analysis, GDPD5 and GDPD6 enzyme activity is independent of divalent cations. *E. coli* GlpQ activity was shown to be Ca^{2+}-dependent, while Arabidopsis GDPD1 exhibits differences in cation requirements, as the enzyme depends on Mg^{2+} for optimal enzyme activity (Cheng et al., 2011).

Expression analysis of Arabidopsis *GDPD5* revealed moderate expression in all tested tissues except shoots from 10 days old seedlings. However, *GDPD6* is only expressed in flowers and siliques under Pi sufficient conditions (Cheng et al., 2011). Expression of the two genes is strongly induced under Pi starvation (Gaude et al., 2008; Cheng et al., 2011). The same results were obtained after testing the transcript levels of the other *GDPD* genes under Pi starvation in Arabidopsis (Cheng et al., 2011). Microarray analysis also revealed that the expression of different *LAH* genes is significantly upregulated by Pi starvation (Ryu, 2004; Mission, 2005; Morcuende et al., 2007), indicating that LAH-mediated phospholipid degradation is promoted by Pi deprivation. Special Pi response elements binding to the MYB-related transcription factor *PHR1* (*phosphate starvation response 1*) (Rubio et al., 2001; Pant et al., 2015) can be found in the promoter region of five *GDPD* genes in Arabidopsis (Cheng et al., 2011). MYB proteins are a superfamily of transcription factors that play regulatory roles in developmental processes and defense responses in plants. Recent studies revealed that PHR1 regulates the lipid remodeling and TAG accumulation in Arabidopsis during Pi starvation (Pant et al., 2015). The glycerolipid composition as well as the expression of most lipid-remodeling gene transcripts analyzed by Pant and co-workers (2015), were altered in the *phr1* mutant under Pi starvation. It has been shown that *GDPD6* transcript levels were also significantly reduced in the *phr1* mutant during Pi deprivation (Gaude et al., 2008), indicating a link between the regulation of the phospholipid degradation pathways upon Pi depletion.

Since the degradation of membrane phospholipids occurs in several intracellular membrane systems including the plasma membrane, mitochondria, tonoplast, ER and the

chloroplasts, the hydrolysis pathways mediated by LAH and GDPD are present in various subcellular compartments. Subcellular localization analysis revealed that GDPD1 is plastid localized (Cheng et al., 2011). Preliminary results obtained by van der Rest and co-workers (2004) detected Arabidopsis GDPD5 in the vacuoles. On the contrary, results obtained in this study revealed that GDPD5 and GDPD6 are targeted to the ER. Several LAHs such as *AtPLA$_2$*-β, *AtPLA$_2$*-γ, and *AtPLA$_2$*-δ are localized to the ER (Mongrand et al., 1997; Mongrand et al., 2000; Kim et al., 2011), indicating that lipid deacylation actively occurs at the ER. Thus, many enzymes required for releasing Pi from phospholipids, especially PC, can be found at the ER.

4.2.1 Physiological Characterization of the *gdpd5* and *gdpd6* Mutants

Arabidopsis T-DNA mutants, harboring insertions in the coding region were available for *GDPD5* and *GDPD6*. RT-PCR products for *gdpd5-2*, and *gdpd6-2* were observed in semi-quantitative RT-PCR when analyzed with primers 5' to the insertion site, indicating residual expression of truncated proteins. PCR amplification of *gdpd5-1* with primers 3' to the insertion resulted in the production of a truncated cDNA band, indicating promoter activity on the T-DNA driving expression of this *GDPD* sequence part. For *gdpd6-1,* no PCR product was detected using primers around or 3' to the insertion site. The homozygous single mutant lines for *GDPD5* and *GDPD6* were comparable in growth and morphology to Arabidopsis Col-0 WT plants on soil as well as under Pi starved conditions. Hence, the insertions did not appear to interfere with stress response and vegetative plant development. In addition, lipid composition and G3P levels of plants grown under Pi sufficient and Pi-deprived conditions were analyzed since both genes show highest transcript levels under Pi deficiency. Glycerolipid content, as well as molecular species composition were analyzed in Arabidopsis WT Col-0, *gdpd5*, and *gdpd6* T-DNA insertion mutant lines. The replacement of phospholipids by galactolipids could be observed in all lines, but no differences in individual lipid classes were detected between the WT and the mutant lines in leaves and roots under normal growth or Pi-starved conditions. Furthermore, the lipid composition of leaves and roots was different. This can be explained by the abundance of photosynthetic membranes in leaves, containing high proportions of galactolipids. However, roots contain plastids lacking internal membranes, hence the galactolipid content in roots is rather low. Furthermore, in leaves, DGDG increases about 2-fold, accompanied by an equivalent decrease in phospholipids (Härtel et al., 2000, 2001) (Kelly et al., 2003; Li et al., 2006). While in roots the DGDG increase is much stronger by about 8 to 10-fold, but not sufficient to substitute for the decrease in phospholipids, leading to the reduction in total lipid content by 42 % (Li et al., 2006). Results obtained in this work show that DGDG accumulation and the decrease in phospholipids are not compromised in the different *gdpd5 and gdpd6* insertion lines, indicating that *GDPD5* and *GDPD6* are not primarily involved in the replacement of phospholipids by glycolipids in leaves and in roots or act redundantly. These results are in line with previous

studies on different *GDPD* genes in Arabidopsis (Gaude et al., 2008; Cheng et al., 2011) (see below).

Contrary to the well-characterized biosynthetic pathways for DGDG and SQDG under Pi deficiency (Essigmann et al., 1998; Yu et al., 2002; Gaude et al., 2008; Kobayashi et al., 2009; Okazaki et al., 2009), some mechanisms in the degradation of phospholipids upon Pi starvation remain enigmatic. As shown previously, GDPDs from different organisms are involved in the hydrolysis of glycerophosphodiesters resulting in the release of G3P, the main precursor for DAG synthesis, which is employed for galactolipid and PC/PE synthesis (Van Der Rest et al., 2004; Fisher et al., 2005; Cheng et al., 2011). The Arabidopsis *gdpd1* loss-of-function mutant showed a significant reduction in G3P levels in both shoots and roots under Pi-depleted conditions (Cheng et al., 2011), and a Pi starvation-induced growth phenotype, accompanied with a decrease in root length and fresh weight of 4 to 12 day-old seedlings. This phenotype could be rescued by adding G3P to the growth medium (Cheng et al., 2011), indicating that glycerophosphodiester metabolism is crucial to salvage free Pi from G3P, as seen in bacteria. G3P levels were examined in Arabidopsis *GDPD5* and *GDPD6* mutants. The G3P amount in the mutants measured by GC was comparable to that of the WT, when plants were grown on Pi-replete conditions. Since both genes are highly expressed upon Pi starvation, G3P levels were also examined under Pi-depleted conditions. A reduction in G3P levels was detected for *gdpd5-2*, *gdpd6-1*, as well as *gdpd6-2* mutant lines as compared to WT. Under Pi plus conditions, Arabidopsis WT contained around 1500 nmol G3P g^{-1} FW, while under Pi starved conditions around 175 nmol G3P g^{-1} FW were detected, in contrast to Cheng and co-workers (2011) who measured lower amounts of G3P under +Pi or -Pi conditions. They also measured around 120 nmol G3P g^{-1} FW (Cheng et al., 2011), while approximately 50 nmol G3P g^{-1} FW were detected by Arrivault and co-workers (Arrivault et al., 2009). This difference in G3P content under Pi-replete conditions is not caused by the GC-MS method used for G3P quantification, because similar results were obtained by spectrophotometric measurement (appendix). Further experiments are required to explain the different results obtained in this study compared to the literature.

In addition to serving as a precursor for lipid synthesis, G3P is a key metabolite that carries reducing equivalents from the cytosol to the mitochondria. The cytosolic G3P dehydrogenase, GPDHc1, is a component of the G3P shuttle, channeling cytosolic reducing equivalents to mitochondria for respiration (Shen et al., 2006). The Arabidopsis *gpdhc1* T-DNA insertion mutant is affected in mitochondrial respiration, exhibiting an increased $NADH/NAD^+$ ratio compared with WT plants under standard growth conditions and an impaired adjustment of $NADH/NAD^+$ ratios under stress conditions (Shen et al., 2006). G3P serves as a chemical signal that contributes to systemic acquired resistance, which is form of plant defense, providing immunity against diverse pathogens (Chanda et al., 2011; Mandal et al., 2011; Yu et al., 2013). It was also shown, that G3P level in plant cells has an impact on Arabidopsis root development.

Primary root development is inhibited in mutants with increased G3P levels, due do alterations in the glycerol catabolism (Hu et al., 2014). G3P is also crucial for lipid metabolic processes. It plays a prominent role in the prokaryotic and eukaryotic pathways of glycerolipid biosynthesis, because it is the substrate for glycerol-3-phosphate acyltransferase (GPAT), forming the backbone for glycerolipids in Arabidopsis. G3P is the main precursor for phosphatidic acid, synthesized by the acylation of G3P. PA is dephosphorylated resulting in DAG, which is the precursor for glycerolipid biosynthesis. Diminished levels of G3P, as seen in the *GDPD5* and *GDPD6* mutant lines under Pi starvation, may impair subsequent steps in glycerolipid biosynthesis. It has been shown that different GPATs are essential for the normal development of reproductive tissue in Arabidopsis (Zheng et al., 2003; Chen et al., 2014). Arabidopsis has eight GPAT genes required for several biosynthetic processes e.g. the synthesis of cutin and suberin (Beisson et al., 2012; Yang et al., 2012), substrate availability for GPAT activity was decreased in *gdpd5* and *gdpd6* single mutants, probably affecting glycerolipid biosynthesis. G3P is not only crucial for the glycerolipid biosynthesis, but is also believed to modulate the balance of the prokaryotic and eukaryotic pathways in Arabidopsis by influencing the metabolic flux, as well as gene transcription levels (Shen et al., 2010). The Arabidopsis mutant *ats1* (formerly designated *act1*), carries a block in the first step of glycerolipid biosynthesis in the chloroplast, due to a loss-of-function mutation in the soluble chloroplastic glycerol-3-phosphate acyltransferase (ATS1/ACT1) (Kunst et al., 1988). The membrane lipids of *ats1* are exclusively derived from the eukaryotic pathway, showing that this pathway can provide sufficient amounts of lipids for chloroplast biogenesis. G3P, derived from different pathways, can be generated by GPDH via the reduction of DHAP in the cytosol and the plastids. G3P produced by this reaction can be transported between the cytosol and plastidial stroma. Another way of G3P synthesis is the glycerol kinase-mediated phosphorylation of glycerol. It is believed that the G3P synthesized through GPDH- and glycerol kinase-catalyzed reactions might be used in different cellular processes and may be located in different cellular compartments (Chanda et al., 2011).

The overlapping expression patterns in each subfamily observed by Cheng and co-workers (2011) indicate functional redundancy of the *GDPD* genes in Arabidopsis. The remaining gene function of the other *GDPD*s in the single T-DNA insertion lines might be able to compensate for the loss of *GDPD5* or *GDPD6*. Especially *GDPD1* was found to be the main GDPD isoform expressed in response to Pi starvation, particularly in roots (Cheng et al., 2011). The T-DNA insertion mutants *gdpd5-1*, *gdpd5-2*, and *gdpd6-1* still have residual expression of truncated transcripts, as shown by semi-quantitative RT-PCR. RT-PCR analysis using primers binding across the insertion site did not lead to a PCR product in either of the single mutant lines. However, the analysis using different primer sets resulted in the expression of RT-PCR fragments upstream and downstream from the insertion site. For *gdpd5-1* harboring the insertion in the second exon, a RT-PCR fragment was obtained using primers on exon 7 and 9

downstream of the insertion site. The residual expression of the *gdpd5-1* allele may be due to the presence of the 35S promoter close to the T-DNA border in the same orientation as the *GDPD5* gene. For the *gdpd5-2* and *gdpd6-2* alleles, transcripts were detected upstream from the insertion site, but no transcript was detected spanning the insertion site. It cannot be ruled out that the *gdpd5-2* and *gdpd6-2* alleles retain some *GDPD* function since both alleles appeared to express the 5'-portion of the *GDPD5* and *GDPD6* genes, respectively. Arabidopsis GDPDs of subfamily type-A contain a conserved GDPD domain, which is similar to those discovered in bacteria and animals (Cheng et al., 2011). The critical residues for the active site are highly conserved within the GDPD domain in Arabidopsis GDPD type-A family, indicating that they may have enzymatic function. The highly conserved regions are located approximately 45 amino acids downstream of the N-terminal start methionine. Thus the predicted active sites of the two proteins are still transcribed in *gdpd5-2* and *gdpd6-2*. Therefore, it is likely that the predicted truncated GDPD5 and GDPD6 proteins in *gdpd5-1*, *gdpd5-2*, and *gdpd6-2* still exhibit enzymatic functions. Only for the *gdpd6-1* insertion mutant, no transcript across or downstream the insertion site could be detected. The *gdpd6-1* mutant line harbors the insertion in the third exon.

4.2.2 The *gdpd5-1$^{+/-}$gdpd6-1$^{+/-}$* Mutant Shows High Percentage of Non-Viable Pollen

The roles of *GDPD5* and *GDPD6* in Arabidopsis appear to be redundant since no phenotypic differences were found in the single T-DNA insertion lines compared to WT. For this reason, crosses of the different homozygous T-DNA insertion lines were done, and the T_2 progeny was tested for the presence of double homozygous mutants by PCR analysis. Double homozygous plants were obtained from *gdpd5-1 gdpd6-2*, *gdpd5-2 gdpd6-1*, *and gdpd5-2 gdpd6-2* crosses after several rounds of self-pollination and PCR analysis. All of these double homozygous mutant plants were similar in growth and morphology as well as in lipid composition compared to WT. The *gdpd5-1 gdpd6-1* cross resulted in double heterozygous *gdpd5-1$^{+/-}$gdpd6-1$^{+/-}$* or heterozygous/WT (*gdpd5-1$^{+/-}$gdpd6-1$^{+/+}$ or gdpd5-1$^{+/+}$gdpd6-1$^{+/-}$)* progeny. No homozygous/heterozygous (*gdpd5-1$^{-/-}$gdpd6-1$^{+/-}$, gdpd5-1$^{+/-}$gdpd6-1$^{-/-}$)* or double homozygous (*gdpd5-1$^{-/-}$gdpd6-1$^{-/-}$)* plants could be recovered. These results suggested that double homozygous (*gdpd5-1$^{-/-}$gdpd6-1$^{-/-}$)* embryos might be lethal. Analysis of the siliques of several double heterozygous plants revealed approximately 45 ± 3.2 % of the ovules were not fertilized. Following the Mendelian inheritance, only 31.25 % of the ovules should be not fertilized, when representing the missing double homozygous or homozygous/heterozygous phenotype in the progeny of a double heterozygous mutant line. The number of 45 % of non-fertilized ovules in double heterozygous *gdpd5-1$^{+/-}$gdpd6-1$^{+/-}$* mutant plants indicates the presence of an additional defect. In this study, the failure to obtain double homozygous plants led to the unexpected discovery that the *gdpd5-1$^{+/-}$gdpd6-1$^{+/-}$* plants harbor gametophytic mutations in pollen

development. The double heterozygous *gdpd5-1*$^{+/-}$*gdpd6-1*$^{+/-}$ line showed a high percentage of non-viable pollen grains. The Alexander test revealed approximately 50 % of the pollen grains to be aberrant. 25 % of the pollen grains in the double heterozygous *gdpd5-1*$^{+/-}$*gdpd6-1*$^{+/-}$ mutant line harbor the haplotype "ab" (*gdpd5-1*$^{-/-}$*gdpd6-1*$^{-/-}$). The high number of non-viable pollen grains indicates that also pollen grains harboring the haplotypes "aB" or "Ab" only partially contributes to fertilization. Electron microscopy revealed differences in shape and size of the aberrant pollen. They are deformed and distorted indicating less turgor than the WT pollen. In order to exclude a possible contribution of the female gametophyte to the decreased fertility, reciprocal crosses were done. Reciprocal crossing revealed a severe transmission defect for the male, but not for the female gametophyte. This is in line with the expression pattern for Arabidopsis *GDPD5* and *GDPD6*, which are most abundantly expressed in flowers and stamen but not in pistills. All *GDPD* genes are highly expressed in flowers and stamen except *GDPD4*, suggesting a role of the *GDPD* family genes during development of reproductive organs (Cheng et al., 2011).

One hypothesis that could account for the pollen lethal phenotype is a defect in the availability of G3P, which provides the glycerol backbone for glycerolipid biosynthesis. During pollen maturation in different species of the Brassicaceae, lipids and proteins are deposited (Baker et al., 1997). Several types of lipidic structures can be found in pollen, which are essential for pollen development (Preuss et al., 1993; Wolters-Arts et al., 1998). Pollen grains accumulate lipid bodies, comparable to the storage oil bodies in cotyledons. These lipid bodies function as storage reserves of energy and as a carbon source for pollen germination. The developing pollen has a high demand in lipid biosynthesis due to storage reserve formation within lipid bodies. TAG is the major form of carbon storage in pollen and biosynthesis encompasses the sequential acylation and the subsequent dephosphorylation of G3P. Lipid bodies, mainly consisting of TAG, gradually appear shortly after pollen mitosis I and increase in number in the vegetative cell of pollen (Park and Twell, 2001). Thus, oil bodies can be found in mature pollen but not in young microspores. It has been shown that acyl-CoA: diacylglycerol acyltransferase 1 (DGAT1) and phospholipid: diacylglycerol acyltransferase 1 (PDAT1) have overlapping function that are essential for pollen viability (Zhang et al., 2009). Both genes contribute to glycerolipid biosynthesis and especially TAG formation in pollen (Zhang et al., 2009). The *dgat1 pdat1* double mutant lacks oil bodies in pollen grains and is severely pollen lethal. The decrease in oil bodies, as seen in *dgat1-1pdat1-2* (Zhang et al., 2009) as well as *gdpd5-1*$^{+/-}$*gdpd6-1*$^{+/-}$ double mutants might not directly be lethal, but the severe impairment in lipid biosynthesis may initiate an autolytic process leading to cell death. Therefore, mutations of several genes involved in glycerolipid biosynthesis lead to an impairment in pollen development.

Lipid biosynthesis occurs within two distinct pathways, the prokaryotic pathway of the chloroplast inner envelope, producing chloroplastic lipids, or the eukaryotic pathway, using

acyl-CoA esters at the ER. The decrease of G3P in the *gdpd5-1*$^{+/-}$*gdpd6-1*$^{+/-}$ double mutant may also cause changes in the flux of fatty acids into the different pathways of lipid biosynthesis, since this is sensitive to changes in the G3P levels (Miquel et al., 1998). Differences in PC levels and a shift from 18:3 fatty acids, representing the most abundant fatty acid in pollen grains (Table 4.1), to 18:1 and 18:2 containing molecular species, were found in the pollen grains of the double heterozygous *gdpd5-1*$^{+/-}$*gdpd6-1*$^{+/-}$ mutant line. The relative amount of PC is significantly reduced in mutant pollen compared to the WT control, and also major differences in the molecular species composition were detected. 18:3 containing molecular species of PC, PE, PI, and PA are drastically decreased, while 18:1 and 18:2 fatty acids are increased in PC, PI and PA at the expense of the 18:3 decrease. This shift might be underestimated and might be even more severe if it would have been possible to analyze only pollen grains affected by the mutation. The pollen analyzed for lipids were a mixture of viable and non-viable pollen grains, produced by the double heterozygous *gdpd5-1*$^{+/-}$*gdpd6-1*$^{+/-}$ mutant. Hence the changes in lipid composition might be attenuated. The decreased levels in 18:3 content might point to a defect in acyl editing of PC, resulting in a decreased amount of 18:3 content and the concomitant accumulation of 18:1 and 18:2 fatty acids. It has previously been shown that the quantity of 18:3 fatty acids is crucial for pollen development in Arabidopsis. The *fad3fad7-2fad8* triple mutant deficient in the activity of different membrane-bound desaturases showed only trace levels of 18:3 (<0.1 %) and no levels of 16:3 fatty acids in leaf membrane lipids (McConn, 1996; McConn and Browse, 1998). Around 84 % of the mutant pollen was non-viable and showed a reduced germination rate (McConn, 1996; McConn and Browse, 1998). Since 18:3 fatty acids are not essential for photosynthesis the only important requirement for 18:3 appears to be as a substrate for the octadecanoid pathway, producing jasmonic acid. The amount of jasmonic acid in *fad3fad7-2fad8* triple mutant plants was only 3 % of that produced in WT plants. Jasmonic acid has essential roles in pollen maturation and release (McConn and Browse, 1998). Nevertheless, small amounts of 18:3 fatty acids are sufficient for proper maturation. Hence, it is rather unlikely that the pollen lethal phenotype in double heterozygous *gdpd5-1*$^{+/-}$*gdpd6-1*$^{+/-}$ mutant is caused by the lack of jasmonic acid, but it is more likely caused by a defect in storage lipid accumulation.

Table 4.1: Fatty acid composition of the lipids from pollen grains of Arabidopsis WT plants (Zheng et al., 2003).

	Proportion of Fatty Acid (mol %)					
	14:0	16:0	18:0	18:1	18:2	18:3
WT	4.75	27.21	9.64	7.75	13.69	36.96

Independent efficiency for the essential role of *GDPD5* and *GDPD6* during pollen development stems from the analysis of *GDPD5* RNAi lines in the *gdpd6-1* background. The *gdpd6-1* T-DNA insertion line represented a complete null mutant, showing no transcript when tested by semi-quantitative RT-PCR. Two independent *GDPD5* RNAi *gdpd6-1* lines were isolated which showed reduced *GDPD5* expression. With approximately 30 and 26 % non-viable pollen grains, the pollen development in the RNAi lines #45 and #47 was impaired. Therefore, the two RNAi lines provide independent evidence for the role of *GDPD5* and *GDPD6* in male gametophyte development.

4.2.3 Inheritance of *GDPD5* and *GDPD6* Insertion Lines and Complementation

The mechanisms involved in the integration of T-DNA into the plant genome mediated by *A. tumefaciens* are still not well characterized. The complexity of the integration mechanisms leads to transgenic loci consisting of one, two or many copies of the transgene (Takano et al., 1997; De Neve et al., 1998). The transgene is inherited as a dominant trait (Christou et al., 1989; Misra and Gedamu, 1989; Theuns et al., 2002), showing a progeny conforming a 3:1 Mendelian ratio (Shrawat, 2007). Next to the Mendelian inheritance, 10 to 50 % of the segregation does not occur following the Mendelian ratio, due to an unstable transmission of the transgene, a poor expression (Deroles and Gardner, 1988; Register III et al., 1994), or second site insertions. *GDPD5* and *GDPD6* are on two different chromosomes. Therefore, these non-linked genes are expected to segregate randomly. The double mutant line generated by crossing the homozygous *gdpd5-1* and *gdpd6-1* single mutants resulted in a progeny lacking double homozygous or homozygous/heterozygous plants, whereas double homozygous mutants could be recovered after crossing the other available T-DNA insertion lines of *GDPD5* and *GDPD6*. The varying effects of the T-DNA insertional mutagenesis in the different *GDPD* single mutant lines is most likely due to the expression of truncated proteins, which might harbor enzymatic function. The fact that no *gdpd5-1*$^{-/-}$*gdpd6-1*$^{-/-}$ double mutant plants could be obtained, while at the same time, homozygous double mutant lines of all other combinations of alleles could be produced, indicates that the lethality of the combination of *gdpd5-1 with gdpd6-1* might be caused by the severity of the respective mutations. Therefore, studies were focused on double heterozygous *gdpd5-1*$^{+/-}$*gdpd6-1*$^{+/-}$ mutant. Genetic complementation with a genomic construct for *GDPD6*, which harbors the 5' and 3' non-transcribed region and the genomic sequence of *GDPD6*, did not result in double homozygous *gdpd5-1*$^{-/-}$*gdpd6-1*$^{-/-}$ or heterozygous/homozygous *gdpd5-1*$^{+/-}$ *gdpd6-1*$^{-/-}$ mutants in the F1 progeny. Complementation of the pollen lethal phenotype was not found with the genomic construct for *GDPD6*. It might be necessary to test a larger number of plants of different independently transformed plant lines. Genetic complementation with the *35S::GDPD6* overexpression construct resulted in a progeny lacking double homozygous mutants. But it was possible to obtain homozygous/heterozygous *gdpd5-1*$^{-/-}$*gdpd6-1*$^{+/-}$ mutants,

which could not be found in the progeny of double heterozygous *gdpd5-1*$^{+/-}$*gdpd6-1*$^{+/-}$ mutants. It should be noted that the 35S promoter is almost silent during pollen development in Arabidopsis (Wilkinson et al., 1997). This could explain at least in part the incomplete complementation. Nevertheless, the ectopic expression of *GDPD6* under the control of the 35S promoter was partially able to complement the phenotype.

This study has shown that the loss of *GDPD5* or *GDPD6* function in single mutants did not lead to alterations in overall lipid composition under Pi deprived conditions compared to WT plants. The results obtained showed no overt impact on the hydrolysis of major phospholipids or on the synthesis of galactolipids through the remodeling or the de novo biosynthetic pathway in the *GDPD5* and *GDPD6* single mutant lines, probably due to genetic redundancy and residual expression. However, the content of G3P, which is the enzymatic product of GDPD activity, was decreased in single mutant lines under Pi starvation, indicating an important role upon Pi starvation. The double mutant line generated by crossing of the homozygous *gdpd5-1* and *gdpd6-1* single mutants resulted in a progeny lacking double homozygous or homozygous/heterozygous mutants. Plants, which were double heterozygous, produced viable and non-viable pollen, with alterations in lipid composition. The pollen lethal phenotype was also obtained to a lesser extent in *GDPD5* RNAi lines with *gdpd6-1* background. The results obtained in this study indicate that *GDPD5* and *GDPD6* might not be involved in lipid remodeling under Pi starvation, but are crucial for male gametophyte development. A possible involvement of other *GDPD* genes has to be analyzed, since there are several *GDPD* genes in Arabidopsis, which await their characterization.

5 Summary

Chloroplasts are the site of the *de novo* synthesis of the predominant proportion of fatty acids in plant cells. During fatty acid synthesis, the acyl chain is bound to acyl carrier protein (ACP). Acyl-ACP thioesterases hydrolyze acyl-ACPs in the chloroplast releasing free fatty acids, thereby regulating their chain lengths. The free fatty acids are exported from the plastid and activated by long chain fatty acid-CoA synthetases to serve as substrates for glycerolipid synthesis at the endoplasmic reticulum (ER). Plant cells harbor two types of acyl-ACP thioesterases, FatA and FatB. They differ in amino acid sequence and substrate specificity. FatA thioesterases are highly active towards oleoyl-ACPs (18:1-ACP), while FatB thioesterases show highest activity with saturated acyl-ACPs but also with 18:1-ACP. Arabidopsis contains two genomic loci encoding FatA thioesterases, *FatA1* and *FatA2*. Fatty acids are major components of glycerolipids in plants. Lipids play crucial roles in the plant's ability to survive and adapt to environmental changes. In response to low levels of phosphate (Pi) in the rhizosphere, plants degrade membrane phospholipids, which harbor up to 1/3 of organically bound Pi, to provide Pi for other important cellular processes. During Pi deprivation, membrane phospholipids are replaced by non-phosphorous glycolipids.

Heterologous expression of *FatA1* and *FatA2* in the *E. coli fadD* mutant led to the accumulation of $16:1^{\Delta 9}$ and $18:1^{\Delta 11}$ fatty acids, demonstrating that the two proteins harbor acyl-ACP thioesterase A activities. Two *fatA1-2* and *fatA2-2* loss-of-function mutants were obtained. Seeds of the two single mutants showed a reduced total fatty acid content as well as a shift in TAG molecular species composition with a decrease of 18:1, 18:2, and 18:3 and a concomitant increase in 20:1 and 22:1 containing molecular species. Expression of *FatA1* and *FatA2* was most prominent in the developing embryo. After crossing fatA1-2 and fatA2-2, only homozygous/heterozygous *fatA1-2*$^{+/-}$*fatA2-2*$^{-/-}$ mutants were obtained, because homozygous *fatA1-2*$^{-/-}$*fatA2-2*$^{-/-}$ double mutant embryos are lethal. Light microscopy revealed that embryo development was arrested at the late heart to early torpedo stage. The mutant embryos showed a fatty acid composition comparable to WT heart/torpedo stage embryos. When compared to WT heart/torpedo stage embryos, the total amount of diacylglycerol and triacylglycerol was increased in the double mutant embryos. Phosphatidylethanolamine in the mutant embryos still contained C18 acyl groups indicating that the export of 18:1 from the plastid was still active, probably due to the remaining enzymatic function of FatB. At heart stage, fatty acid export from the chloroplast drastically increases along with the onset of triacylglycerol synthesis. This might explain why a total block in FatA activity becomes lethal at this stage of embryo development. Complementation experiments to rescue the lethal phenotype of the double mutant embryos using acyl-ACP thioesterases (FatA or FatB) from Arabidopsis and *Umbellularia californica* with specificities for different acyl-ACPs under the control of either the 35S, CvMV, glycinin, or the Arabidopsis *FatA1* promoter region in all possible combinations were not successsful. In no case, plants with the genotype *fatA1-2*$^{-/-}$*fatA2-2*$^{-/-}$ expressing a *FatA* or *FatB* complementation

construct were observed in the progeny. This might be due to insufficient promoter activity during heart stage. Alternatively, *FatB* constructs might be incapable of complementation because fatty acid export via FatB might be insufficient to compensate for the loss of the two *FatA* genes. The fact that a total block of the *FATA1* and *FATA2* expression in the double mutant becomes embryo lethal indicates that the export of sufficient amounts of unsaturated fatty acids (18:1) is absolutely essential for plant physiology, in particular during embryo development.

In the second part of this work, the regulation of the replacement of membrane phospholipids with non-phosphorous lipids during Pi depletion was studied. Glycerophosphodiester phosphodiesterases (GDPD) hydrolyze glycerophosphodiesters, which are phospholipid metabolites generated by phospholipase A activity, thereby releasing glycerol-3-phosphate (G3P) and the aminoalcohol. These enzymes are presumably involved in phospholipid degradation upon Pi starvation. Arabidopsis contains six *GDPD* genes and the expression of most of the genes is induced under low Pi conditions. Transient expression of *GDPD5* and *GDPD6* in *N. benthamiana* revealed activity towards different glycerophosphodiesters with preference for GPC and GPE. Subcellular localization experiments of GDPD5 and GDPD6 with eGFP fusion constructs indicated that the two proteins were associated with the ER, the presumed site of phospholipid degradation during Pi starvation. Different Arabidopsis T-DNA insertion lines for *GDPD5* and *GDPD6* (*gdpd5-1*, *gdpd5-2*, *gdpd6-1*, *gdpd6-2*) were subjected to Pi starvation experiments. A reduction in G3P levels was detected for *gdpd5-2*, *gdpd6-1*, as well as *gdpd6-2* leaves under Pi depleted conditions as compared to WT. G3P is the main precursor in glycerolipid synthesis. The *gdpd5* and *gpdp6* mutant lines were crossed in all combinations. Double homozygous mutants (*gdpd5-1 gdpd6-2*, *gpdp5-2 gpdp6-1*, *gpdp5-2 gdpd6-2*) were readily obtained in the F2 population. Analysis by semi-quantitative RT-PCR showed residual expression of sequences upstream and downstream from the insertion sites except for *gdpd6-1*. No double homozygous or homozygous/heterozygous *gdpd5-1 gdpd6-1* plants were obtained. The pollen formation was affected in the double heterozygous *gdpd5-1*$^{+/-}$ *gdpd6-1*$^{+/-}$ line. Electron microscopic analysis revealed differences in shape and size of the aberrant pollen, which are deformed and distorted. Lipid analysis of *gdpd5-1*$^{+/-}$*gdpd6-1*$^{+/-}$ pollen grains showed decreased PC level and a shift from 18:3 to 18:1 and 18:2 containing molecular PC species. Two independent *GDPD5* RNAi *gdpd6-1* lines were isolated which also showed a reduced number of viable-pollen grains. Therefore, the two RNAi lines provide independent evidence for the crucial role of *GDPD5* and *GDPD6* in male gametophyte development. After expression of *GDPD6* under the control of the 35S promoter in the double heterozygous *gdpd5-1*$^{+/-}$*gdpd6-1*$^{+/-}$ mutant, heterozygous/homozygous plants could be found in the F1 progeny. These results suggest that GDPD5 and GDPD6 are not directly involved in phospholipid degradation during Pi deprivation, but that they are essential during pollen development in Arabidopsis. The mechanism by which GDPD enzymes contribute to pollen development remains unclear.

6 References

Alexander M (1969) Differential staining of aborted and nonaborted pollen. *In* Biotechnology & Histochemistry **44:** 117-122

Alvarez-Buylla ER, Benítez M, Corvera-Poiré A, Cador ÁC, de Folter S, de Buen AG, Garay-Arroyo A, García-Ponce B, Jaimes-Miranda F, Pérez-Ruiz RV (2010) Flower development. *In* The Arabidopsis book/American Society of Plant Biologists **8**

Alvarez H, Steinbüchel A (2002) Triacylglycerols in prokaryotic microorganisms. *In* Applied Microbiology and Biotechnology **60:** 367-376

Andersson MX, Larsson KE, Tjellström H, Liljenberg C, Sandelius AS (2005) Phosphate-limited oat. The plasma membrane and the tonoplast as major targets for phospholipid-to-glycolipid replacement and stimulation of phospholipases in the plasma membrane. *In* Journal of Biology Chemistry **280:** 27578-27586

Andre C, Haslam RP, Shanklin J (2012) Feedback regulation of plastidic acetyl-CoA carboxylase by 18: 1-acyl carrier protein in *Brassica napus*. *In* Proceedings of theNational Academy of Sciences of the United States of America **109:** 10107-10112

Arrivault S, Guenther M, Ivakov A, Feil R, Vosloh D, Van Dongen JT, Sulpice R, Stitt M (2009) Use of reverse-phase liquid chromatography, linked to tandem mass spectrometry, to profile the Calvin cycle and other metabolic intermediates in Arabidopsis rosettes at different carbon dioxide concentrations. *In* The Plant Journal **59:** 826-839

Ausubel FM, Brent R, Kingston R, Moore D, Seidman J, Smith J, Struhl K (1995) Short protocols in molecular biology NY: John Willey and Sons Inc **29:** 130-135

Awai K, Maréchal E, Block MA, Brun D, Masuda T, Shimada H, Takamiya K, Ohta H, Joyard J (2001) Two types of MGDG synthase genes, found widely in both 16:3 and 18:3 plants, differentially mediate galactolipid syntheses in photosynthetic and nonphotosynthetic tissues in *Arabidopsis thaliana*. *In* Proceedings of theNational Academy of Sciences of the United States of America **98:** 10960-10965

Bajon C, Horlow C, Motamayor J, Sauvanet A, Robert D (1999) Megasporogenesis in *Arabidopsis thaliana* L.: an ultrastructural study. *In* Sexual Plant Reproduction **12:** 99-109

Baker SC, Robinson-Beers K, Villanueva JM, Gaiser JC, Gasser CS (1997) Interactions among genes regulating ovule development in Arabidopsis thaliana. *In* Genetics **145:** 1109

Banas A, Dahlqvist A, Stahl U, Lenman M, Stymne S (2000) The involvement of phospholipid: diacylglycerol acyltransferases in triacylglycerol production. *In* Biochemistry Society Transactions **28:** 703-704

Barber S, Walker J, Vasey E (1963) Mechanisms for movement of plant nutrients from soil and fertilizer to plant root. *In* Journal of Agricultural and Food Chemistry **11:** 204-207

Baud S, Bellec Y, Miquel M, Bellini C, Caboche M, Lepiniec L, Faure JD, Rochat C (2004) gurke and pasticcino3 mutants affected in embryo development are impaired in acetyl-CoA carboxylase. *In* EMBO reports **5:** 515-520

Baud S, Guyon V, Kronenberger J, Wuillème S, Miquel M, Caboche M, Lepiniec L, Rochat C (2003) Multifunctional acetyl-CoA carboxylase 1 is essential for very long chain fatty acid elongation and embryo development in Arabidopsis. *In* The Plant Journal **33:** 75-86

Baud S, Lepiniec L (2008) Compared analysis of the regulatory systems controlling lipogenesis in hepatocytes of mice and in maturing oilseeds of Arabidopsis. *In* Comptes Rendus Biologies **331:** 737-745

Baud S, Wuillème S, Lemoine R, Kronenberger J, Caboche M, Lepiniec L, Rochat C (2005) The AtSUC5 sucrose transporter specifically expressed in the endosperm is involved in early seed development in Arabidopsis. *In* The Plant Journal **43:** 824-836

Beisson F, Koo AJ, Ruuska S, Schwender J, Pollard M, Thelen JJ, Paddock T, Salas JJ, Savage L, Milcamps A, Mhaske VB, Cho Y, Ohlrogge JB (2003) Arabidopsis genes involved in acyl lipid metabolism. A 2003 census of the candidates, a study of the distribution of

expressed sequence tags in organs, and a web-based database. *In* Plant Physiology **132:** 681-697

Beisson F, Li-Beisson Y, Pollard M (2012) Solving the puzzles of cutin and suberin polymer biosynthesis. *In* Current Opinion in Plant Biology **15:** 329-337

Bieleski R (1973) Phosphate pools, phosphate transport, and phosphate availability. *In* Annual Review of Plant Physiology **24:** 225-252

Bligh EG, Dyer WJ (1959) A rapid method of total lipid extraction and purification. *In* Canandian Journal of Biochemistry and Physiology **37:** 911-917

Bohanec B (2009) Doubled haploids via gynogenesis. Springer

Bonaventure G, Bao X, Ohlrogge J, Pollard M (2004) Metabolic responses to the reduction in palmitate caused by disruption of the FATB gene in Arabidopsis. *In* Plant Physiology **135:** 1269-1279

Bonaventure G, Salas JJ, Pollard MR, Ohlrogge JB (2003) Disruption of the FATB gene in Arabidopsis demonstrates an essential role of saturated fatty acids in plant growth. *In* The Plant Cell **15:** 1020-1033

Bowman J (1994) Arabidopsis: an atlas of morphology and development. Springer-Verlag New York

Brisson D, Vohl MC, St-Pierre J, Hudson TJ, Gaudet D (2001) Glycerol: a neglected variable in metabolic processes? Bioessays **23:** 534-542

Browse J, McCourt PJ, Somerville CR (1986) Fatty acid composition of leaf lipids determined after combined digestion and fatty acid methyl ester formation from fresh tissue. *In* Analytical Biochemistry **152:** 141-145

Browse J, Somerville, C. (1991) Glycerolipid synthesis: Biochemistry and regulation. *In* Annual Review of Plant Physiology and Plant Molecular Biology **42:** 467-506

Browse J, Warwick N, Somerville CR, Slack CR (1986) Fluxes through the prokaryotic and eukaryotic pathways of lipid synthesis in the '16:3' plant *Arabidopsis thaliana*. *In* Biochemical Journal **235:** 25-31

Buseman CM, Tamura P, Sparks AA, Baughman EJ, Maatta S, Zhao J, Roth MR, Esch SW, Shah J, Williams TD, Welti R (2006) Wounding stimulates the accumulation of glycerolipids containing oxophytodienoic acid and dinor-oxophytodienoic acid in Arabidopsis leaves. *In* Plant Physiology **142:** 28-39

Byers DM, Gong H (2007) Acyl carrier protein: structure-function relationships in a conserved multifunctional protein family. *In* Biochemistry and Cell Biology **85:** 649-662

Carman GM, Han GS (2006) Roles of phosphatidate phosphatase enzymes in lipid metabolism. *In* Trends in Biochemical Sciences **31:** 694-699

Carman GM, Henry, SA (2007) Phosphatidic Acid Plays a Central Role in the Transcriptional Regulation of Glycerophospholipid Synthesis in *Saccharomyces cerevisiae*. *In* Journal of Biological Chemistry **282**

Chanda B, Venugopal SC, Kulshrestha S, Navarre DA, Downie B, Vaillancourt L, Kachroo A, Kachroo P (2008) Glycerol-3-phosphate levels are associated with basal resistance to the hemibiotrophic fungus Colletotrichum higginsianum in Arabidopsis. *In* Plant Physiology **147:** 2017-2029

Chanda B, Xia Y, Mandal MK, Yu K, Sekine KT, Gao Q-m, Selote D, Hu Y, Stromberg A, Navarre D (2011) Glycerol-3-phosphate is a critical mobile inducer of systemic immunity in plants. Nature Genetics **43:** 421-427

Chapman KD (1998) Phospholipase activity during plant growth and development and in response to environmental stress. *In* Trends in Plant Science **3:** 419-426

Chen M, Han G, Dietrich CR, Dunn TM, Cahoon EB (2006) The essential nature of sphingolipids in plants as revealed by the functional identification and characterization of the Arabidopsis LCB1 subunit of serine palmitoyltransferase. *In* The Plant Cell Online **18:** 3576-3593

Cheng Y, Zhou W, Peters C, Li M, Wang X, Huang J (2011) Characterization of the Arabidopsis glycerophosphodiester phosphodiesterase (GDPD) family reveals a role of the plastid-localized AtGDPD1 in maintaining cellular phosphate homeostasis under phosphate starvation. *In* The Plant Journal **66:** 781-795

Chomczynski P, Sacchi N (1987) Single-step method of RNA isolation by acid guanidinium thiocyanate-phenol-chloroform extraction. *In* Analytical Biochemistry **162:** 156-159.

Christensen CA, Subramanian S, Drews GN (1998) Identification of gametophytic mutations affecting female gametophyte development in Arabidopsis. *In* Developmental Biology **202:** 136-151

Christou P, Swain WF, Yang N-S, McCabe DE (1989) Inheritance and expression of foreign genes in transgenic soybean plants. *In* Proceedings of the National Academy of Sciences of the United States of America **86:** 7500-7504

Clarke NG, Dawson R (1981) Alkaline O leads to N-transacylation. A new method for the quantitative deacylation of phospholipids. *In* Biochemical Journal **195:** 301-306

Cruz-Ramírez A, Oropeza-Aburto A, Razo-Hernández F, Ramírez-Chávez E, Herrera-Estrella L (2006) Phospholipase DZ2 plays an important role in extraplastidic galactolipid biosynthesis and phosphate recycling in Arabidopsis roots. *In* Proceedings of the National Academy of Sciences of the United States of America **103:** 6765-6770

Custers J, Cordewener J, Fiers M, Maassen B, Campagne MVL, Liu C (2001) Androgenesis in Brassica. In Current Trends in the Embryology of Angiosperms. Springer, pp 451-470

Custers J, Snepvangers S, Jansen H, Zhang L, van Lookeren Campagne M (1999) The 35S-CaMV promoter is silent during early embryogenesis but activated during nonembryogenic sporophytic development in microspore culture. *In* Protoplasma **208:** 257-264

Dahlqvist A, Ståhl U, Lenman M, Banas A, Lee M, Sandager L, Ronne H, Stymne S (2000) Phospholipid:diacylglycerol acyltransferase: an enzyme that catalyzes the acyl-CoA-independent formation of triacylglycerol in yeast and plants. *In* Proceedings of the National Academy of Sciences of the United States of America **97:** 6487-6492

Daxinger L, Hunter B, Sheikh M, Jauvion V, Gasciolli V, Vaucheret H, Matzke M, Furner I (2008) Unexpected silencing effects from T-DNA tags in Arabidopsis. *In* Trends in Plant Science **13:** 4-6

Daxinger L, Kanno T, Huettel B, Matzke M, Matzke A (2007) MSAP-An approach to identify endogenous targets of RNA-directed DNA methylation and Pol IV in *Arabidopsis thaliana*. Febs Journal, Vol 274. Blackwell Publishing 9600 Garsington Rd, Oxford, England, pp 74-74

De Neve M, Van Houdt H, Bruyns A-M, Van Montagu M, Depicker A (1998) Screening for transgenic lines with stable and suitable accumulation levels of a heterologous protein. *In* Recombinant Proteins from Plants. Springer, pp 203-227

Dehesh K, Jones A, Knutzon DS, Voelker TA (1996) Production of high levels of 8:0 and 10:0 fatty acids in transgenic canola by overexpression of Ch FatB2, a thioesterase cDNA from Cuphea hookeriana. *In* The Plant Journal **9:** 167-172

Deroles SC, Gardner RC (1988) Expression and inheritance of kanamycin resistance in a large number of transgenic petunias generated by Agrobacterium-mediated transformation. *In* Plant Molecular Biology **11:** 355-364

Ding S-H, Huang L-Y, Wang Y-D, Sun H-C, Xiang Z-H (2006) High-level expression of basic fibroblast growth factor in transgenic soybean seeds and characterization of its biological activity. *In* Biotechnology letters **28:** 869-875

Dörmann P, Frentzen M, Ohlrogge JB (1994) Specificities of the Acyl-Acyl carrier protein (ACP) thioesterase and glycerol-3-phosphate acyltransferase for octadecenoyl-ACP isomers (Identification of a petroselinoyl-ACP thioesterase in Umbelliferae). *In* Plant Physiology **104:** 839-844

Dörmann P, Hoffmann-Benning S, Balbo I, Benning C (1995) Isolation and characterization of an Arabidopsis mutant deficient in the thylakoid lipid digalactosyl diacylglycerol. *In* The Plant Cell **7:** 1801-1810

Dörmann P, Voelker TA, Ohlrogge JB (1995) Cloning and expression in *Escherichia coli* of a novel thioesterase from *Arabidopsis thaliana* specific for long-chain acyl-acyl carrier proteins. *In* Archives of Biochemistry and Biophysics **316:** 612-618

Dörmann P, Voelker TA, Ohlrogge JB (2000) Accumulation of palmitate in *Arabidopsis* mediated by the acyl-acyl carrier protein thioesterase FATB1. *In* Plant Physiology **123:** 637-644

Douce R, Joyard J (1990) Biochemistry and function of the plastid envelope. *In* Annual Review of Cell Biology **6:** 173-216

Eastmond P, Quettier AL, Kroon JT, Craddock C, Adams N, Slabas AR (2010) Phosphatidic acid phosphohydrolase1 and 2 regulate phospholipid synthesis at the endoplasmic reticulum in Arabidopsis. *In* The Plant Cell **22:** 2796-2811

Eccleston VS, Ohlrogge JB (1998) Expression of lauroyl-acyl carrier protein thioesterase in brassica napus seeds induces pathways for both fatty acid oxidation and biosynthesis and implies a set point for triacylglycerol accumulation. *In* The Plant Cell **10:** 613-622

Essigmann B, Güler S, Narang RA, Linke D, Benning C (1998) Phosphate availability affects the thylakoid lipid composition and the expression of *SQD1*, a gene required for sulfolipid biosynthesis in *Arabidopsis thaliana*. *In* Proceedings of theNational Academy of Sciences of the United States of America **95:** 1950-1955

Fait A, Angelovici R, Less H, Ohad I, Urbanczyk-Wochniak E, Fernie AR, Galili G (2006) Arabidopsis seed development and germination is associated with temporally distinct metabolic switches. *In* Plant Physiology **142:** 839-854

Fang Z, Shao C, Meng Y, Wu P, Chen M (2009) Phosphate signaling in *Arabidopsis* and *Oryza sativa*. Plant Science **176:** 170-180

Fernández-Murray JP, McMaster CR (2005) Glycerophosphocholine catabolism as a new route for choline formation for phosphatidylcholine synthesis by the Kennedy pathway. *In* Journal of Biological Chemistry **280:** 38290-38296

Fisher E, Almaguer C, Holic R, Griac P, Patton-Vogt J (2005) Glycerophosphocholine-dependent growth requires Gde1p (YPL110c) and Git1p in Saccharomyces cerevisiae. *In* Journal of Biological Chemistry **280:** 36110-36117

Focks N, Benning C (1998) wrinkled1: A novel, low-seed-oil mutant of Arabidopsis with a deficiency in the seed-specific regulation of carbohydrate metabolism. *In* Plant Physiology **118:** 91-101

Frentzen M (1990) Comparison of certain properties of membrane bound and solubilized acyltransferase activities of plant microsomes. *In* Plant Science **69:** 39-48

Frentzen M (2004) Phosphatidylglycerol and sulfoquinovosyldiacylglycerol: anionic membrane lipids and phosphate regulation. *In* Current Opinion of Plant Biology **7:** 270-276

Fuchs J, Podda M (2005) Ligase chain reaction (LCR) and ligase detection reaction. *In* Encyclopedia of Medical Genomics and Proteomics 713-717.

Gaude N, Nakamura Y, Scheible W-R, Ohta H, Dörmann P (2008) Phospholipase C5 (NPC5) is involved in galactolipid accumulation during phosphate limitation in leaves of Arabidopsis. *In* The Plant Journal **56:** 28-39

Gifford EM, Foster AS (1989) Morphology and evolution of vascular plants. WH Freeman and Company New York

Härtel H, Benning C (2000) Can digalactosyldiacylglycerol substitute for phosphatidylcholine upon phosphate deprivation in leaves and roots of Arabidopsis? *In* Biochemical Society Transaction **28:** 729-732

Härtel H, Dörmann P, Benning C (2000) DGD1-independent biosynthesis of extraplastidic galactolipids after phosphate deprivation in Arabidopsis. *In* Proceedings of theNational Academy of Sciences of the United States of America **97:** 10649-10654

Härtel H, Dörmann P, Benning C (2001) Galactolipids not associated with the photosynthetic apparatus in phosphate-deprived plants. *In* Journal of Photochemistry and Photobiology B **61:** 46-51

Harwood J (1980) Plant acyl lipids: structure, distribution and analysis. *In* The Biochemistry of Plants **4:** 1-55

Heath RJ, Rock CO (1995) Regulation of malonyl-CoA metabolism by acyl-acyl carrier protein and β-ketoacyl-acyl carrier protein synthases in *Escherichia coli*. *In* Journal of Biological Chemistry **270:** 15531-15538

Heinz E (1977) Enzymatic reactions in galactolipid biosynthesis. *In* M Tevini, HK Lichtenthaler, eds, Lipids and Lipid Polymers in Higher Plants. Springer Verlag, Berlin, pp 102-120

Hellyer A, Leadlay PF, Slabas AR (1992) Induction, purification and characterisation of acyl-ACP thioesterase from developing seeds of oil seed rape (*Brassica napus*). *In* Plant Molecular Biology **20:** 763-780

Horton P, Park K-J, Obayashi T, Fujita N, Harada H, Adams-Collier C, Nakai K (2007) WoLF PSORT: protein localization predictor. *In* Nucleic Acids Research **35:** W585-W587

Hruz T, Laule O, Szabo G, Wessendorp F, Bleuler S, Oertle L, Widmayer P, Gruissem W, Zimmermann P (2008) Genevestigator v3: a reference expression database for the meta-analysis of transcriptomes. Advances in Bioinformatics **2008**

Hu J, Zhang Y, Wang J, Zhou Y (2014) Glycerol affects root development through regulation of multiple pathways in Arabidopsis. *In* Plos One **9**

Huynh TT, Pirtle RM, Chapman KD (2002) Expression of a *Gossypium hirsutum* cDNA encoding a FatB palmitoyl-acyl carrier protein thioesterase in *Escherichia coli*. *In* Plant Physiology and Biochemistry **40:** 1-9

Jelitto T, Sonnewald U, Willmitzer L, Hajirezeai M, Stitt M (1992) Inorganic pyrophosphate content and metabolites in potato and tobacco plants expressing *E. coli* pyrophosphatase in their cytosol. *In* Planta **188:** 238-244

Jha J, Maiti M, Bhattacharjee A, Basu A, Sen PC, Sen S (2006) Cloning and functional expression of an acyl-ACP thioesterase FatB type from *Diploknema* (Madhuca) *butyracea* seeds in *Escherichia coli*. *In* Journal of Plant Physiology and Biochemistry **44:** 645-655

Johnson-Brousseau SA, McCormick S (2004) A compendium of methods useful for characterizing Arabidopsis pollen mutants and gametophytically-expressed genes. The *In* The Plant Journal **39:** 761-775

Jones A, Davies M, Voelker T (1995) Palmitoyl-acyl carrier protein (ACP) thioesterase and the evolutidnary origin of plant acyl-ACP thioesterases. *In* The Plant Cell **7:** 359-371

Jürgens G, Ruiz RAT, Laux T, Mayer U, Berleth T (1994) Early events in apical-basal pattern formation in Arabidopsis. *In* Plant molecular biology. Springer, pp 95-103

Kameda K, Nunn W (1981) Purification and characterization of acyl coenzyme A synthetase from *Escherichia coli*. *In* Journal of Biological Chemistry **256:** 5702-5707

Kandasamy MK, Nasrallah JB, Nasrallah ME (1994) Pollen-pistil interactions and developmental regulation of pollen tube growth in Arabidopsis. *In* Development **120:** 3405-3418

Katagiri T, Ishiyama K, Kato T, Tabata S, Kobayashi M, Shinozaki K (2005) An important role of phosphatidic acid in ABA signaling during germination in *Arabidopsis thaliana*. *In* The Plant journal **43:** 107-117

Kelly AA, Dörmann P (2002) DGD2, an *Arabidopsis* gene encoding a UDP-galactose-dependent digalactosyldiacylglycerol synthase is expressed during growth under phosphate-limiting conditions. *In* Journal of Biological Chemistry **277:** 1166-1173

Kelly AA, Froehlich JE, Dörmann P (2003) Disruption of the two digalactosyldiacylglycerol synthase genes DGD1 and DGD2 in *Arabidopsis* reveals the existence of an additional enzyme of galactolipid synthesis. *In* The Plant Cell **15:** 2694-2706

Kennedy EP (1961) Biosynthesis of complex lipids. *In* Federation proceedings, Vol 20, p 934

Kim HJ, Ok SH, Bahn SC, Jang J, Oh SA, Park SK, Twell D, Ryu SB, Shin JS (2011) Endoplasmic reticulum–and golgi-localized phospholipase A2 plays critical roles in Arabidopsis pollen development and germination. *In* The Plant Cell **23:** 94-110

Kim S, Yamaoka Y, Ono H, Kim H, Shim D, Maeshima M, Martinoia E, Cahoon EB, Nishida I, Lee Y (2013) AtABCA9 transporter supplies fatty acids for lipid synthesis to the endoplasmic reticulum. Proceedings of the National Academy of Sciences of the United States of America **110:** 773-778

Kobayashi K, Awai K, Nakamura M, Nagatani A, T M, Ohta H (2009) Type-B monogalactosyldiacylglycerol synthases are involved in phosphate starvation-induced lipid remodeling, and are crucial for low-phosphate adaptation. *In* The Plant Journal **57:** 322-331

Konishi T, Shinohara K, Yamada K, Sasaki Y (1996) Acetyl-CoA carboxylase in higher plants: most plants other than gramineae have both the prokaryotic and the eukaryotic forms of this enzyme. *In* Plant and Cell Physiology **37:** 117-122

Koo A, Ohlrogge J, Pollard M (2004) On the export of fatty acids from the chloroplast. *In* Journal of Biological Chemistry **279:** 16101-16110

Kunst L, Browse J, Somerville C (1988) Altered regulation of lipid biosynthesis in a mutant of *Arabidopsis* deficient in chloroplast glycerol-3-phosphate acyltransferase activity. *In* Proceedings of theNational Academy of Sciences of the United States of America **85:** 4143-4147

Laemmli UK (1970) Cleavage of structural proteins during the assembly of the head of bacteriophage T4. *In* Nature **227:** 680-685

Larson T, Ehrmann M, Boos W (1983) Periplasmic glycerophosphodiester phosphodiesterase of *Escherichia coli*, a new enzyme of the glp regulon. *In* Journal of Biological Chemistry **258:** 5428-5432

Lemieux B, Miquel M, Somerville C (1990) Mutants of Arabidopsis with alterations in seed lipid fatty acid composition. *In* Theoretical and applied genetics **80:** 234-240

Li M, Welti R, Wang X (2006) Quantitative profiling of Arabidopsis polar glycerolipids in response to phosphorus starvation. Roles of phospholipases D zeta1 and D zeta2 in phosphatidylcholine hydrolysis and digalactosyldiacylglycerol accumulation in phosphorus-starved plants. *In* Plant Physiology **142:** 750-761

Lush WM (1999) Whither chemotropism and pollen tube guidance? Trends in Plant Science **4:** 413-418

Maeo K, Tokuda T, Ayame A, Mitsui N, Kawai T, Tsukagoshi H, Ishiguro S, Nakamura K (2009) An AP2-type transcription factor, WRINKLED1, of *Arabidopsis thaliana* binds to the AW-box sequence conserved among proximal upstream regions of genes involved in fatty acid synthesis. *In* The Plant Journal **60:** 476-487

Maheshwari P, Johri B (1950) Development of the embryo sac, embryo and endosperm in helixanthera ligustrina (wall.) dans. *In* Nature **165:** 978-979

Mandal MK, Chanda B, Xia Y, Yu K, Sekine K, Gao Q-m, Selote D, Kachroo A, Kachroo P (2011) Glycerol-3-phosphate and systemic immunity. *In* Plant signaling and Behavior **6:** 1871-1874

Mansfield S, Bowman J (1993) Embryogenesis. Arabidopsis: An atlas of morphology and development, J. Bowman, ed (Berlin: Springer-Verlag)**:** 349-362

Mansfield S, Briarty L (1992) Cotyledon cell development in *Arabidopsis thaliana* during reserve deposition. *In* Canadian Journal of Botany **70:** 151-164

Matos AR, Pham-Thi A-T (2009) Lipid deacylating enzymes in plants: old activities, new genes. *In* Plant Physiology and Biochemistry **47:** 491-503

Matzke A, Neuhuber F, Park Y, Ambros P, Matzke M (1994) Homology-dependent gene silencing in transgenic plants: epistatic silencing loci contain multiple copies of methylated transgenes. *In* Molecular and General Genetics MGG **244:** 219-229

McConn M (1996) The critical requirement for linolenic acid is pollen development, not photosynthesis, in an Arabidopsis mutant. The Plant Cell Online **8:** 403-416

McConn M, Browse J (1998) Polyunsaturated membranes are required for photosynthetic competence in a mutant of Arabidopsis. *In* The Plant Journal **15:** 521-530

McKee J, Hawke J (1979) The incorporation of [14C] acetate into the constituent fatty acids of monogalactosyldiglyceride by isolated spinach chloroplasts. *In* Archives of Biochemistry and Biophysics **197:** 322-332

Meinke DW, Franzmann LH, Nickle TC, Yeung EC (1994) Leafy cotyledon mutants of Arabidopsis. *In* The Plant Cell Online **6:** 1049-1064

Miège C, Maréchal E, Shimojima M, Awai K, Block MA, Ohta H, Takamiya K, Douce R, Joyard J (1999) Biochemical and topological properties of type A MGDG synthase, a spinach chloroplast envelope enzyme catalyzing the synthesis of both prokaryotic and eukaryotic MGDG. *In* European Journal Biochemistry **265:** 990-1001

Miquel M, Cassagne C, Browse J (1998) A new class of Arabidopsis mutants with reduced hexadecatrienoic acid fatty acid levels. Plant Physiology **117:** 923-930

Misra RC (1962) Contribution to the embryology of *Arabidopsis thaliana* (Gay and Monn.). *In* Agra University Journal Research (Sciences) **11:** 191–199

Misra S, Gedamu L (1989) Heavy metal tolerant transgenic *Brassica napus* L. and *Nicotiana tabacum* L. plants. *In* Theoretical and Applied Genetics **78:** 161-168

Mission J, Raghothama K, Jain A, Jouhet J, Block M, Blingy R, Ortet P, Creff A, Somerville S, Rolland N, Doumas P, Nacry P, Herrerra-Estrella L, Nussaume L, Thibaud, MC (2005) A genome-wide transcriptional analysis using Arabidopsis thaliana Affymetrix gene chips determined plant responses to phosphate deprivation. *In* Proceedings of the National Academy of Sciences of the United States of America **102:** 11934-11939

Mongrand S, Bessoule J, Cassagne C (1997) A re-examination in vivo of the phosphatidylcholine–galactolipid metabolic relationship during plant lipid biosynthesis. *In* Biochemistry Journal **327:** 853-858

Mongrand S, Cassagne C, Bessoule JJ (2000) Import of lyso-phosphatidylcholine into chloroplasts likely at the origin of eukaryotic plastidial lipids. *In* Plant Physiology **122:** 845-852

Morcuende R, Bari R, Gibon Y, Zheng W, Pant BD, BLÄSING O, Usadel B, Czechowski T, Udvardi MK, Stitt M (2007) Genome-wide reprogramming of metabolism and regulatory networks of Arabidopsis in response to phosphorus. *In* Plant, Cell & Environment **30:** 85-112

Moreno-Pérez AJ, Venegas-Calerón M, Vaistij FE, Salas JJ, Larson TR, Garcés R, Graham IA, Martínez-Force E (2012) Reduced expression of FatA thioesterases in Arabidopsis affects the oil content and fatty acid composition of the seeds. *In* Planta **235:** 629-639

Nakamura Y, Awai K, Masuda T, Yoshioka Y, Takamiya K, Ohta H (2005) A novel phosphatidylcholine-hydrolyzing phospholipase C induced by phosphate starvation in *Arabidopsis*. *In* Journal of Biological Chemistry **280:** 7469-7476

Nakamura Y, Koizumi R, Shui G, Shimojima M, Wenk MR, Ito T, Ohta H (2009) Arabidopsis lipins mediate eukaryotic pathway of lipid metabolism and cope critically with phosphate starvation. *In* Proceedings of the National Academy of Sciences of the United States of America **106:** 20978-20983

Nakamura Y, Ohta H. (2010) Phosphatidic Acid Phosphatases in Seed Plants. *In* Lipid Signaling in Plants **16:** 131-141

Nielsen N (1989) In Vitro Modification and Assembly of Soybean Glycinin1. *In* Proceedings of the World Congress on Vegetable Protein Utilization in Human Foods and Animal Feedstuffs. *In* The American Oil Chemists Society, p 487

Ohlrogge J, Browse J (1995) Lipid biosynthesis. Plant Cell **7:** 957-970

Ohlrogge JB, Browse J, Somerville CR (1991) The genetics of plant lipids. *In* Biochimica et Biophysica Acta **1082:** 1-26

Ohlrogge JB, Jaworski JG (1997) Regulation of fatty acid synthesis. *In* Annual Review of Plant Physiology and Plant Molecular Biology **48:** 109-136

Ohshima N, Yamashita S, Takahashi N, Kuroishi C, Shiro Y, Takio K (2008) *Escherichia coli* cytosolic glycerophosphodiester phosphodiesterase (UgpQ) requires Mg2+, Co2+, or Mn2+ for its enzyme activity. *In* Journal of bacteriology **190:** 1219-1223

Okazaki Y, Otsuki H, Narisawa T, Kobayashi M, Sawai S, Kamide Y, Kusano M, Aoki T, Hirai MY, Saito K (2013) A new class of plant lipid is essential for protection against phosphorus depletion. *In* Nature Communications **4:** 1510

Okazaki Y, Shimojima M, Sawada Y, Toyooka K, Narisawa T, Mochida K, Tanaka H, Matsuda F, Hirai A, Hirai MY, Ohta H, Saito K (2009) A chloroplastic UDP-glucose pyrophosphorylase from *Arabidopsis* is the committed enzyme for the first step of sulfolipid biosynthesis. *In* The Plant Cell **21:** 892-909

Pappan K, Austin-Brown S, Chapman KD, Wang XM (1998) Substrate selectivities and lipid modulation of plant phospholipase D alpha, -beta, and -gamma. *In* Archives of Biochemistry and Biophysics **353:** 131-140

Paradisa S, Villasusob AL, Aguayoa SS, Maldineya R, Habricota Y, Zalejskia C, Machadoa E, Sottaa B, Miginiaca B, Jeannettea E (2011) *Arabidopsis thaliana* lipid phosphate

phosphatase 2 is involved in abscisic acid signalling in leaves. *In* Plant Physiology and Biochemistry **49:** 357-362

Pant BD, Burgos A, Pant P, Cuadros-Inostroza A, Willmitzer L, Scheible WR (2015) The transcription factor PHR1 regulates lipid remodeling and triacylglycerol accumulation in Arabidopsis thaliana during phosphorus starvation. *In* Journal of Experimental Botany eru535

Park SK, Twell D (2001) Novel Patterns of ectopic cell Plate growth and Lipid Body Distribution in the Arabidopsis gemini pollen1Mutant. *In* Plant Physiology **126:** 899-909

Pech-Canul Á, Nogales J, Miranda-Molina A, Álvarez L, Geiger O, Soto MJ, López-Lara IM (2011) FadD is required for utilization of endogenous fatty acids released from membrane lipids. *In* Journal of Bacteriology **193:** 6295-6304

Perry SE, Wang H (2003) Rapid isolation of *Arabidopsis thaliana* developing embryos. *In* Biotechniques **35:** 278-280, 282

Pierrugues O, Brutesco C, Oshiro J, Gouy M, Deveaux Y, Carman GM, Thuriaux P, Kazmaier M (2001) Lipid phosphate phosphatases in Arabidopsis. Regulation of the AtLPP1 gene in response to stress. *In* Journal of Biological Chemistry **276:** 20300-20308

Poirier Y, Thoma S, Somerville C, Schiefelbein J (1991) Mutant of *Arabidopsis* deficient in xylem loading of phosphate. *In* Plant Physiology **97:** 1087-1093

Pollard MR, Anderson L, Fan C, Hawkins DJ, Davies HM (1991) A specific acyl-ACP thioesterase implicated in medium-chain fatty acid production in immature cotyledons of *Umbellularia californica*. *In* Archives of Biochemistry and Biophysics **284:** 306-312

Preuss D, Lemieux B, Yen G, Davis R (1993) A conditional sterile mutation eliminates surface components from Arabidopsis pollen and disrupts cell signaling during fertilization. *In* Genes & Development **7:** 974-985

Pruitt RE, Hülskamp M (1994) 18 From pollination to fertilization in Arabidopsis. Cold Spring Harbor Monograph Archive **27:** 467-483

Raghothama KG (1999) Phosphate Acquisition. Annual Review of Plant Physiology and Plant *In* Molecular Biology **50:** 665-693

Register JC, Peterson DJ, Bell PJ, Bullock WP, Evans IJ, Frame B, Greenland AJ, Higgs NS, Jepson I, Jiao S (1994) Structure and function of selectable and non-selectable transgenes in maize after introduction by particle bombardment. *In* Plant Molecular Biology **25:** 951-961

Rietz S, Dermendjiev G, Oppermann E, Tafesse FG, Effendi Y, Holk A, Parker JE, Teige M, Scherer GF (2010) Roles of Arabidopsis patatin-related phospholipases A in root development are related to auxin responses and phosphate deficiency. *In* Molecular Plant **3:** 524-538

Riggs KG, McLachlan A (1986) A simplified screening procedure for large number of mini preparation. *In* Biotechnique **4:** 310-313

Rosso MG, Li Y, Strizhov N, Reiss B, Dekker K, Weisshaar B (2003) An *Arabidopsis thaliana* T-DNA mutagenized population (GABI-Kat) for flanking sequence tag-based reverse genetics. *In* Plant Molecular Biology **53:** 247-259

Roughan PG, Slack, C.R. (1982) Cellular organization of glycerolipid metabolism. *In* Annual Review of Plant Physiology **33:** 97-132

Rubio V, Linhares F, Solano R, Martín AC, Iglesias J, Leyva A, Paz-Ares J (2001) A conserved MYB transcription factor involved in phosphate starvation signaling both in vascular plants and in unicellular algae. *In* Genes & Development **15:** 2122-2133

Ryu SB (2004) Phospholipid-derived signaling mediated by phospholipase A in plants. *In* Trends in Plant Science **9:** 229-235

Salas J, Ohlrogge J (2002) Characterization of substrate specificity of plant FatA and FatB acyl-ACP thioesterases. *In* Archives of Biochemistry Biophysics **403:** 25-34

Sambrook J, Fritsch EF, Maniatis T (1989) Molecular cloning: A laboratory manual. Cold Spring Harbor Laboratory Press, New York

Sánchez-García A, Moreno-Pérez AJ, Muro-Pastor AM, Salas JJ, Garcés R, Martínez-Force E (2010) Acyl-ACP thioesterases from castor (*Ricinus communis*): An enzymatic system

appropriate for high rates of oil synthesis and accumulation. *In* Phytochemistry **71:** 860-869

Sanders PM, Bui AQ, Weterings K, McIntire K, Hsu Y-C, Lee PY, Truong MT, Beals T, Goldberg R (1999) Anther developmental defects in *Arabidopsis thaliana* male-sterile mutants. *In* Sexual Plant Reproduction **11:** 297-322

Schneitz K, Hülskamp M, Pruitt RE (1995) Wild-type ovule development in *Arabidopsis thaliana*: a light microscope study of cleared whole-mount tissue. *In* The Plant Journal **7:** 731-749

Seguí-Simarro JM (2010) Androgenesis revisited. *In* The Botanical Review **76:** 377-404

Shanklin J, Somerville C (1991) Stearoyl-acyl-carrier-protein desaturase from higher plants is structurally unrelated to the animal and fungal homologs. *In* Proceedings of the National Academy of Sciences of the United States of America **88:** 2510-2514

Shen W, Li JQ, Dauk M, Huang Y, Periappuram C, Wei Y, Zou J (2010) Metabolic and transcriptional responses of glycerolipid pathways to a perturbation of glycerol 3-phosphate metabolism in Arabidopsis. *In* Journal of Biological Chemistry **285:** 22957-22965

Shen W, Wei Y, Dauk M, Tan Y, Taylor DC, Selvaraj G, Zou J (2006) Involvement of a glycerol-3-phosphate dehydrogenase in modulating the NADH/NAD+ ratio provides evidence of a mitochondrial glycerol-3-phosphate shuttle in Arabidopsis. *In* The Plant Cell Online **18:** 422-441

Shimojima M, Ohta H, Iwamatsu A, Masuda T, Shioi Y, Takamiya K (1997) Cloning of the gene for monogalactosyldiacylglycerol synthase and its evolutionary origin. *In* Proceedings of the National Academy of Sciences of the United States of America **94:** 333-337

Shintani DK, Ohlrogge JB (1995) Feedback inhibition of fatty acid synthesis in tobacco suspension cells. *In* The Plant Journal **7:** 577-587

Shrawat AK (2007) Genetic transformation of cereals mediated by Agrobacterium: potential and problems. *In* ISB News Report

Siebers M, Dörmann P, Hölzl G (2015) Membrane remodelling in phosphorus-deficient plants. *In* Annual Plant Reviews **48**, 237-264

Šimočková M, Holic R, Tahotná D, Patton-Vogt J, Griač P (2008) Yeast Pgc1p (YPL206c) controls the amount of phosphatidylglycerol via a phospholipase C-type degradation mechanism. *In* Journal of Biological Chemistry **283:** 17107-17115

Sims TL, Goldberg RB (1989) The glycinin Gy1 gene from soybean. *In* Nucleic acids research **17:** 4386

Smith P, Krohn RI, Hermanson G, Mallia A, Gartner F, Provenzano M, Fujimoto E, Goeke N, Olson B, Klenk D (1985) Measurement of protein using bicinchoninic acid. *In* Analytical Biochemistry **150:** 76-85

Soriano M, Li H, Boutilier K (2013) Microspore embryogenesis: establishment of embryo identity and pattern in culture. *In* Plant Reproduction **26:** 181-196

Sussman MR, Amasino RM, Young JC, Krysan PJ, Austin-Phillips S (2000) The Arabidopsis knockout facility at the University of Wisconsin-Madison. *In* Plant Physiology **124:** 1465-1467

Svetlichnyy V (2007) Funktionelle Charakterisierung von Acyl-ACP-Thioesterasen in *Arabidopsis thalina*. Diploma thesis, Max-Planck-Institute of Molecular Plant Physiology, Golm

Takano M, Egawa H, Ikeda JE, Wakasa K (1997) The structures of integration sites in transgenic rice. *In* The Plant Journal **11:** 353-361

Terzaghi WB (1986) A System for Manipulating the Membrane Fatty Acid Composition of Soybean Cell Cultures by Adding Tween-Fatty Acid Esters to Their Growth Medium Basic Parameters and Effects on Cell Growth. *In* Plant Physiology **82:** 771-779

Theuns I, Windels P, De Buck S, Depicker A, Van Bockstaele E, De Loose M (2002) Identification and characterization of T-DNA inserts by T-DNA fingerprinting. *In* Euphytica **123:** 75-84

Tjellström H, Andersson MX, Larsson KE, Sandelius AS (2008) Membrane phospholipids as a phosphate reserve: the dynamic nature of phospholipid-to-digalactosyl diacylglycerol exchange in higher plants. *In* Plant, Cell & Environment **31:** 1388-1398

To A, Joubès J, Barthole G, Lécureuil A, Scagnelli A, Jasinski S, Lepiniec L, Baud S (2012) WRINKLED transcription factors orchestrate tissue-specific regulation of fatty acid biosynthesis in Arabidopsis. The Plant Cell Online **24:** 5007-5023

Tommassen J, Eiglmeier K, Cole ST, Overduin P, Larson TJ, Boos W (1991) Characterization of two genes, *glpQ* and *ugpQ*, encoding glycerophosphoryl diester phosphodiesterases of *Escherichia coli*. *In* Molecular and General Genetics **226:** 321-327

Towbin H, Staehelin T, Gordon J (1979) Electrophoretic transfer of proteins from polyacrylamide gels to nitrocellulose sheets: procedure and some applications. *In* Proceedings of the National Academy of Sciences of the United States of America **76:** 4350-4354

Van Der Rest B, Rolland N, Boisson A, Ferro M, Bligny R, Douce R (2004) Identification and characterization of plant glycerophosphodiester phosphodiesterase. *In* Biochemical Journal **379:** 601-607

Vance CP, Uhde-Stone C, Allan DL (2003) Phosphorus acquisition and use: critical adaptations by plants for securing a nonrenewable resource. *In* New Phytologist **157:** 423–447

Vaucheret H (1993) Identification of a general silencer for 19S and 35S promoters in a transgenic tobacco plant: 90 bp of homology in the promoter sequence are sufficient for trans-inactivation. Comptes rendus de l'Académie des sciences. Série 3, *In* Sciences de la Vie **316:** 1471-1483

Venugopal SC, Chanda B, Vaillancourt L, Kachroo A, Kachroo P (2009) The common metabolite glycerol-3-phosphate is a novel regulator of plant defense signaling. *In* Plant Signaling and Behavior **4:** 746-749

Verdaguer B, de Kochko A, Fux CI, Beachy RN, Fauquet C (1998) Functional organization of the cassava vein mosaic virus (CsVMV) promoter. *In* Plant Molecular Biology **37:** 1055-1067

Voelker TA, Davies HM (1994) Alteration of the specificity and regulation of fatty acid synthesis of Escherichia coli by expression of a plant medium-chain acyl-acyl carrier protein thioesterase. *In* Journal of Bacteriology **176:** 7320-7327

Voelker TA, Worrell AC, Anderson L, Bleibaum J, Fan C, Hawkins DJ, Radke SE, Davies HM (1992) Fatty acid biosynthesis redirected to medium chains in transgenic oilseed plants. *In* Science **257:** 72-74

Voinnet O, Lederer C, Baulcombe DC (2000) A Viral Movement Protein Prevents Spread of the Gene Silencing Signal in *Nicotiana benthamiana. In* Cell **103:** 157-167

Wang G, Ryu S, Wang X (2012) Plant phospholipases: an overview. *In* Lipases and Phospholipases. Springer, pp 123-137

Wang Q, Sullivan RW, Kight A, Henry RL, Huang J, Jones AM, Korth KL (2004) Deletion of the chloroplast-localized thylakoid formation1 gene product in Arabidopsis leads to deficient thylakoid formation and variegated leaves. *In* Plant Physiology **136:** 3594-3604

Wang X (2002) Phospholipase D in hormonal and stress signaling. *In* Current Opinion in Plant Biology **5:** 408-414

Webb MC, Gunning BE (1990) Embryo sac development in Arabidopsis thaliana. *In* Sexual Plant Reproduction **3:** 244-256

Wei Y, Shen W, Dauk M, Wang F, Selvaraj G, Zou J (2004) Targeted gene disruption of glycerol-3-phosphate dehydrogenase in Colletotrichum gloeosporioides reveals evidence that glycerol is a significant transferred nutrient from host plant to fungal pathogen. *In* Journal of Biological Chemistry **279:** 429-435

Weimar JD, DiRusso CC, Delio R, Black PN (2002) Functional role of fatty acyl-coenzyme A synthetase in the transmembrane movement and activation of exogenous long-chain fatty acids. Amino acid residues within the ATP/AMP signature motif of Escherichia coli FadD are required for enzyme activity and fatty acid transport. *In* Journal of Biological Chemistry **277:** 29369-29376

Welti R, Li W, Li M, Sang Y, Biesiada H, Zhou H-E, Rajashekar C, Williams T, Wang X (2002) Profiling membrane lipids in plant stress responses. Role of phospholipase D in freezing-induced lipid changes in *Arabidopsis*. *In* Journal of Biological Chemistry **277:** 31994-32002

Wilhelmi LK, Preuss D (1997) Blazing New Trails (Pollen Tube Guidance in Flowering Plants). *In* Plant Physiology **113:** 307

Wilhelmi LK, Preuss D (1999) The mating game: pollination and fertilization in flowering plants. *In* Current Opinion in Plant Biology **2:** 18-22

Wilkinson JE, Twell D, Lindsey K (1997) Activities of CaMV 35S and nos promoters in pollen: implications for field release of transgenic plants. *In* Journal of Experimental Botany **48:** 265-275

Willemse M, Van Went J (1984) The female gametophyte. *In* Embryology of Angiosperms. Springer, pp 159-196

Wolters-Arts M, Lush WM, Mariani C (1998) Lipids are required for directional pollen-tube growth. *In* Nature **392:** 818-821

Wu G-Z, Xue H-W (2010) Arabidopsis β-ketoacyl-[acyl carrier protein] synthase I is crucial for fatty acid synthesis and plays a role in chloroplast division and embryo development. *In* The Plant Cell **22:** 3726-3744

Yadegari R, Drews GN (2004) Female gametophyte development. *In* The Plant Cell Online **16:** S133-S141

Yamaryo Y, Dubots E, Albrieux C, Baldan B, Block MA (2008) Phosphate availability affects the tonoplast localization of PLDζ2, an *Arabidopsis thaliana* phospholipase D. *In* FEBS letters **582:** 685-690

Yang W, Simpson JP, Li-Beisson Y, Beisson F, Pollard M, Ohlrogge JB (2012) A land-plant-specific glycerol-3-phosphate acyltransferase family in Arabidopsis: substrate specificity, sn-2 preference, and evolution. *In* Plant Physiology **160:** 638-652

Yu B, Xu C, Benning C (2002) *Arabidopsis* disrupted in *SQD2* encoding sulfolipid synthase is impaired in phosphate-limited growth. *In* Proceedings of the National Academy of Sciences of the United States of America **99:** 5732-5737

Yu K, Soares JM, Mandal MK, Wang C, Chanda B, Gifford AN, Fowler JS, Navarre D, Kachroo A, Kachroo P (2013) A feedback regulatory loop between G3P and lipid transfer proteins DIR1 and AZI1 mediates azelaic-acid-induced systemic immunity. *In* Cell Reports **3:** 1266-1278

Yuan L, Voelker TA, Hawkins DJ (1995) Modification of the substrate specificity of an acyl-acyl carrier protein thioesterase by protein engineering. *In* Proceedings of the National Academy of Sciences of the United States of America **92:** 10639-10643

Zhang M, Fan J, Taylor DC, Ohlrogge JB (2009) DGAT1 and PDAT1 acyltransferases have overlapping functions in Arabidopsis triacylglycerol biosynthesis and are essential for normal pollen and seed development. *In* The Plant Cell Online **21:** 3885-3901

Zhang X, Ferguson-Miller SM, Reid GE (2009) Characterization of ornithine and glutamine lipids extracted from cell membranes of *Rhodobacter sphaeroides*. *In* Journal of America Society for Mass Spectrometry **20:** 198-212

Zheng B, Berrie CP, Corda D, Farquhar MG (2003) GDE1/MIR16 is a glycerophosphoinositol phosphodiesterase regulated by stimulation of G protein-coupled receptors. *In* Proceedings of the National Academy of Sciences of the United States of America **100:** 1745-1750

Zinkl GM, Zwiebel BI, Grier DG, Preuss D (1999) Pollen-stigma adhesion in Arabidopsis: a species-specific interaction mediated by lipophilic molecules in the pollen exine. *In* Development **126:** 5431-5440

7 Appendix

7.1 Triacylglycerol Species Compositions of Arabidopsis *fatA1-2fatA2-2* Mutant Embryos at Heart Stage

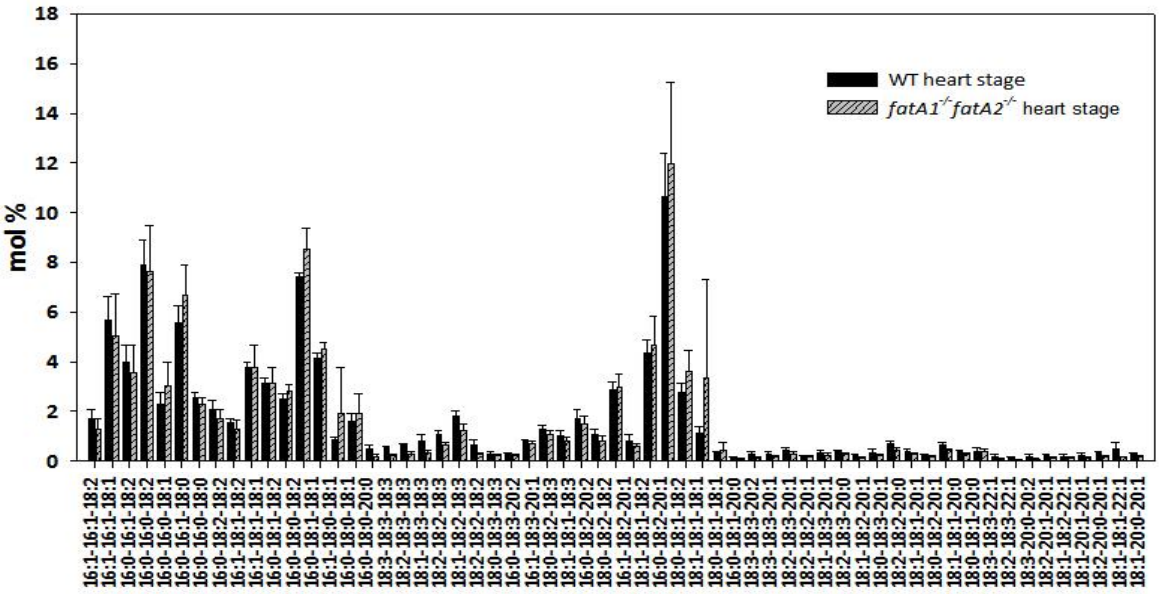

Figure 7.1: Triacylglycerol species composition (mol %) from Arabidopsis WT and *fatA1-2*$^{-/-}$*fatA2-2*$^{-/-}$ heart stage embryos. Lipids were extracted from heart stage embryos ca. 12 days after flowering by chloroform/methanol extraction and analyzed by Q-TOF MS/MS. Data present means and standard deviations of five independent determinations.

7.2Alignment of Nucleic Acid Sequences of Arabidopsis *GDPD5* and *GDPD6* Coding Region

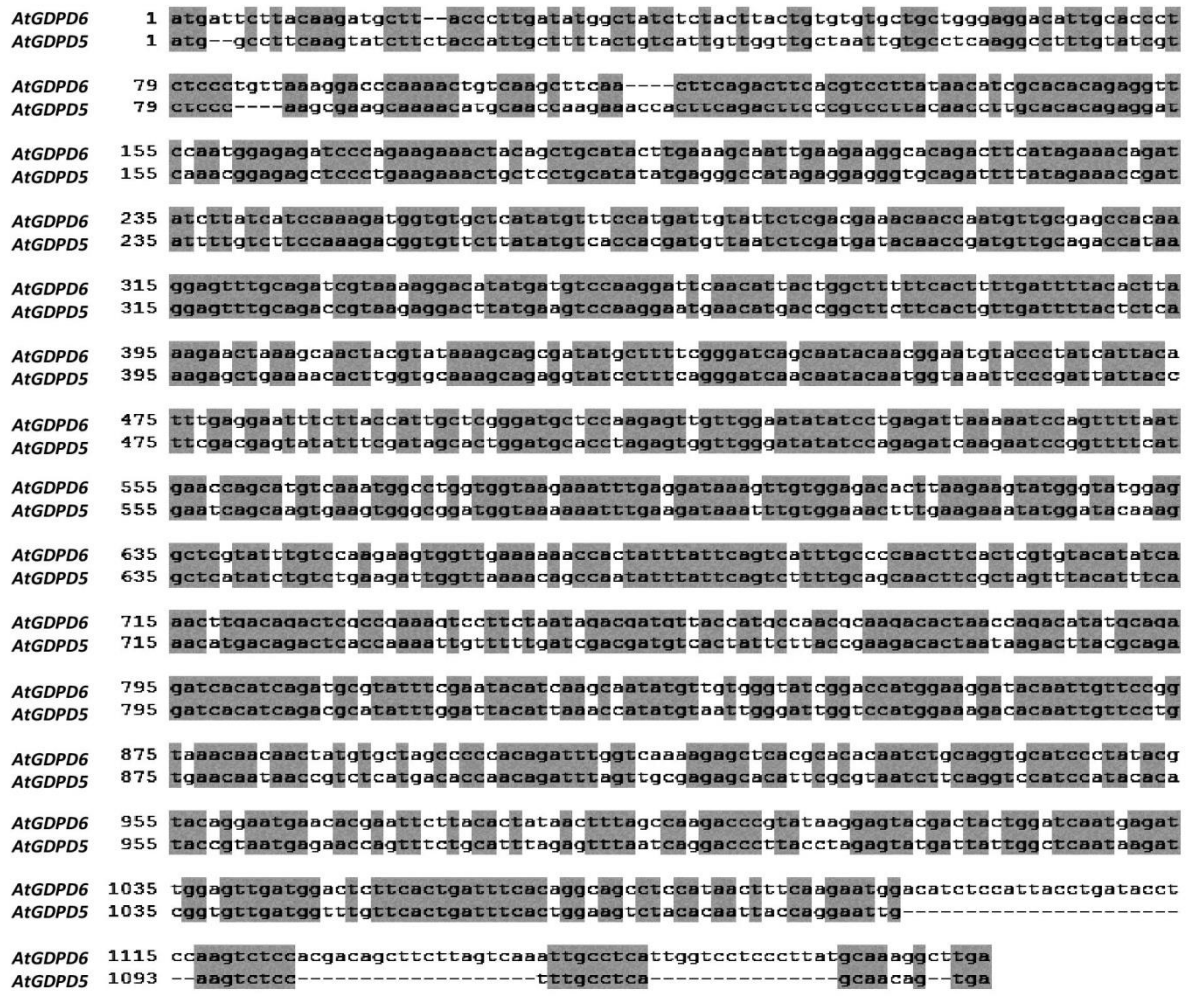

Figure 7.2: Nucleic acid sequences of the *GDPD5* and *GDPD6* predicted coding region. Alignment of the nucleotide sequences of Arabidopsis glycerophosphodiester phosphodiesterases (*AtGDPD5*, *AtGDPD6*). The alignment was derived from the amino acid sequences comparison using CloneManager Scoring Matrix: Blosum62.

7.3 Membrane lipid composition of mutants affected in Different Genes Involved in Membrane Lipid Remodeling During Phosphate Limitation

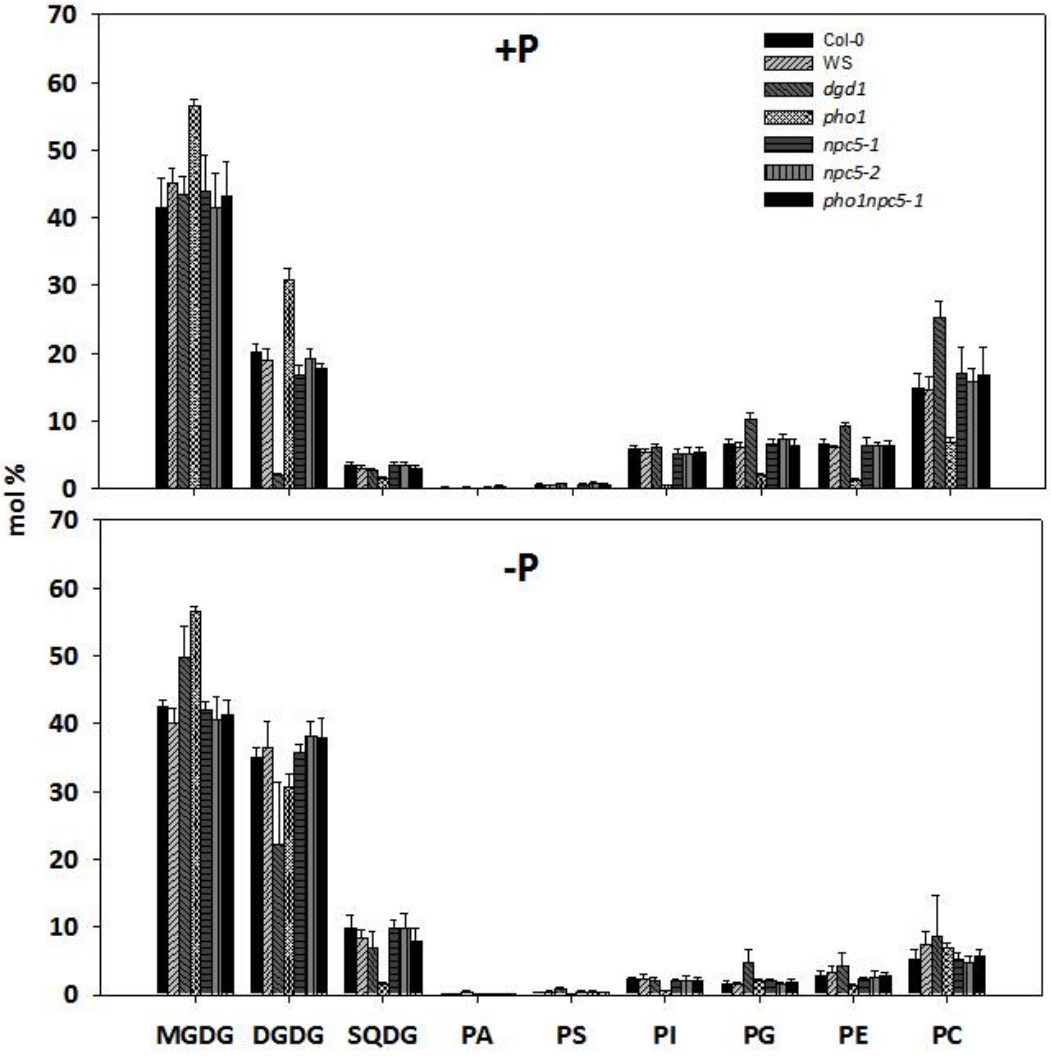

Figure 7.3: Glycerolipid composition (mol %) from Arabidopsis WT (different ecotypes) and different mutants affected in genes presumably involved in membrane lipid remodeling upon phosphate starvation. Plants were grown on synthetic agar medium with or without phoshate. Lipids were extracted from leaves by chloroform/methanol and analyzed by Q-TOF MS/MS. Data present means and standard deviations of five independent determinations.

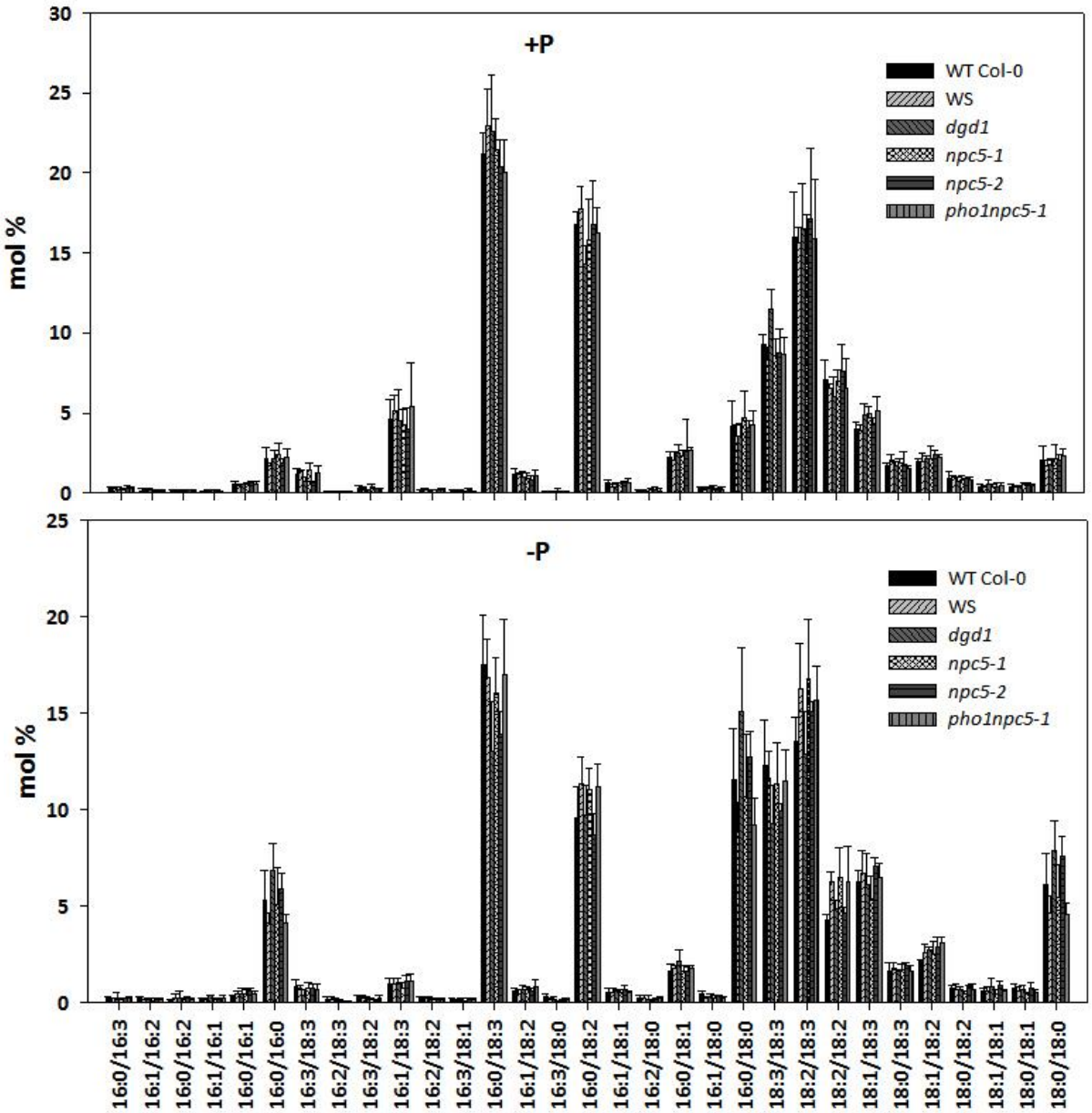

Figure 7.4: Diacylglycerol composition (mol %) from Arabidopsis WT (different ecotypes) and different mutants affected in genes presumably involved in membrane lipid remodeling upon phosphate starvation. Lipids were extracted from leaves with chloroform/methanol and analyzed by Q-TOF MS/MS. Data present means and standard deviations of five independent determinations.

7.4 Alexander Staining of the Different *GDPD5* and *GDPD6* Single Mutants

Table 7.1: Viability test of pollen from WT and *GDPD5* and *GDPD6* single mutants.

Pollen viability of GDPD single mutants					
Plant	**WT**	***gdpd5-1***	***gdpd5-2***	***gdpd6-1***	***gdpd6-2***
Total numbers counted	1896	2582	1659	1263	1155
Viable (%)	99	98	95	99	96
Non-viable (%)	1	2	5	1	4

7.5 G3P Measurement in Arabidopsis WT

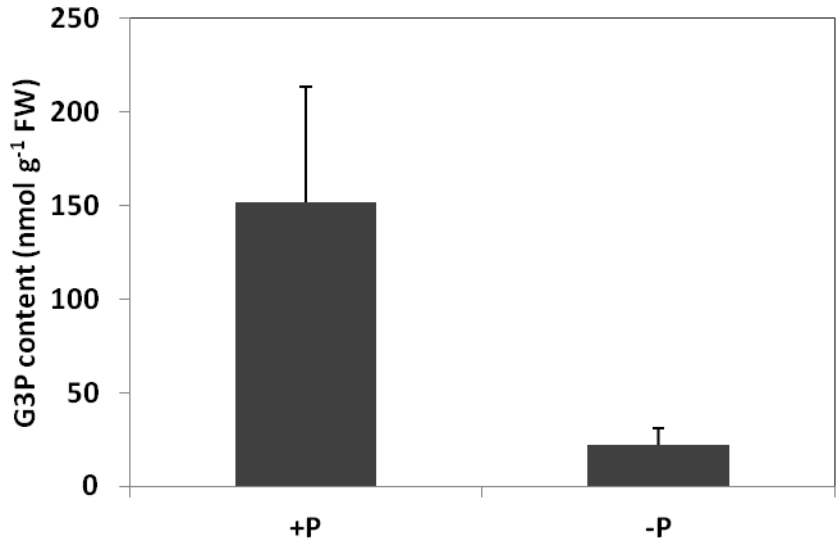

Figure 7.5: G3P content in Arabidopsis Col-0 roots grown on phosphate plus or minus conditions. G3P was isolated by chloroform/methanol extraction and analyzed by GC-MS. Data present means and standard deviations of four independent determinations.

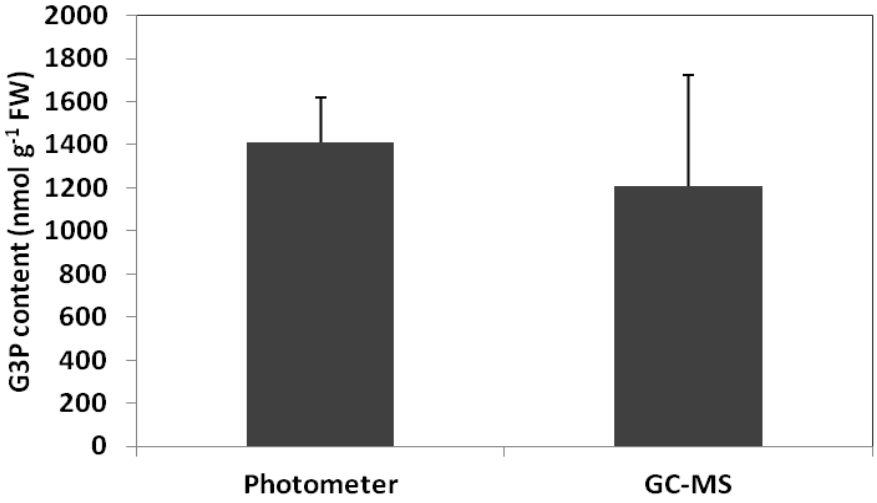

Figure 7.6: G3P content in Arabidopsis Col-0 leaves of plants grown on soil. G3P was isolated by chloroform/methanol extraction and analyzed with a photometer or by GC-MS. Data present means and standard deviations of at least three independent determinations. Similar G3P contents were obtained when leaves were extracted with TCA, and G3P was measured with the photometer.

7.6 Synthetic Oligonucleotides

Synthetic oligonucleotides used in this work were ordered from IDT Genomics (Leuven, BE).

Table 7.2: Synthetic oligonucleotides

Stock number	Sequence
bn78	ATTTTGCCGATTTCGGAAC
bn142	CCCATTTGGACGTGAATGTAGACAC
bn122	TTTTCTGGGTTTTGTATGCATG
bn123	TTCCAACAGCCAAAATACAGG
bn207	AGGGGGATTGAGTTTGATTTG
bn208	ACCATTTGGTTCAATTTGCAG
bn209	TCCAAATATGCGTCTGATGTG
bn210	TCAAATTCAGTCATGGCCTTC
bn212	CGTGTGCCAGGTGCCCACGGAATAGT
bn287	TTGGTCATCTCATCTCTTCCG
bn288	ATTTGGAAACTTGTGCAGGTG
bn433	GAATTCATGTTGAAGCTTTCGTGTAATG
bn434	GTCGACGCAATGGTTTCAACAGTAGCG
bn435	CTGCAGATGTTGAAGCTTTCGTGTAATG
bn436	GGATCCGCAATGGTTTCAACAGTAGCG
bn451	GAATTCCCAATGTTGCGAGCC
bn452	GTCGACACGAGCCTCCATACC
bn453	CTGCAGCCAATGTTGCGAGCC
bn454	GGATCCACGAGCCTCCATACC
bn460	GTGGATCCATGTTGAAGCTTTCGTGTAA
bn461	GTGGTACCTTAACTTGAAGGCTTCTTTC
bn462	GTGGATCCATGTTGAAGCTTTCGTGTAA
bn463	GTGGTACCTCATCTTGATGACTTCTTTC
bn465	GTGGTACCTCACTGTTGCTGAGGCAAAG
bn467	GTGGTACCTCAAGCCTTTGCATAAGGGA
bn579	ACGCAGAGATCACATCAGAC
bn580	TCACTGTTGCTGAGGCAAAG
bn581	TGGGTATCGGACCATGGAAG
bn582	CATAAGGGAGGACCAATGAG
bn670	GTACTAGTATGTTGAAGCTTTCGTGTAA
bn671	GTGTCGACTTAACTTGAAGGCTTCTTTC
bn672	GTACTAGTATGTTGAAGCTTTCGTGTAA
bn673	GTGTCGACTCATCTTGATGACTTCTTTC
bn674	GTACTAGTATGGCCTTCAAGTATCTTCT
bn675	GTGTCGACTCACTGTTGCTGAGGCAAAG
bn676	GTACTAGTATGATTCTTACAAGATGCTT
bn677	GTGTCGACTCAAGCCTTTGCATAAGGGA
bn682	AGACTTCCCGTCCTTACAAC
bn683	CCCACTTCACTTGCTGATTC
bn684	GCACCCTCTCCCTGTTAAAG
bn685	GCATCCCGAGCAATGGTAAG
bn887	TGGATCCATGCGTGCTGTTGTATCTGCTGA
bn888	TGGATCCATGCGGGCAATTCTCTCTGCTGA
bn1160	ACACGCGTATGGTGGCCACCTCTGCTAC
bn1161	ACCTCGAGTTACGGTGCAGTTCCCCAAG
bn1162	AcagatctATGGTGGCCACCTCTGCTAC
bn1163	ACGTCGACTTACGGTGCAGTTCCCCAAG
bn1181	GTGGATCCATGTCCCGTCCTTACAACCTTGC
bn1182	GTGGATCCATGTCACGTCCTTATAACATCGC
bn1210	GTCTCGAGATGTCCCGTCCTTACAACCTTGC
bn1212	GTCTCGAGATGTCACGTCCTTATAACATCGC

Stock number	Sequence
bn1220	GTATTAATCTGTTGCTGAGGCAAAG
bn1221	GTATTAATAGCCTTTGCATAAGGGA
bn1276	CACTAGTATGGCCTTCAAGTATCTTC
bn1277	CGGATCCCTGTTGCTGAGGCAAAGGAG
bn1278	CACTAGTATGATTCTTACAAGATGCTT
bn1279	CGGATCCAGCCTTTGCATAAGGGAGGA
bn1280	CGGATCCATGGTGAGCAAGGGCGAGGA
bn1281	CGTCGACTTACTTGTACAGCTCGTCCA
bn1350	GTACGCGTATGTTGAAGCTTTCGTGTAA
bn1366	CGTCGACTTAACTTGAAGGCTTCTTTC
bn1548	AGGCCATGGCGGCCGAAGAAGAATGGAGGATCATG
bn1658	GGCCATGGCGGCCAGAAGGTAATTATCCAAGAT
bn1659	ACTAGTGTTTCGATCCACTTTCTTACAAATTTCTC
bn1721	CAGGCCATGGCGGCCTCTTAACCAACTTAAGATTA
bn1722	GCGCTAGCCTTTTCGAATTTTGAAAATT
bn1737	TAGGCCCTTAAGGCCTTCTAACTTTTAGCATGTTTTG
bn1740	CAACTAGTATGGCTACTACATCTTTGGC
bn1741	ATGTCGACTCACACTCTTGGCTCAGCAG

7.7 Glycerol Stocks

Table 7.3: Glycerol stocks of recombinant *E. coli* strains.

Stock number	recombinant plasmid
223	pQ-*FatA1*
224	pQ-*FatA2*
751	pQ-*FatA1*oTP
752	pQ-*FatA2*oTP
205	pL-35S::RNAi-*FatA1*-DsRed
211	pL-35S::*FatA1*-DsRed
213	pL-35S::*FatA2*-DsRed
753	pL-35S::*FatB*-DsRed
754	pL-35S::*UcFatB*-DsRed
755	pBin-gly::*FatA1*-DsRed
756	pBin-gly::*FatB*-DsRed
757	pBin-gly::*UcFatB*
758	pL-*CMV::FatA1*-DsRed
759	pL-pro*FatA1::FatA1*-DsRed
760	pL-pro*FtaA1::FatB*-DsRed
761	pL-pro*FatA1::UcFatB*-DsRed
286	pQ-*GDPD5*oTMD
285	pQ-*GDPD6*oTMD
290	pLW01-*DsRed::GDPD5*oTMD
289	pLW01-*DsRed::GDPD6*oTMD
217	pL-*35S::GDPD5*-DsRed
215	pL-*35S::GDPD6*-DsRed
762	pDRGDPD5
763	pDRGDPD6
764	pL-*GDPD5::eGFP*
765	pL-*GDPD6::eGFP*
209	pL-*35S::GDPD5*-RNAi-DsRed
766	pL-utr*GDPD6*utr-DsRed

Eidesstattliche Erklärung/Declaration of primary authorship:

Ich versichere persönlich, dass ich die vorstehende Arbeit selbstständig und ohne Benutzung anderer als der angegebenen Hilfsmittel angefertigt habe. Alle Stellen, die wörtlich oder sinngemäß aus Veröffentlichungen entnommen sind, wurden als solche kenntlich gemacht. Die Arbeit hat in gleicher oder ähnlicher Form in keinem anderen Prüfungsamt vorgelegen.

I declare, that I have written the present thesis for doctorate and without help of others. Other than the presented references were not used and quoted results were always marked with the relevant reference. The present thesis was never either abroad or in Germany submitted for examination in the present or a similar version.

Bonn, den 16.03.2015

Meike Siebers

Acknowledgements

Nun zum interessanten Teil dieser Arbeit ...

Für die Bereitstellung des spannenden Themas, die enge fachliche Betreuung der Doktorarbeit und die exzellenten Arbeitsbedingungen am Institut für molekulare Physiologie und Biotechnologie der Pflanzen möchte ich mich herzlich bei Professor Peter Dörmann bedanken.

Bei Professor Lukas Schreiber bedanke ich mich für die freundliche Übernahme des Korreferates.

Michael Melzer vom IPK Gatersleben danke ich für die Durchführung der Elektronenmikroskopie und die Bereitstellung der wunderschönen Mikroskopieaufnahmen.

Ich hätte mir keine bessere Atmosphäre für das Unterfangen Doktorarbeit wünschen können und damit meine ich nicht nur das Chaosbüro. Ich hatte die besten Kollegen die man sich vorstellen kann! Vera, meine moralische Instanz, danke für die vielen Ratschläge und Gespräche die Wissenschaft und das Leben betreffend! Katha, guck mal der Flieder! Du unglaublich beeindruckendes Menschlein, Dir glaube ich tatsächlich alles, selbst wenn es um Wasserbäder geht! Matze Matze Matze, Dir danke ich für die unzähligen unbeschwerten Stunden als Labor- und Büromitbewohner und dafür, dass Du immer ein williges Opfer für alle Sport- und Ess-Experimente warst. Caro, so erfrischend ehrlich, wenn es mehr Menschen wie Dich geben würde, wäre das Leben klarer und einfacher. Es ist schön, wenn aus Kollegen Freunde werden!

Großer Dank gebührt auch Helga Peisker, für die Hilfe bei allen Q-TOF Messungen, Marlies Becker und Andreas Ahrens, für ihre Unterstützung im Labor, Georg Hölzl, meinem Lexikon in allen Klonierungsfragen! Katha und Vera, ohne deren Expertise ich einen Großteil der Q-TOF Messungen gar nicht hätte machen können. Regina, früher eine meiner besten Studenten und heute Kollegin, danke, dass Du Dich durchgebissen hast! Ania, Dir danke ich für die schönen Aufnahmen am konfokalen Mikroskop – ich würde Dir jederzeit wieder meinen Schreibtisch „überlassen“. Auch möchte ich mich bei allen aktuellen und ehemaligen Mitarbeitern des IMBIOs bedanken, besonders jedoch bei Felix Lippold, der mich als Newbie an die Hand genommen hat – „einfach machen!“

P. Narf – wir sollten öfter mal mit Matsch spielen. Danke für die wundervolle Zeit im hohen Norden und Deine kritischen, aber meist hilfreichen Kommentare bezüglich - naja - allem! ☺

Auch möchte ich Gino für seine Unterstützung über so viele Jahre hinweg danken.

Den meisten Dank schulde ich jedoch meiner Familie. Nina - die kleine Schwester und doch großes Vorbild. Endlich zusammen in Bonn! Meinen Eltern Anne und Jürgen danke ich für die Unterstützung auf diesem Weg und die Möglichkeit jederzeit zu Hause Ruhe zu finden. Ihr habt alles richtig gemacht!

Christopher - mein Wunderheiler - danke, dass Du meinen Blick fürs Wesentliche geschärft und mir gezeigt hast, worauf es wirklich ankommt. Es ist ein gutes Gefühl Dich stets an meiner Seite zu wissen! **Danke!**

„Lipide sind wichtiger als Regen!“

Dr. Branols; 08.07.2014, Botanischer Garten Bonn.